NAVAL POSTGRADUATE SCHOOL

MONTEREY, CALIFORNIA

THESIS

PARAMETRIC STUDIES OF DDG-81 SHIP SHOCK TRIAL SIMULATIONS

by

Jarema M. Didoszak

March 2004

Thesis Advisor: Young S. Shin

Approved for public release; distribution is unlimited

THIS PAGE INTENTIONALLY LEFT BLANK

REPORT DOCUMENTATION PAGE			Form Approved OMB No. 0704-0188
Public reporting burden for this collection of information is estimated to average 1 hour per response, including the time for reviewing instruction, searching existing data sources, gathering and maintaining the data needed, and completing and reviewing the collection of information. Send comments regarding this burden estimate or any other aspect of this collection of information, including suggestions for reducing this burden, to Washington headquarters Services, Directorate for Information Operations and Reports, 1215 Jefferson Davis Highway, Suite 1204, Arlington, VA 22202-4302, and to the Office of Management and Budget, Paperwork Reduction Project (0704-0188) Washington DC 20503.			
1. AGENCY USE ONLY ***(Leave blank)***	**2. REPORT DATE** March 2004	**3. REPORT TYPE AND DATES COVERED** Master's Thesis	
4. TITLE AND SUBTITLE: Parametric Studies of DDG-81 Ship Shock Trial Simulations			**5. FUNDING NUMBERS**
6. AUTHOR(S) Jarema M. Didoszak			
7. PERFORMING ORGANIZATION NAME(S) AND ADDRESS(ES) Naval Postgraduate School Monterey, CA 93943-5000			**8. PERFORMING ORGANIZATION REPORT NUMBER**
9. SPONSORING /MONITORING AGENCY NAME(S) AND ADDRESS(ES) N/A			**10. SPONSORING/MONITORING AGENCY REPORT NUMBER**
11. SUPPLEMENTARY NOTES The views expressed in this thesis are those of the author and do not reflect the official policy or position of the Department of Defense or the U.S. Government.			
12a. DISTRIBUTION / AVAILABILITY STATEMENT Approved for public release; distribution is unlimited			**12b. DISTRIBUTION CODE**

13. ABSTRACT (maximum 200 words)

Motivated by the sizable ledger of ships sent to the ocean floor without ever sustaining a direct hit during World War II, a heightened interest in ship shock survivability spread throughout the Naval Engineering community. As a result, over the last fifty years, Live Fire Test & Evaluations, otherwise known as ship shock trials, have been conducted in order to determine the seaworthiness of each new class of ship commissioned in the U.S. Fleet. While beneficial in determining the overall survivability of a ship and its mission essential equipment in a severe shock environment, these Navy-mandated tests pose serious danger to the crew, ship and environment.

As an alternative to these labor intensive, costly and time consuming at-sea tests, the recent advances in computer processing power have made it possible to employ finite element methods involving complex geometries in the modeling and simulation of shock response for the ship and surrounding fluid. This thesis examines the accuracy of shock simulation predictions as compared to the ship shock trials conducted on USS WINSTON S. CHURCHILL (DDG-81). An investigation of the effects of sensor location, damping and shot geometry is presented as validation of the Naval Postgraduate School modeling and simulation methodology.

14. SUBJECT TERMS Underwater Explosion, UNDEX, Modeling and Simulation, Shock and Vibration, Ship Shock, Shock Response, Underwater Shock Analysis, Dynamic Shock Simulation, Computer Simulation, USS Winston S. Churchill, DDG-81			**15. NUMBER OF PAGES** 166
			16. PRICE CODE
17. SECURITY CLASSIFICATION OF REPORT Unclassified	**18. SECURITY CLASSIFICATION OF THIS PAGE** Unclassified	**19. SECURITY CLASSIFICATION OF ABSTRACT** Unclassified	**20. LIMITATION OF ABSTRACT** UL

NSN 7540-01-280-5500 Standard Form 298 (Rev. 2-89)
Prescribed by ANSI Std. 239-18

THIS PAGE INTENTIONALLY LEFT BLANK

Approved for public release; distribution is unlimited.

PARAMETRIC STUDIES OF DDG-81
SHIP SHOCK TRIAL SIMULATIONS

Jarema M. Didoszak
Lieutenant, United States Navy
B.S. NA & ME, University of Michigan, 1994

Submitted in partial fulfillment of the
requirements for the degree of

MASTER OF SCIENCE IN MECHANICAL ENGINEERING

from the

NAVAL POSTGRADUATE SCHOOL
March 2004

Author: Jarema M. Didoszak

Approved by: Young S. Shin
Thesis Advisor

Anthony J. Healey
Chairman, Department of Mechanical and Astronautical Engineering

THIS PAGE INTENTIONALLY LEFT BLANK

ABSTRACT

Motivated by the sizable ledger of ships sent to the ocean floor without ever sustaining a direct hit during World War II, a heightened interest in ship shock survivability spread throughout the Naval Engineering community. As a result, over the last fifty years, Live Fire Test & Evaluations, otherwise known as ship shock trials, have been conducted in order to determine the seaworthiness of each new class of ship commissioned in the U.S. Fleet. While beneficial in determining the overall survivability of a ship and its mission essential equipment in a severe shock environment, these Navy-mandated tests pose serious danger to the crew, ship and environment.

As an alternative to these labor intensive, costly and time consuming at-sea tests, the recent advances in computer processing power have made it possible to employ finite element methods involving complex geometries in the modeling and simulation of shock response for the ship and surrounding fluid. This thesis examines the accuracy of shock simulation predictions as compared to the ship shock trials conducted on USS WINSTON S. CHURCHILL (DDG-81). An investigation of the effects of sensor location, damping and shot geometry is presented as validation of the Naval Postgraduate School modeling and simulation methodology.

THIS PAGE INTENTIONALLY LEFT BLANK

TABLE OF CONTENTS

LIST OF FIGURES

LIST OF TABLES

THIS PAGE INTENTIONALLY LEFT BLANK

ACKNOWLEDGMENTS

I would like to extend my sincerest gratitude to Dr. Young S. Shin for his support and expert guidance throughout the course of this research and my study at the Naval Postgraduate School. His dedication to this field and the expertise that he brings were instrumental in the successful completion of this effort.

There are also some of the other individuals that helped make this study possible and deserve to be recognized for their contributions:

CAPT David Lewis and CDR Jeff Riedel from PEO Ships, for their foresight, support and funding of the Naval Postgraduate School's ship shock modeling and simulation program,

Steve Rutgerson of UERD, who was always there to answer the myriad of questions that I had about sensors locations and the shock trial data examined during the course of my research and analysis,

Tom Christian, our Shock and Vibration Computational Laboratory manager, technician and computer problem solver extraordinaire; his skilled management of the computer systems helped avert disaster time and again.

And finally, I would like to thank my loving wife Robin most of all, for her patience and understanding during my time working on this project. I dedicate this work to my three wonderful sons, Danylo, Stefan and Yuri.

THIS PAGE INTENTIONALLY LEFT BLANK

I. INTRODUCTION

A. BACKGROUND

To the dismay of many World War II naval leaders, scores of ships, both combatants and those in service with the merchant marine, were sent to the ocean floor without ever taking a direct hit from an enemy bomb, mine or torpedo. These ships sank as a result of underwater explosions (UNDEX) occurring in the surrounding waters adjacent to the ship. In the ensuing years a buzz-phrase sharing the title of a training film on underwater explosions, "near is close enough", proved to signal a shift in naval warfare. With the ability to effectively deliver ever-increasing charge sizes it became readily evident that hitting the hull of the ship was no longer as important as once had been the case. It had been generally accepted throughout the Fleet that one of the best ways to sink a ship was to open a large hole in the hull beneath the waterline. This was done with the expectation that the ensuing flooding would reduce stability to a point from which the ship could not recover. Delivering a direct hit to a weapons magazine or fuel storage tanks that would facilitate the cascade of internal explosions and ultimate catastrophic loss due to conflagration was also deemed highly desirable and practical. However, through insightful analysis of the wartime ship losses suffered during the first half of the 20th century, it was determine that incident shock wave and bubble pulse forces resulting from UNDEX events were one of the primary initiators of structural damage, material failure and ultimate loss mechanism in the sinking of numerous ships [Ref. 1].

Over the last fifty years much research has been accomplished in the UNDEX field, resulting in a greater appreciation of the true power encapsulated in the UNDEX shock phenomena. Accordingly, having understood the necessity for ships that were resilient in an UNDEX environment, specifications were established for the design and testing requirements of all naval surface combatants. The Department of the Navy set forth guidance for shock hardening of surface ships in OPNAVINST 9072.2 [Ref. 2], with additional requirements delineated in NAVSEA 0908-LP-000-3010A [Ref. 3] and MIL-S-901D [Ref. 4]. Carried out in the summer of 2001, the DDG-81 Ship Shock

Trials are the latest set of Live Fire Testing & Evaluations (LFT&E) to be conducted in fulfillment of these standing requirements.

Referred to as "shots", a series of underwater explosions, produced by the detonation of charges placed at varying locations in the water adjacent the ship, are designed to test the ship at "near combat conditions" [Ref. 2]. The response of the ship, weapons systems, specific equipment and the crew are all measured and recorded in order to evaluate their performance in a shock environment. Taken from one of the first ships in the class, or from a ship incorporating major design changes during construction, this data is then analyzed and recommendations are made for the alteration of existing ships or for a change in the design of subsequent ships to be built within that same ship class.

Even though these ship shock trials provide a true record of the system response of the ship as well as excellent training for the ship's crew, they are very costly, and inherently dangerous. Such events require extensive planning and coordination and are potentially damaging to the ship structure, electronics and multi-million dollar weapons systems. Inasmuch as these shock trials are good measures of the ship's potential performance in a shock environment, they are limited by the safety risk involved and thus only test to two-thirds the design limit. These limitations of the LFT&E program raise concerns over the validity of the ship shock trials and their associated costs, which could range as high as 5% of the $950million delivery cost, as in the case of the USS JOHN PAUL JONES (DDG-53) ship shock trials conducted in 1994 [Ref. 5].

In recent years, unprecedented advances in computer modeling and simulation have created the potential to mitigate some of the costs associated with the LFT&E activities through the use of virtual shock environment analysis [Ref. 6]. By implementing these current technologies, simulations that accurately predict the initial peak response of a surface ship subjected to an underwater shock event enhance traditional analysis methods and hold great promise in replacing certain types of at sea live fire testing [Ref. 7]. With the two major elements of the modeling and simulation process, model refinement and computer runtime, amounting to only a fraction of the ship shock trial costs, engineers can subject the finite element ship model and corresponding fluid mesh to an exhaustive battery of simulations over an extensive range

of charge sizes and geometries. These simulations conducted in the virtual UNDEX environment allow for evaluation of the ship system at and beyond its design limits, without bringing harm to the ship, crew or the environment. This approach has the added benefit of incorporating predictive results obtained from the simulations into the final stages of the ship design spiral. Making corrective changes while the ship is still in the construction phase, rather than during the post-production timeframe as is done with current LFT&E results, greatly reduces the rework costs.

Though not considered reliable enough at this time to completely replace the LFT&E process, it is expected that the use of simulated UNDEX events will continue to be used as a predictive design tool. The insight gained in the virtual UNDEX environment would eliminate the need for broad scope shots and foster focused investigation of UNDEX events through use of scalable charges placed at specific locations corresponding to the points of interest found in pre-shock trial simulations.

B. SCOPE OF RESEARCH

Using the data obtained from the shock trials conducted on USS WINSTON S. CHURCHILL (DDG-81) in June of 2001 as a basis, this paper serves as further validation of the modeling and simulation methodology established by the Shock and Vibration Computation Laboratory at the Naval Postgraduate School (NPS). Recent work completed by Schneider [Ref. 8] at NPS concentrated mainly on the refinement of the modeling and simulation process of the DDG-81 as well as analysis on the overall vertical response velocities at the shipwide level. This paper will expound upon the work presented by Schneider in June 2003. Using the NPS modeling and simulation process, this paper further investigates the results of localized vertical velocity response in the critical Combat Information Center (CIC) area as well as the shipwide velocity response in the athwartship direction. Comparisons between the measured ship shock trial data and the simulated response predictions were also conducted for two sets of ship system proportional damping coefficients. The findings of these comparisons will also be presented herein.

THIS PAGE INTENTIONALLY LEFT BLANK

II. UNDERWATER EXPLOSION PHENOMENA

In order to truly understand the devastating effects that are associated with the underwater shock phenomena it is necessary to start with some background information on this subject. Since there are many complex layers to the underwater shock phenomena and its corresponding system response, only the most relevant factors will be presented in order to provide some degree of familiarization.

A. FLUID BEHAVIOR

There is a defined sequence of events that makes up the underwater explosion (UNDEX). We shall begin with a simple discussion of the underwater shock and where and how it comes exist. To set the process in motion, a sudden chemical reaction within the initiator charge, typically composed of a primer explosive such as mercury fulminate, results from an electronic or mechanical detonation. This action then ignites the high explosive. Commonly used high explosives are HBX-1, RDX, TNT and PETN. Their detonation and ensuing conflagration causes a high temperature, high pressure gas to be formed. Almost immediately a shock wave propagates outward from the nucleus of the charge at a velocity on the order of 25,000 ft/sec [Ref. 9]. With the reaction initiated, a pressure wave proceeds to moves through the surrounding explosive material, creating additional pressure waves. The generated explosive energy exists in a gaseous state with temperatures and pressures approaching 3000 degrees Celsius and 50,000 atmospheres, respectively [Ref. 10]. This initial process takes only nanoseconds to occur in most high explosives [Ref. 11]. With the pressure wave velocity exceeding the acoustic velocity of the explosive material by anywhere from three to fives times, a shock wave is formed. This combination of extremely high heat and compressive pressures facilitates the self-perpetuating nature of the explosive process. The resulting shock wave is then released into the surrounding fluid.

Typically when dealing with water in engineering applications, it is taken to be an incompressible fluid in all but the most rare of cases. However, in UNDEX applications, the water immediately surrounding the explosive charge actually compresses slightly as a

result of the extreme pressure of the shock wave. This compression results in a high pressure shock wave in the water that in turn spreads outward from the charge location. Though this shock wave initially moves through the water at velocities much greater than the speed of sound, it quickly retards to match the acoustic velocity of the water. Generally approximated as 5000 ft/sec, the actual speed of sound through water is affected by such factors as temperature, hydrostatic pressure, and salinity of the medium [Ref. 10]. For the simulations discussed herein a value of 5057 ft/sec is used in all cases.

The pressure wave generated during the detonation process has an incredible amount of force driving it outward from the charge center. For example, in the case of TNT, it is on the order of 2×10^6 lb/in^2. Figure 1 shows an example of the pressure profile for a TNT charge [Ref. 9]. The initial shock wave shows a discontinuous pattern of exponential decay as the radial distance from the detonation point increases.

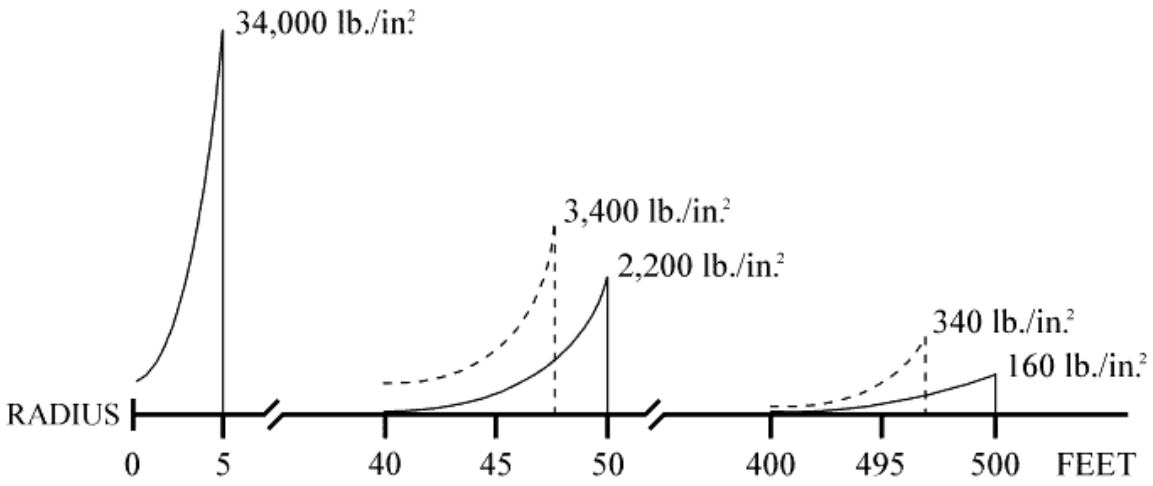

Figure 1. Shock Wave Profiles for 300 lb TNT Charge [from Ref. 9]

A series of empirical equations have been formulated to characterize the shock wave pressure profile, $P(t)$ [Ref. 10]. These formulae, Equations (1) through (5), are good from 10-100 charge radii and for up to one time decay constant after the initial detonation.

$$P(t)=P_{max}e^{-\frac{t-t_1}{\theta}} \qquad \text{(psi)} \qquad (1)$$

$$P_{max}=K_1\left(\frac{W^{\frac{1}{3}}}{R}\right)^{A_1} \qquad \text{(psi)} \qquad (2)$$

$$\theta=K_2W^{\frac{1}{3}}\left(\frac{W^{\frac{1}{3}}}{R}\right)^{A_2} \qquad \text{(msec)} \qquad (3)$$

$$T=K_5\frac{W^{\frac{1}{3}}}{(D+33)^{\frac{5}{6}}} \qquad \text{(sec)} \qquad (4)$$

$$A_{max}=K_6\frac{W^{\frac{1}{3}}}{(D+33)^{\frac{1}{3}}} \qquad \text{(ft)} \qquad (5)$$

where the preceding variables are defined as:

t_1 = arrival time of shock wave (msec)

t = time of interest (msec)

P_{max} = the peak magnitude of the pressure of the shock front (psi)

θ = shock wave decay constant (msec)

R = standoff distance, radial (ft)

W = weight of the explosive (lb)

D = charge depth (ft)

K_1, K_2, K_5, K_6, A_1, A_2 = constants specific to explosive type

A_{max} = maximum bubble radius (ft)

B. GAS BUBBLE OSCILLATION

After the shock wave is produced it quickly expands radially, leaving behind the highly compressed, superheated gases that formed it. This spherical gaseous bubble continues to expand to relieve its pressure until the internal pressure falls below the surrounding hydrostatic pressure of the water. In the interim the bubble actually expands past its equilibrium due to the momentum of the expansion, growing to nearly twice its equilibrium diameter. Equation (5) is used to calculate the maximum bubble radius [Ref. 9].

This equation illustrates that the maximum bubble radius has a one-third power relationship with the charge weight and an inverse proportionality to the one-third power of the charge depth. At the instant that the gas bubble reaches its maximum diameter, there is a sizable positive pressure gradient between the bubble and the encompassing water, which causes the gas bubble to implode upon itself. The bubble then shrinks down to a point where the pressure within the bubble is high enough to prevent further collapse. A negative pressure gradient now exists between the bubble and the water that surrounds it. Once again the bubble attempts to expand to its equilibrium state and reaches a maximum diameter smaller than the initial gas bubble diameter, yet still larger than its expected equilibrium point, though the overshoot is less than in the first case. Henceforth this oscillatory process repeats until the energy contained within the bubble is insufficient to continue the cycle or the bubble has come in close proximity with the free surface of the water, allowing the exhaust gases to freely vent to the air above. The cyclic expansion and contraction of the bubble along with its migration path to the free surface are shown in Figure 2.

The vertical migration velocity experience by the bubble in its ascent to the air-water interface is calculated by using Equation(6). The vertical velocity (U) is a function of the gas bubble radius,

$$U=\frac{2g}{a^3(t)}\int_0^t a^3(t)dt \qquad \text{(ft/sec)} \qquad (6)$$

where:

g = gravitational acceleration constant

a = gas bubble radius

Even though the gas bubble pulse is highly dependent on charge geometry, specifically charge size and detonation depth, it is important to the simulation of the UNDEX event. This is especially true in the case of the DDG-81 shock trial simulations since the gas bubble pulse has a low oscillation frequency that approaches the values of the first bending mode of the ship. It could potentially result in even more destructive forces than the incident pressure wave, given the proximity of the phenomena [Ref. 10].

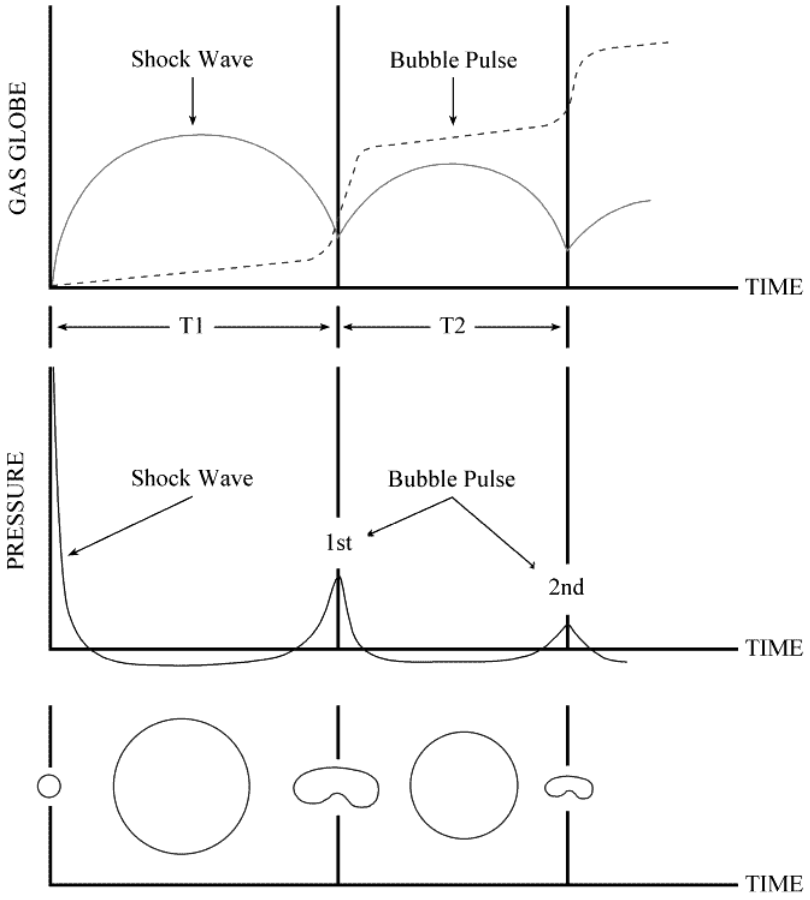

Figure 2. Gas Bubble Oscillation and Migration Path [after Ref. 9]

C. CAVITATION

In general, cavitation is described as the phenomenon that occurs when there is a region of absolute negative pressure present in a body of water at a nearly constant temperature. Vapor cavities are formed where the negative pressure causes the tensile force of the water, which cannot be sustained, to implode, in turn causing high pressure pulses to emanate. During an UNDEX event there are two types of cavitation present, bulk cavitation and local cavitation. The first type, bulk cavitation, can be thought of as a large area of low pressure at the free surface of the water forming above the charge detonation point, while the second, local cavitation is a small area of low pressure generally found to occur at the fluid-structure interface. Both types of cavitation can figure in very prominently to the overall response of the ship during an UNDEX event and are important factors that must be accounted for in the simulation process [Ref. 11].

1. Bulk Cavitation

In an UNDEX event the blast, and likewise the shock wave, propagate in a spherical expanding circle from the detonation point. Figure 3 is a two-dimensional representation of the geometries involved in a typical UNDEX event. The incident pressure wave, a compressive pressure wave, is first to strike the target. As this shock wave reaches the free surface it is reflected at the boundary as a rarefaction wave, which means that the water flow is directed opposite to the direction of propagation. This tensile pressure wave contributes to the creation of bulk cavitation due to the marked reduction in image pressure once the incident pressure wave has decayed. The pressure decay rate is defined in accordance with Equation (1). This point is termed “cut-off”. The cavitation pressure can be as low as negative three to four psi [Ref. 12]. Figure 4 illustrates the shock wave profiles and the “cut-off” time.

There may also exist be a bottom reflection wave, caused by the reflection of the shock wave off of the ocean floor, though this type of pressure wave is customarily of less significance in the UNDEX event pertaining to surface ships since this type of pressure wave is heavily dependent on the ocean floor characteristics and its proximity to the target [Ref. 9].

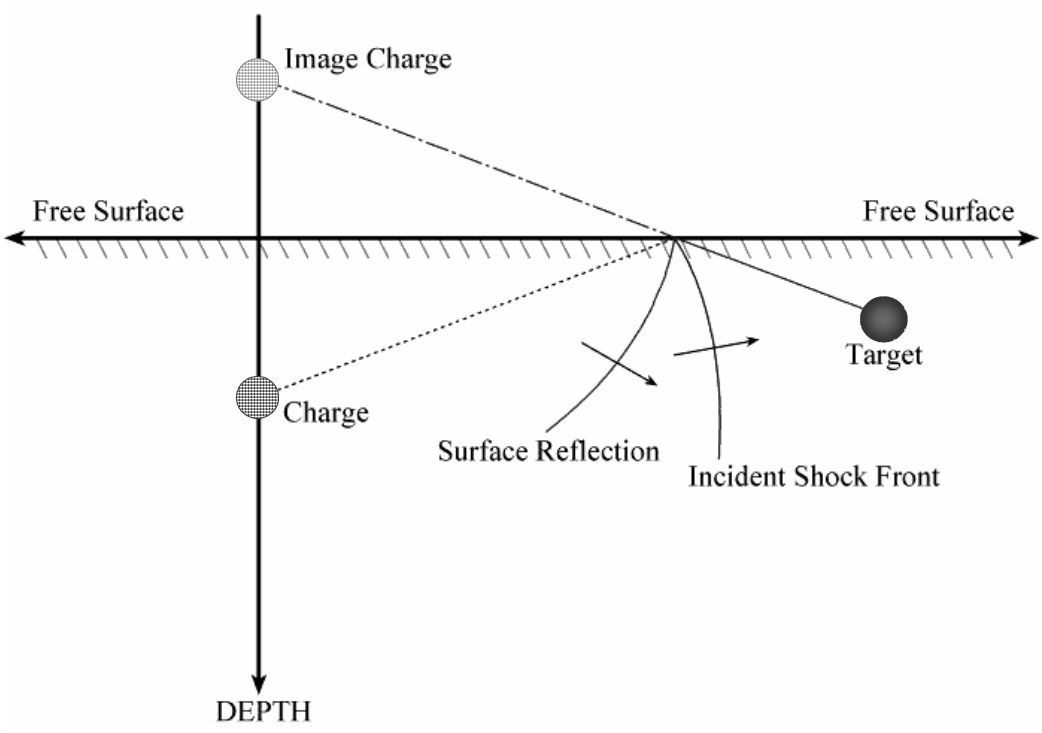

Figure 3. Underwater Explosion Geometry [after Ref. 9]

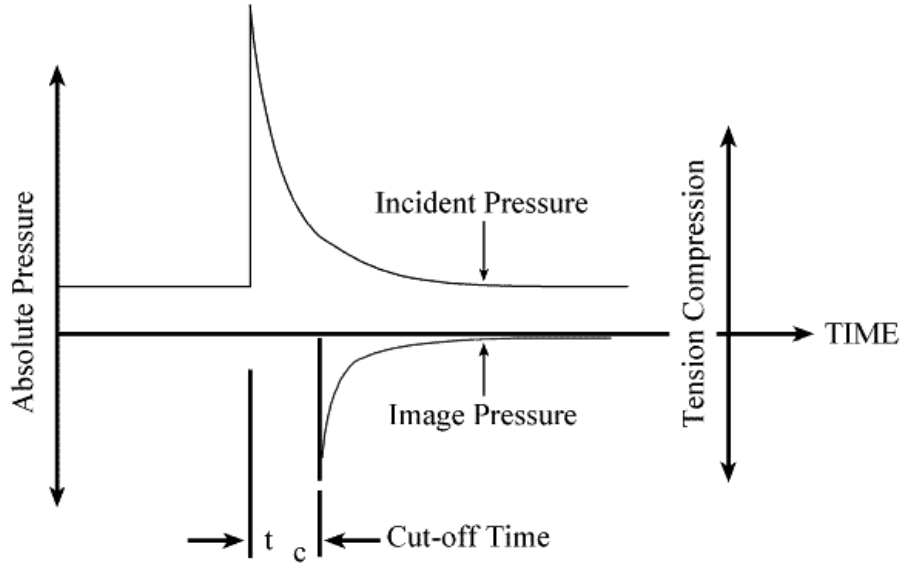

Figure 4. Shock Wave Pressure Profile with Cut-off Time [after Ref. 9]

The bulk cavitation area is formed due to the water's inability to support the negative pressure resulting from the tensile forces of the reflected incident pressure wave. The water vapor cavity that is created consists of two separate boundary regions, an

upper boundary and a lower boundary. These boundaries are a function of the size, type and depth of the charge that is detonated in an UNDEX event. An example of this dependence is shown in Figure 5. This series of subplots, generated for a 100 lb Pentaerythritol Tetranitrate (PETN) charge at varying depths, illustrates the difference in resulting bulk cavitation zones. The MATLAB® code used to generate this figure is provided in APPENDIX A.

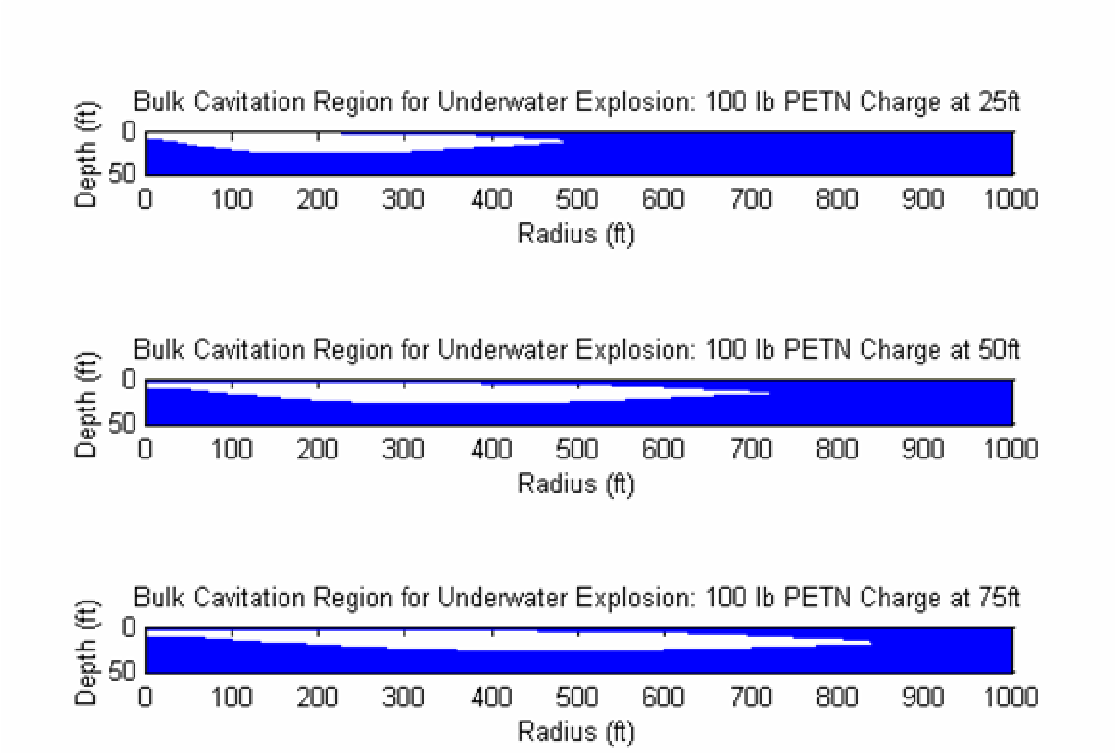

Figure 5. Bulk Cavitation Zone for 100 lb PETN Charge Detonated at Varying Depths

In order to find the upper cavitation zone boundary, which is defined as the area in which the net pressure equals zero, Equation (7) is used in conjunction with Equations (8) and (9).

$$F(x,y) = K_1\left(\frac{W^{\frac{1}{3}}}{r_1}\right)^{A_1} e^{-\frac{(r_2-r_1)}{C\theta}} + P_A + \gamma y - K_1\left(\frac{W^{\frac{1}{3}}}{r_2}\right)^{A_1} = 0 \qquad (7)$$

$$r_1 = \sqrt{(D-y)^2 + x^2} \qquad \text{and} \qquad r_2 = \sqrt{(D+y)^2 + x^2} \qquad (8) \text{ and } (9)$$

where $x, y =$ the horizontal range and the vertical depth of the point

r_1 = standoff distance from the charge to the point

r_2 = standoff distance from the image charge to the point

C = acoustic velocity in the water

D = charge depth

θ = decay constant

P_a = atmospheric pressure

γ = weight density of water

W = charge weight

$K_1, A_1, K_2, A_2 =$ shock wave parameters (charge type dependent)

In order to determine the lower cavitation zone boundary, the decay rates of the absolute pressure and the reflected wave must be equated. The formula for this calculation is shown in Equation (10), using the same variables as in Equations (7) through (9).

$$G(x,y) = -\frac{P_i}{C\theta}\left\{1 + \left[\frac{r_2 - 2D\left(\frac{D+y}{r_2}\right)}{r_1}\right]\left[\frac{A_2 r_2}{r_1} - A_2 - 1\right]\right\}$$
$$-\frac{A_1 P_i}{r_1^2}\left[r_2 - 2D\left(\frac{D+y}{r_2}\right)\right] + \gamma\left(\frac{D+y}{r_2}\right) + \frac{A_1}{r_2}(P_i + P_A + \gamma y) = 0 \qquad (10)$$

P_i, the incident pressure at cut-off, is given by,

$$P_i = P_{\max} e^{-\left[\frac{(r_2 - r_1)}{C\theta}\right]} \tag{11}$$

Bulk cavitation will continue to exist in the area of the water vapor cavity until its absolute pressure has risen above zero psi. The bulk cavitation area, when viewed during an UNDEX event occurring near to the surface, can be witnessed as a white flattened cardioid-like shape just beneath the air-water interface. Figure 6 is a cross section view representative of the bulk cavitation zone created by a 100 lb PETN charge detonated 75 feet below the free surface of the water.

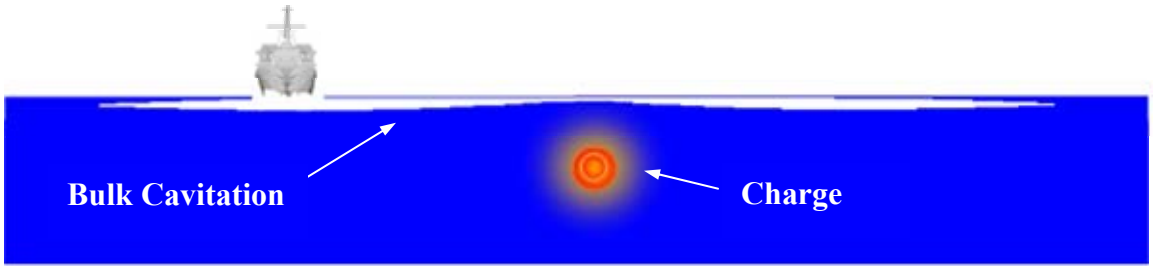

Figure 6. Bulk Cavitation Zone Resulting from an Underwater Explosion

2. Local Cavitation

Shock pressure pulses occurring as a result of an UNDEX event excite the ship structure as they impinge on the hull, causing dynamic responses. As this fluid-structure interaction occurs, the total pressure along the hull becomes negative. Unable to sustain the tension, the water pressure reduces to vapor pressure and cavitation occurs. Taylor flat plate theory will be used to describe how the phenomenon of local cavitation occurs. Figure 7 shows a Taylor flat plate subjected to a plane wave.

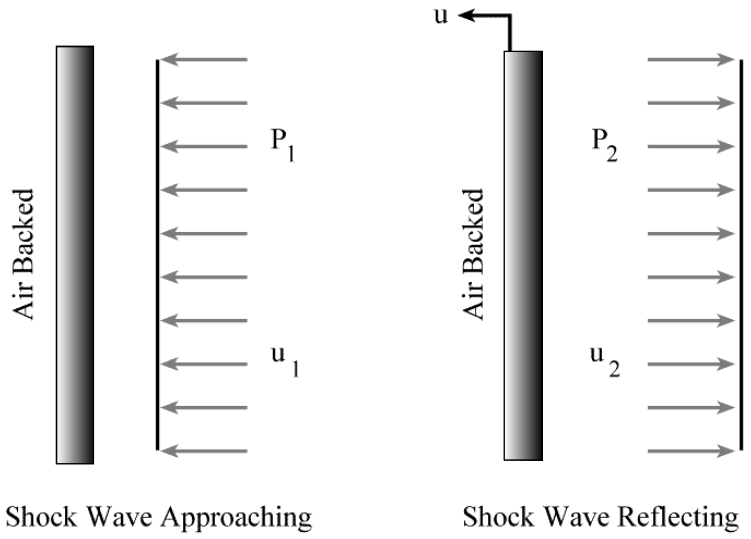

Figure 7. Taylor Plate Subjected to a Plane Wave [after Ref. 9]

The plate is subjected to an incident shock wave, $P_1(t)$, which is taken to be a planar wave. As is interacts with the plate, the reflected pressure wave, $P_2(t)$, is created and reflected off of the plate. The velocity of the plate is defined as $u(t)$. Using Newton's 2nd Law the equation of motion for a flat plate is written as

$$m\frac{du(t)}{dt} = P_1(t) + P_2(t) \tag{12}$$

The velocities behind the incident shock wave and the reflected shock wave are defined as $u_1(t)$ and $u_2(t)$, respectively. From this the plate interface between the surface of the plate and the fluid is described as

$$u(t) = u_1(t) - u_2(t) \tag{13}$$

It can be shown for a one-dimensional wave, that the that incident and reflected shock wave pressures reduce to,

$$P_1(t) = \rho C u_1(t) \tag{14}$$

$$P_2(t) = \rho C u_2(t) \tag{15}$$

where ρ = fluid density and C = acoustic velocity in the medium.

Hence, Equations (1), (14) and (15) can be used to formulate the solution of the reflected pressure wave equation as follows:

$$P_2(t) = P_{\max} e^{-\left(\frac{t-t_1}{\theta}\right)} - \rho C u(t) \tag{16}$$

Equation (16) can then be re-written as a first order linear differential equation,

$$m\left(\frac{du}{dt}\right) + \rho C u(t) = 2P_{\max} e^{-\left(\frac{t-t_1}{\theta}\right)} \tag{17}$$

for which the solution is of the plate velocity is found to be

$$u(t) = \frac{2P_{\max}\theta}{m(1-\beta)}\left\{e^{-\left[\frac{\beta(t-t_1)}{\theta}\right]} - e^{-\left[\frac{(t-t_1)}{\theta}\right]}\right\} \tag{18}$$

where $\beta = \frac{\rho C \theta}{m}$ and t > 0. The net pressure at the plate can then be expressed as

$$P_1 + P_2 = \frac{2P_{\max}\theta}{(1-\beta)}\left\{e^{-\left[\frac{(t-t_1)}{\theta}\right]} - \beta e^{-\left[\frac{\beta(t-t_1)}{\theta}\right]}\right\} \tag{19}$$

Equation (19) then shows that as β increases to a large value, which represents a lightweight plate, the total net pressure becomes negative at a very early time. Thus, cavitation occurs as the vapor pressure of water is reached. The plate separates from the fluid and attains a maximum velocity [Ref. 9].

D. FLUID-STRUCTURE INTERACTION

The fluid-structure interaction between the ship's hull and the surrounding water is primarily in the vertical direction as a result of an underwater explosion. It has been found that the response of the ship can be approximated with some appreciable degree of accuracy by using the Doubly Asymptotic Approximation (DAA) [Ref. 11]. The underlying equation used to define the structural motion is the discretized differential equation,

$$[M]\{\ddot{x}(t)\}+[C]\{\dot{x}(t)\}+[K]\{x(t)\}=\{f(t)\} \tag{20}$$

where $[M]$, $[C]$ and $[K]$ are the symmetric linear structural mass, damping and stiffness matrices, and $\{f\}$ is the external force vector.

Equation (20) represents the dynamic response of the ship structure. It can be thought of as a balance of all of the forces acting upon the ship's structure. These forces include the inertial forces, damping forces, internal forces and acoustic fluid pressure forces [Ref. 13].

In dealing with a submerged structure excited by an acoustic wave, the external forcing function is equal to,

$$f = -GA_f(p_I + p_s) + f_D \tag{21}$$

where p_I is the nodal pressure vector for the wetted-surface fluid mesh pertaining to the incident wave and p_s is the nodal vector corresponding to the scattering wave.

The dry-structure applied force vector is f_D, the transformational matrix relating the nodal surface forces is denoted as G, while A_f is the diagonal area matrix associated with the elements in the fluid mesh [Ref. 13].

The DAA is the preferred method for solution of this problem since it accounts for the approximation of both early time (high frequency) and late time (low frequency) motions [Ref. 14]. The First Order Doubly Asymptotic Approximation (DAA_1) is used for long cylindrical shell structures such as a surface ship or submarine since the DAA is not valid in the cavitation region. The DDA_1 equation is expressed as,

$$[M_f]\{\dot{p}_S\}+\rho c[A_f]\{p_S\}=\rho c[M_f]\{\dot{u}_S\} \tag{22}$$

where $\{u_s\}$ is the scattered wave fluid particle velocities vector, $\{p_s\}$ is the scattered wave pressure vector, $[M_f]$ is the fluid mass matrix, $[A_f]$ is the diagonal area matrix of the fluid mesh, ρ is the fluid density, and c is the sound velocity of the fluid [Ref. 15].

In the early time response Equation (22) reduces to $p_s = \rho c u_s$, a plane wave approximation, while for the late time response, it reduces to $A_f p_s = M_f \dot{u}_s$, a virtual mass approximation [Ref. 16].

Since this method allows for the solution of the fluid-structure interaction in terms of wetted-surface response only, $\{f\}$, the excitation of the wetted-surface structure by the incident shock wave is given by Equation (23), where p_I and p_s correspond to the incident pressure and scattered shock wave pressure vectors, respectively [Ref. 17].

$$f = GA_f(p_I + p_s) \tag{23}$$

The scattered wave fluid particle velocities are then tied to the structure response through the following relationship:

$$G^T \dot{x} = u_I + u_s \tag{24}$$

where T represents matrix transpose.

By means of mathematical manipulation of the aforementioned equations the resulting DDA Interaction Equations are found to be:

$$[M]\{\ddot{x}\} + [C]\{\dot{x}\} + [K]\{x\} = -[G][A_f](p_I + p_s) \tag{25}$$

$$[M_f]\{\dot{p}_s\} + \rho c[A_f]\{p_s\} = \rho c[M_f]\left([G^T\{\ddot{x}\} - \{\dot{u}_I\}\right) \tag{26}$$

Equations (25) and (26) leave two unknowns, x and p_s, which can be solved using a staggered solution scheme [Ref. 14].

THIS PAGE INTENTIONALLY LEFT BLANK

II. SHIP SHOCK MODELING AND SIMULATION

A. SHIP MODEL

The finite element model of the USS WINSTON S. CHURCHILL (DDG-81) that was used as the basis of the research reported in this paper was built by the DDG-51 Class ship design firm, Gibbs and Cox, Inc. [Ref. 18]. Figure 8 shows the Flight IIA model alongside the original DDG-51 model used during the DDG-53 simulation effort.

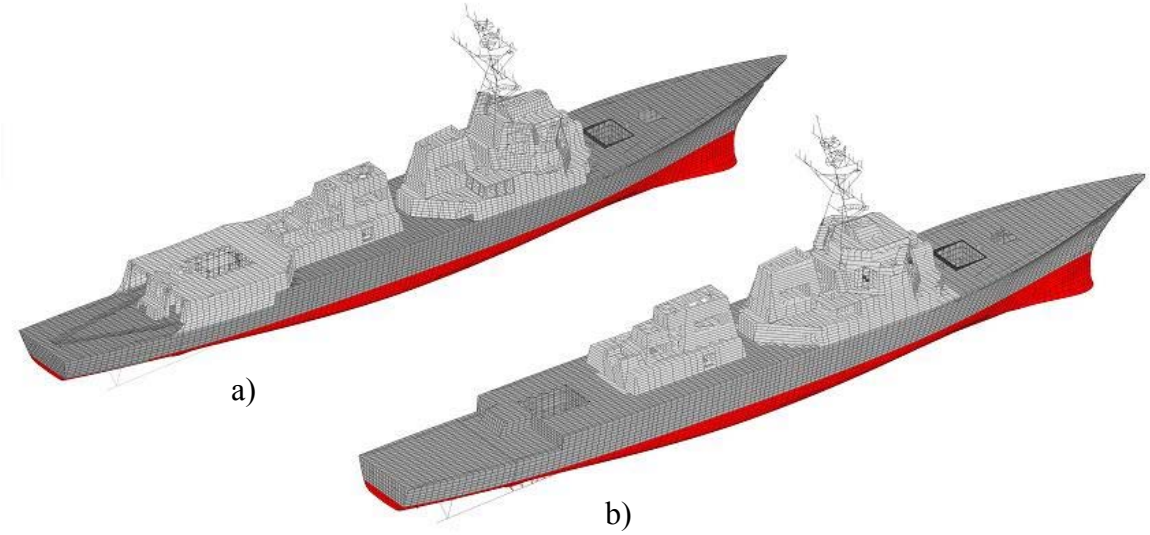

Figure 8. DDG-81 (a) and DDG-53 (b) Finite Element Models [from Ref. 18]

The major modifications that were made to the Flight IIA Arleigh Burke Class destroyer initial production design were as follow:

- Extension of the transom by five feet
- Replacement of both Vertical Launch System (VLS) handling cranes by six additional VLS cells, for a total of 96 VLS cells
- Replacement of the 5”/54 caliber gun with the 5”/62 caliber gun
- Increased thickness of scantlings amidships
- Installation of dual helicopter hangers

Detailed descriptions of the alterations made to DDG-81 are provided in Figure 9.

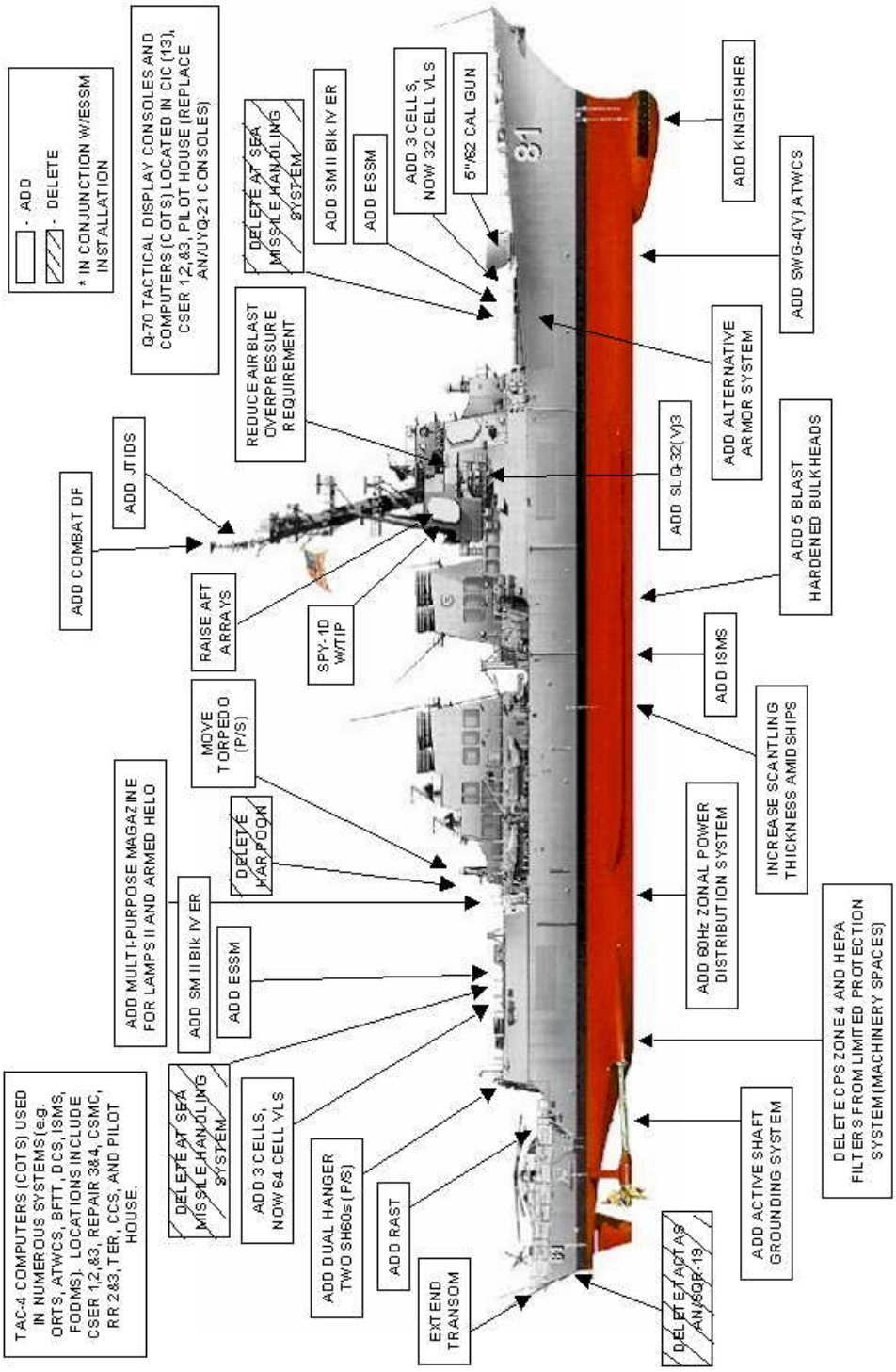

Figure 9. Illustration of Alterations Made to the Flight IIA Arleigh Burke Class Destroyer [from Ref. 19]

For each one of the three shots, Gibbs and Cox, Inc. provided a separate finite element model to the Naval Postgraduate School shock simulation team. Details such as the liquid tank levels, exact weapons load-out, temporarily installed equipment and even the number of personnel onboard at the time of each shot, were accounted for in order to obtain the most accurate model possible for simulation of the ship shock trials. The complex finite element model included many additional improvements over previous models, such as more realistic mass distribution through the use of a significantly superior weight tape.

Figure 10 shows some of the simplified spring-mass models that were developed from existing detailed equipment models. This was done for items that could significantly influence the ship response at the keel, bulkheads and sensor locations. The gas turbines, main reduction gears and 5"/62 gun are some examples of critical items that were incorporated into the overall ship model [Ref. 18].

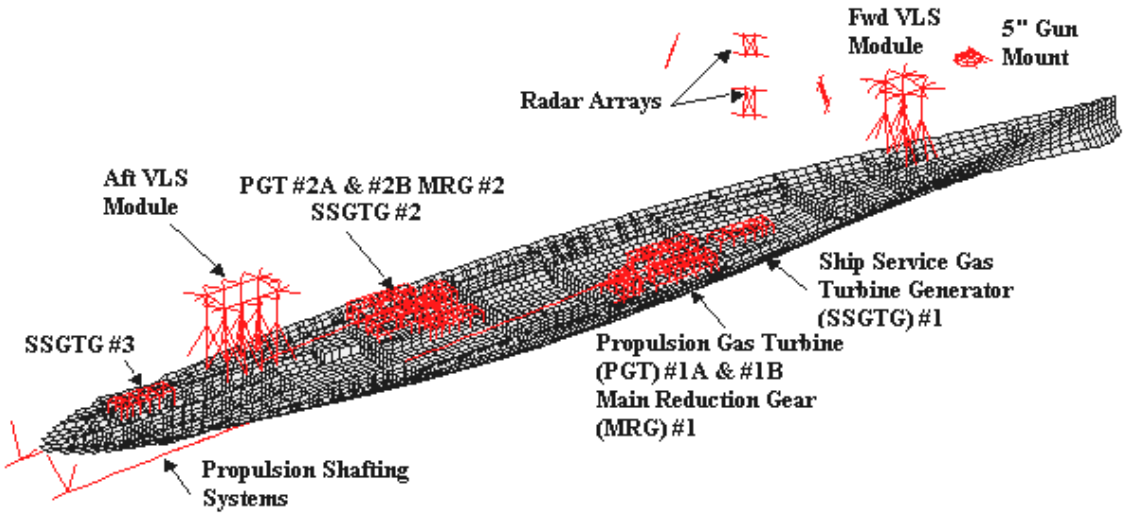

Figure 10. Equipment Models in the Finite Element Model of DDG-81 [from Ref. 18]

The nominal mesh size of the finite element model was 27 in x 48 in. The level of detail and complexity of the ship model are shown in Figure 11, a cut-away view looking from the centerline toward the port side, astern of Frame 300.

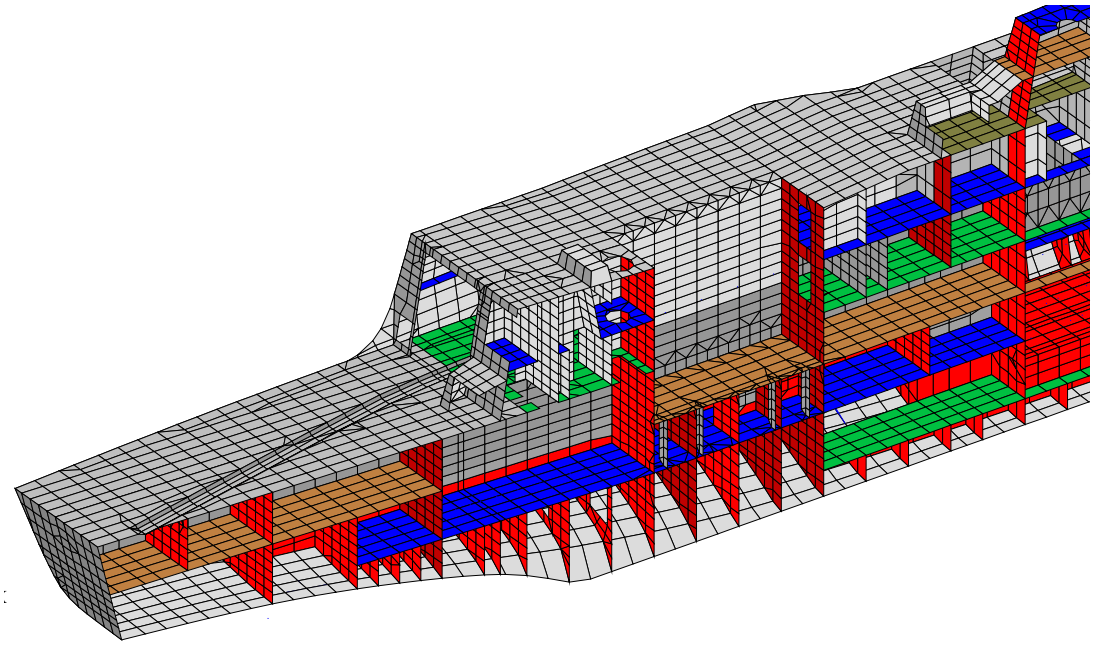

Figure 11. Cut-away View of the DDG-81 Finite Element Model [from Ref. 18]

Table 1 provides a list of some of the key properties associated with the DDG-81 finite element models.

Table 1. List of Finite Element Model Properties [from Ref. 18]

Number of Nodes	40,514
Number of Degrees of Freedom	243,084
Number of Beam Elements	49,397
Number of Thin Shell Elements	48,662
Number of Lumped Masses	92,541

Figure 12 gives a general representation of where the charges were located during the at sea ship shock trial performed on DDG-81. The exact locations and charge sizes will not be discussed herein as these parameters are classified. Shot 3 was the closest in proximity to the ship when its charge was detonated. Inasmuch as this was the most severe shot of the three, the Shot 3 data will be used in most of the comparisons since it most closely approximates an actual surface ship UNDEX event experienced during combat.

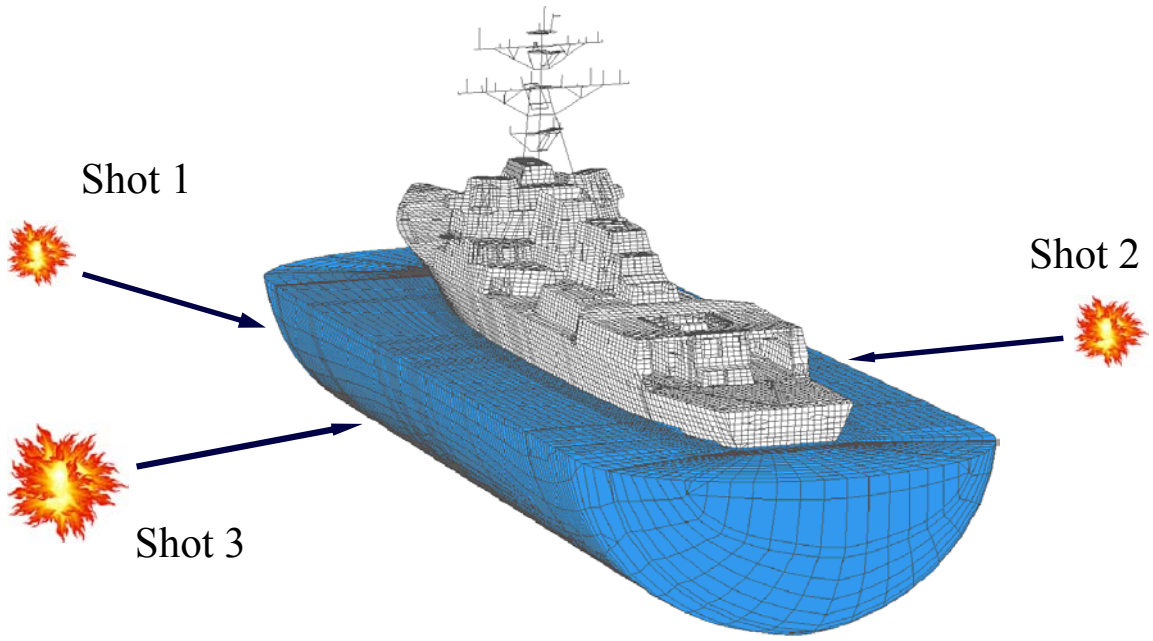

Figure 12. DDG-81 Ship Shock Trial Shot Geometry

B. SHOCK TRIAL SIMULATION

An overview of the process used to conduct the ship shock trial simulations is shown in Figure 13. First the finite element model provided by Gibbs and Cox, Inc. was converted from a MSC/NASTRAN input deck into a nonlinear dynamic analysis code (LS-DYNA) keyword file. A fluid mesh was created in TrueGrid, a high quality hexahedral mesh program by XYZ Scientific Applications, Inc. During March through June 2003, Schneider [Ref. 8] developed the fluid mesh that is currently being employed for all shock trial simulations at NPS. Next the fluid mesh and converted model were run joined together in LS-DYNA, which was coupled with the Underwater Shock Analysis code (USA). This is where the actual shock simulation is conducted. The node output data generated by LS-DYNA was transferred to Ceetron's GLview for post-processing. Finally, UERD Tools was used to compare the measured ship shock trial data with the shock simulation response results. A more detailed explanation of the NPS modeling and simulation process follows.

1. Pre-Processing

After receiving the finite element model it was translated into LS-DYNA keyword format. A corresponding fluid mesh for each shot's model was built in TrueGrid. The industry standard LS-DYNA software, which is commonly used to analyze the dynamic response of large structures, including those coupled to fluids was chosen as a primary means in which to perform the simulations. It is a non-linear three-dimensional analysis code that performs the time integration for the structure.

2. Underwater Shock Analysis Code

The USA code [Ref. 14] was used to calculate the transient response of the ship's wetted-surface structure to an incident shock wave. USA is a boundary element code that solves the ship's structure interaction equations using the DAA formulation given in Equation 14. As previously stated, by using the DAA approach, the response is modeled solely in terms of the wetted-surface variables. This eliminates the need for a separate fluid volume. This technique has been shown to work well for a submerged structure,

such as a submarine, but has some difficulty addressing ship shock phenomena close to the air-water interface due to the addition of bulk cavitation associated with the surface ship UNDEX event. To overcome this problem, a finite element model of the surrounding fluid elements was created to properly account for the presence of bulk cavitation within the UNDEX environment so that the calculations could be performed. In recent work completed by Hart [Ref. 20], it was concluded that the surrounding fluid mesh must extend radially outward from the hull to a radius equal to the maximum depth of the lower cavitation boundary. Accordingly, the DAA boundary is truncated at the outer surface of the surrounding fluid mesh [Ref. 9].

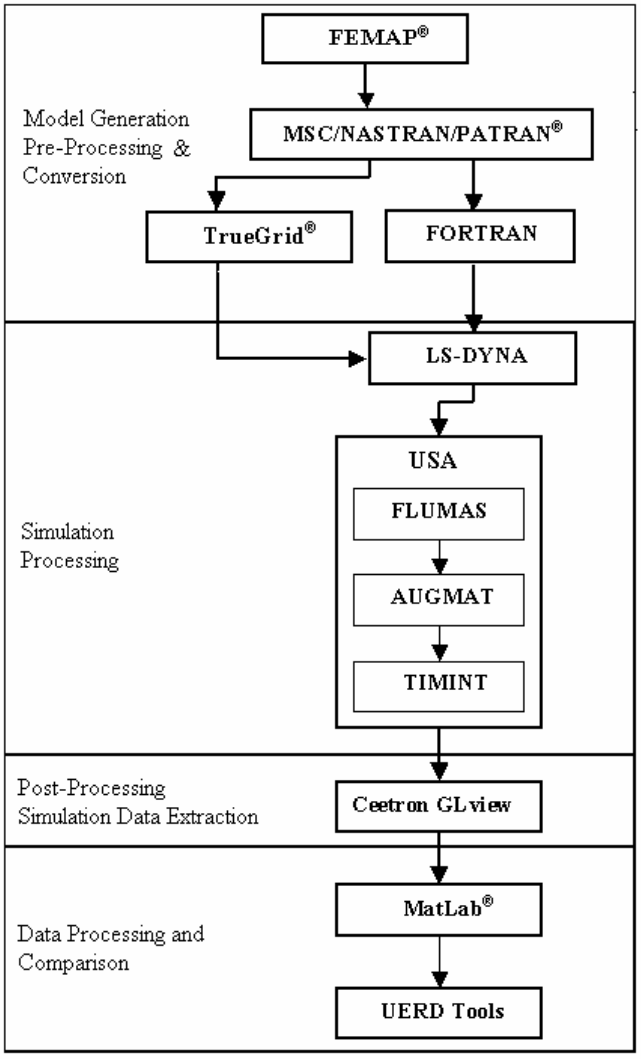

Figure 13. NPS Modeling and Simulation Process Flow Chart [from Ref. 8]

The USA code is formed from three parts, a) the Fluid Mass Processor (FLUMAS), b) the Augmented Matrix Processor (AUGMAT), and c) the Time Integration Processor (TIMINT) [Ref. 11].

a. FLUMAS

The FLUMAS processor creates the fluid mass matrix for the ship's wetted-surface structure in an infinite, in viscid and incompressible fluid. Based on user-defines inputs which include: fluid mesh and element definitions, frees surface location, working medium fluid properties and atmospheric properties, the FLUMAS processor calculates the number of independent coordinates required to define the hull's structural and fluid degrees of freedom (DOF) on the wetted-surface [Ref. 17, 22]. In addition, the FLUMAS processor generates the directional cosines for the normal pressure force and the nodal weights for the fluid element pressure forces [Ref. 16, 21].

b. AUGMAT

The AUGMAT processor is where the fluid and structural matrices are linked together. The output from the FLUMAS processor, specifically the symmetric fluid mass matrix, is sent to the AUGMAT processor for use along with the LS/DYNA generated structural mass matrix, to create input matrices for the TIMINT processor. The combination of these matrices within the same file makes for a more efficient manner in which the TIMIT processor is able to access the data [Ref. 22].

c. TIMINT

The final processor in the USA code is the TIMINT processor. It then compiles the output information from the AUGMAT processor and uses this data to execute the direct integration of Equations (17) and (18). These are the structural and fluid interactions, respectively. The TIMINT processor solves the fluid equations whereas the LS-DYNA processor solves the structural equations. Both of these equation sets are solved at every time step by using an unconditionally stable staggered integration scheme. The TIMINT processor output data is saved as a binary history file, (D3THDT),

and as an ASCII file, (NODOUT). Thus, a time history of displacement, velocity and wetted-surface pressure is recorded for those nodes that were previously designated in the LS-DYNA keyword input file. Since the TIMINT processor is the most time intensive in the entire simulation process, response data information is only retained for those nodes that have been chosen based on their correlation to actual sensor locations from the ship shock trials [Ref. 23].

3. Post-Processing

The results obtained from the LS-DYNA and USA codes are then transferred into a graphical post-processing software package for further conversion of the data into a visual representation of the ship shock trial simulation response data. This transformation accomplished in Ceetron's GLview Pro Suite. The GLview output is then exported to the UERD Tools software where velocity time history response plots are generated for comparison of the simulation against the measured ship shock trial data.

a. GLview

Ceetron's GLview Pro Suite is a commercial application that caters to the thee-dimensional visualization and interactive animation of simulations run on large complex Finite Element models. GLview has the ability to directly import binary and ASCII type data files generated by the LS-DYNA/USA processors. Possessing not only the capability of three-dimensional model visualization but also an ability to create time-dependent data plots, GLview Pro's animation software is able to display time-dependent results in both scalar and vector formats for the stresses, strains, displacement, velocities and accelerations within the fluid-structure model [Ref. 24]. Unfortunately, GLview Pro is unable to directly import ship shock trial data for comparison. Thus the ASCII history files for each sensor/node location must be extracted from the LS-DYNA NODOUT file and individually exported to the UERD Tools data analysis and plotting program.

b. UERD

Underwater Explosions Research Department (UERD) is a RTD&E organization within the Naval Surface Warfare Center, Carderock Division. The data analysis program, UERD Tools, is a custom software package designed specifically for the analysis of ship shock trial data. This extremely versatile software contains many features for the manipulation and filtering of raw data as well as the conditioning of imported data of various formats. UERD Tools enables the user to create high quality data plots of shock response. As the final step in the NPS modeling and simulation process, the LS-DYNA/USA simulation data is imported in the ASCII type file format generated in GLview Pro. Prior to comparison of the simulation data against the measured sensor data the time steps of all response frequency curves are normalized and scaled to ensure proper fit of dimensional units. Lastly, the actual data analysis/correlation is conducted using built-in analysis tools within the UERD Tools program.

IV. DATA COLLECTION AND ANALYSIS

The methods described within this section were used in the data processing and error correlation of all of the sensor and simulation considered in the series of studies presented in this paper.

A. SHOCK RESPONSE DATA PROCESSING

In order to properly compare the simulation data and the measured data each set must be analyzed for anomalies and inherent errors embedded within the data. High frequency "noise" and low frequency "drift" are two such factors. They must first be minimized by established methods so that their influence does not skew the data comparison.

1. High Frequency "Noise"

The sensors used in the measurement and recording of actual ship shock trial data not only collect the desired frequency response but also gather unwanted high frequency "noise". These additional frequencies, which are well beyond the interest range for UNDEX events, tend to clutter the data. The unfiltered data, shown in red in Figure 14 has a less defined frequency curve as compared to the low-pass filtered data, in blue, for the same sensor. The time history plot for this velocity meter, V2010V was taken from the Shot 2 data set. By using the low-pass filtering technique, all of the frequencies greater than 250 Hz were removed, leaving a much cleaner plot.

The aforementioned process of noise reduction has been an accepted practice for some time, however it has only recently been postulated that the same procedure should be applied to the simulated data as well. A statistical study based on 233 accelerometer measurements indicated that the simulation data, when low-pass filtered at 250Hz, correlated much better with the low-pass filtered raw data for the same sensor [Ref. 8]. Table 2 shows a summary of the statistical results of this study. Consequently, all response data comparisons in this study were low pass filtered at 250 Hz.

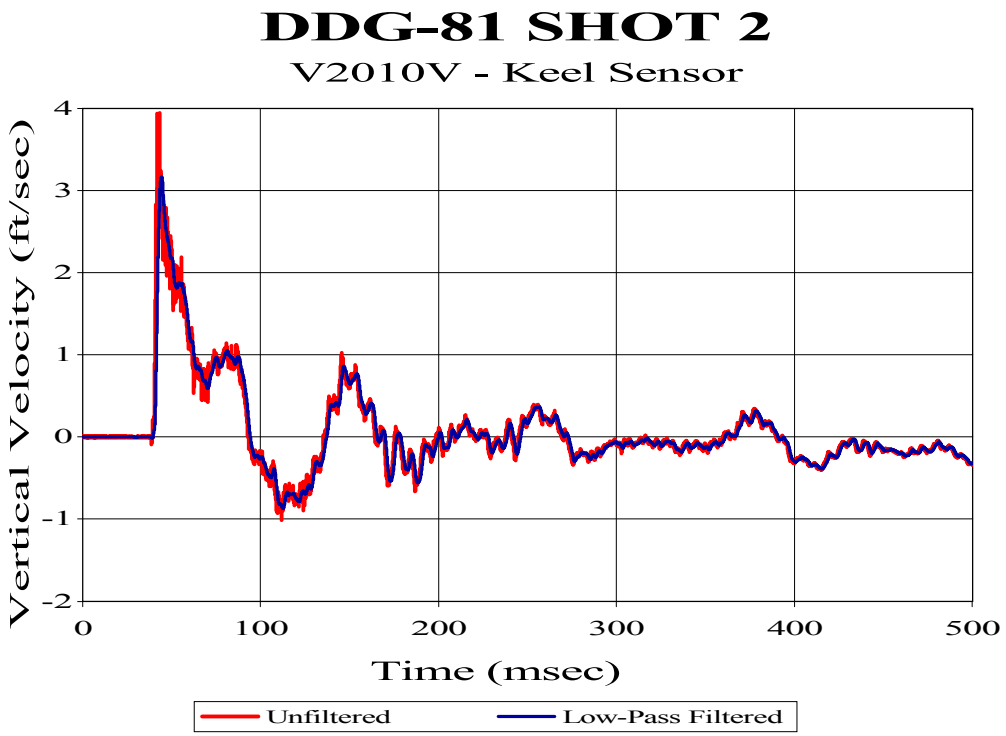

Figure 14. Comparison of Unfiltered and Low-Pass Filtered Sensor Data

Table 2. Summary of Filtered and Unfiltered Simulation Data [from Ref. 8]

	Shock Trial Data (Filtered)	Simulation Data (Unfiltered)	Simulation Data (Filtered)
Mean	26.225	82.985	34.297
Variance	520.229	5775.711	606.426
Standard Deviation	22.809	75.998	24.626

2. Velocity Response "Drift"

For the analysis conducted in this work, two types of sensor data were used, namely that collected from accelerometers and velocity meters. Though they were designed to capture the transient response motion of the system, these sensors are routinely used to gather data for up to 2500 msec during an UNDEX event. Consequently, the sensors acquire a larger range of frequencies than are desired. Velocity meters require seismic correction, an integration process, to correct their error. The drift associated with data taken from accelerometers is a result of the integration process that transforms it into velocity response data.

The time response history for sensor A4100V data shown in Figure 15 was taken from the Shot 2 data set. A gradual trailing off of the sensor's time history data is seen after the first 250 msec. This trend away from the zero equilibrium point is the drift in the sensor data.

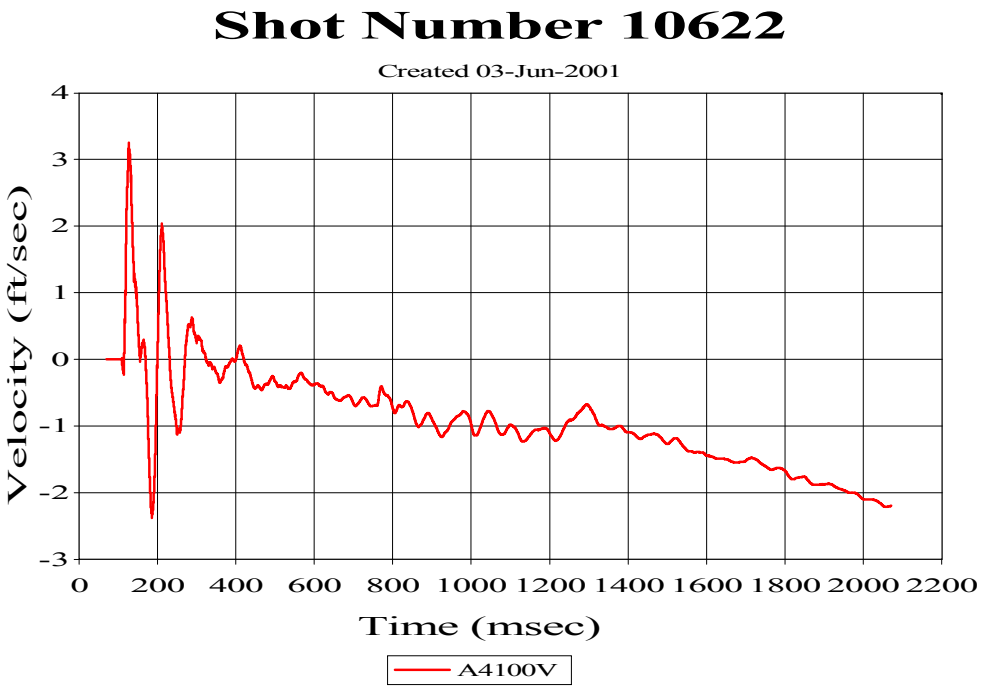

Figure 15. Accelerometer Output Data Prior to Drift Compensation being Applied

There have been numerous studies conducted concerning the problem of sensor drift. In this study, the built-in "Drift Compensation" function within UERD Tools was chosen as a means to eliminate the drift present in the measured accelerometer data. Though this technique does not always produce a time response history entirely free from drift, it maintains the magnitude of the response and does not introduce a phase shift. It follows a set algorithm as opposed to some other curve fitting processes that require the skill and judgment of the user to identify the point where the drift is introduced into the record.

Figure 16 shows an example of velocity response data acquired from same accelerometer A4100V after it has been integrated and modified using the UERD Tools Drift Compensation function.

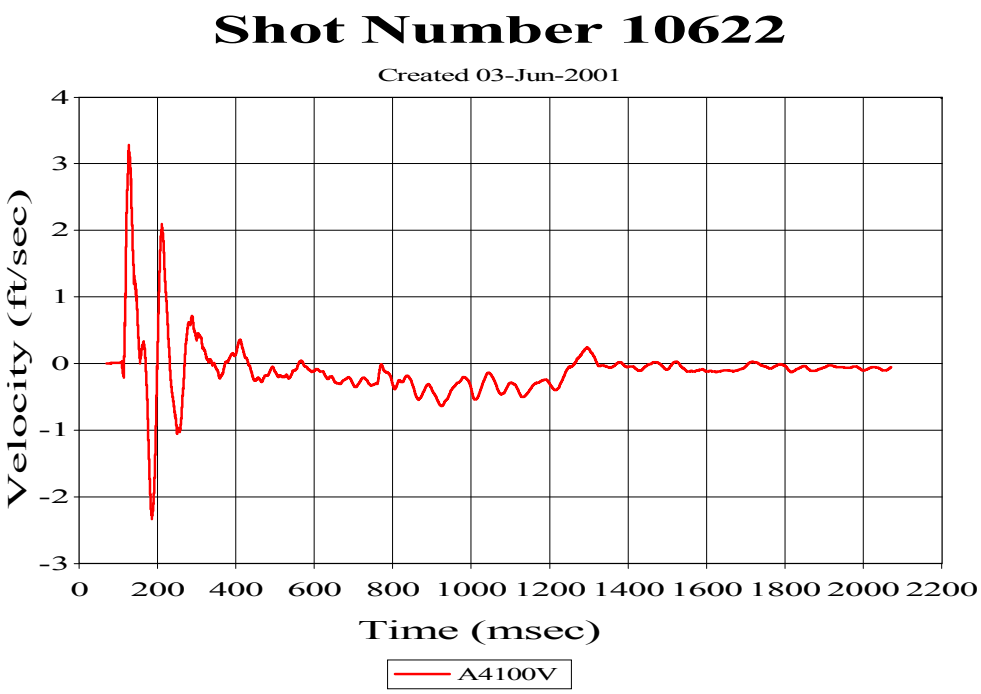

Figure 16. Accelerometer Output Data After Drift Compensation has been Applied

Table 3 provides results from a study comparing the vertical velocity response data taken from accelerometers versus that obtained from velocity meters. Overall, there was a much better correlation between the simulated data and the measured data when using the accelerometer data. In order to minimize error introduced into the data by physical drift of the velocity meters, accelerometer data was used whenever possible.

Table 3. Average Comprehensive Russell's Error Factor [from Ref. 8]

SENSOR TYPE	Average Comprehensive Russel's Error Factor			
	SHOT 1	SHOT 2	SHOT 3	OVERALL
ACCELEROMETER	0.1845	0.1434	0.1910	0.1730
VELOCITY METER	0.2269	0.2196	0.2315	0.2260

B. DATA ANALYSIS AND COMPARISON

1. Sensor and Node Location

There were approximately 620 sensors installed in USS WINSTON S. CHURCHILL during the summer of 2001 ship shock trials conducted at sea approximately 100 nautical miles off the coast of Mayport, Florida. Strain gauges, velocity meters and accelerometers were installed in DDG-81 to capture the time history response data during each of the three UNDEX events. Figures 17 and 18 show the locations where the vertical, athwartship and longitudinal sensors. In order to facilitate sensor correlation during the analysis, specific nodes corresponding to sensor installations were built into the structural model in many instances. If a sensor location did not exactly correspond to a node, the closet node was found from the finite element model. The selected nodes were then designated in the LS-DYNA input deck as nodes for which to retain time history response data for comparison.

Typically the vertical velocity response is analyzed for an UNDEX event, since it is the principal response direction. Accordingly, for the analysis of the Combat Information Center (CIC) area, the vertical velocities were chosen for comparison. However, in the second part of the analysis that is presented, the athwartship velocities were compared to investigate whether or not the athwartship simulations were accurate.

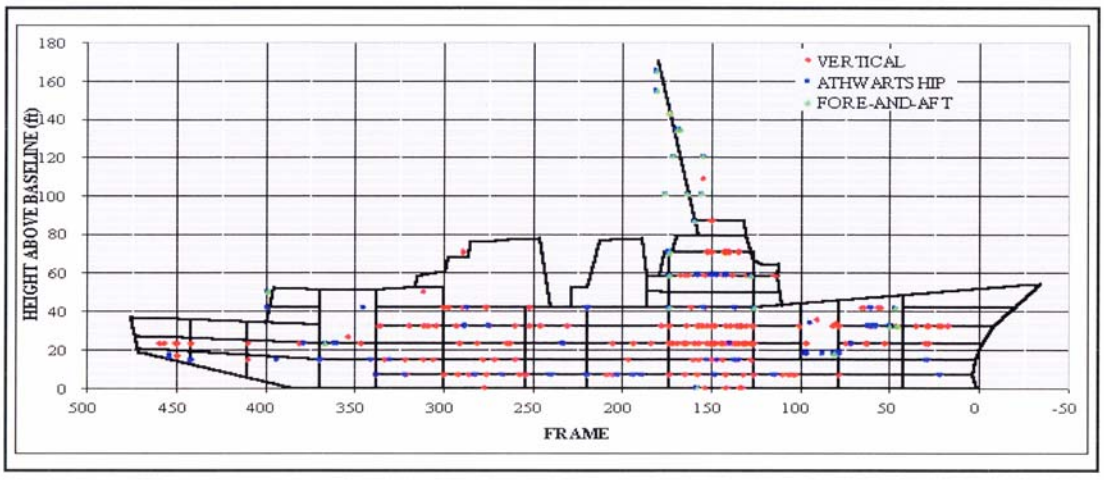

Figure 17. Sensor Locations Depicted in Profile View of DDG-81 [from Ref. 19]

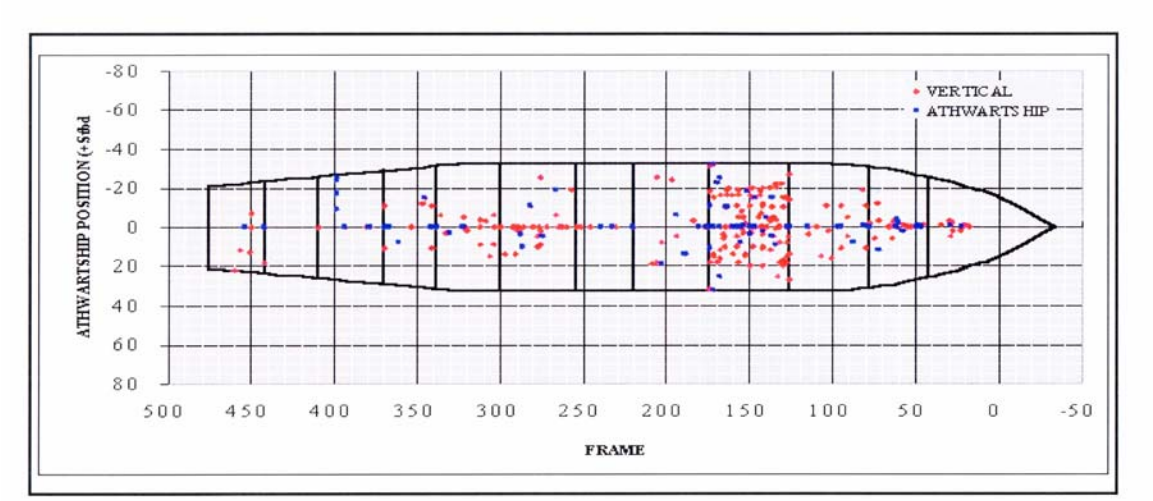

Figure 18. Sensor Locations Depicted in Top View of DDG-81 [from Ref. 19]

2. Error Measurements

Though always somewhat subjective, there must exist away to quantify how well two data sets correlate to one another. As has been the case in previous studies concerning the simulation of the DDG-81 shock trials, this paper shall also use Russell's error factor [Ref. 25, 26] as an unbiased measure of error between the simulated data and the measured data.

In order to calculate the Russell's error, first, two variables are defined as,

$$A = \sum_{i=1}^{N} f_1(i)^2 \tag{27}$$

and

$$B = \sum_{i=1}^{N} f_2(i)^2 \tag{28}$$

where $f_1(i)$ and $f_2(i)$ are the measured and predicted response magnitudes at each time step, which is denoted as i. Using the variables A and B from Equations (27) and (28), the relative magnitude error of the correlation is,

$$m = \frac{(A - B)}{\sqrt{AB}} \tag{29}$$

From Equation (29) the magnitude error is calculated as,

$$RM = \mathrm{s}ign(m)\log_{10}(1 + |m|) \tag{30}$$

The phase error is found as follows,

$$p = \hat{\phi}_1 \bullet \hat{\phi}_2 \tag{31}$$

where $\hat{\phi}$ is the normalized unit vector of the transient response. The phase correlation between the two data sets can be computed as,

$$p = \frac{C}{\sqrt{AB}} \tag{32}$$

where C is defined by,

$$C = \sum_{i=1}^{N} f_1(i) f_2(i) \tag{33}$$

The phase error is calculated as,

$$RP = \frac{\cos^{-1}(p)}{\pi} \tag{34}$$

Equations (30) and (34) are used in conjunction with Equation (35) to determine the comprehensive error.

$$RC = \sqrt{\frac{\pi}{4}(RM^2 + RP^2)} \tag{35}$$

Now that the correlation has been defined in terms of a comprehensive error factor, a range must be set, delineating what will be deemed an acceptable span of error values. Though there is no definitive number that characterizes a "satisfactory" correlation between the data sets, the values listed in Table 4 have been used as the acceptance criteria in both the earlier DDG-53 and current DDG-81 ship shock trial simulation projects [Ref. 27].

Table 4. Russell's Comprehensive Error Factor Acceptance Criteria

RC < 0.15	EXCELLENT
0.15 ≤ RC ≤ 0.28	ACCEPTABLE
RC > 0.28	POOR

Figure 19 is a plot of the data set that was used in determining the criteria presented in Table 4. Notice that in some cases a comparison with a RC = 0.25 or 0.26 was considered poor while conversely some plots having correlations as high as 0.33 or 0.34 were given an acceptable rating.

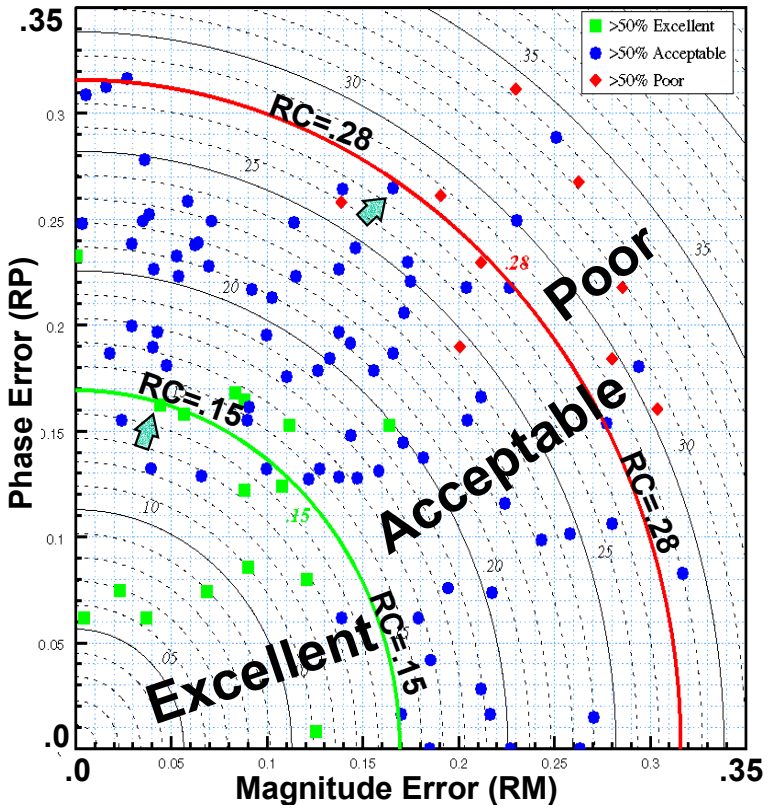

Figure 19. Russell's Error Criteria Determination Data [from Ref. 25]

The criteria established in Table 4 were suggested to be a valid measure of acceptance based on comparison of 500 msec in length using fully conditioned velocity response data comparisons. The data used in these comparisons was subjected to drift correction and low-pass filtering at 250 Hz as previously described. The acceptance criteria from Table 4 were determined to be valid for only the aforementioned data processing method.

THIS PAGE INTENTIONALLY LEFT BLANK

V. SIMULATION RESULTS

During the DDG-81 ship shock trials a total of three underwater explosions or "shots" took place. All three of these shots have been simulated using the NPS modeling and simulation process. The primary focus of this thesis is to further validate the DDG-81 simulation process developed at NPS by investigating the shipwide athwartship velocity response and the localized vertical velocity response in the Combat Information Center area. Additionally, the effects of using a new set of proportional damping coefficients will be studied and compared with those used in the DDG-53 simulation effort conducted at the NPS.

A. CIC AREA VERTICAL VELOCITY RESPONSE DATA

The Combat Information Center (CIC) is one of the focal points in ship's operational life. The main objective of the CIC personnel is to ensure combat readiness by acting as a central hub for the gathering, processing, and dissemination of all Command and Control, Communications, Computers and Intelligence (C4I) data and information throughout the ship. With all of its electronic equipment, communications devices and weapons systems consoles, determining the motion response values for CIC was a NAVSEA priority during the DDG-81 ship shock trials program [Ref. 19]. The addition of upgraded consoles such as the AN/UYQ-70(V) Advanced Display System and the physical rearrangement of the CIC layout helped spur the effort to quantify the response that the equipment and watchstanders would be subjected to during an UNDEX event. Figure 20 displays the layout of the CIC as modeled and the location of select sensors within the compartment. Figure 21 shows the location of CIC with respect to the ship's profile.

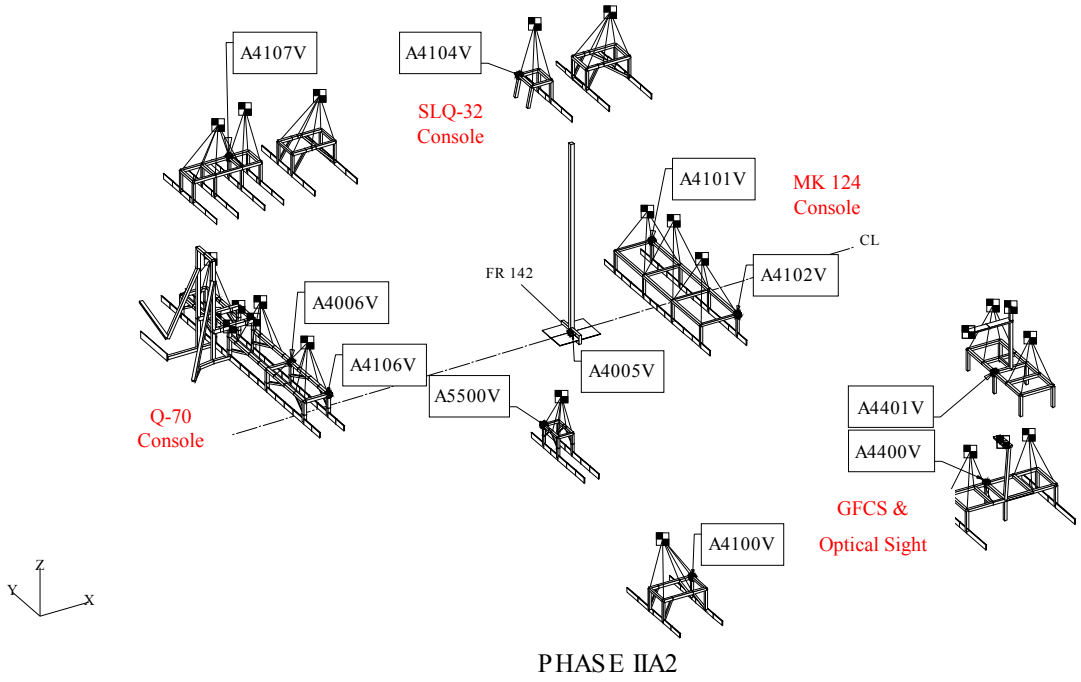

Figure 20. DDG-81 CIC Console and Sensor Locations [from Ref. 18]

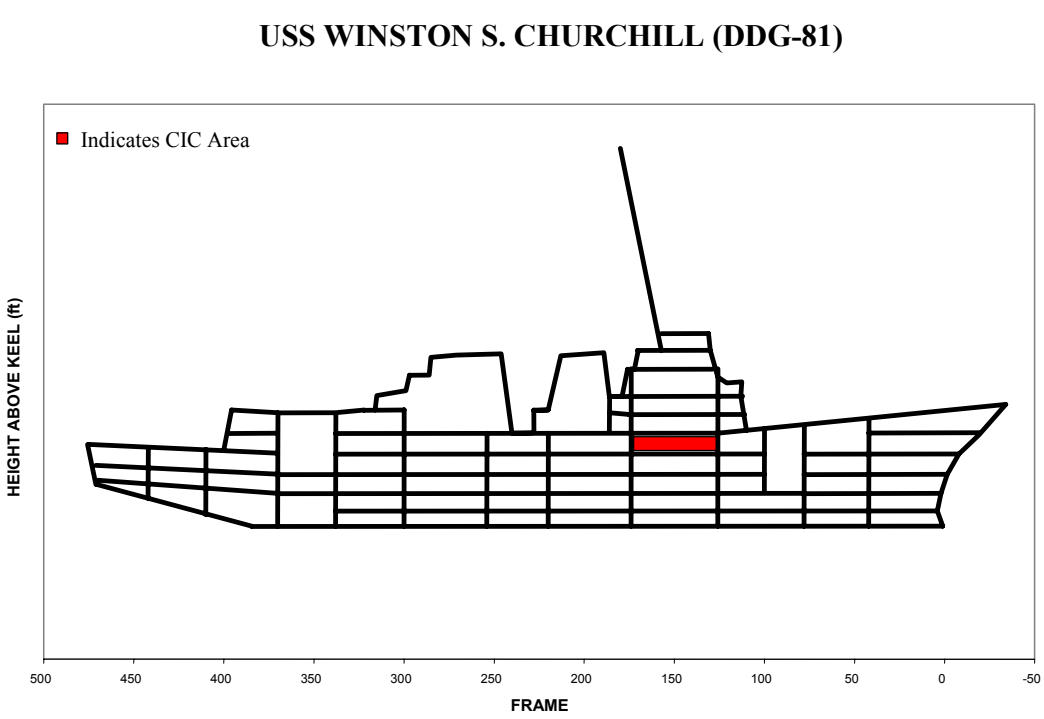

Figure 21. Location of Combat Information Center [after Ref. 27]

Vertical velocity comparisons of the simulated response data and the ship shock trial data were made for all three of the shots. Table 5 lists the sensor types and locations of those that were evaluated in this series of comparisons. All sensors analyzed in this section were deck mounted.

Table 5. CIC Vertical Velocity Response Sensor Locations

Sensor	Compartment	Grid ID	X (inches)	Y(inches)	Z(inches)	General Location Description
A4005V	CIC	212054	3888	0	390	BASE OF CENTER COMPARTMENT STANTION
A4025V	CIC	212075	3744	54	390	FOUNDATION OF AAWC CONSOLE
A4100V	CIC	211924	3888	-270	390	BTWN GFCS & OPTICAL SIGHT CONSOLES
A4101V	CIC	212068	3936	27	390	MK 124 CONSOLE BASE
A4102V	CIC	212042	3936	-27	390	UNDER MK 124 CONSOLE
A4104V	CIC	212156	3984	216	390	FOUNDATION OF OJ-446C/SLQ-32(V)
A4106V	CIC	212025	3744	-54	390	FOUNDATION OF Q-70 CONSOLE
A4108V	CIC	212153	3840	216	390	BTWN RSC & TIC CONSOLES
A4109V	CIC	211924	3888	-270	390	BTWN SWS & ASUWC CONSOLES
A4110V	CIC	211973	3744	-162	390	FOUNDATION OF ASWCSO CONSOLE
A4111V	CIC	212155	3936	216	390	FOUNDATION OF Q70 CONSOLE
A4408V	CIC	211979	4032	-162	390	BTWN FOUNDATION OF LC01 & LC02 CONSOLE
A4409V	CIC	211926	3984	-270	390	FOUNDATION OF ATDC-1
A5503V	CIC	211974	3792	-162	390	AT L6S, CENTER OF FOUNDATION
A2104V	CIC ANNEX	222240	3504	0	390	AT BULKHEAD 174 CENTELINE
A2101V	CIC PROJECTION RM	212058	4080	0	390	AT BULKHEAD 126 CENTERLINE
A4105V	CIC PROJECTION RM	212031	4032	-54	390	FOUNDATION OF CLSD
A2102A	CIC PROJECTION RM	212058	4080	0	390	AT BULKHEAD 126 CENTERLINE
A2105AI	CIC ANNEX	222240	3504	0	390	AT BULKHEAD 174 CENTELINE
A2106F	CIC ANNEX	222240	3504	0	390	AT BULKHEAD 174 CENTELINE
A2103F	CIC PROJECTION RM	212058	4080	0	390	AT BULKHEAD 126 CENTERLINE

While the true magnitudes of the simulation data comparison contained both positive and negative values, indicating simulated responses that were both smaller and larger than the measured magnitudes of the sensor response data, for ease of plotting, all magnitudes errors are plotted as their absolute value. The true calculated magnitudes are found in the corresponding data tables for each set of plots. Figure 22 is a plot of the complete data set for all three shots used in the CIC area analysis.

In all but a few exceptions, the vertical velocity response values fall into the excellent or acceptable range. Even those falling outside the acceptable region are just barely greater than the 0.28 cut-off value, and do not necessarily constitute an undesirable correlation. The magnitude error is consistently low throughout the data set, while it is the relationship of the phase that inevitably drives the overall comprehensive error higher in most cases.

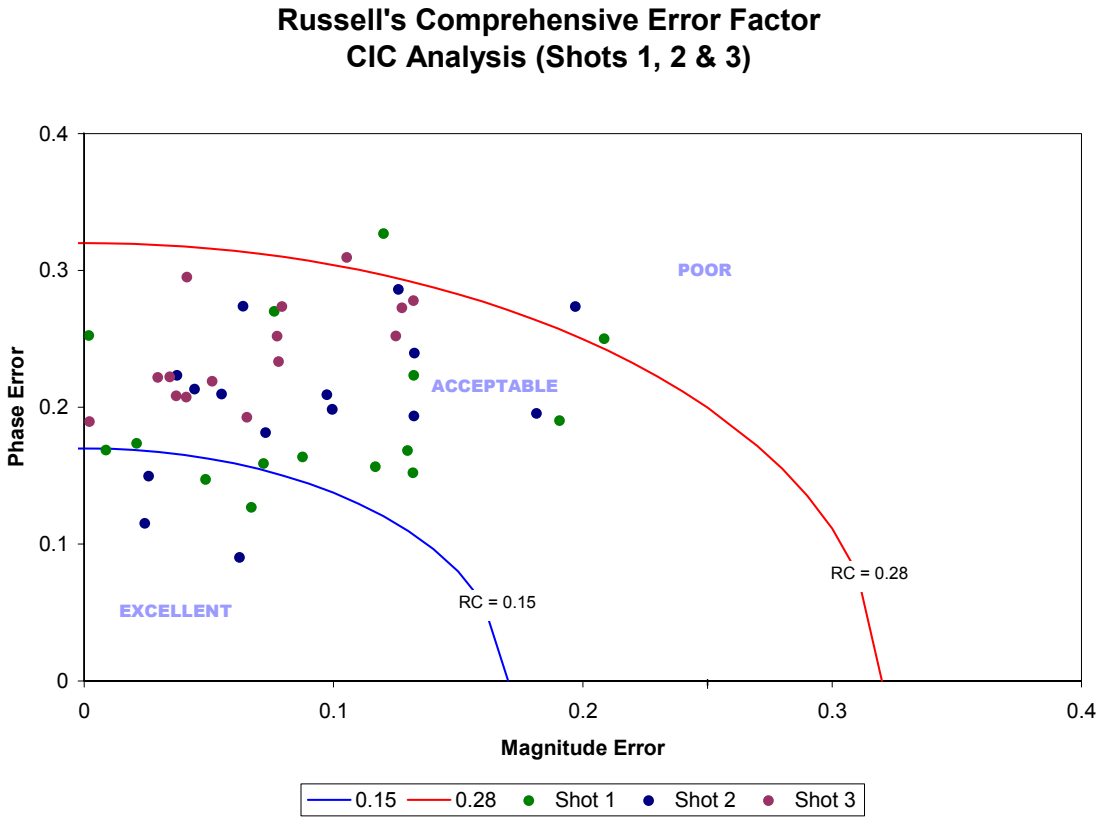

Figure 22. Russell's Comprehensive Error Factor for CIC

1. Shot 1

Shot 1 was located furthest from the ship, making it the least severe. This shot was detonated forward of the port bow, well off of its intended mark, which was abeam the port side of the ship. Consequently it had the most extreme aspect as was shown in Figure 12. Based on previous studies of the DDG-81 ship shock trial simulations it was surmised that this asymmetric geometry would not negatively impact the course of the current study.

a. Error Comparison

Using a fluid mesh model that extended down to the cavitation depth of 75 ft, an average Russell's Comprehensive error factor was previously found to be 0.2162 during the shipwide vertical sensor analysis of Shot 1 [Ref. 8]. In comparison the mean

value of the localized CIC area analysis for shot 1 was only 0.1978. This improvement in Russell's Comprehensive error factor was anticipated since a general trend of improvement as the z-direction coordinate of the sensor location increases with respect to the ship's keel, or baseline was previously discovered [Ref. 8]. Figure 23 shows a graphical representation of the Russell's Comprehensive error factor while Table 6 provides the supporting data.

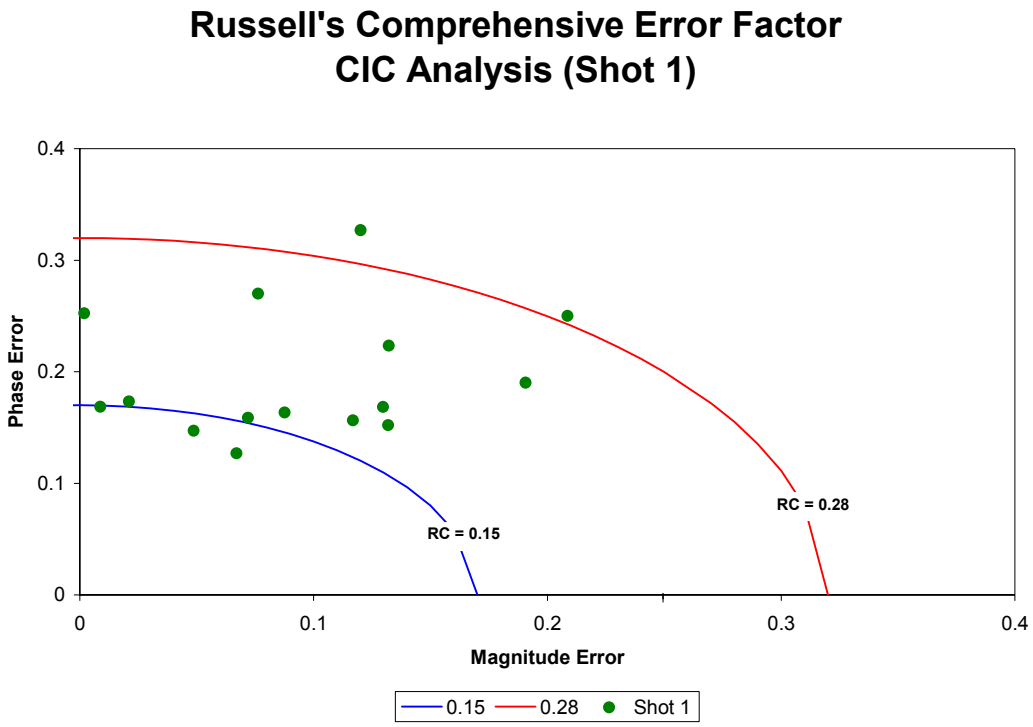

Figure 23. Russell's Error Factor for CIC (Shot 1)

Table 6. Russell's Error Factors for CIC (Shot 1)

Simulation runtime = 500 msec						SHOT 1		
Sensor	NODE	Mounting Type	Location (in)*			738in Cavitation - Medium		
						SHIP SHOCK TRIAL DATA (<250HZ)		
						LS-DYNA/USA DATA (<250HZ)		
			x	y	z	RM	RP	RC
A4005V	212054	Deck	3888	0	390	0.0876	0.1637	0.1645
A4025V	212075	Deck	3744	54	390	-0.1318	0.1522	0.1784
A4100V	211924	Deck	3888	-270	390	-0.1168	0.1566	0.1732
A4101V	212068	Deck	3936	27	390	0.0087	0.1687	0.1497
A4102V	212042	Deck	3936	-27	390	0.1321	0.2234	0.2300
A4104V	212156	Deck	3984	216	390	-0.0018	0.2525	0.2238
A4106V	212025	Deck	3744	-54	390	-0.1906	0.1903	0.2387
A4108V	212153	Deck	3840	216	390	0.1201	0.3270	0.3087
A4109V	211924	Deck	3888	-270	390	-0.1297	0.1685	0.1885
A4110V	211973	Deck	3744	-162	390	0.0487	0.1472	0.1374
A4111V	212155	Deck	3936	216	390	-0.0762	0.2701	0.2487
A4408V	211979	Deck	4032	-162	390	0.2086	0.2501	0.2886
A4409V	211926	Deck	3984	-270	390	0.0719	0.1589	0.1545
A2104V	222240	Deck	3504	0	390	-0.0670	0.1270	0.1272
A2101V	212058	Deck	4080	0	390	0.0210	0.1736	0.1551
Russell Error Correlation					Sum(E(X))	-0.01520	2.92980	2.96700
	> 0.28	Poor			Sum(E(X^2))	0.18558	0.61683	0.63021
	< 0.15	Excellent			**Mean**	**-0.00101**	**0.19532**	**0.19780**
					Standard Deviation	0.11513	0.05643	0.05564

* Referenced to the G&C NASTRAN Model with coordinate origin located at the stern.

b. Velocity Plot

The following plots are of the vertical velocity comparison conducted between the measured ship shock trial data and the simulation data at typical sensor locations and their corresponding nodes. Figure 24 shows the time history response of the aft CIC bulkhead which had one of the best overall correlation factors with an RC = 0.1272 while Figure 25 shows the time history response of a sensor, A4108V, with one of the poorest correlations with an RC = 0.3087. Even so, this correlation value is just beyond the acceptable range, but still well within one standard deviation of the mean.

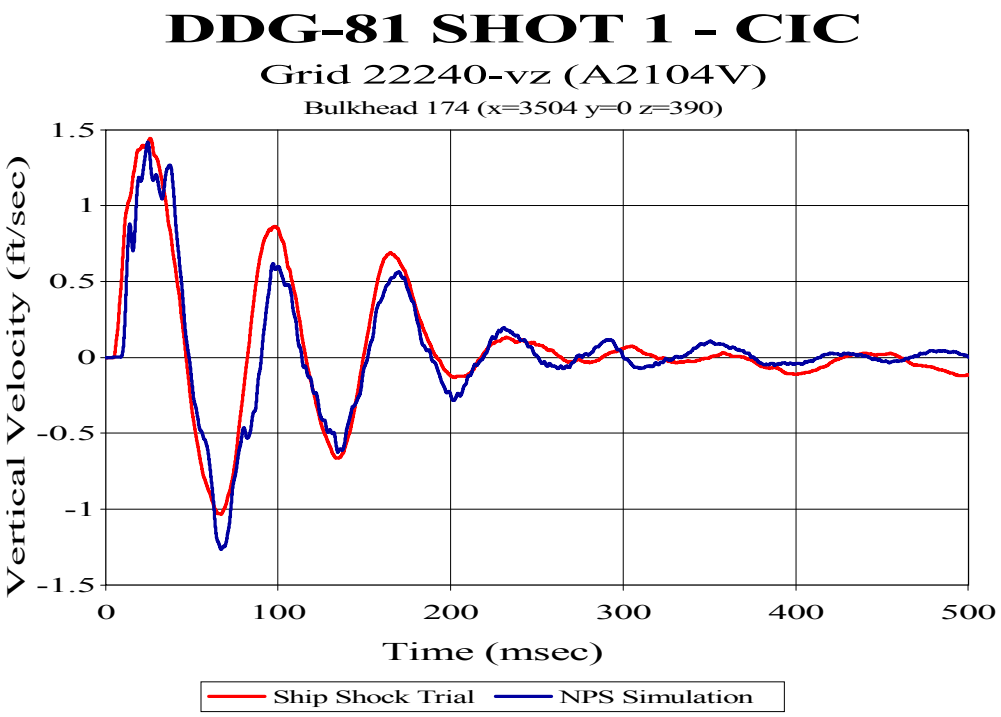

Figure 24. Deck Sensor A2104V

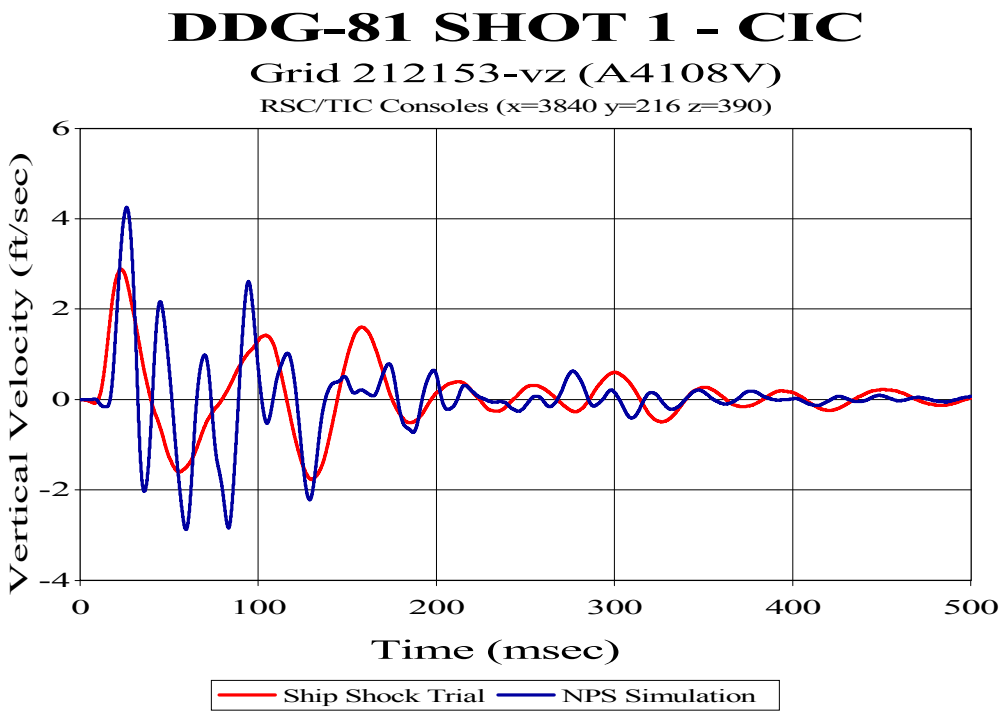

Figure 25. Deck Sensor A4108V

2. Shot 2

As shown in Figure 12, Shot 2 was detonated directly abeam the starboard side of DDG-81 during the ship shock trials. The charge severity was the intermediary value of the three shots, with its standoff distance lying nearer the ship than it had in Shot 1.

a. Error Comparison

In the shipwide comparison of vertical velocity response for Shot 2 the mean Russell's Comprehensive error factor was determined to be 0.1912 [Ref. 8]. The mean value of the localized CIC area analysis for Shot 2 was found to be 0.2006. In this case the results are comparable with those obtained from the shipwide analysis. Figure 26 is a graphical representation of the Russell's Comprehensive error factor for Shot 2.

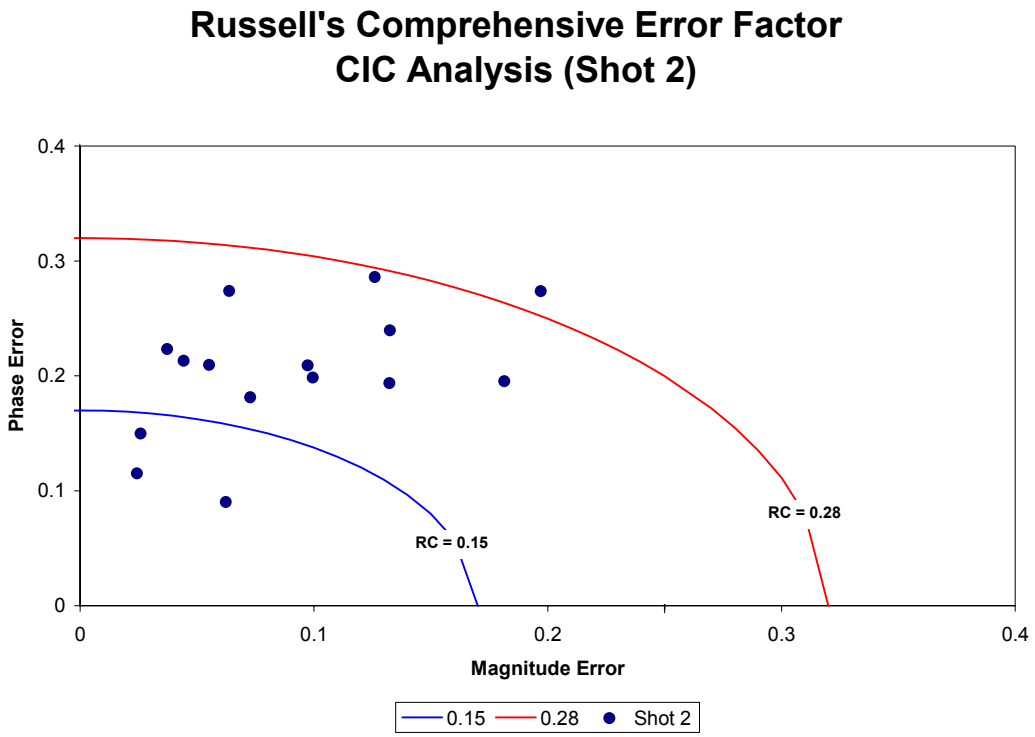

Figure 26. Russell's Error Factor for CIC (Shot 2)

Contrary to the slight increase in overall RC value, the data distribution throughout the shot has a better accuracy and precision associated with it. Three of the

sensors evaluated fall in the excellent range and only one in the poor correlation category. Figure 27 of sensor A2104V, which had the best correlation at RC = 0.0972, shows the similitude of both curves in magnitude as well as in phase. The error in magnitude and phase are, RM = 0.0623, RP = 0.0902, respectively. Further analysis conducted for a 200 msec time history response found that the comprehensive effort factor fell to a value of RC = 0.0799. Table 7 provides a complete description of the error factors for Shot 2.

Table 7. Russell's Error Factors for CIC (Shot 2)

Simulation runtime = 500 msec						SHOT 2		
Sensor	NODE	Mounting Type	Location (in)*			738in Cavitation - Medium		
						SHIP SHOCK TRIAL DATA (<250HZ)		
						LS-DYNA/USA DATA (<250HZ)		
			x	y	z	RM	RP	RC
A4005V	212054	Deck	3888	0	390	0.0727	0.1815	0.1733
A4025V	212075	Deck	3744	54	390	-0.0243	0.1152	0.1044
A4100V	211924	Deck	3888	-270	390	-0.1322	0.1937	0.2079
A4101V	212068	Deck	3936	27	390	0.0995	0.1985	0.1968
A4102V	212042	Deck	3936	-27	390	0.0372	0.2234	0.2007
A4104V	212156	Deck	3984	216	390	-0.0637	0.2739	0.2492
A4106V	212025	Deck	3744	-54	390	-0.0973	0.2091	0.2044
A4108V	212153	Deck	3840	216	390	-0.1260	0.2862	0.2771
A4109V	211924	Deck	3888	-270	390	-0.1814	0.1955	0.2364
A4110V	211973	Deck	3744	-162	390	0.0442	0.2132	0.1930
A4111V	212155	Deck	3936	216	390	-0.1970	0.2737	0.2988
A4408V	211979	Deck	4032	-162	390	0.1324	0.2397	0.2434
A4409V	211926	Deck	3984	-270	390	-0.0551	0.2097	0.1921
A2104V	222240	Deck	3504	0	390	-0.0623	0.0902	0.0972
A2101V	212058	Deck	4080	0	390	0.0258	0.1498	0.1347
Russell Error Correlation					Sum(E(X))	-0.52750	3.05330	3.00940
	> 0.28	Poor			Sum(E(X^2))	0.16282	0.66429	0.64998
	< 0.15	Excellent			**Mean**	**-0.03517**	**0.20355**	**0.20063**
					Standard Deviation	0.10151	0.05528	0.05746

* Referenced to the G&C NASTRAN Model with coordinate origin located at the stern.

b. Velocity Plots

Figures 27 and 28 are representative of the result obtained from the Shot 2 analysis of the vertical velocity response in CIC and are provided as a sample of the complete set of time history response plot found in APPENDIX B. The Russell's Comprehensive error factors for sensors A2104V and A4025V are, RC = 0.0972 and RC = 0.1044, respectively.

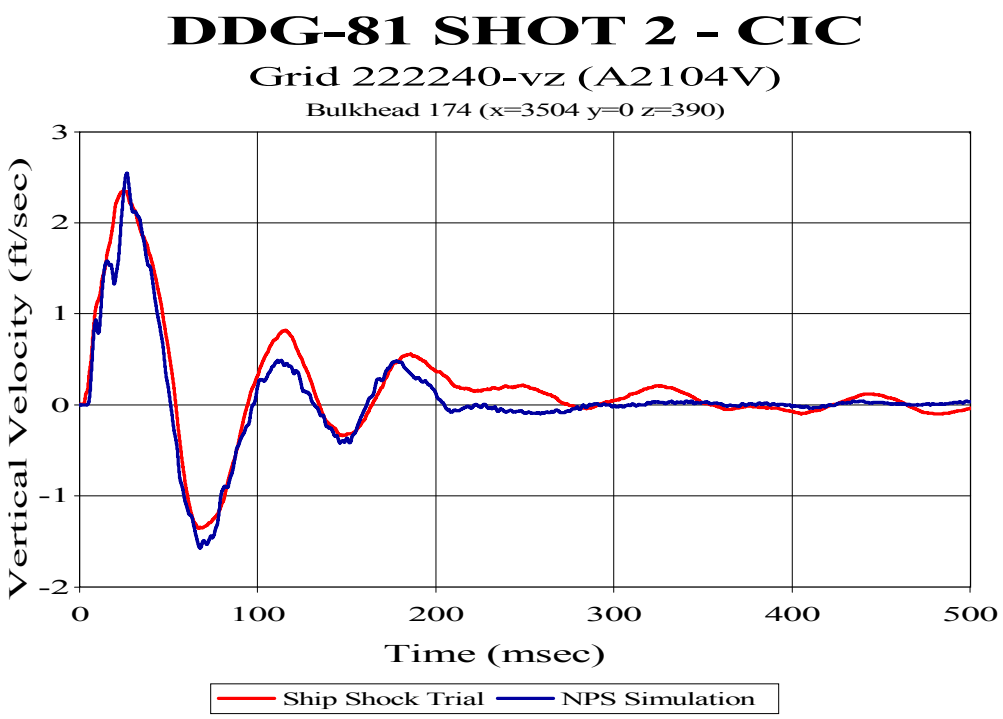

Figure 27. Deck Sensor A2104V

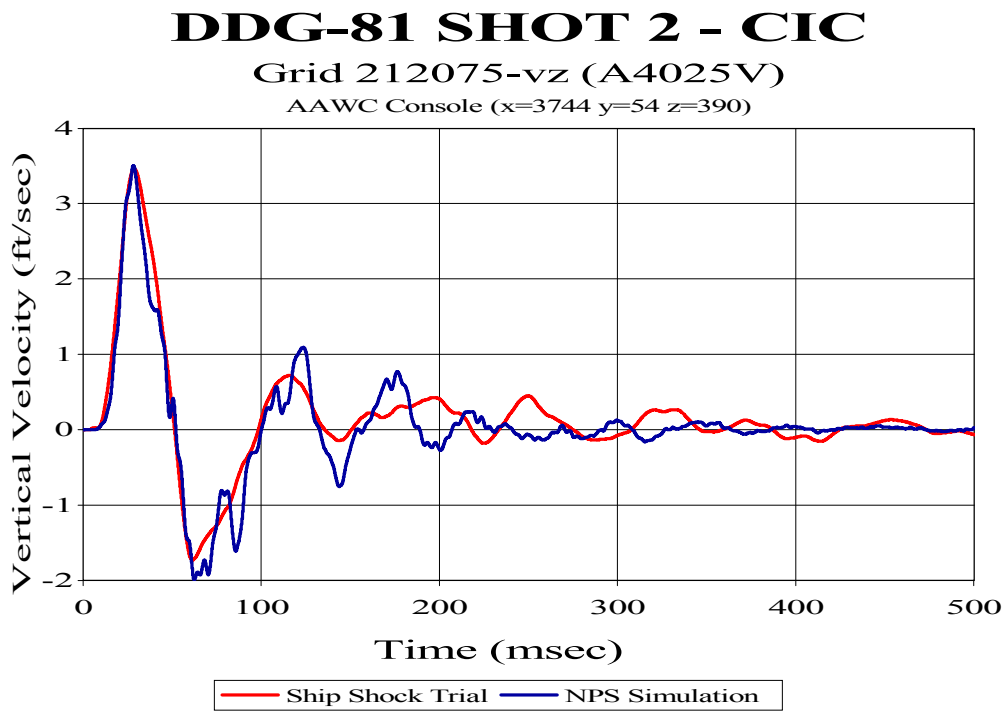

Figure 28. Deck Sensor A4025V

3. Shot 3

Shot 3 was the most severe of the three shots conducted during the DDG-81 ship shock trials. During this UNDEX event the charge was detonated at the closest point to the ship in order to create a two-thirds design level blast. The charge was located almost exactly amidships along the port beam, as shown in Figure 12.

a. Error Comparison

In the shipwide comparison of vertical velocity response for Shot 3 the mean Russell's Comprehensive error factor was determined to be 0.2114 [Ref. 8]. Once again the CIC area specific mean value was comparable but just slightly higher, with a Russell's Comprehensive error factor of 0.2238. In the case of Shot 3, there were no excellent correlations however, as shown in Figure 29, the data falls in a much more accurate manner. All but one sensor was deemed to have acceptable correlation with respect to the acceptance criteria, with sensor A4108V possessing a marginal value of RC = 0.2897 as the sole poor correlation.

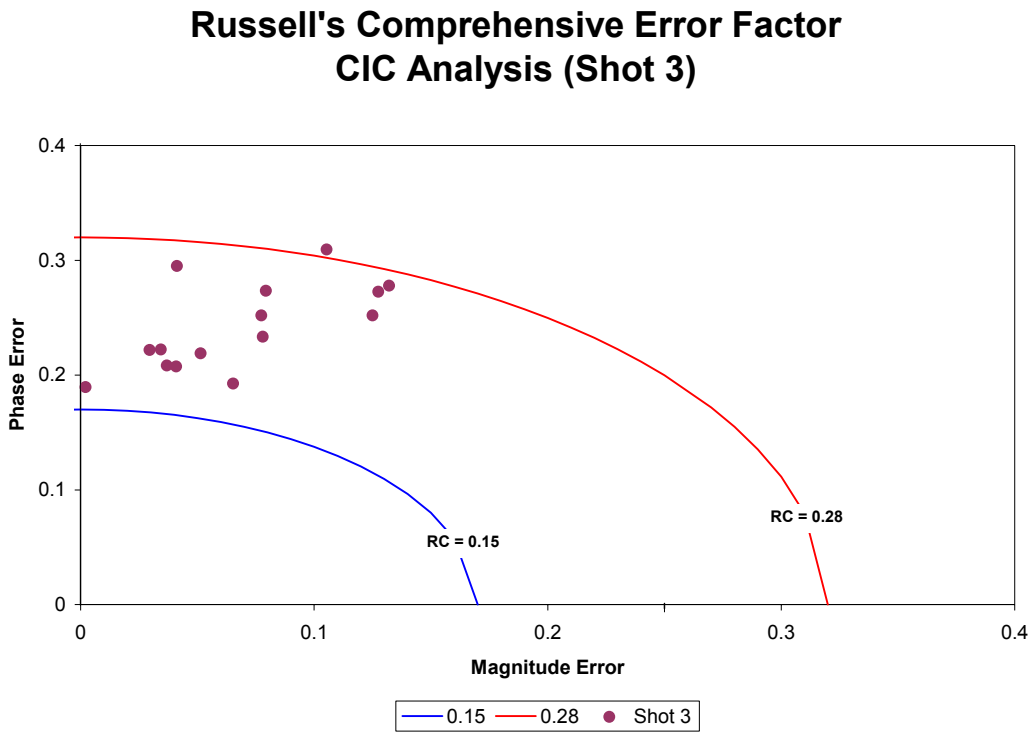

Figure 29. Russell's Error Factor for CIC (Shot 3)

Nevertheless, all of the results for Shot 3 are tightly clustered in the acceptable range (with the exception of sensor A4108V) nearer the ordinate, indicating a minimal deviation in magnitude error. The greatest error in magnitude correlation was a RM = 0.1320 for sensor A2104V. Based on the summary of Russell's error factors presented in Table 8, almost 80% of the sensors have a RM $\leq$ 0.10.

Table 8. Russell's Error Factors for CIC (Shot 3)

Simulation runtime = 500 msec						SHOT 3		
Sensor	NODE	Mounting Type	Location (in)*			738in Cavitation - Coarse		
						SHIP SHOCK TRIAL DATA (<250HZ)		
						LS-DYNA/USA DATA (<250HZ)		
			x	y	z	RM	RP	RC
A4005V	212054	Deck	3888	0	390	0.1250	0.2521	0.2494
A4025V	212075	Deck	3744	54	390	0.0369	0.2084	0.1876
A4100V	211924	Deck	3888	-270	390	-0.0513	0.2190	0.1994
A4101V	212068	Deck	3936	27	390	0.0773	0.2520	0.2336
A4102V	212042	Deck	3936	-27	390	0.1320	0.2779	0.2727
A4104V	212156	Deck	3984	216	390	0.0793	0.2736	0.2525
A4106V	212025	Deck	3744	-54	390	-0.0780	0.2334	0.2181
A4108V	212153	Deck	3840	216	390	0.1053	0.3095	0.2897
A4109V	211924	Deck	3888	-270	390	-0.0653	0.1927	0.1803
A4110V	211973	Deck	3744	-162	390	0.0409	0.2075	0.1874
A4111V	212155	Deck	3936	216	390	-0.0412	0.2951	0.2641
A4408V	211979	Deck	4032	-162	390	0.1274	0.2727	0.2667
A4409V	211926	Deck	3984	-270	390	0.0343	0.2223	0.1993
A2104V	222240	Deck	3504	0	390	-0.0020	0.1895	0.1680
A2101V	212058	Deck	4080	0	390	0.0295	0.2219	0.1896
Russell Error Correlation					Sum(E(X))	0.55010	3.62760	3.35840
	> 0.28	Poor			Sum(E(X^2))	0.09239	0.89701	0.77374
	< 0.15	Excellent			**Mean**	**0.03667**	**0.24184**	**0.22389**
					Standard Deviation	0.07182	0.03752	0.03947

* Referenced to the G&C NASTRAN Model with coordinate origin located at the stern.

b. Velocity Plots

Figures 30 and 31 are vertical velocity plots chosen from analysis of Shot 3 CIC sensor locations. The Russell's Comprehensive error factors for sensors A4110V and A4100V are, RC = 0.1874 and RC = 0.1994, respectively.

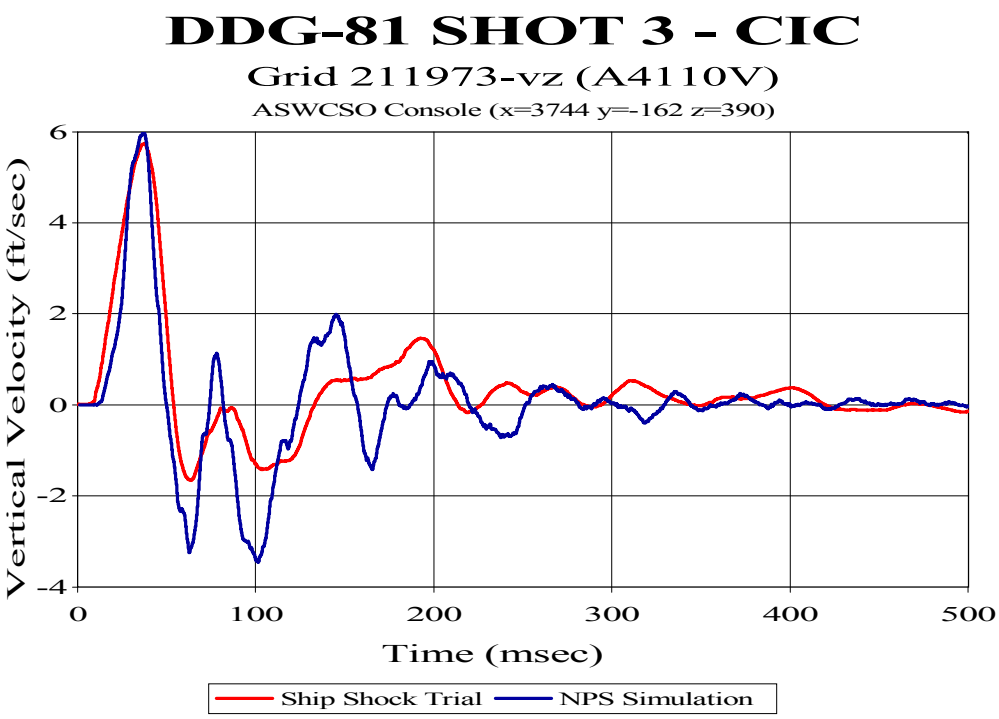

Figure 30. Deck Sensor A4110V

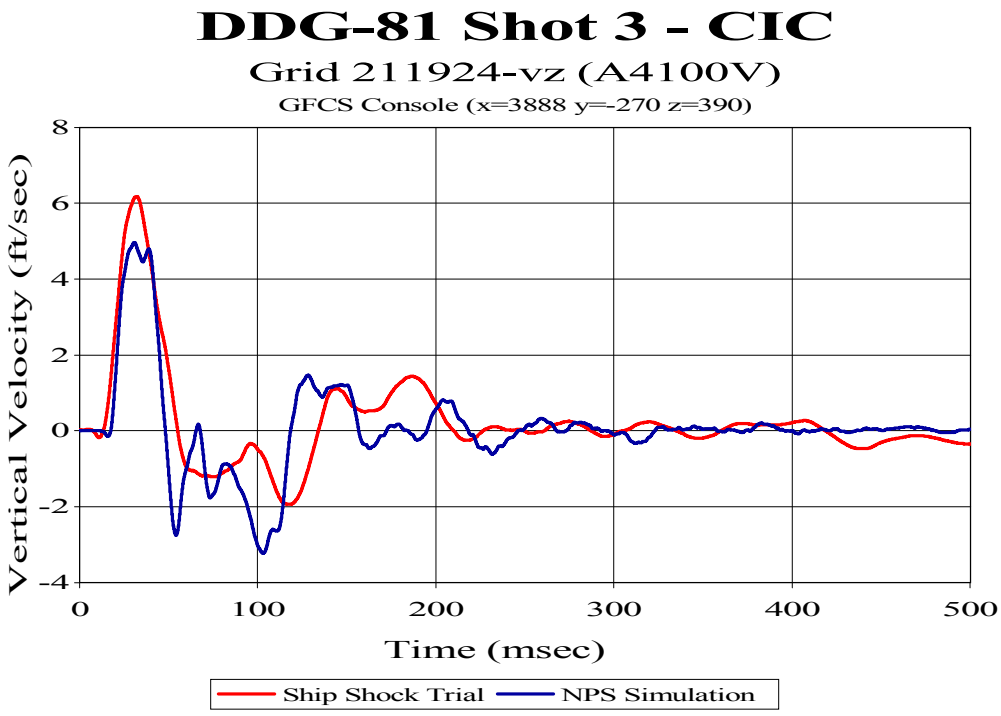

Figure 31. Deck Sensor A4100V

4. Statistical Analysis of CIC Velocity Response

Table 9 presents statistical results from each of the three shots. This table has been included as an overview of the data that has been presented with regard to the vertical velocity response analysis conducted on the CIC area. As is shown in Table 9 there is a high rate of correlation for all three shots.

Table 9. Statistical Data for CIC Response Analysis of Shots 1, 2 & 3

Russell's Comprehensive Error	Shot 1	Shot 2	Shot 3
RC < 0.30	93%	100%	100%
RC < 0.28	87%	87%	87%
RC < 0.25	87%	87%	67%
RC < 0.20	60%	40%	47%
RC < 0.18	53%	27%	6%
RC < 0.15	20%	20%	6%
Mean RC	0.1978	0.2006	0.2239
Standard Deviation	0.0564	0.0576	0.0395
Mean + Standard Deviation	0.2542	0.2582	0.2634
Data within One Standard Deviation	87%	87%	73%

The preceding results obtained from the CIC response data indicates that the NPS modeling and simulation methodology does in fact consistently produce satisfactory results as compared to the measured data.

B. SHIPWIDE ATHWARTSHIP VELOCITY RESPONSE DATA

The primary response of an UNDEX event is in the vertical direction. Accordingly, the athwartship direction and the longitudinal direction responses are significantly smaller in magnitude than those in the vertical direction. For this reason the vertical response of the system, which is the ship in this case, has always been the focus of previous analysis conducted in this area. In the following study the athwartship motion response of the DDG-81 was simulated and compared to the measured ship shock trial data in a similar manner to that previously discussed. The goal of this study was to

ascertain whether or not the NPS modeling and simulation methodology accurately captured the more subtle athwartship velocity response as well as it did the primary vertical velocity response of the ship. Data from all three shots was incorporated into the athwartship analysis.

1. Error Comparison

As a result of its secondary nature in the over response of the ship, the athwartship motion of the ship is not as well documented as the vertical response. Of the over 600 sensors installed during the ship shock trial in DDG-81 only about 10% were used to collect athwartship response data. Table 10 is the list of sensors used in the athwartship analysis. Though this is a relatively small set of data points, the sensor locations chosen were well distributed throughout the ship.

Table 10. Athwartship Velocity Response Sensor Locations

Sensor	Compartment	Grid ID	X (inches)	Y(inches)	Z(inches)	General Location Description
A2001A	PASSAGE	120217	5328	0	82	VERTICAL CENTERLINE STIFFNER
A2102A	CIC PROJECTION RM	212058	4080	0	390	AT BULKHEAD 126 CENTERLINE
A2110A	RADAR ROOM #1	414953	4059	0	722.8	ON BULKHEAD
A2105AI	CIC ANNEX	222240	3504	0	390	AT BULKHEAD 174 CENTELINE
A2117AI	RADAR ROOM #2	414367	3504	0	702	AT BULKHEAD 174
A2238AI	PORT MAST	416419	3504	135	848	MAST LEG PORT
A2241A	STARBOARD MAST	416269	3504	-135	848	MAST LEG STARBOARD
A2015AI	AUX MACH RM #2	230461	2952	0	85.5	CENTRELINE BULKHEAD
A2311A	A/C MACHINERY RM	320746	1536	0	177	AT BULKHEAD 338
A2033A	FAN ROOM	330764	1152	0	196	ABOVE 3RD DECK
A2021A	AFTER STEERING	350052	288	0	211	KEEL BEAM AT BULKHEAD 442

Sensors A2001 and A2021 were originally included in the study but do not appear in the final analysis for Shot 1 and Shot 2. These two sensors correspond to accelerometers located in the bow and at the stern of the ship. They exhibit very poor correlation characteristics as compared to the rest of the data. The data points for these sensors fell well of the chart shown in Figure 32, which is a comparison of Russell's Comprehensive error factor for all three shots. Considered to be outliers, they were ultimately excluded.

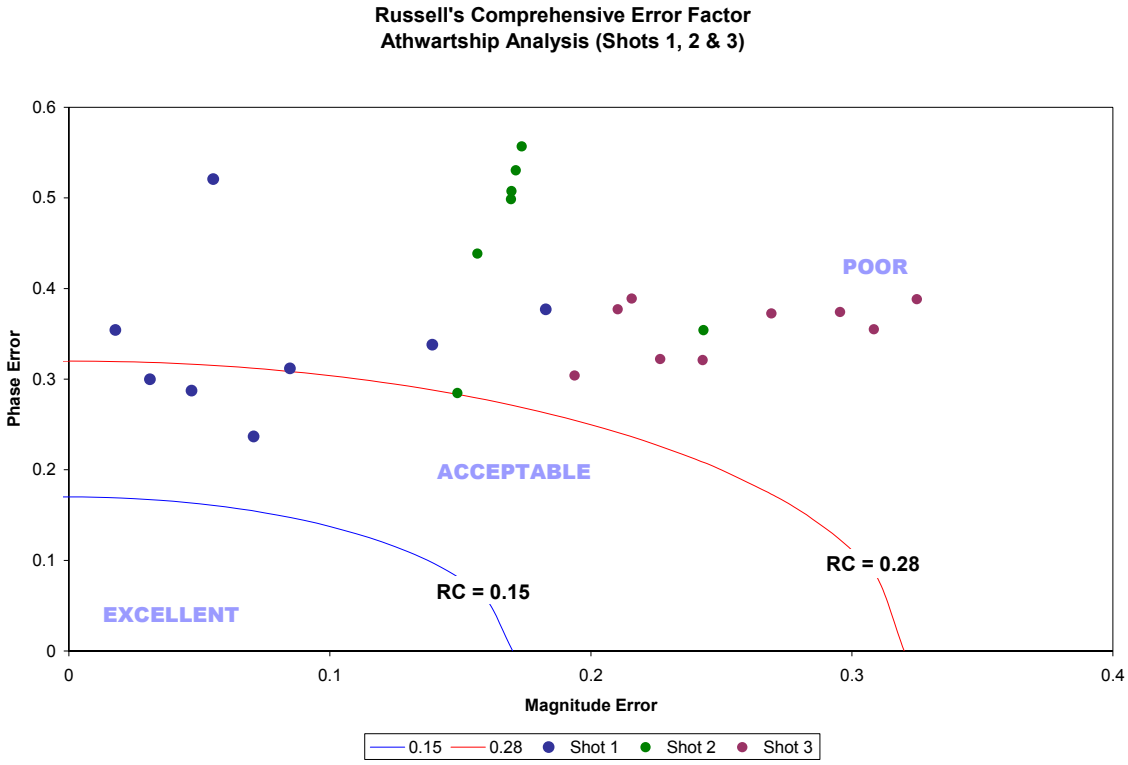

Figure 32. Russell's Comprehensive Error Factor for Athwartship Response

Table 11 contains the complete list of data used for the analysis and computation of Russell's error factors for the athwartship velocity response.

2. Velocity Plots

The figures that follow provide some examples of the athwartship velocity plots. A complete set of athwartship velocity plots are provided in APPENDIX C. Figure 33 shows a time history response plot for sensor A2015A from Shot 2. The correlation for this accelerometer located nearly amidships near the keel has a value of RC = 0.2847. This correlation is just outside the acceptable range.

Table 11. Russell's Error Factor for Athwartship Response

Runtime = 500 msec						SHOT 1			SHOT 2			SHOT 3		
Sensor	NODE	Mounting Type	Location (in)*			738in Cavitation - Medium			738in Cavitation - Medium			738in Cavitation - Coarse		
						SHIP SHOCK TRIAL DATA (<250HZ)			SHIP SHOCK TRIAL DATA (<250HZ)			SHIP SHOCK TRIAL DATA (<250HZ)		
						LS-DYNA/USA DATA (<250HZ)			LS-DYNA/USA DATA (<250HZ)			LS-DYNA/USA DATA (<250HZ)		
			x	y	z	RM	RP	RC	RM	RP	RC	RM	RP	RC
A2001A	120217	Keel	5328	0	82	-0.7292	0.4376	0.7537	-0.7416	0.4804	0.7830	-0.4587	0.4203	0.5513
A2102A	212058	Bulkead	4080	0	390	0.0708	0.2367	0.2189	-0.2431	0.3542	0.3807	-0.2265	0.3223	0.3491
A2110A	414953	Bulkhead	4059	0	722.8	0.1393	0.3381	0.3241	-0.1565	0.4387	0.4127	-0.2156	0.3889	0.3941
A2105Al	222240	Bulkhead	3504	0	390	-0.0470	0.2873	0.2580	-0.1694	0.4986	0.4667	-0.2691	0.3725	0.4072
A2117Al	414367	Bulkhead	3504	0	702	-0.0311	0.2997	0.2670	-0.1695	0.5077	0.4744	-0.3084	0.3551	0.4168
A2238Al	416419	Bulkhead	3504	135	848	0.0179	0.3542	0.3143	-0.1712	0.5305	0.4940	-0.3248	0.3883	0.4487
A2241A	416269	Bulkhead	3504	-135	848	0.0847	0.3119	0.2864	-0.1735	0.5570	0.5170	-0.2954	0.3741	0.4224
A2015Al	230461	Keel	2952	0	85.5	-0.1827	0.3769	0.3712	-0.1488	0.2847	0.2847	-0.2428	0.3212	0.3568
A2311A	320746	Bulkhead	1536	0	177							-0.1937	0.3040	0.3194
A2033A	330764	Keel	1152	0	196	-0.0553	0.5207	0.4641	-0.4303	0.4568	0.5562	-0.2102	0.3771	0.3826
A2021A	350052	Keel	288	0	211	-0.6853	0.5050	0.7547	-0.7211	0.5100	0.7827	-0.4226	0.4295	0.5340
Russell Error Correlation					Sum(E(X))	-0.00340	2.72550	2.50400	-1.66230	3.62820	3.58640	-3.16780	4.05330	4.58240
> 0.28		Poor			Sum(E(X^2))	0.07153	0.97862	0.82480	0.40773	1.70568	1.65986	0.98772	1.50961	1.96127
< 0.15		Excellent			**Mean**	**-0.00042**	**0.34069**	**0.31300**	**-0.20779**	**0.45353**	**0.44830**	**-0.28798**	**0.36848**	**0.41658**
					Standard Deviation	0.10108	0.08458	0.07658	0.09436	0.09273	0.08625	0.08686	0.04006	0.07233

* Referenced to the G&C NASTRAN Model coordinate origin

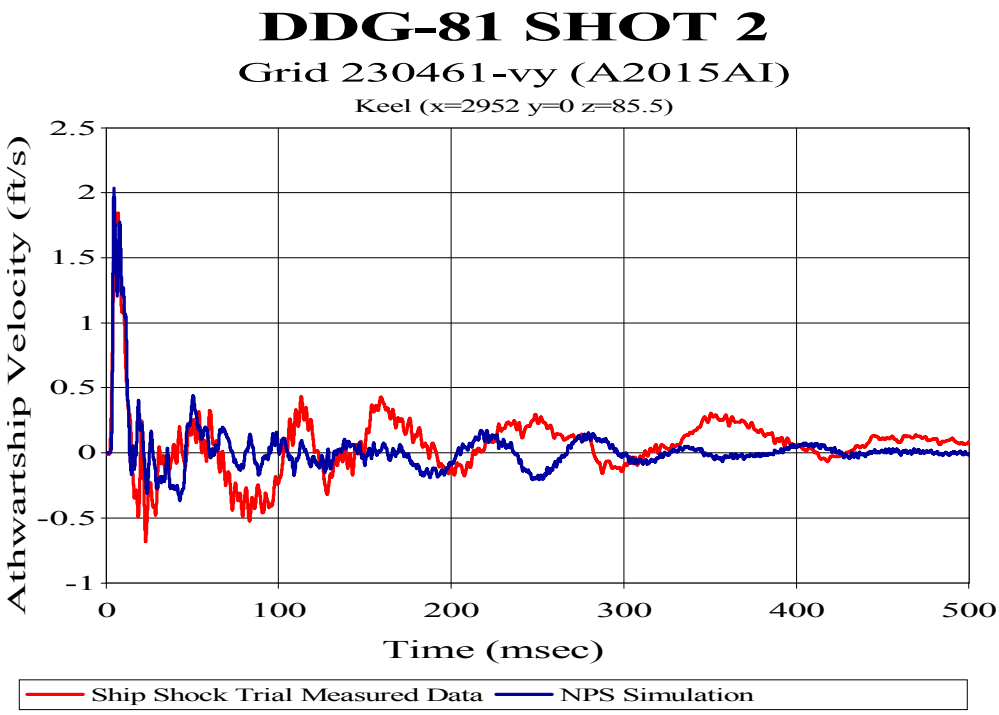

Figure 33. Keel Sensor A2015AI

The next set of figures illustrates some of the deficiencies discovered while analyzing the athwartship response data. Analysis of the early time response for keel sensor A2033A, shown in Figure 34, revealed that it suffered from serious drift error within the first 100 msec. The standard drift compensation technique had been applied, with the result being displayed in Figure 35. There is a definite trailing off of the measured shock trial data curve away from the abscissa. Without manual manipulation of the shock trial curve it was impossible to generate a valid comparison of the simulated data. Similar in nature to the drift correction issues experienced in the CIC area analysis, this problem appears to be magnified by the much smaller magnitudes that are witnessed in the athwartship response. In most cases, the magnitudes in the athwartship direction are on the order of one magnitude smaller when compared to the corresponding vertical direction response for the same sensor location.

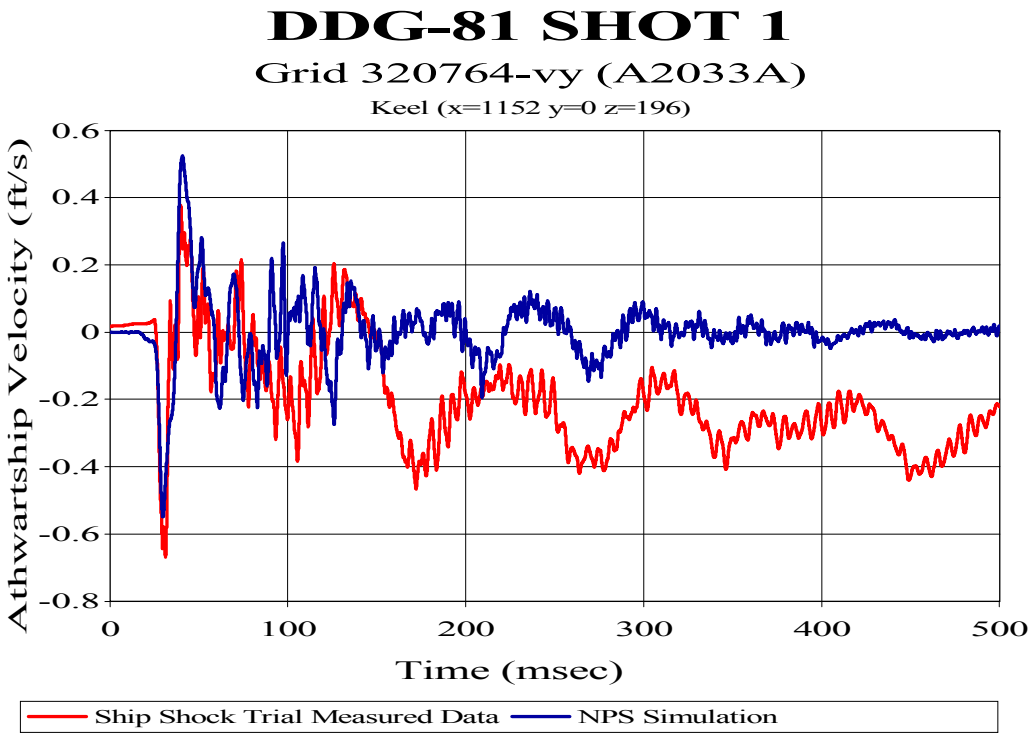

Figure 34. Keel Sensor A2033A

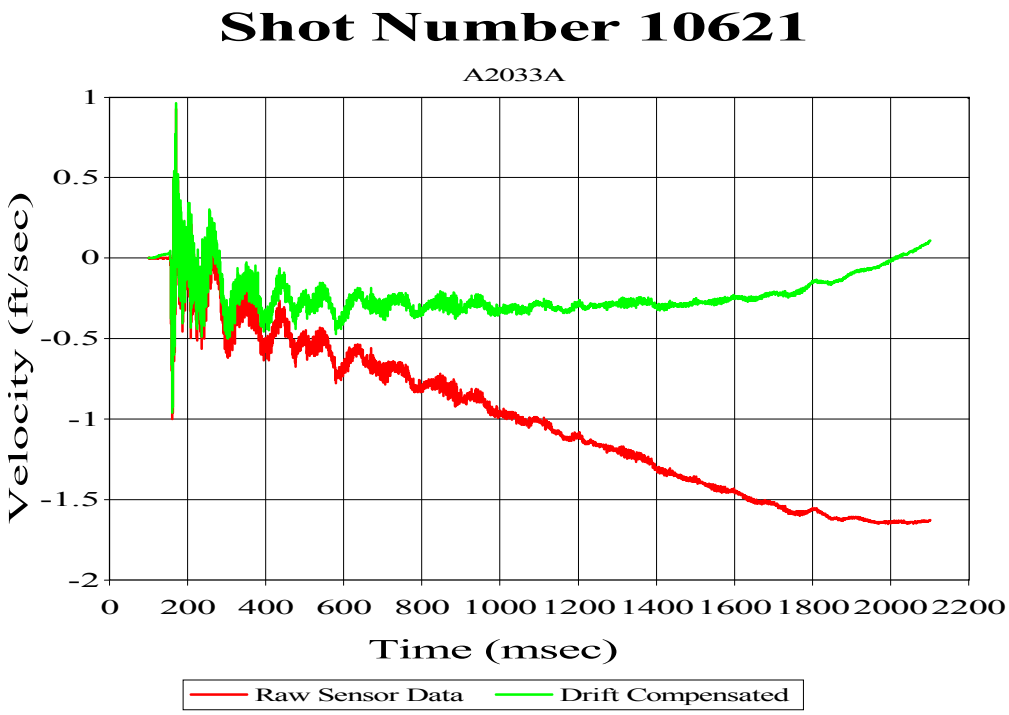

Figure 35. Sensor A2033A: Application of Drift Compensation

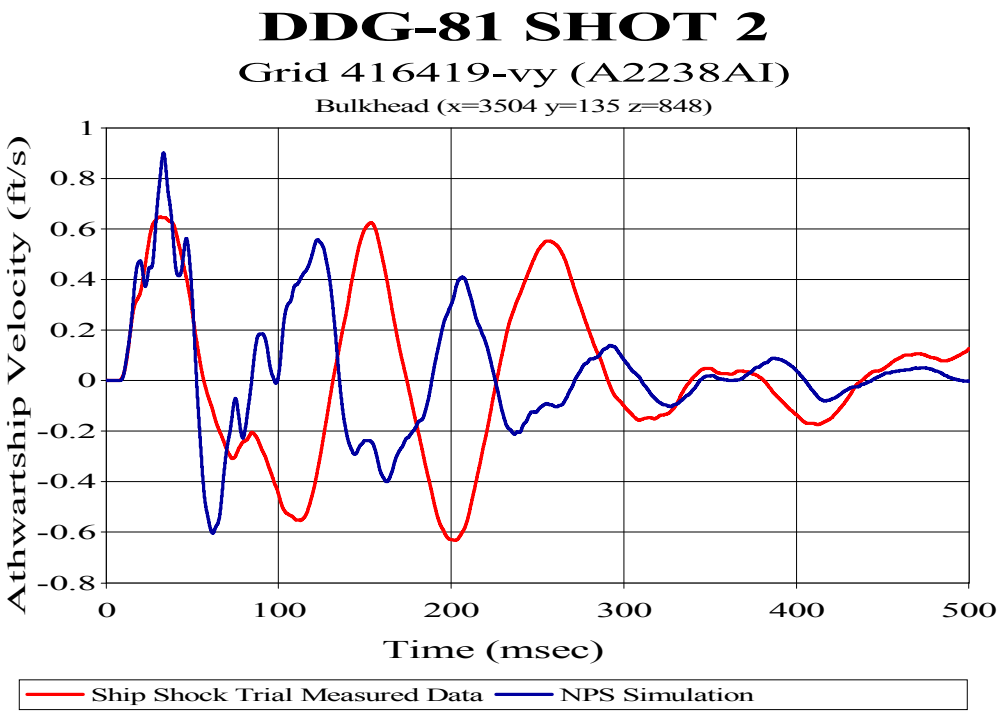

Figure 36. Bulkhead Sensor A2238AI

The bulkhead sensor shown in Figure 36, A2238AI, appears to have good initial correlation in phase, but quickly goes out of phase. For the 500 msec time history plot shown, the RP = 0.5305, with the RC = 0.4940. The simulated data generally under-predicted the response after the initial peak with the RM = 0.1712. In general this was a poor correlation, even though both of the curves appear to be of almost same wave pattern.

3. Comparison Results

Overall the results in the athwartship direction were found to be much less promising than those in vertical velocity comparison. Using the same 250Hz low-pass filtering and standard drift correction via the UERD Tools built in function, the mean correlation in the athwartship direction was determined to be RC = 0.3922; well beyond the RC = 0.28 acceptable limit. Table 12 further summarizes the finding for athwartship velocity response.

Table 12. Statistical Data for Athwartship Response Analysis of Shots 1, 2 & 3

Russell's Comprehensive Error	Shot 1	Shot 2	Shot 3
RC < 0.33	75%	13%	9%
RC < 0.30	50%	13%	0%
RC < 0.28	25%	0%	0%
RC < 0.25	13%	0%	0%
RC < 0.20	0%	0%	0%
Mean RC	0.3130	0.4483	0.4166
Standard Deviation	0.0766	0.0865	0.0732
Mean + Standard Deviation	0.3896	0.5348	0.4898
Data within One Standard Deviation	88%	88%	82%

The results obtained from the small sampling of sensors that were studied produced generally unacceptable athwartship response correlations based on the criteria established in Table 4. Even so, the Russell's Magnitude error factor was equal to value of 0.20 or lower, considerably lower in most cases. This would indicate that the simulation did in fact accurately capture the range of the motion. However, as in the CIC vertical velocity response comparison where it had also been witnessed, though to a lesser degree, the phase error dominated the error correlation due to its pronounced excursion from the measured data. In the athwartship direction the Russell's Phase error factor was determined to lie in the range of 0.30 or higher in nearly all cases.

One of the possible contributors to the less favorable correlation in the athwartship direction is the inherently smaller magnitudes found in the velocity response as compared to those in the vertical direction. With the ever present problem of sensor drift, as previously shown in Figure 35, the induced error and method of correction impact the ultimate curve comparison much more significantly in the athwartship direction due to the smaller range of motion in the actual response for a particular point.

Additionally, the physical placement of the sensor in some cases is suspect. In review of the sensor installation descriptions it was discovered that some sensors were mounted to the web section of stiffeners, equipment foundations, longitudinal bulkheads and other locations off of the true deck. It is postulated that the placement of these various sensors could impact the phase response of the actual sensor during the UNDEX

event, skewing the recorded data by measuring the motion of the lightweight component that it is affixed to rather than the ship itself. This type of motion, at a presumably at higher rate of oscillation would not be present in the computer simulation of that node point in the finite element model.

V. SHIP SYSTEM DAMPING

Almost all of the damping within a structure is a result of frictional energy that is being dissipated at physical connection points such as bolted or riveted joints. However, in a ship the majority of connections are welded rather than mechanically joined, so there is much less energy dissipation through the welds. Ships do however provide a viable means for energy to escape the system. This occurs through long cable runs, hangers, snubbers and out to the fluid surrounding the hull itself [Ref. 28].

A. PROPORTIONAL DAMPING COEFFICIENTS

A study comparing the effects of ship system damping effects was completed for the DDG-81 [Ref. 28]. Different proportional damping values were applied to the LS-DYNA input deck and simulations were conducted for Shot 2 of the DDG-81 ship shock trials. A dense fluid mesh model was used for the simulation in this comparison. The time history plots of two of these sets of simulations employing different damping coefficients were compared against the measured ship shock trial data in the standard manner which was outlined in the previous chapter of this paper.

Rayleigh damping, a particular form of proportional damping, defines the damping matrix, [C], as

$$C = \alpha[M] + \beta[K] \tag{36}$$

in the general expression for the structural equation of motion, Equation (37).

$$[M]\{\ddot{x}\} + [C]\{\dot{x}\} + [K]\{x\} = \{F\} \tag{37}$$

The damping coefficients α and β are constants. Equation (36) can be normalized using mass normalization such that

$$[\phi]^T[C][\phi] = [2\zeta_r\omega_r]_{diag} = \alpha[I] + \beta[\omega_r^2]_{diag} \tag{38}$$

In a complex system such as a ship, the subscript *r,* which signifies the number of modes, greatly exceeds the two modes necessary to determine the solution of the equation. In the case that the system is over determined, the coefficients can be found using the measured data and a least squares curve fitting method.

For each mode of the ship response the modal damping ratio is calculated using Equation (39).

$$\zeta_i = \frac{1}{2}\left(\frac{\alpha}{\omega_i} + \beta\omega_i\right) \tag{39}$$

1. NPS Damping Values

A new set of damping coefficient values was determined by extensive analysis of measured data taken from the DDG-53 ships shock trials. The ship was divided into 67 area groups for the damping analysis, which included data from 773 sensors. For the frequency spectrum of interest, 0 to 250Hz, both the athwartship and vertical response were measured and recorded. A least squares curve fit, as shown in Figure 37, was applied to each area group. The area groups were given weighted averages based on the number of modes used in the curve fitting process necessary to find α and β, which are shown in Tables 13 and 14.

Table 13. Weighted Mean of α [from Ref. 28]

Athwartship Direction	Vertical Direction
18.4	19.2

Table 14. Weighted Mean of β [from Ref. 28]

Athwartship Direction	Vertical Direction
2.82E-06	2.09E-06

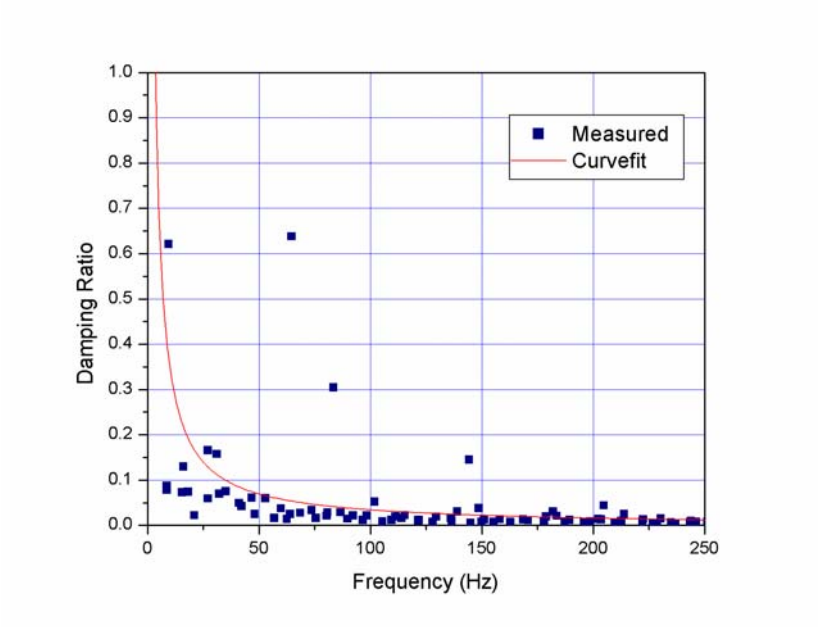

Figure 37. Modal Damping Ratio at Area 6, Athwartship Direction [from Ref. 28]

Thus, the new NPS Damping values are defined as $\alpha = 19.2$ and $\beta = 2.09E\text{-}6$, in the vertical direction, of which shall be compared in this study. Similarly, in the athwartship direction the NPS Damping values were found to be, $\alpha = 18.4$ and $\beta = 2.82E\text{-}6$. The great disparity in the two damping coefficients indicates that the damping in the system is mass driven.

2. DDG-53 Simulation Damping Values

Table 15 gives the damping coefficient values that were previously used in the modeling and simulation effort of DDG-53 and the early DDG-81 investigations.

Table 15. Damping Values from the DDG-53 Simulation Effort [from Ref. 29]

Damping Value	α	β
4%	2.64	4.99E-05
8%	4.93	9.89E-05

The values listed in Table 15 were found by fixing the damping ratio, ζ, at two particular frequencies, namely 5Hz and 250Hz. The complete curves were then generated across the frequency spectrum using Equation (39). Figures 38 and 39 illustrate the various damping curves considered. The points at 5Hz and 250Hz indicate where the 4% and 8% damping curves were fixed to those particular values of ζ. The MATLAB® code used to generate the following plots is provided as APPENDIX D.

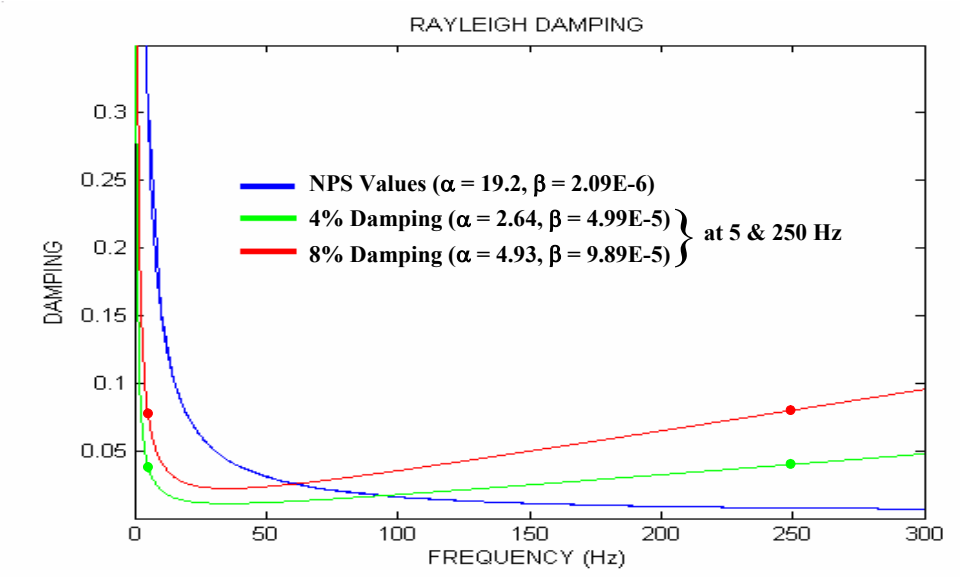

Figure 38. Proportional System Damping (Linear Scale)

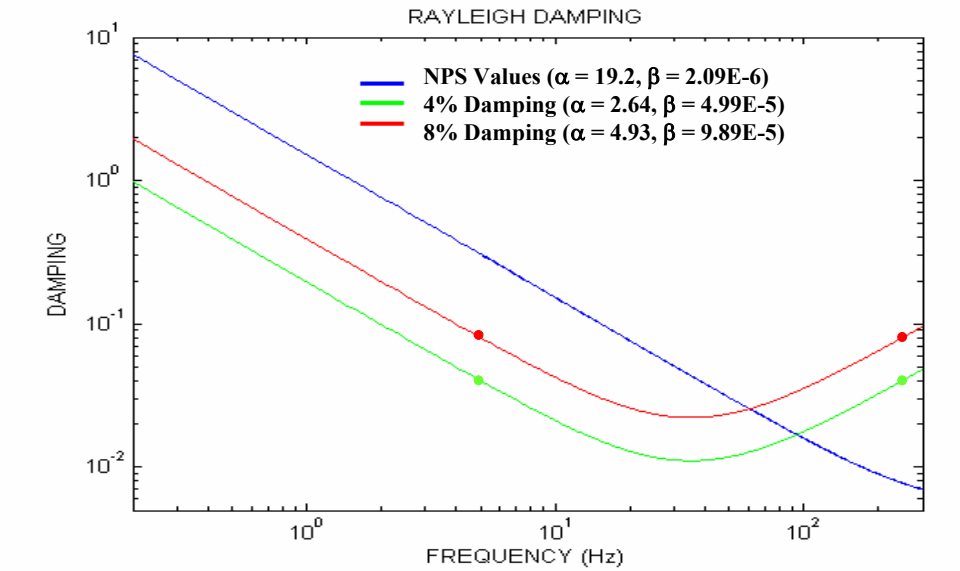

Figure 39. Proportional System Damping (Logarithmic Scale)

B. DAMPING SYSTEM COMPARISONS

In this study the discussion shall be limited to a comparison between the new "NPS Damping Values" as presented by Shin and Ham [Ref. 28], and the fixed 4% damping used in the DDG-53 ship shock trial simulation analysis and the preliminary DDG-81 ship shock trial simulation analysis conducted at NPS.

1. Error Comparison

The following series of velocity response plots compares the Rayleigh damping coefficients, α and β, presented in Tables 13 and 14 with coefficients that were used in previous studies conducted on the DDG-53 and DDG- 81, which appear in Table 15.

Russell's error factor was once again chosen as a means of comparing the simulated velocity response data against the measured actual ship shock trial data. For the purpose of this study, an established set of acceptance criteria was taken from the values presented in Table 4.

2. Velocity Plots

The following velocity plots, which were taken from the analysis conducted on Shot 2, and are typical of the results discovered in this portion of the study. Additional time history response plots are found in APPENDIX E.

In these figures the approximate location of each sensor is indicated on the ship accompanying the time history plots by a red dot. The Russell's Comprehensive (RC) error correlation factor was computed for each sensor. As the velocity response plot comparisons in Figure 40 through Figure 43 show, there is a noticeably closer correlation between the NPS damping values and the ship shock trial data, than with the fixed 4% damping. The mean RC for the 4% Damping cases was 0.25 while in comparison when the new NPS damping values from Table 13 and Table 14 were used, the mean RC value was only 0.18. Recalling that by Russell's correlation criteria, a value below 0.15 is considered an excellent correlation, the simulations using the new NPS damping values consistently showed better correlation and an average reduction of approximately 28% in deviation from the recorded shock trial data versus those using the fixed 4% damping.

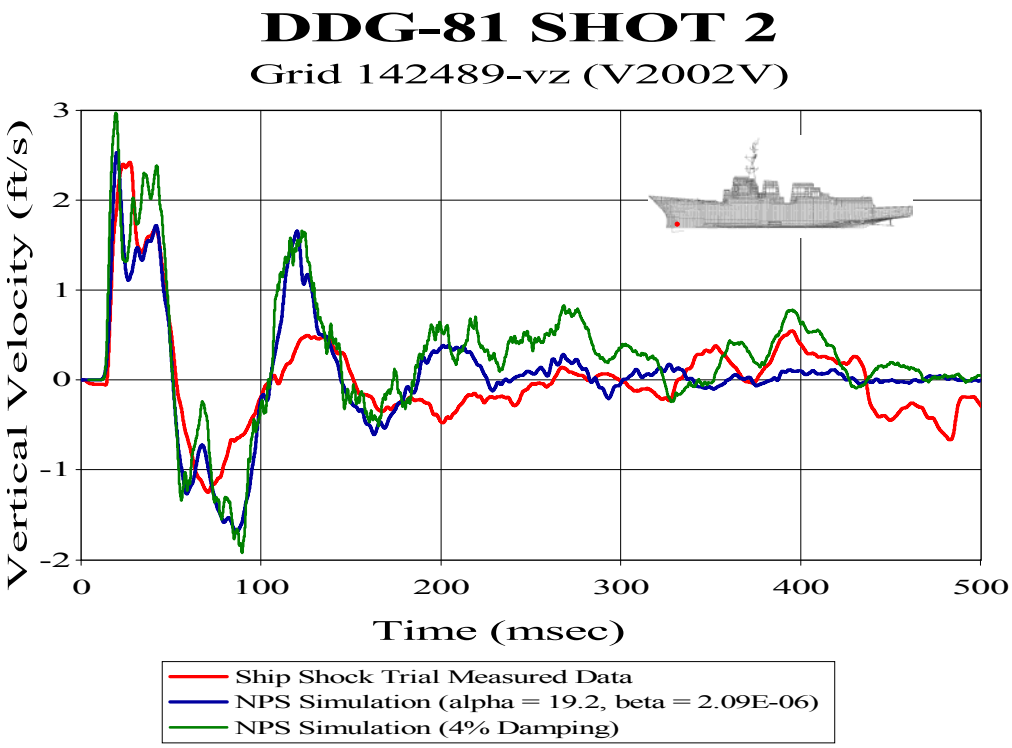

Figure 40. Vertical Velocity Response: Deck Sensor V2002V

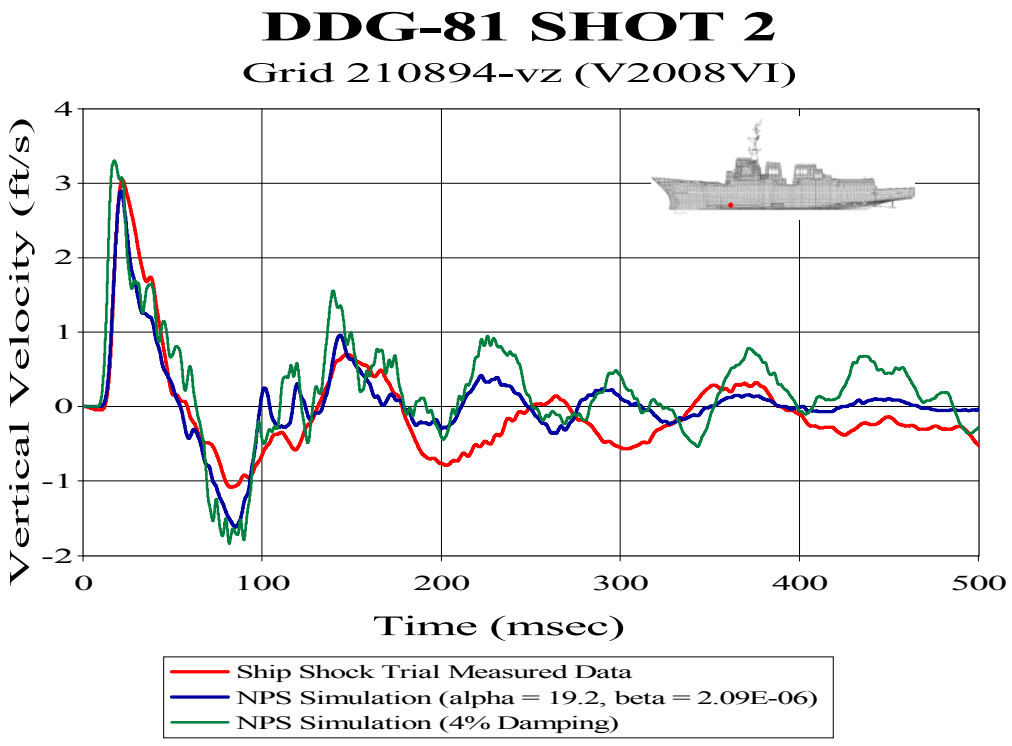

Figure 41. Vertical Velocity Response: Deck Sensor V2008VI

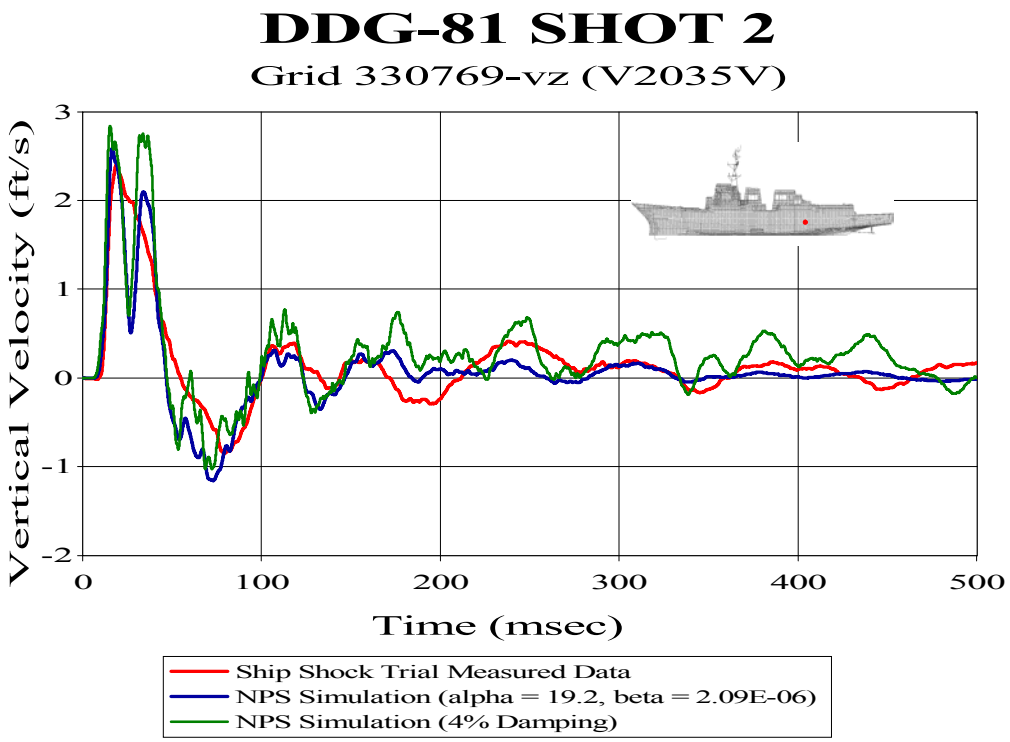

Figure 42. Vertical Velocity Response: Keel Sensor V2035V

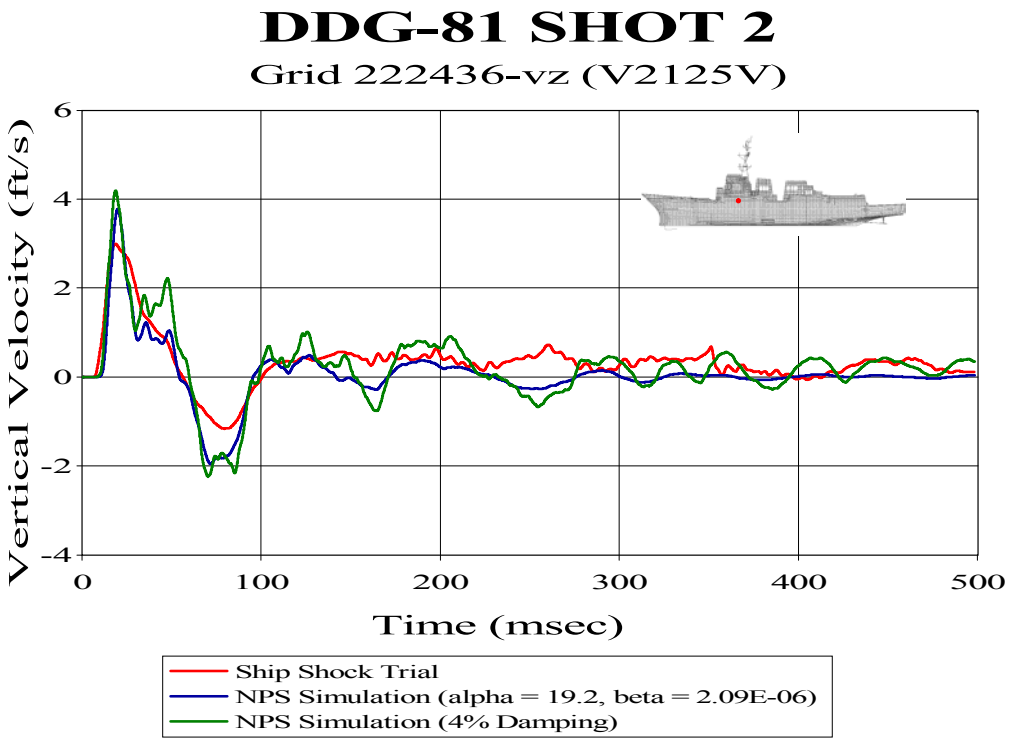

Figure 43. Vertical Velocity Response: Bulkhead Sensor V2125V

3. Damping Effects on Correlation

Table 16 provides the supporting data with Russell's error factors computed for all sensors used in this portion of the system damping comparison study. Figure 44 is a graphical representation of the data presented in Table 16. The Russell's Comprehensive error factor for the simulations using the NPS damping values all fall in the highly acceptable range, with the exception of two sensors. These two sensors, as in the earlier studies, correspond to sensors located at the extremities of the ship, namely the bow and stern. As before, there is some hesitation in accepting these data points that fall well outside of the pattern of the others within their own grouping. These data points should be considered suspect, but are being included in this portion of the study for completeness.

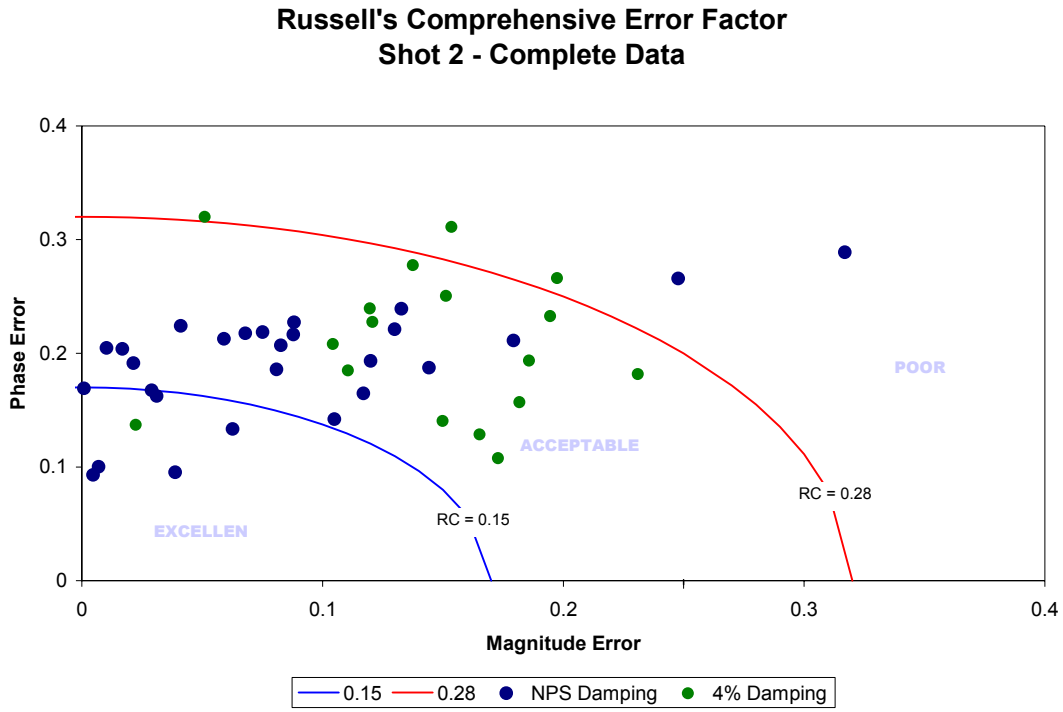

Figure 44. Russell's Error Factor for DDG-81 Shot 2 (Vertical Velocities)

Table 16. Russell's Comprehensive Error Factor Correlation for DDG-81 Shot 2

Ship Shock Simulation with Shot 2 Geometry, Dense Mesh and 738 in Cavitation Depth						Shock Trial Data vs. 4% Damping			Shock Trial Data vs. NPS Damping		
						SHIP SHOCK TRIAL DATA (<250HZ)			SHIP SHOCK TRIAL DATA (<250HZ)		
						LS-DYNA/USA DATA (<250HZ)			LS-DYNA/USA DATA (<250HZ)		
Sensor	Node	Mounting Type	Location (in)*			RM	RP	RC	RM	RP	RC
			x	y	z						
V2000V	120217	Keel	5328	0	82	0.0223	0.3351	0.2976	-0.3169	0.2887	0.38
V2002V	142489	Keel	4656	24	85	0.1974	0.2715	0.2975	0.0679	0.2175	0.2019
V2007V	210430	Keel	4080	0	82	0.1728	0.2297	0.2547	-0.0879	0.2164	0.207
V2009VI	210808	Bulkhead	4080	-176	171	0.1857	0.3342	0.3388	-0.0882	0.2272	0.2160
V2008VI	210894	Deck	4064	176	171	0.1207	0.2689	0.258	0.1200	0.1932	0.2016
A8516V	210993	Bulkhead	1591	36	453	0.1945	0.1927	0.2426	0.0311	0.1623	0.1464
V2108V	212196	Bulkhead	4080	312	390	0.1042	0.1844	0.1877	-0.0809	0.1858	0.1796
V2010V	220589	Keel	3504	0	86	0.1512	0.2174	0.2347	-0.0827	0.2070	0.1975
V2012VI	221102	Bulkhead	3504	-216	177	0.1374	0.2605	0.2610	-0.1299	0.2211	0.2273
V2011VI	221188	Bulkhead	3504	216	177	0.2309	0.2008	0.2712	0.0411	0.2240	0.2018
V2013V	221601	Bulkhead	3504	0	280	0.1105	0.1372	0.1561	-0.1049	0.1420	0.1565
V2124V	222060	Bulkhead	3504	-375	390	0.0510	0.2662	0.2402	-0.1793	0.2113	0.2456
A2104V	222240	Bulkhead	3504	0	390	0.1535	0.1079	0.1663	-0.0388	0.0953	0.0912
V2125V	222436	Bulkhead	3504	375	390	0.1651	0.1936	0.2255	-0.0214	0.1914	0.1707
V2014V	230461	Keel	2952	0	86	0.1196	0.2278	0.2281	-0.0590	0.2126	0.1956
A3565V	231696	Bulkhead	2952	-81	317	0.1817	0.2328	0.2617	0.0290	0.1675	0.1506
V2016V	242399	Keel	2544	0	116	0.1498	0.2083	0.2274	-0.0169	0.2038	0.1812
V2026V	312302	Keel	1992	0	55	0.0999	0.2505	0.2390	-0.0751	0.2185	0.2047
A2310V	320746	Bulkhead	1536	0	177	0.1948	0.2776	0.3005	0.0103	0.2047	0.1816
V2034V	330759	Keel	1152	-135	193	0.0360	0.1819	0.1644	-0.1442	0.1874	0.2095
V2035V	330769	Keel	1152	135	193	0.1643	0.1849	0.2192	0.0009	0.1692	0.1500
V2019V	340167	Keel	672	0	197	0.0877	0.3200	0.2940	-0.1327	0.2391	0.2423
V2020V	350052	Keel	288	0	211	-0.0697	0.3111	0.2825	-0.2477	0.2657	0.3219
A2116V	414367	Deck	3528	-346	1446	0.1844	0.1288	0.1993	0.0070	0.1003	0.0891
A2109V	414953	Bulkhead	4059	0	723	0.2963	0.2395	0.3376	0.1170	0.1647	0.1790
A2240V	416269	Mast	3504	-135	848	0.1459	0.1571	0.1900	-0.0626	0.1335	0.1307
A2237V	416419	Mast	3504	135	848	0.1815	0.1405	0.2034	0.0047	0.0931	0.0826
Russell Error Correlation					Sum(E(X))	3.76940	6.06090	6.57900	-1.44008	5.14330	5.14190
	> 0.28	Poor			Sum(E(X^2))	0.66230	1.46227	1.66684	0.34077	1.03935	1.08392
	< 0.15	Excellent			**Mean**	**0.13961**	**0.22448**	**0.24367**	**-0.05334**	**0.19049**	**0.19044**
Runtime = 500 msec					Standard Deviation	0.07234	0.06255	0.04952	0.10076	0.04787	0.06346

* Referenced to the G&C NASTRAN Model coordinate origin located at the stern.

Figure 44 shows that the results from the simulations performed using the fixed 4% damping values were only marginally acceptable in most cases. The fixed 4% damping response data is loosely grouped whereas there is considerable improvement in the accuracy, especially in terms of the magnitude correlation in the simulations using the NPS damping values. This is demonstrated by the large grouping of NPS damping value derived data points nearer the ordinate.

4. Velocity Meter Data

This section examines the data collected from select velocity meters. In comparison to the overall data, using only the velocity meter data shows an increase in deviation between the simulated response and measured ship shock trial data. In Figure 45 there is a noticeable absence of data points with excellent correlation that were obtained using the NPS damping values.

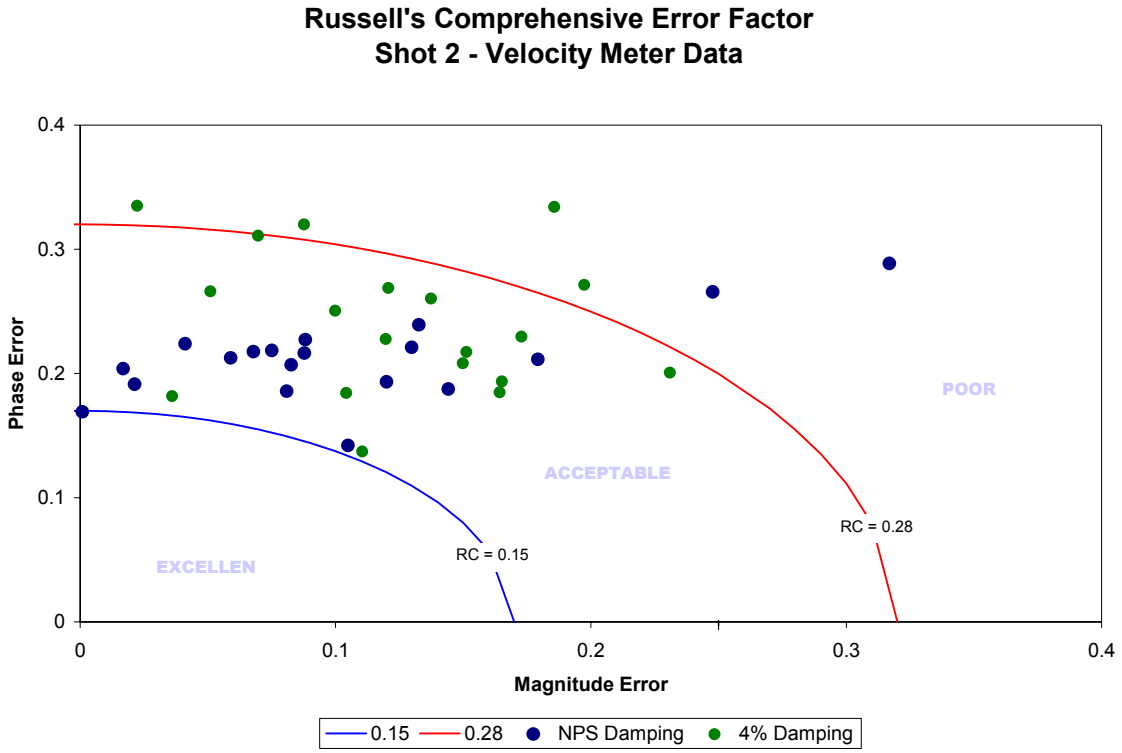

Figure 45. Russell's Comprehensive Error Factor for Shot 2 (Velocity Meter Data)

The weaker correlation is also indicated through the rise in the Russell's Comprehensive error factor as shown in the mean values listed in Table 17. Part of the reason for the degradation in the overall correlation is the inclusion of the two sensors, V2000V and V2020V, which were located at the bow and stern of the ship, respectively. Yet a weaker correlation at the ship's extremities is inline with the results obtained by Schneider's [Ref. 8] shipwide analysis of the vertical velocities. That work indicated that there was a direct correlation between the longitudinal position of a node within the finite element model and the accuracy of the simulated data when compared to the corresponding sensor data. The bow and stern areas consistently showed poor correlation of the simulated data for all three shots. An example of this relationship is shown in Figure 46.

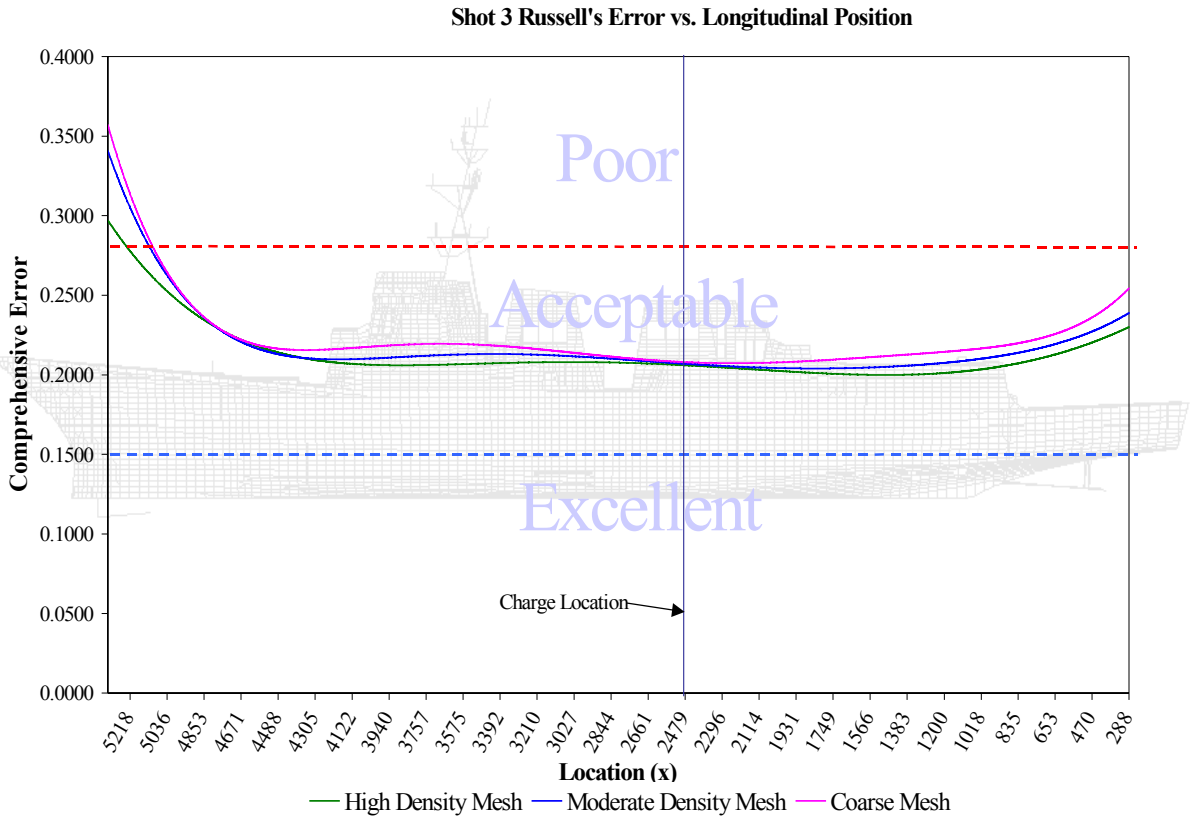

Figure 46. Russell's Comprehensive Error as a Function of Position [from Ref. 8]

Therefore, sensors V2000V and V2020V were removed from further consideration.

Table 17. Damping Comparison Results for DDG-81 Shot 2 (Velocity Meter)

Ship Shock Simulation with Shot 2 Geometry, Dense Mesh and 738 in Cavitation Depth						Shock Trial Data vs. 4% Damping			Shock Trial Data vs. NPS Damping		
						SHIP SHOCK TRIAL DATA (<250HZ)			SHIP SHOCK TRIAL DATA (<250HZ)		
						LS-DYNA/USA DATA (<250HZ)			LS-DYNA/USA DATA (<250HZ)		
Sensor	Node	Mounting Type	Location (in)*			RM	RP	RC	RM	RP	RC
			x	y	z						
V2000V	120217	Keel	5328	0	82	0.0223	0.3351	0.2976	-0.3169	0.2887	0.3800
V2002V	142489	Keel	4656	24	85	0.1974	0.2715	0.2975	0.0679	0.2175	0.2019
V2007V	210430	Keel	4080	0	82	0.1728	0.2297	0.2547	-0.0879	0.2164	0.2070
V2009VI	210808	Bulkhead	4080	-176	171	0.1857	0.3342	0.3388	-0.0882	0.2272	0.2160
V2008VI	210894	Deck	4064	176	171	0.1207	0.2689	0.2580	0.1200	0.1932	0.2016
V2108V	212196	Bulkhead	4080	312	390	0.1042	0.1844	0.1877	-0.0809	0.1858	0.1796
V2010V	220589	Keel	3504	0	86	0.1512	0.2174	0.2347	-0.0827	0.2070	0.1975
V2012VI	221102	Bulkhead	3504	-216	177	0.1374	0.2605	0.2610	-0.1299	0.2211	0.2273
V2011VI	221188	Bulkhead	3504	216	177	0.2309	0.2008	0.2712	0.0411	0.2240	0.2018
V2013V	221601	Bulkhead	3504	0	280	0.1105	0.1372	0.1561	-0.1049	0.1420	0.1565
V2124V	222060	Bulkhead	3504	-375	390	0.0510	0.2662	0.2402	-0.1793	0.2113	0.2456
V2125V	222436	Bulkhead	3504	375	390	0.1651	0.1936	0.2255	-0.0214	0.1914	0.1707
V2014V	230461	Keel	2952	0	86	0.1196	0.2278	0.2281	-0.0590	0.2126	0.1956
V2016V	242399	Keel	2544	0	116	0.1498	0.2083	0.2274	-0.0169	0.2038	0.1812
V2026V	312302	Keel	1992	0	55	0.0999	0.2505	0.2390	-0.0751	0.2185	0.2047
V2034V	330759	Keel	1152	-135	193	0.0360	0.1819	0.1644	-0.1442	0.1874	0.2095
V2035V	330769	Keel	1152	135	193	0.1643	0.1849	0.2192	0.0009	0.1692	0.1500
V2019V	340167	Keel	672	0	197	0.0877	0.3200	0.2940	-0.1327	0.2391	0.2423
V2020V	350052	Keel	288	0	211	-0.0697	0.3111	0.2825	-0.2477	0.2657	0.3219
Russell Error Correlation					Sum(E(X))	2.23680	4.58400	4.67760	-1.53778	4.02190	4.09070
> 0.28		Poor			Sum(E(X^2))	0.35392	1.16387	1.19037	0.31967	0.87029	0.93463
< 0.15		Excellent			**Mean**	**0.11773**	**0.24126**	**0.24619**	**-0.08094**	**0.21168**	**0.21530**
Runtime = 500 msec					Standard Deviation	0.07094	0.05672	0.04643	0.10414	0.03244	0.05472

* Referenced to the G&C NASTRAN Model coordinate origin located at the stem.

Considering only the velocity meter data, it was found that by using the new NPS damping values, the average improvement was approximately 25% over the comparisons made using the 4% fixed damping. These results are shown in Table 18.

Table 18. Relative Improvement Using NPS Damping Values (Shot 2)

Relavtive Percentage of Improvement in Russell's Comprehensive Error Correlation Shot 2 (Vertical Direction)			
Sensor	**Node**	**Ship Compartment Location**	**Percent Relavtive Change**
V2002V	142489	4th Deck, Bow	32.13%
V2007V	210430	4th Deck, Forward	18.73%
V2009VI	210808	4th Deck, Forward	36.25%
V2008VI	210894	4th Deck, Forward	21.86%
V2108V	212196	1st Deck, Bow	4.32%
V2010V	220589	4th Deck, Forward	15.85%
V2012VI	221102	4th Deck, Forward	12.91%
V2011VI	221188	4th Deck, Forward	25.59%
V2013V	221601	4th Deck, Amidships	-0.26%
V2124V	222060	1st Deck, Forward	-2.25%
V2125V	222436	1st Deck, Forward	24.30%
V2014V	230461	4th Deck, Amidships	14.25%
V2016V	242399	4th Deck, Amidships	20.32%
V2026V	312302	4th Deck, Amidships	14.35%
V2034V	330759	3rd Deck, Aft	-27.43%
V2035V	330769	1st Deck, Bow	31.57%
V2019V	340167	3rd Deck, Aft	17.59%
Average Improvement in Correlation			24.58%

From investigation of the velocity meter data it was clear that the magnitude correlation was acceptable in most cases, and that the phase error accounted for the majority of the error. Thus, further analysis was conducted using a time history of only 250 msec, in the order to try and isolate the early time response. Table 19 provides the Russell's Comprehensive error factors for the shorter 250 msec comparisons. Table 20 shows the relative change in Russell's Comprehensive error factor. On average the RC value improved about 30% when the response time was limited to the early time frame.

Table 19. Selected Russell's Error Factors for Shot 2 (250 msec)

Ship Shock Simulation with Shot 2 Geometry, Dense Mesh and 738 in Cavitation Depth												
Sensor	Node	Mounting Type	Location (in)*			Shock Trial Data vs. 4% Damping			Shock Trial Data vs. NPS Damping		
						SHIP SHOCK TRIAL DATA (<250HZ)			SHIP SHOCK TRIAL DATA (<250HZ)		
						LS-DYNA/USA DATA (<250HZ)			LS-DYNA/USA DATA (<250HZ)		
			x	y	z	RM	RP	RC	RM	RP	RC
V2000V	120217	Keel	5328	0	82	-0.1565	0.2703	0.2768	-0.2817	0.2599	0.3397
V2009VI	210808	Bulkhead	4080	-176	171	0.1373	0.2595	0.2600	-0.0630	0.1868	0.1747
V2013V	221601	Bulkhead	3504	0	280	0.1254	0.1142	0.1503	-0.0700	0.0934	0.1034
V2124V	222060	Bulkhead	3504	-375	390	0.0511	0.2024	0.1850	-0.1418	0.1720	0.1976
V2034V	330759	Keel	1152	-135	193	0.0376	0.1439	0.1318	-0.1138	0.1456	0.1638
V2020V	350052	Keel	288	0	211	-0.0962	0.2610	0.2456	-0.2161	0.2423	0.2877
Russell Error Correlation					Sum(E(X))	0.09870	1.25130	1.24950	-0.88640	1.10000	1.26690
	> 0.28	Poor			Sum(E(X^2))	0.07235	0.28324	0.27872	0.16798	0.22066	0.30526
	< 0.15	Excellent			**Mean**	**0.01645**	**0.20855**	**0.20825**	**-0.14773**	**0.18333**	**0.21115**
Runtime = 250 msec					Standard Deviation	0.11893	0.06675	0.06085	0.08606	0.06163	0.08689

* Referenced to the G&C NASTRAN Model coordinate origin located at the stern.

Table 20. Russell's Comprehensive Error Factor for Early Time Response

Sensor	Node	Mounting Type	Location (in)			Relative Change for 250 msec vs. 500 msec	
			x	y	z	4% Damping	NPS Damping
V2000V	120217	Keel	5328	0	82	6.99%	10.61%
V2009VI	210808	Bulkhead	4080	-176	171	23.26%	19.12%
V2013V	221601	Bulkhead	3504	0	280	3.72%	33.93%
V2124V	222060	Bulkhead	3504	-375	390	22.98%	19.54%
V2034V	330759	Keel	1152	-135	193	19.83%	21.81%
V2020V	350052	Keel	288	0	211	13.06%	10.62%
			Mean Relative Change			29.63%	30.97%

5. Accelerometer Data

When looking at only the accelerometer data for the 500 msec time history response comparisons, it was determined that there was an improvement 31% over the complete data set and a 39% improvement over the velocity meter only data comparisons. The excellent precision in the data points obtained from the NPS damping value simulations is clearly shown in Figure 47. Nearly all the points have an excellent correlation rating, while those from the 4% fixed damping simulations are only marginally acceptable or have poor correlation.

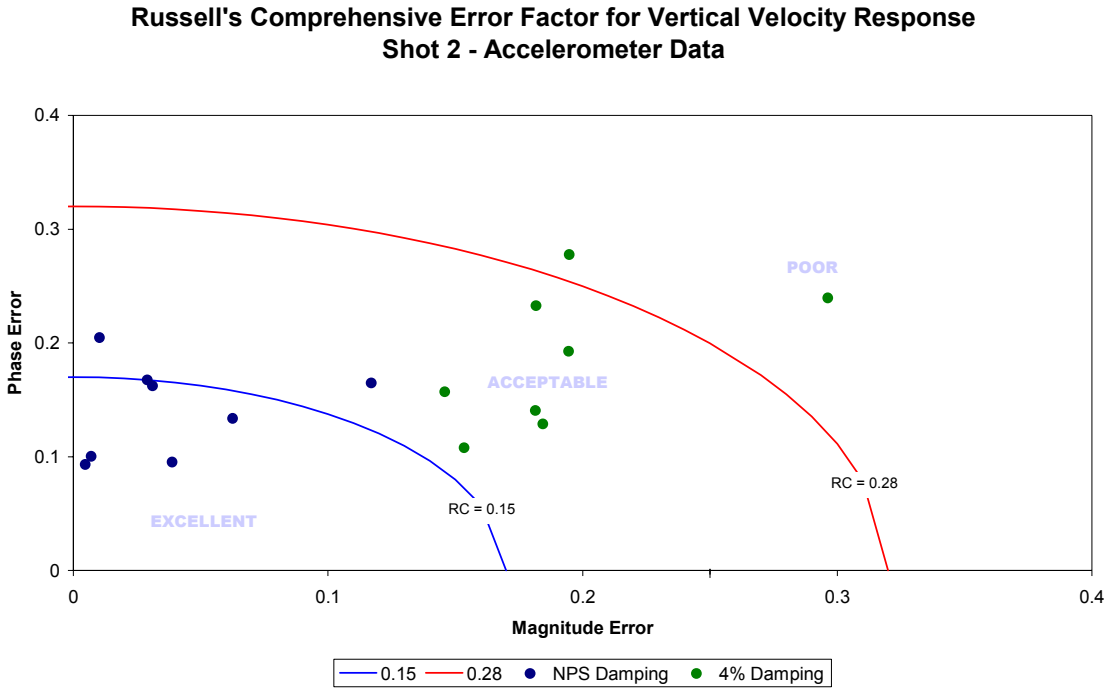

Figure 47. Russell's Comprehensive Error Factor for Shot 2 (Accelerometer Data)

Figures 48 through 55 show the excellent correlation of the accelerometer data from the DDG-81 ship shock trial simulations performed using the new NPS damping coefficient values. The Russell's error factors for these figures are provided in Table 21.

Table 21. Damping Comparison Results for DDG-81 Shot 2 (Accelerometer)

Ship Shock Simulation with Shot 2 Geometry, Dense Mesh and 738 in Cavitation Depth												
Sensor	Node	Mounting Type	Location (in)*			Shock Trial Data vs. 4% Damping SHIP SHOCK TRIAL DATA (<250HZ) LS-DYNA/USA DATA (<250HZ)			Shock Trial Data vs. NPS Damping SHIP SHOCK TRIAL DATA (<250HZ) LS-DYNA/USA DATA (<250HZ)		
			x	y	z	RM	RP	RC	RM	RP	RC
A8516V	210993	Bulkhead	1591	36	453	0.1945	0.1927	0.2426	0.0311	0.1623	0.1464
A2104V	222240	Bulkhead	3504	0	390	0.1535	0.1079	0.1663	-0.0388	0.0953	0.0912
A3565V	231696	Bulkhead	2952	-81	317	0.1817	0.2328	0.2617	0.0290	0.1675	0.1506
A2310V	320746	Bulkhead	1536	0	177	0.1948	0.2776	0.3005	0.0103	0.2047	0.1816
A2116V	414367	Deck	3504	0	702	0.1844	0.1288	0.1993	0.0070	0.1003	0.0891
A2109V	414953	Bulkhead	4059	0	723	0.2963	0.2395	0.3376	0.1170	0.1647	0.1790
A2240V	416269	Mast	3504	-135	848	0.1459	0.1571	0.1900	-0.0626	0.1335	0.1307
A2237V	416419	Mast	3504	135	848	0.1815	0.1405	0.2034	0.0047	0.0931	0.0826
Russell Error Correlation			Sum(E(X))			1.53260	1.47690	1.90140	0.09770	1.12140	1.05120
	> 0.28	Poor	Sum(E(X^2))			0.30838	0.29840	0.47646	0.02110	0.16906	0.14929
	< 0.15	Excellent	**Mean**			**0.19158**	**0.18461**	**0.23768**	**0.01221**	**0.14018**	**0.13140**
Runtime = 500 msec			Standard Deviation			0.04594	0.06065	0.05922	0.05333	0.04117	0.03994

* Referenced to the G&C NASTRAN Model coordinate origin located at the stern.

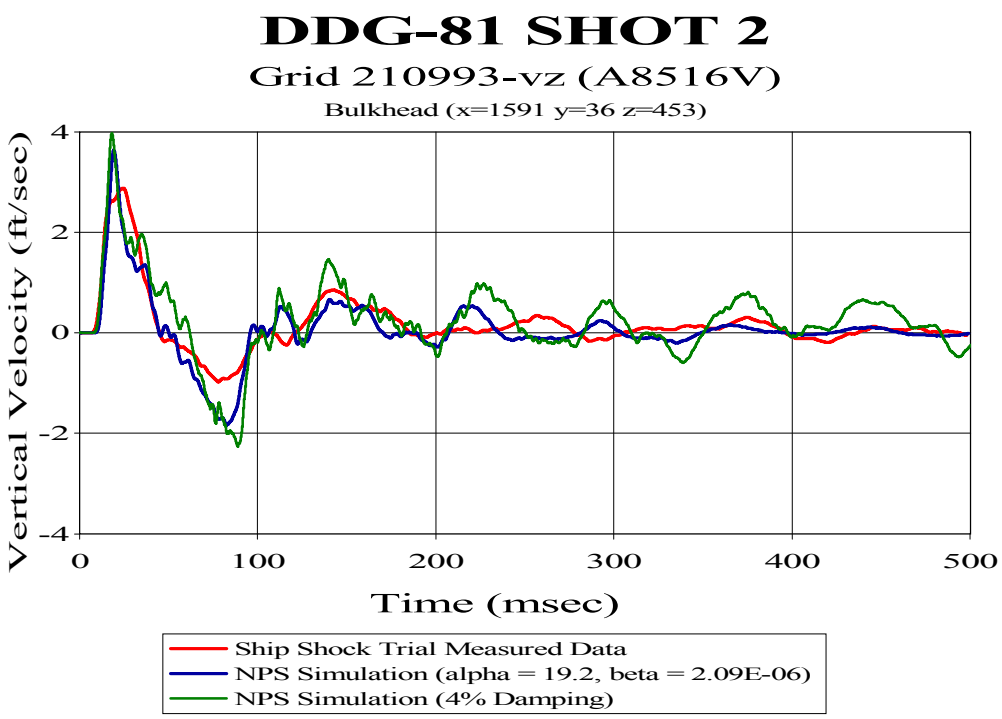

Figure 48. Bulkhead Sensor A8516V

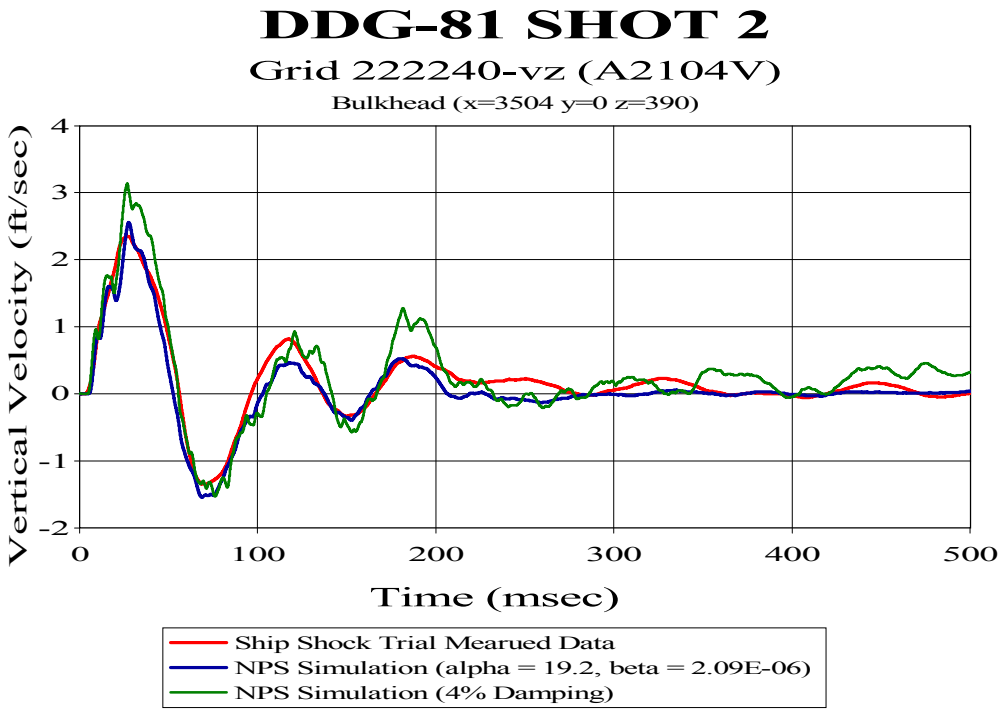

Figure 49. Bulkhead Sensor A2104V

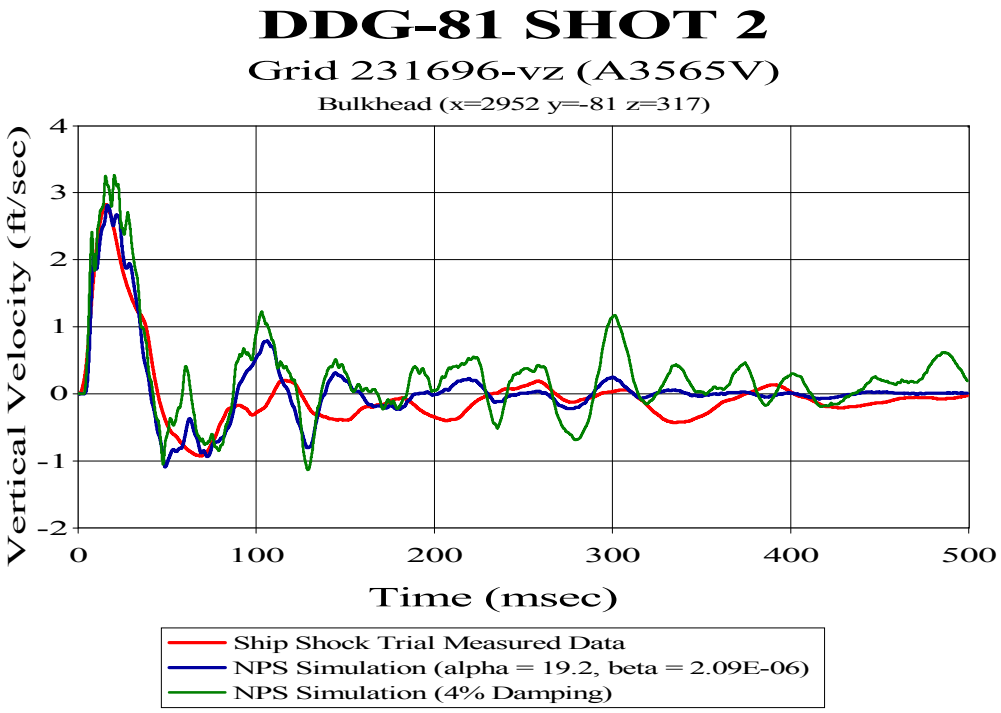

Figure 50. Bulkhead Sensor A3565V

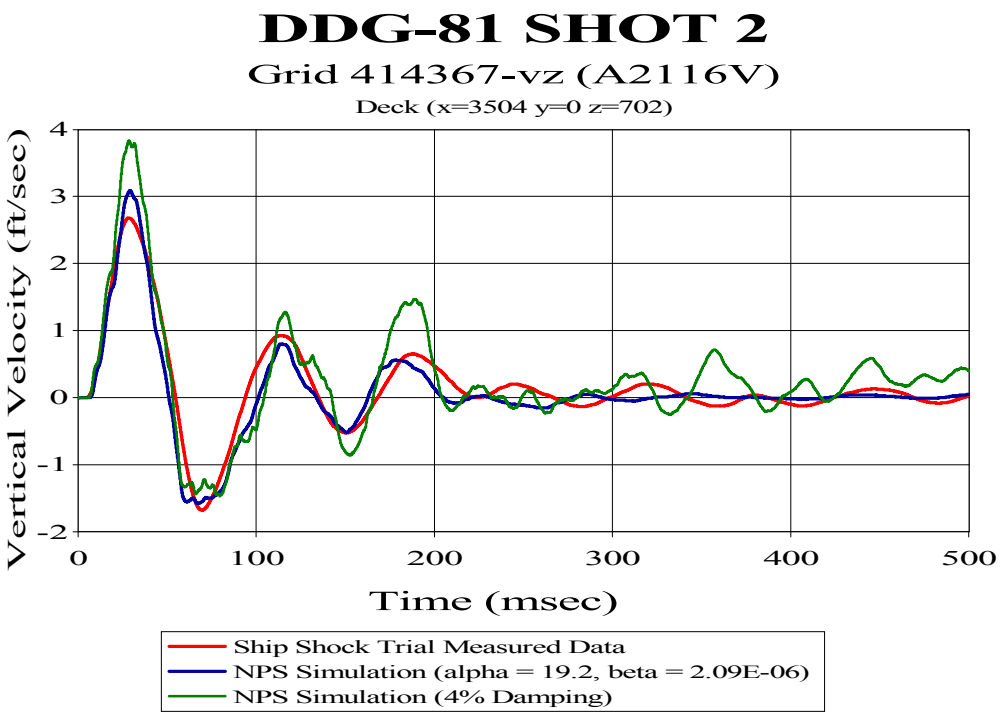

Figure 51. Bulkhead Sensor Bulkhead

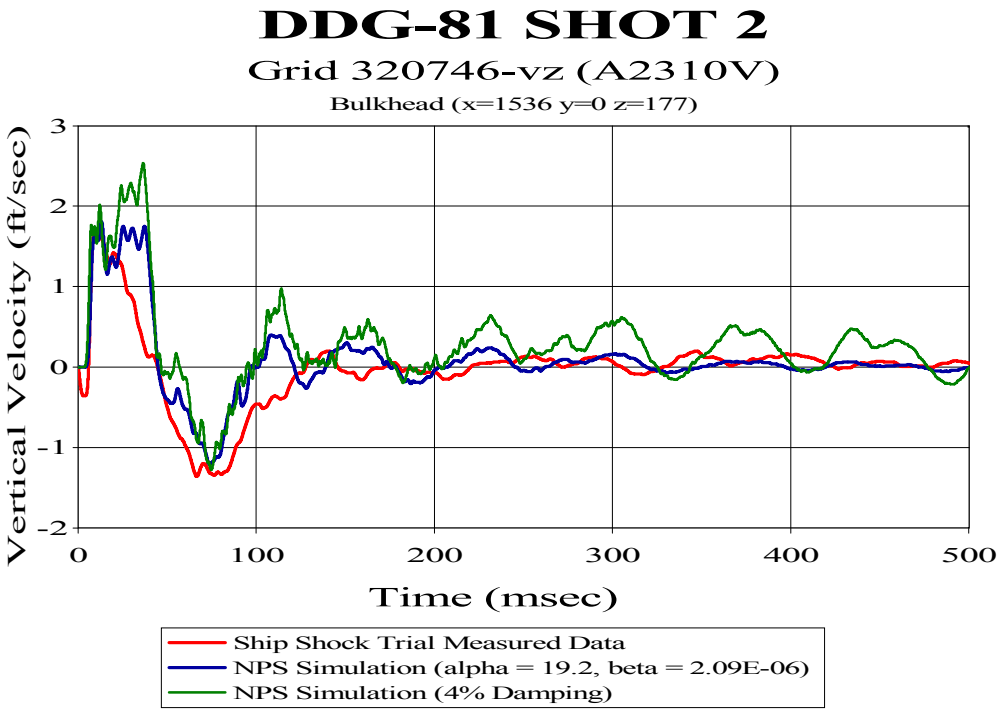

Figure 52. Deck Sensor A2116V

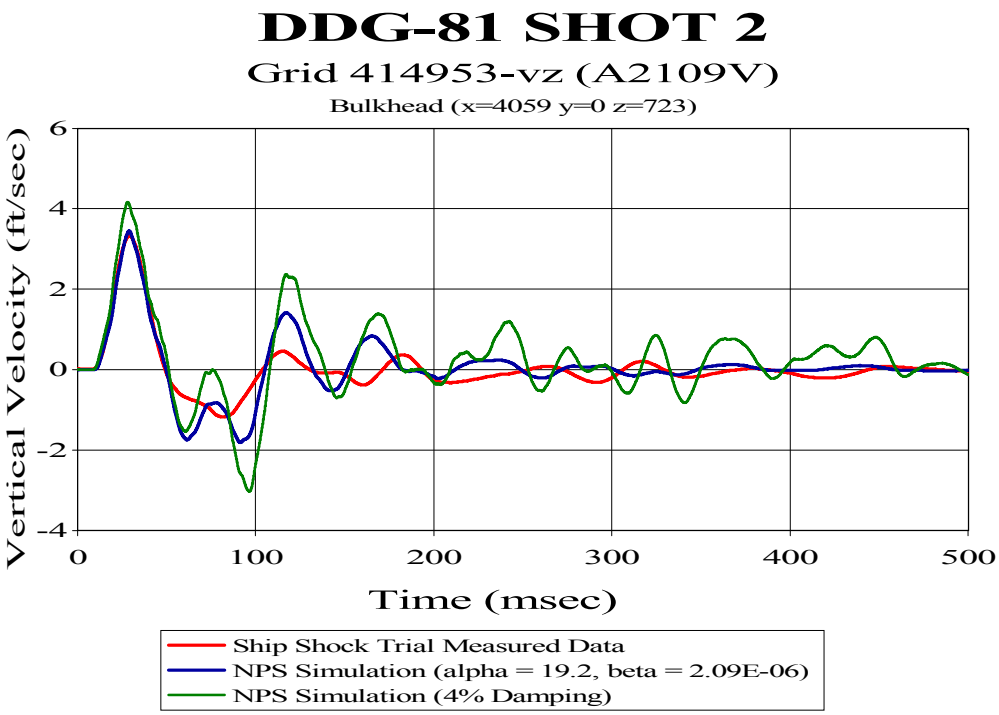

Figure 53. Bulkhead Sensor A2109V

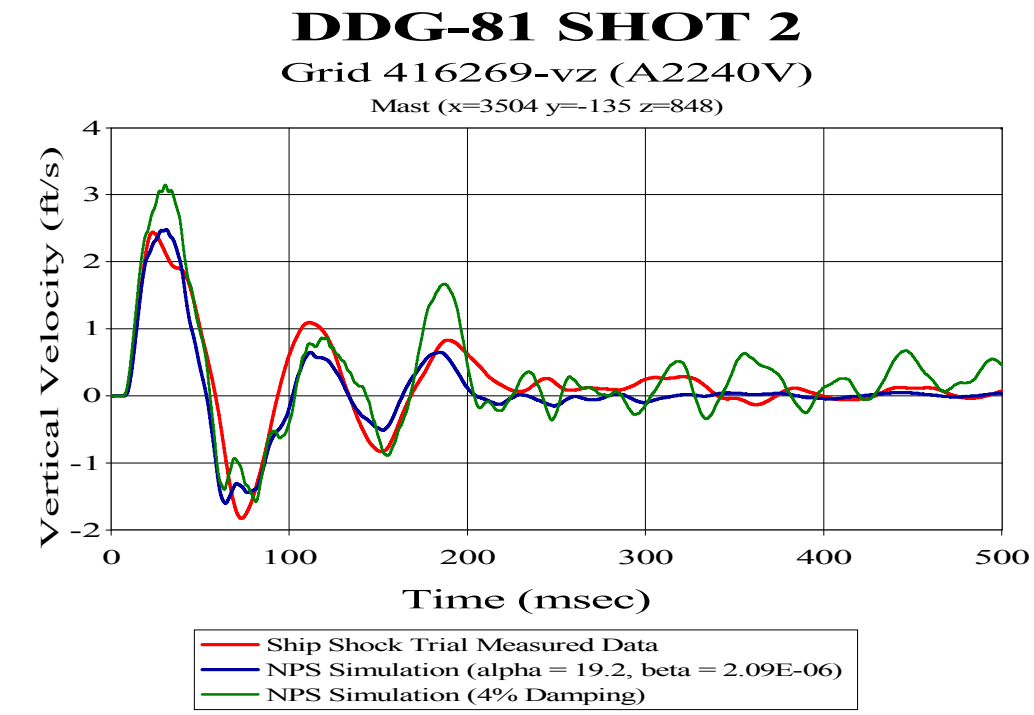

Figure 54. Mast Sensor A2240V

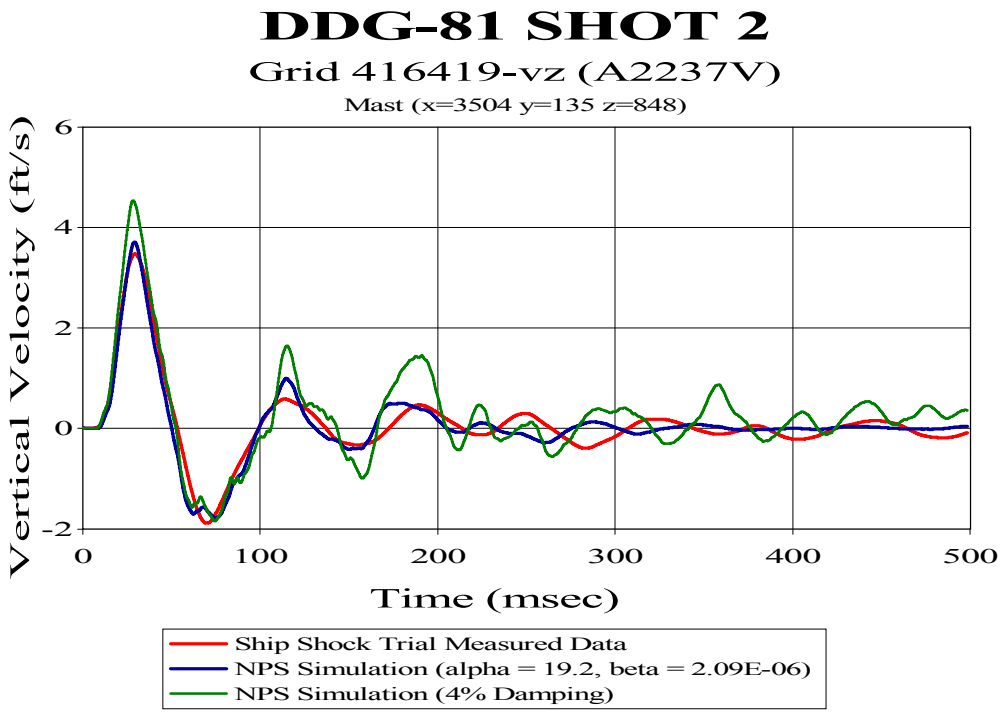

Figure 55. Mast Sensor A2237V

THIS PAGE INTENTIONALLY LEFT BLANK

VII. CONCLUSION AND RECOMMENDATIONS

A. SUMMARY OF FINDINGS

Based upon the finding presented herein, and those referenced throughout this paper, it becomes evident that the modeling and simulation methodology developed at the Naval Postgraduate School Shock and Vibration Computational Laboratory is valid for the simulation of naval surface ship system response resulting from the standard LFT&E UNDEX event designed to test the ship up to a two-thirds design limit. This thesis investigated the primary system response in the Combat Information Center area as well as the shipwide secondary response in the athwartship direction. In addition, the vertical velocity response data obtained through the use of the new Rayleigh damping coefficients developed at the Naval Postgraduate School were compared against existing damping coefficient values previously employed in the DDG-53 ship shock trial simulations. With the exception of the athwartship damping analysis, which determined the simulation data to be only marginally acceptable, the results produces from this series of parametric studies were all highly favorable in nature.

The Combat Information Center is a critical compartment within a naval surface combatant. For this reason it is imperative that the watchstanders and equipment located in this space be able to not only withstand the initial shock but also be able to continue to properly function after being subjected to and UNDEX event. The nodal simulation conducted for the CIC sensors showed a solid correlation with the measured data from the DDG-81 ship shock trial. The results from this localized area, deep in the heart of the ship, proved to be consistent with the primary velocity response correlations performed at the shipwide level.

The athwartship velocity response results were less promising than were anticipate, but not truly unexpected. The very nature of the data is much different from that of the vertical response. The magnitudes witnessed in the athwartship direction are routinely on the order of a magnitude smaller than those in the primary response direction. Although the correlation was less acceptable by the Russell's Comprehensive error factor standards of RC < 0.28, there appeared to be a bias, rather than a random type

error associated with the excursion from the measured response data. Suspect in the analysis was the drift error, which seemed to have overwhelmed the response data comprised of much smaller velocities. Additionally, the pronounced phase error observed in the simulated athwartship data appeared to distort the overall correlation. Further investigation is highly recommended in this area, specifically with respect the late time phase error.

Finally, this study also concluded that the new set of system damping coefficients developed at NPS by Shin and Ham show a distinct improvement in correlation over the previously employed 4% fixed damping. The results of this study support the further use of these new Rayleigh damping coefficients in the DDG-81 ship shock trial modeling and simulation effort. In doing so, it was also confirmed that accelerometer data was better suited for comparison of the simulated data against the measured shock trial data.

B. FUTURE WORK

There is still much work to be done in the modeling and simulation of UNDEX events. A few possibilities for further course of study are offered to that end. Having validated the NPS methodology used in simulating the current two-thirds design limit shock trial, scaling the charge shock factor to full scale shot at the design limit or higher is the next logical step in this simulation effort. Successful completion of a full-scale shock trial simulation would allow ship designers to glean valuable information concerning the limiting design case, previously unobtainable by conventional testing means. The gains attained through the global analysis of the DDG-81 ship shock trial simulation effort suggest focused study of localized phenomena experienced during an UNDEX event such as whipping. In order to further enhance the simulation of DDG-81 ship shock trials the effects derived from the introduction of elasto-plastic material properties within the finite element model of the ship should be investigated. Lastly, as was previously mentioned, the secondary system response in the athwartship direction requires further investigation. Ultimately, it is desired to be able to apply the modeling and simulation techniques that have been developed here at the Naval Postgraduate School to other ship classes through a set of design parameters based on the findings ascertained through the investigation of the DDG-53 and DDG-81 ship shock trials.

APPENDIX A. BULK CAVITATION ZONE PROGRAM

The following program code was written using MATLAB® 6.1 release 12.1. The purpose of this program is to compute the bulk cavitation zone boundaries and create a visualization of the bulk cavitation zone.

```
% Computation of Bulk Cavitation Zone for Underwater Explosions
% LT Jarema M. Didoszak, USN
% APR 2003, Last Modified DEC 2003
% SVCL, Naval Postgraduate School, Monterey, CA

% This program is used to develop the bulk cavitation
% envelope for an underwater charge of PETN at various
% charge weights and depths.

clear; clc;
% Parameter definitions are for PETN type charge
K1 = 24589;       % Pmax
A1 = 1.194;       % Pmax
K2 = 0.052;       % Decay constant
A2 = -0.257;      % Decay constant

% Constants
Pa = 14.7;                  % Atmpospheric pressure (psi)
Gamma = 62.5/144;           % Weight density of water (lb/ft^3)
C = 5;                      % Acoustic velocity of water (ft/msec)

counter = 0;
i = 1;

for W = [100,200,300];              % Equivalent charge weights (lb)
   for D1= [25,50,75];              % Charge location depths (ft)
      counter = counter+1;
      A=zeros(50,1000);
      for y = 1:51;
         for x = 1:1001;
            R1 = sqrt((D1 - (y-1))^2 + (x-1)^2);    % Distance from charge to desired location (ft)
            R2 = sqrt((D1 + (y-1))^2 + (x-1)^2);    % Distance from image charge to desired location (ft)

            theta = K2*(W^(1/3))*(((W^(1/3))/R1)^(A2));                 % Decay Constant (msec)

            Pi = (K1*(W^(1/3)/R1)^(A1))*(exp(-(R2 -R1)/(C*theta)));     % Incident Pressure Wave (psi)
            Ph = Gamma*(y-1);                                           % Hydrostatic Pressure at y (psi)
            Pr = (K1*((W^(1/3)/R2)^(A1)));                              % Refelcted Pressure Wave (psi)



            F =  Pi + Pa + Ph - Pr;                                     % Upper Bulk Caviataion Boundary

            G1 = -Pi/(C*theta)*(1+(((R2-2*D1*((D1+(y-1))/R2))/R1)*(A2*R2/R1-A2-1)));
            G2 = -(A1*Pi/R1^2)*(R2-2*D1*((D1+(y-1))/R2));
```

```
            G3 = Gamma*((D1+(y-1))/R2) ;
            G4 = (A1/R2)*(Pi+Pa + Ph);
            G = G1 + G2 + G3 + G4;                          % Lower Bulk Cavitation Boundary

            if F > 0.001;                                   % Combine Bulk Cavitation Boundaries
               if G < 0;
                  A(y,x) = 1;
               end
            end
            if G > 0;
               A(y,x) = 1;
            end
         end
      end
      temp(:,:,counter) = A;
   end

   charge=num2str(W);
   figure(i)          % Plots for 100 lb charge PETN
   orient landscape
   hold on
   subplot(3,1,1)
   spy(temp(:,:,1))
   title(['Bulk Cavitation Region for Underwater Explosion: ', charge , ...
         ' lb PETN Charge at 25ft'])
   xlabel('Radius (ft)')
   ylabel('Depth (ft)')
   subplot(3,1,2)
   spy(temp(:,:,2))
   title(['Bulk Cavitation Region for Underwater Explosion: ', charge, ...
         ' lb PETN Charge at 50ft'])
   xlabel('Radius (ft)')
   ylabel('Depth (ft)')
   subplot(3,1,3)
   spy(temp(:,:,3))
   title(['Bulk Cavitation Region for Underwater Explosion: ', charge, ...
         ' lb PETN Charge at 75ft'])
   xlabel('Radius (ft)')
   ylabel('Depth (ft)')

   i=i+1;
end
```

APPENDIX B. CIC VERTICAL VELOCITY RESPONSE PLOTS

A. SHOT 1

The following velocity plots are from the analysis of the Combat Information Center for Shot 1. The Russell's error factors for the corresponding data correlation follow each figure caption.

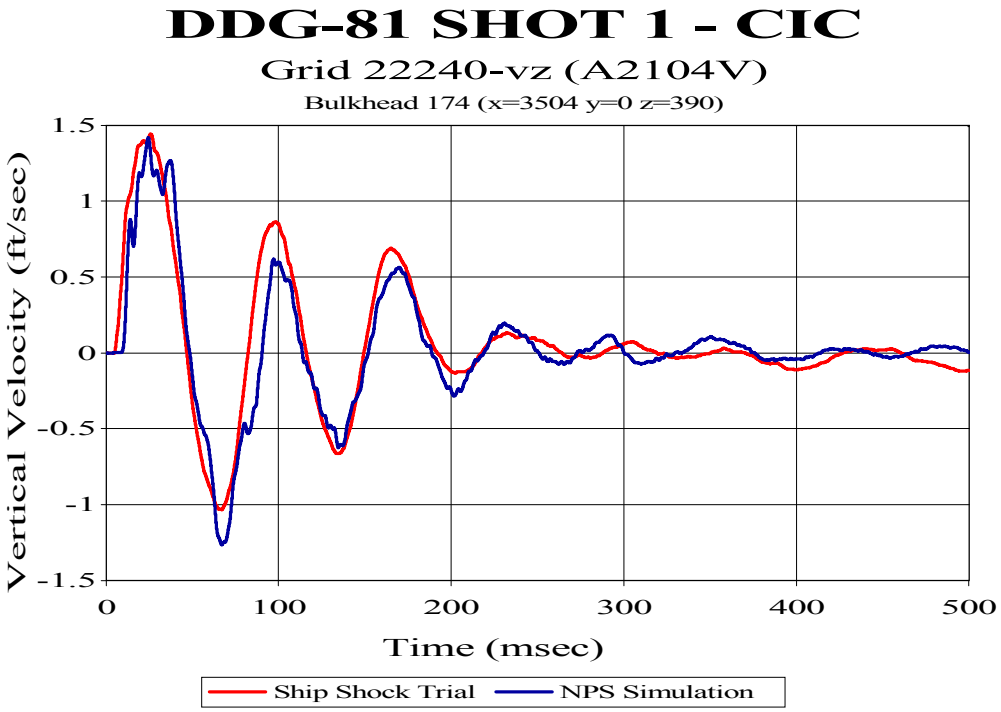

Figure 56. Deck Sensor A2104V: (RM = 0.0670, RP = 0.1270, RC = 0.1272)

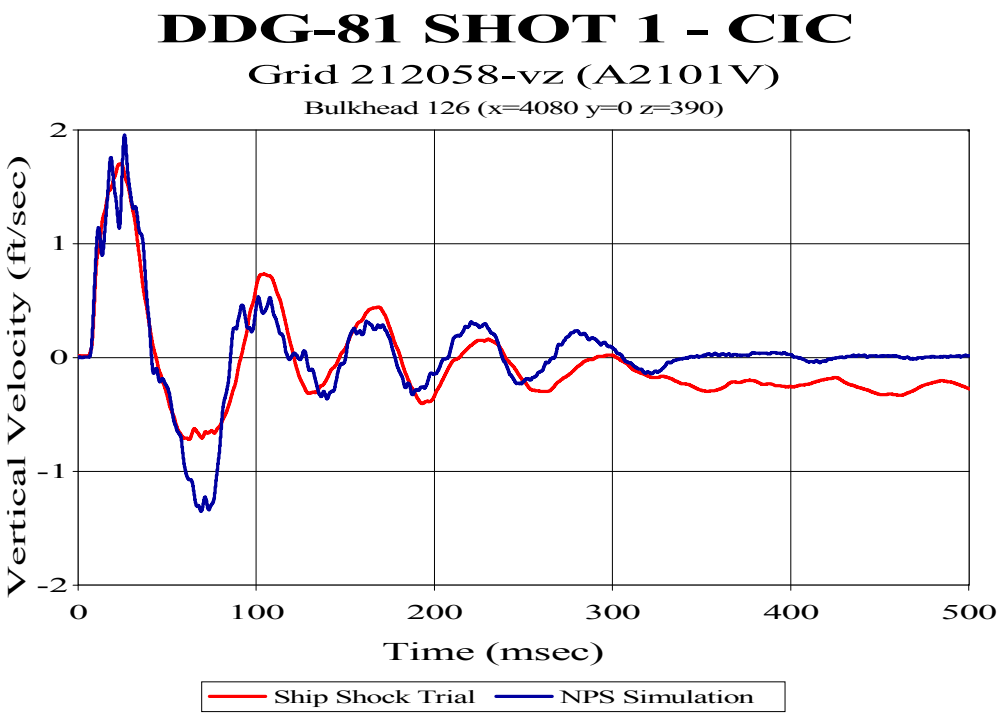

Figure 57. Deck Sensor A2101V: (RM = 0.0210, RP = 0.1736, RC = 0.1551)

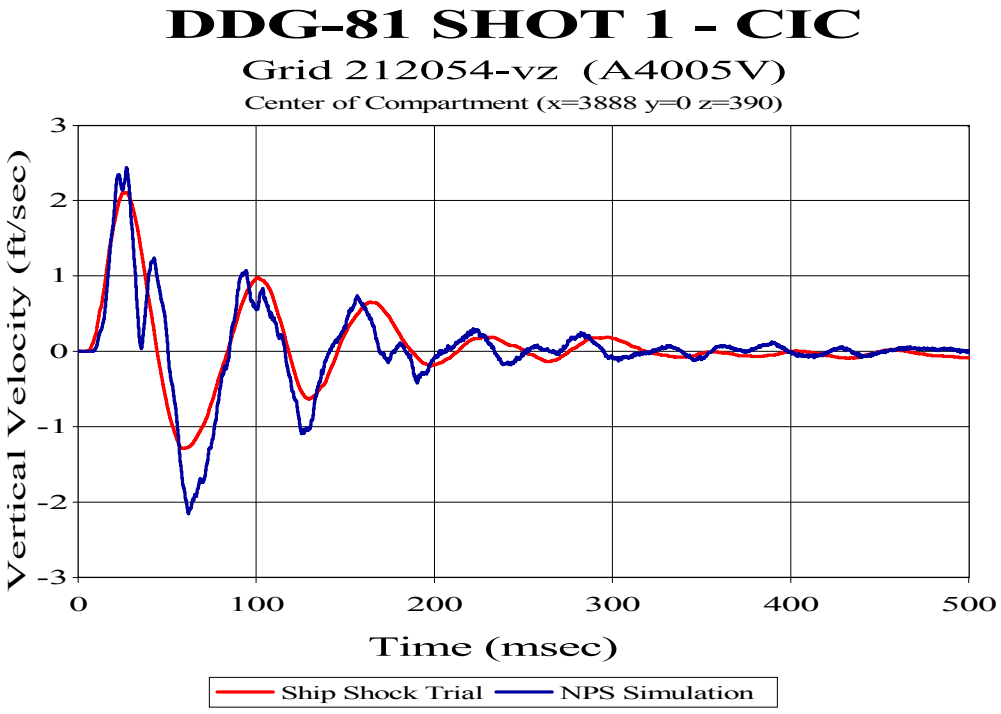

Figure 58. Deck Sensor A4005V: (RM = 0.0876, RP = 0.1637, RC = 0.1645)

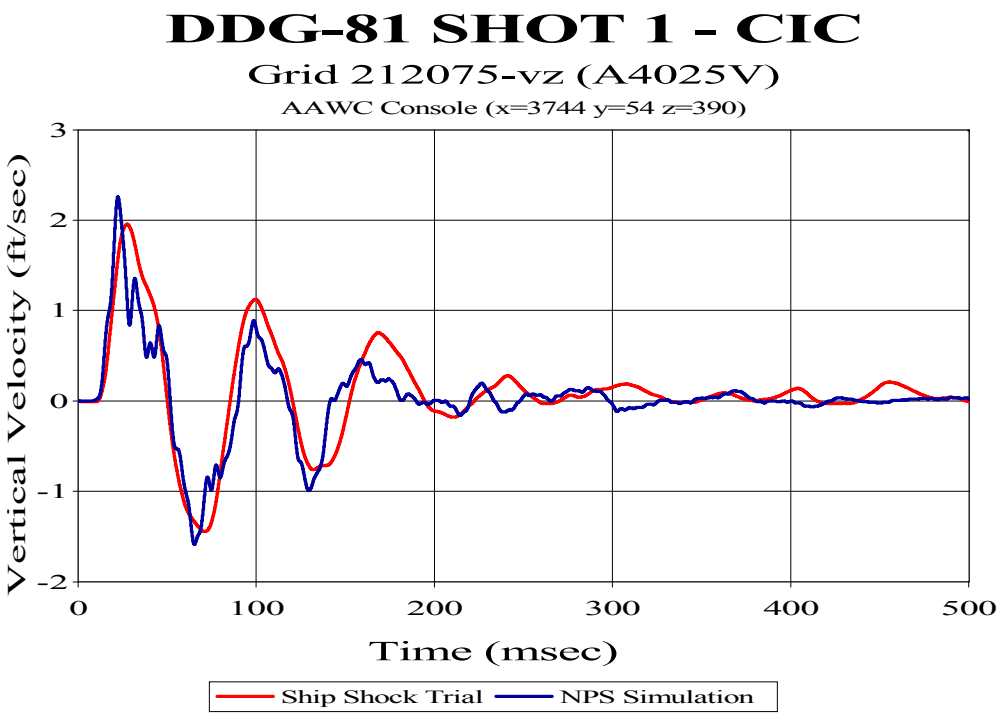

Figure 59. Deck Sensor A4025V: (RM = 0.1318, RP = 0.1522, RC = 0.1784)

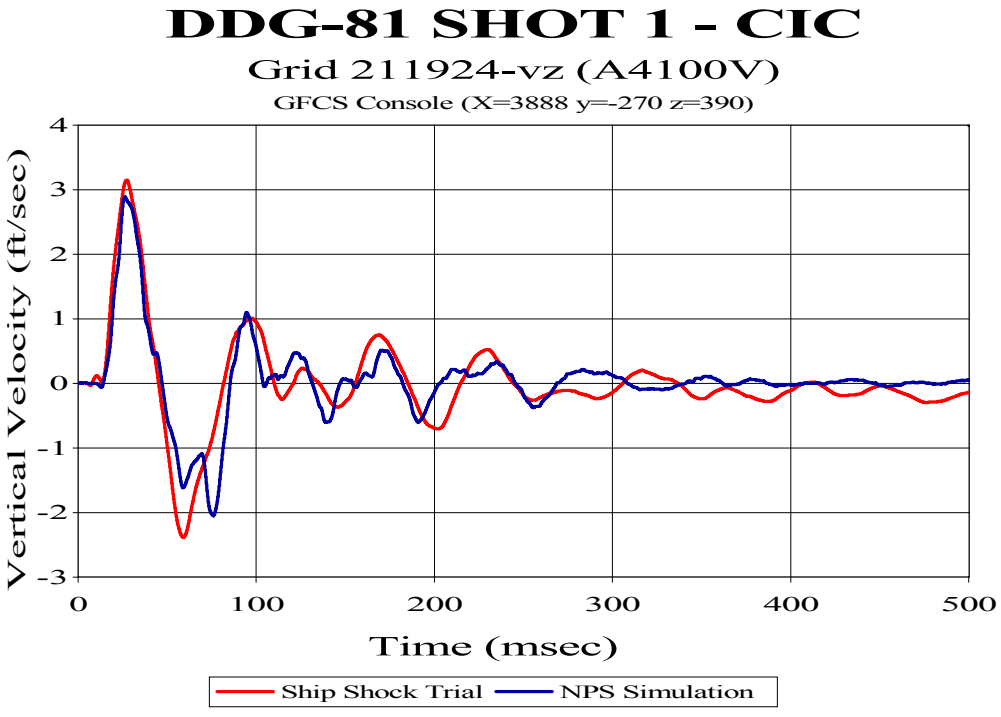

Figure 60. Deck Sensor A4100V: (RM = 0.1168, RP = 0.1566, RC = 0.1732)

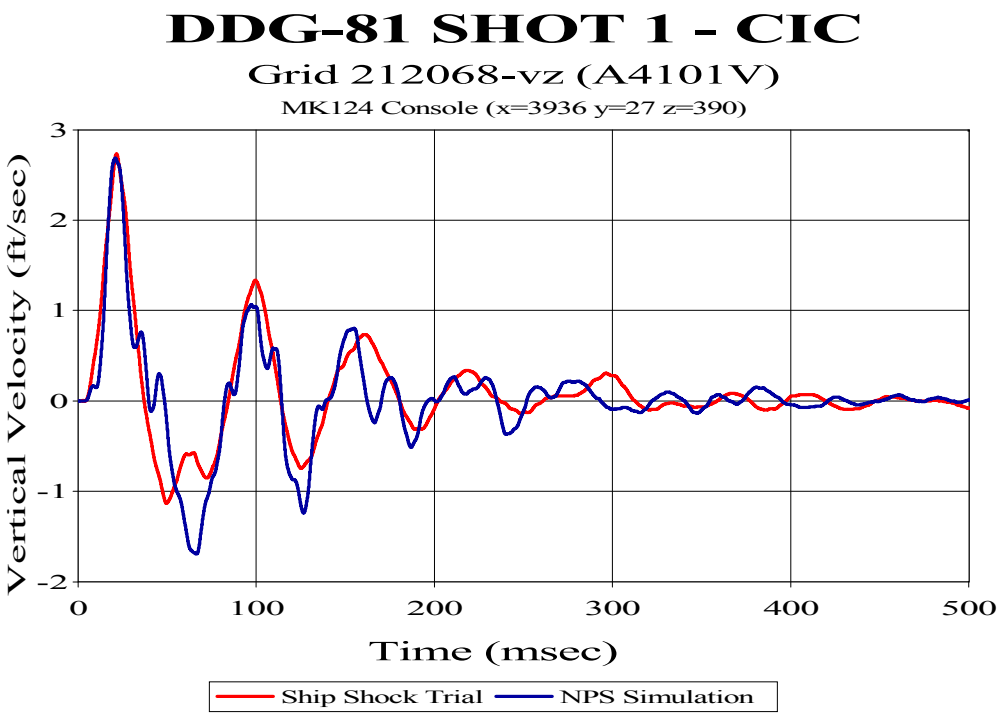

Figure 61. Deck Sensor A4101V: (RM = 0.0087, RP = 0.1687, RC = 0.1497)

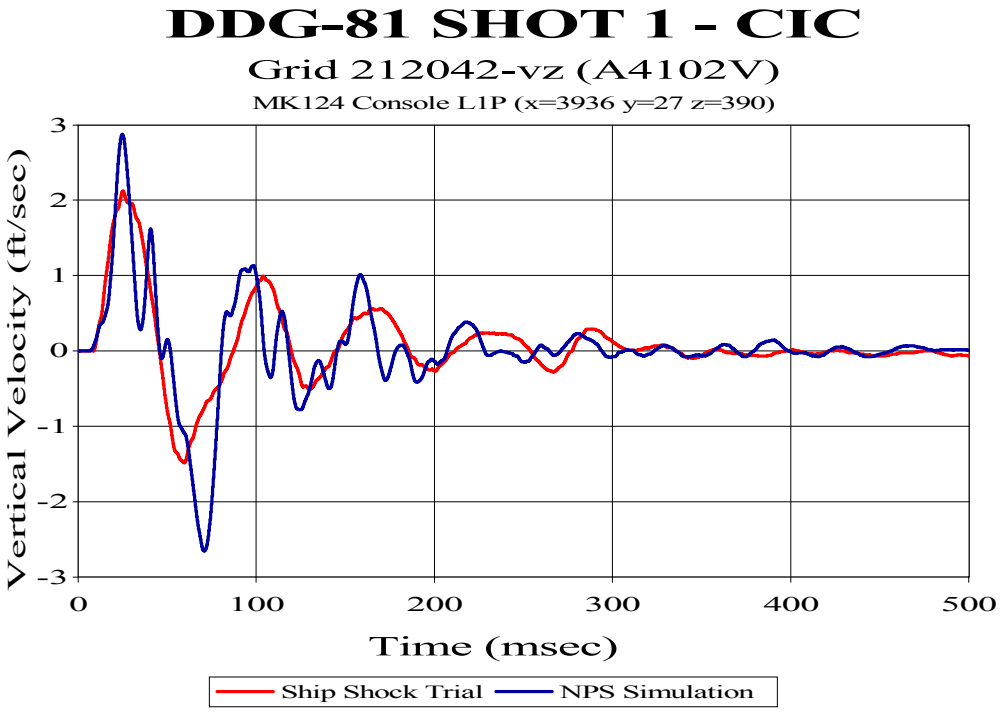

Figure 62. Deck Sensor A4102V: (RM = 0.1321, RP = 0.2234, RC = 0.2300)

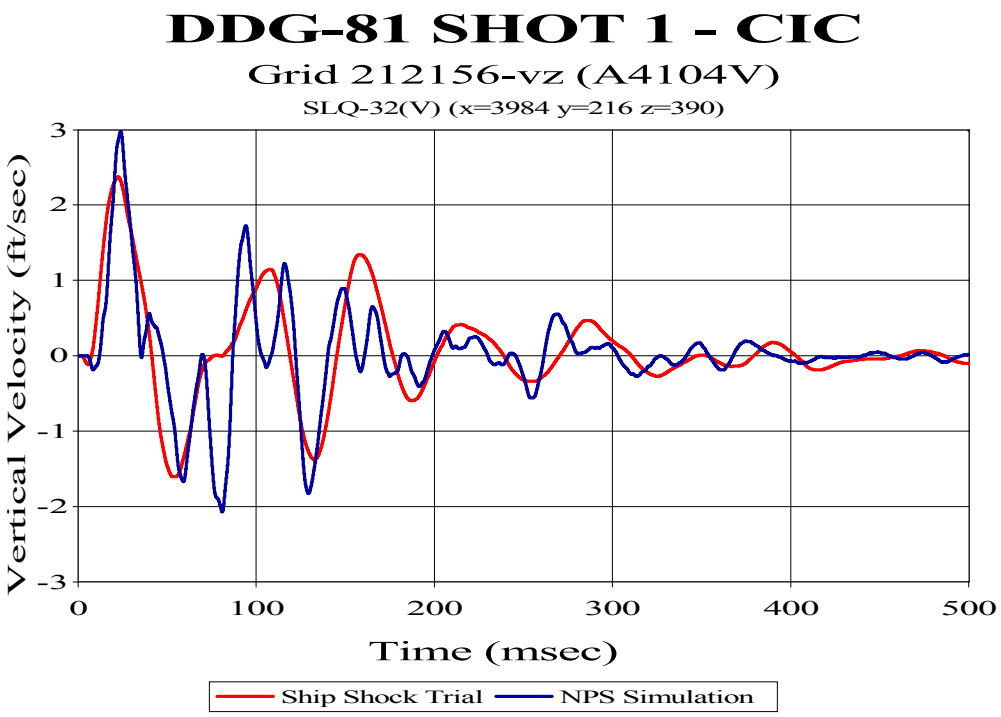

Figure 63. Deck Sensor A4104V: (RM = 0.0018, RP = 0.2525, RC = 0.2238)

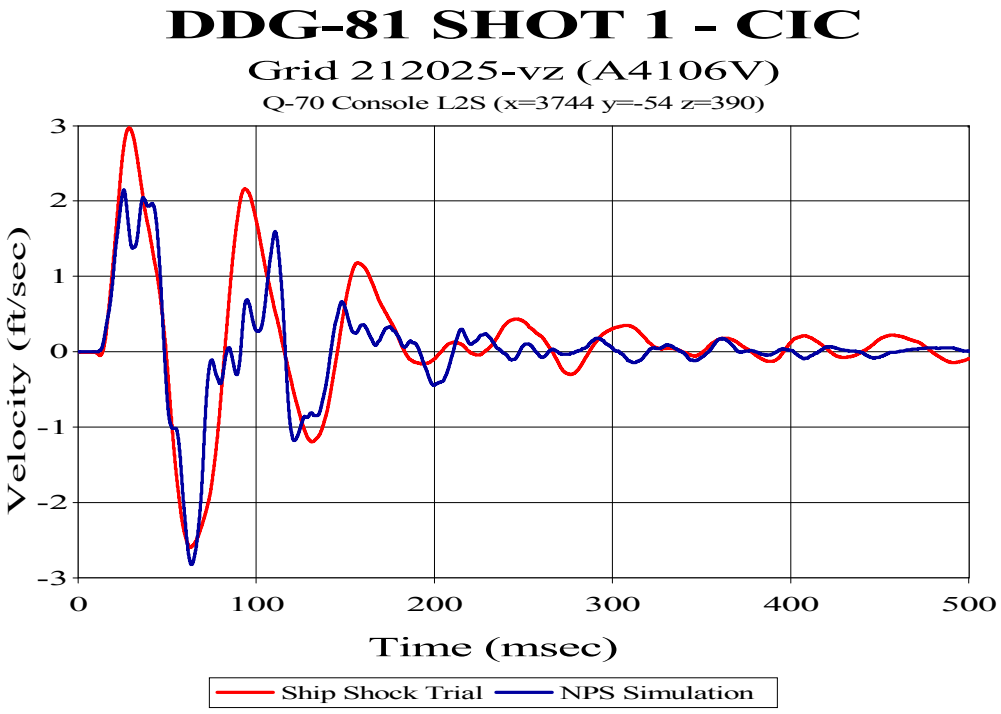

Figure 64. Deck Sensor A4106V: (RM = 0.1906, RP = 0.1903, RC = 0.2387)

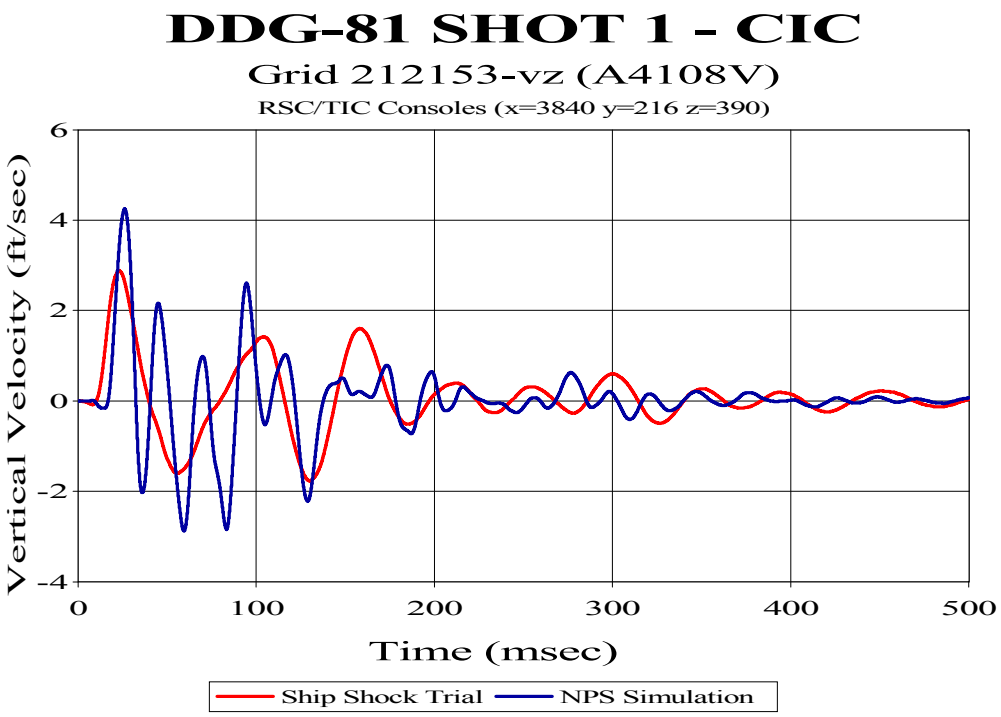

Figure 65. Deck Sensor A4108V: (RM = 0.1201, RP = 0.3270, RC = 0.3087)

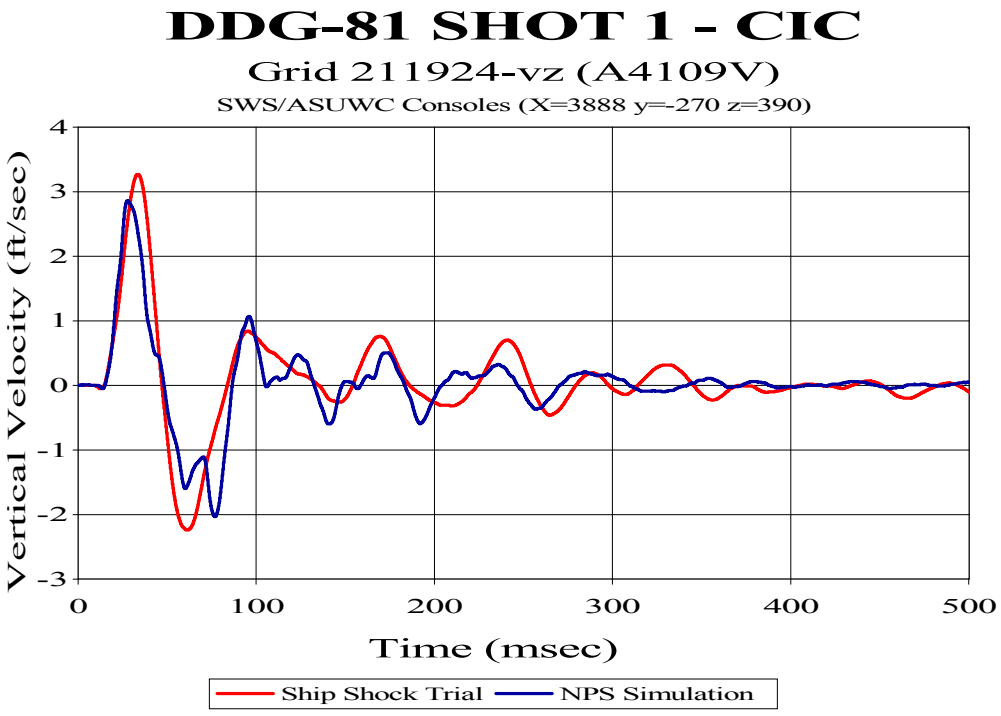

Figure 66. Deck Sensor A4109V: (RM = 0.1297, RP = 0.1685, RC = 0.1885)

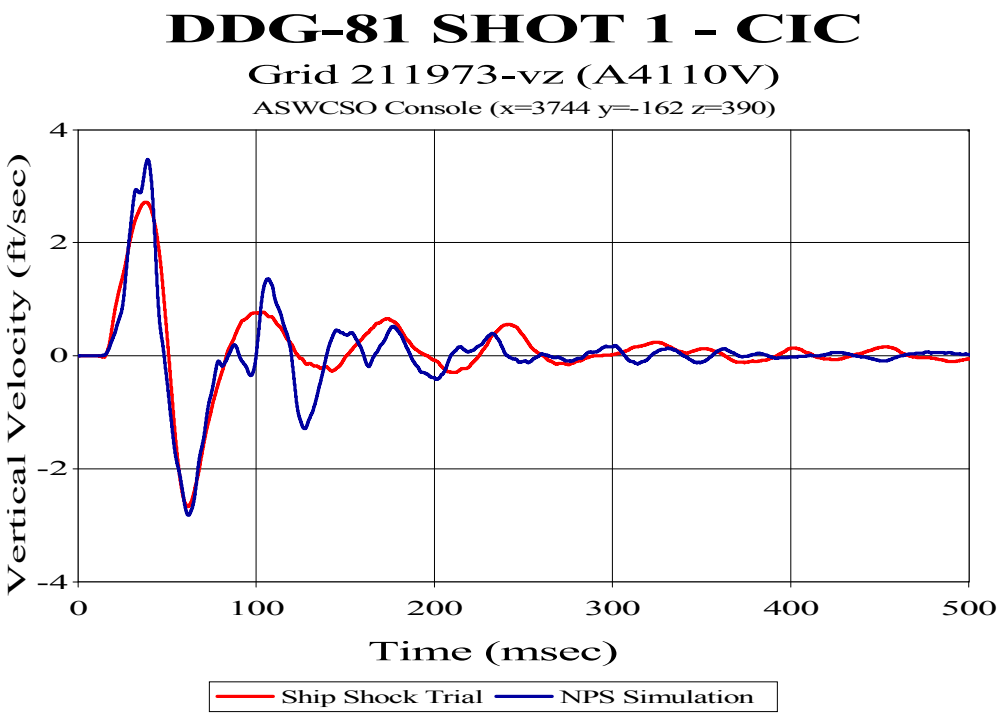

Figure 67. Deck Sensor A4110V: (RM = 0.0487, RP = 0.1472, RC = 0.1374)

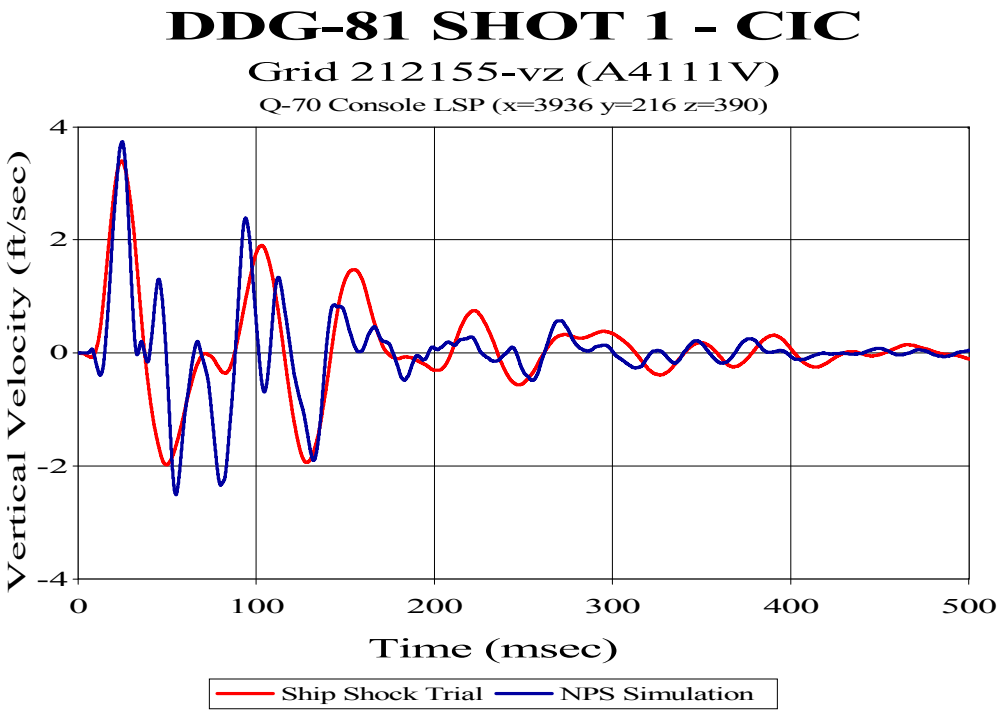

Figure 68. Deck Sensor A4111V: (RM = 0.0762, RP = 0.2701, RC = 0.2487)

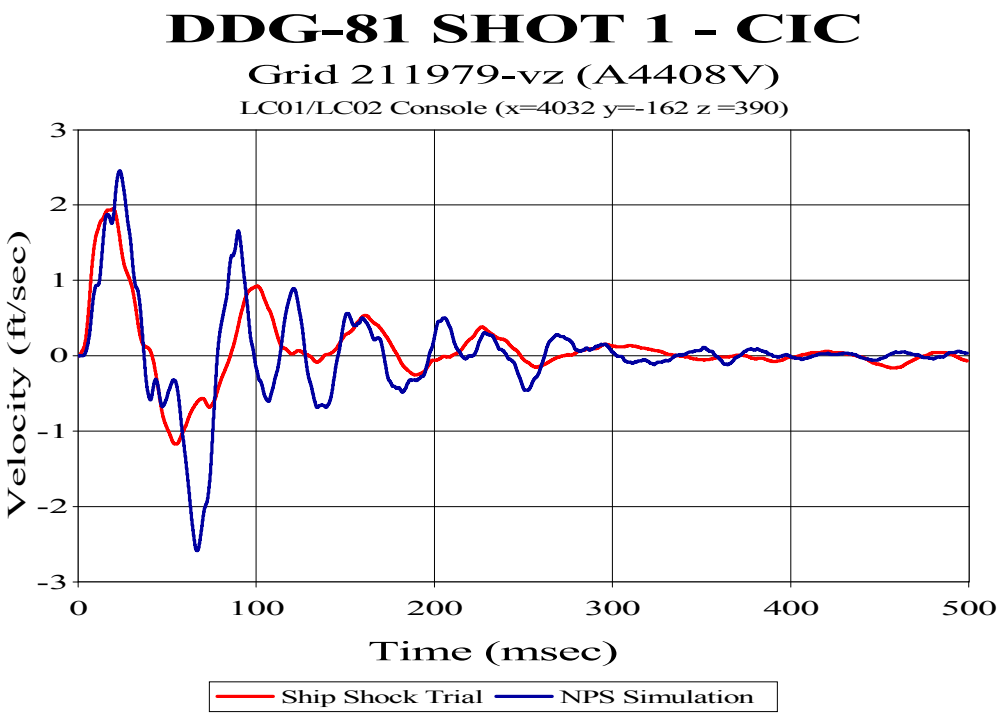

Figure 69. Deck Sensor A4408V: (RM = 0.2086, RP = 0.2501, RC = 0.2886)

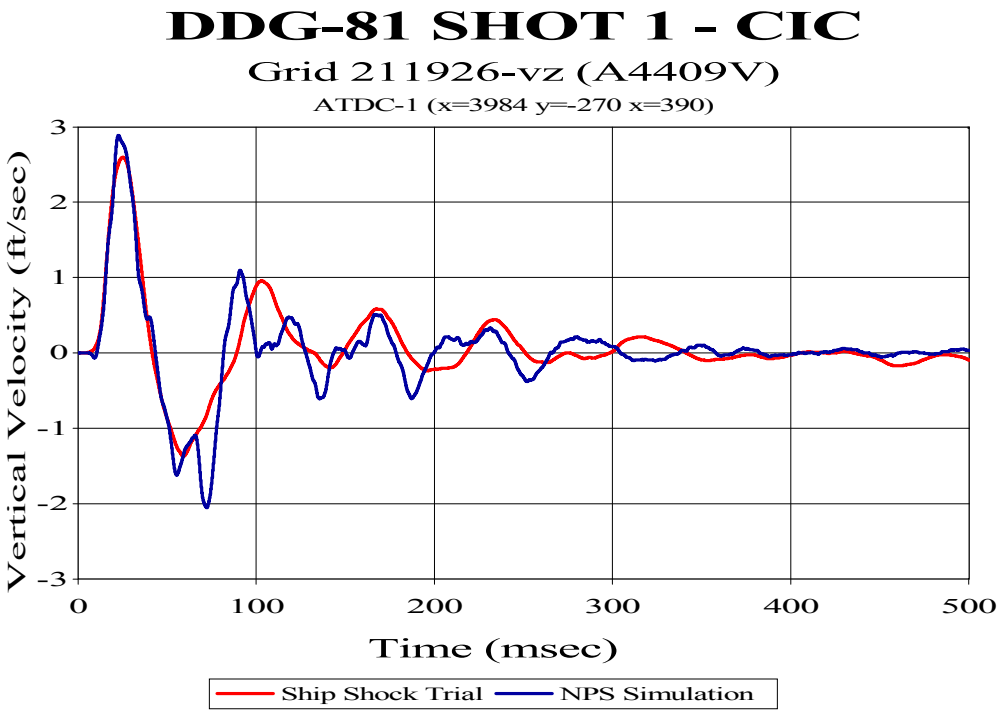

Figure 70. Deck Sensor A4409V: (RM = 0.0719, RP = 0.1589, RC = 0.1545)

B. SHOT 2

The following velocity plots are from the analysis of the Combat Information Center for Shot 2. The Russell's error factors for the corresponding data correlation follow each figure caption.

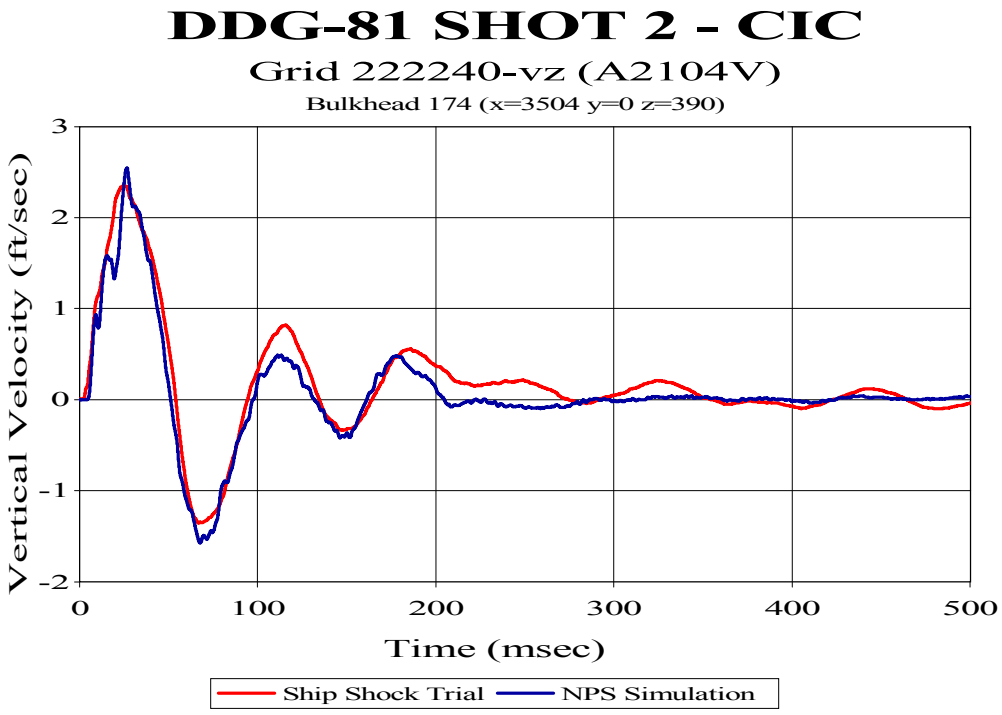

Figure 71. Deck Sensor A2104V: (RM = 0.0623, RP = 0.0902, RC = 0.0972)

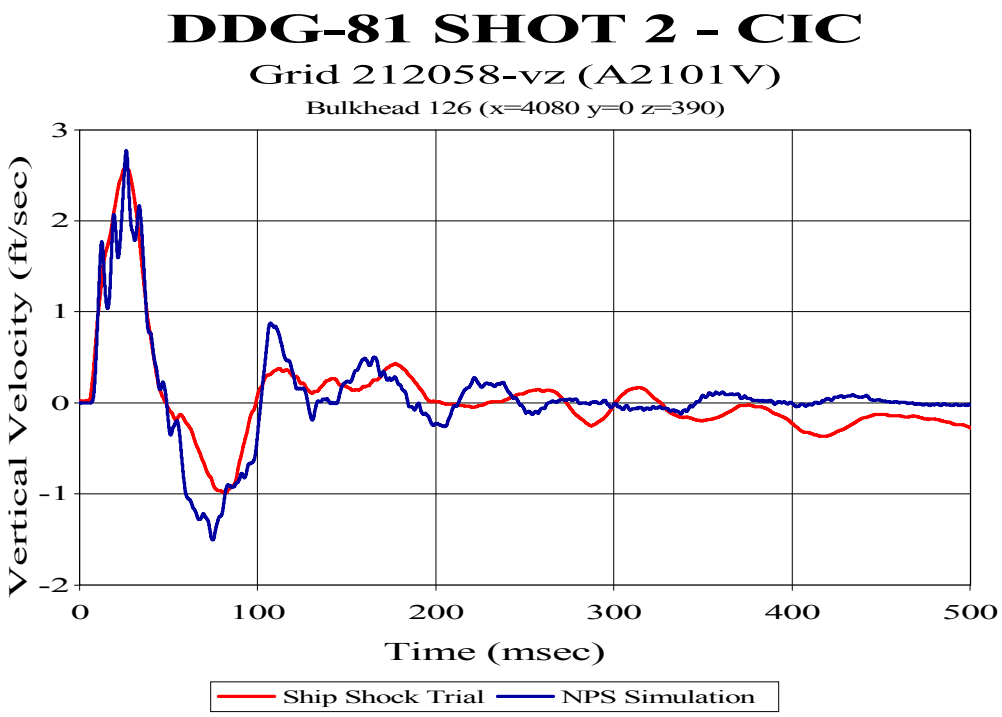

Figure 72. Deck Sensor A2101V: (RM = 0.0258, RP = 0.1498, RC = 0.1347)

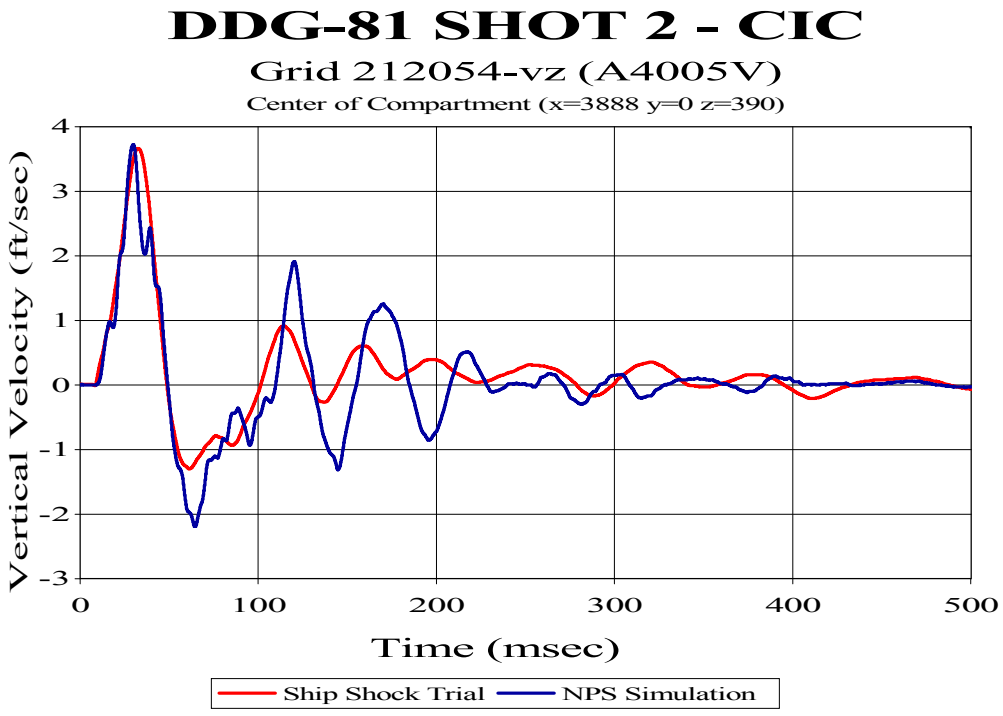

Figure 73. Deck Sensor A4005V: (RM = 0.0727, RP = 0.1815, RC = 0.1733)

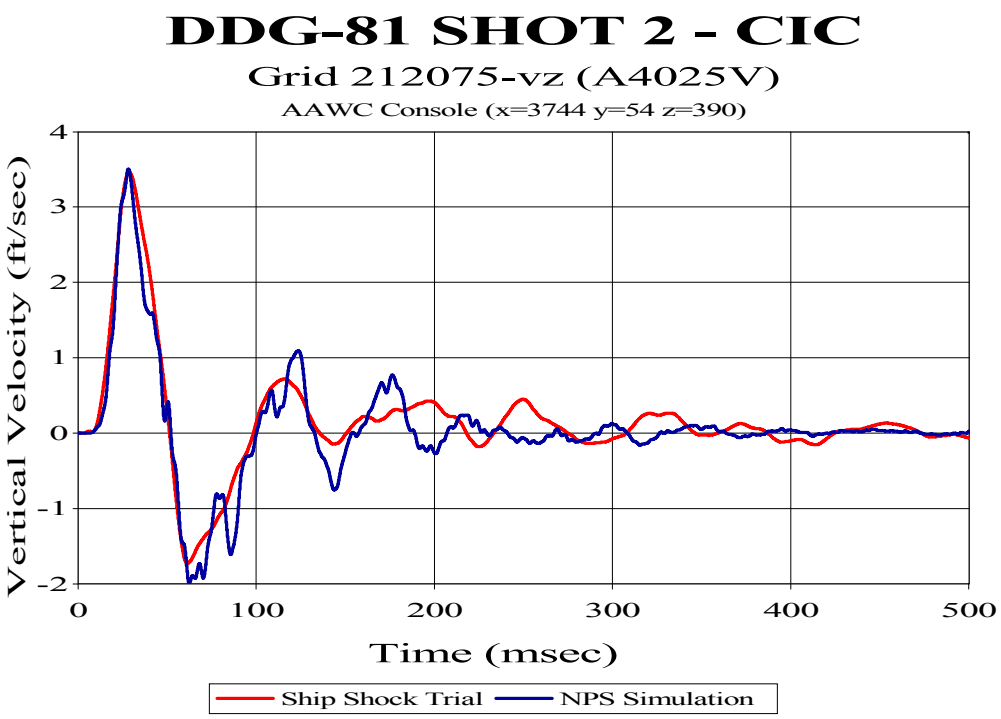

Figure 74. Deck Sensor A4025V: (RM = 0.0243, RP = 0.1152, RC = 0.1044)

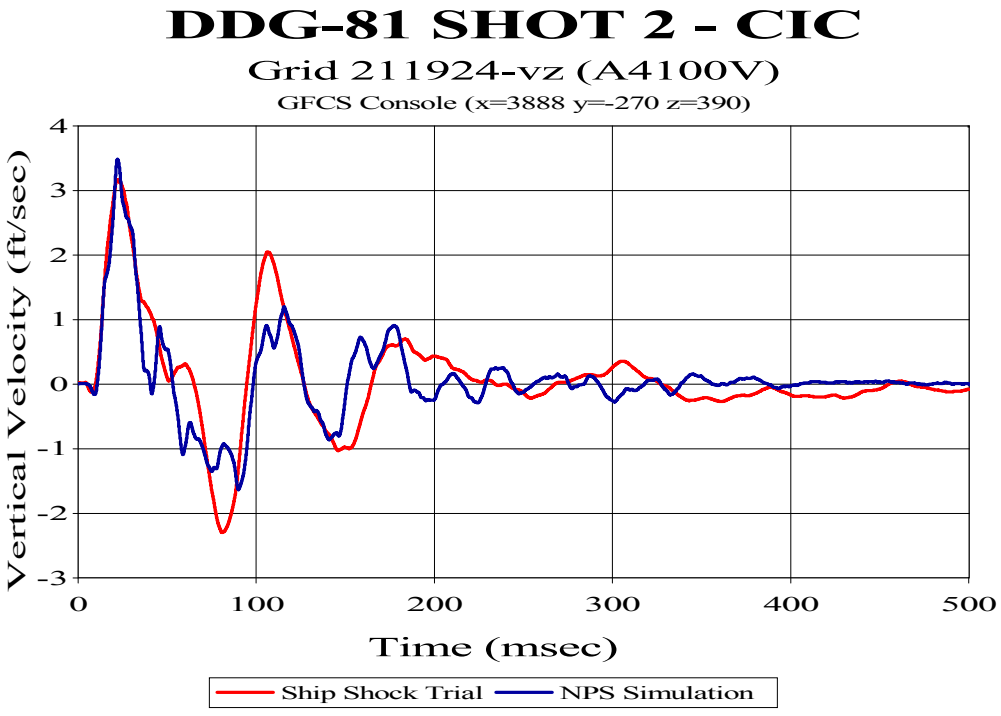

Figure 75. Deck Sensor A4100V: (RM = 0.1322, RP = 0.1937, RC = 0.2079)

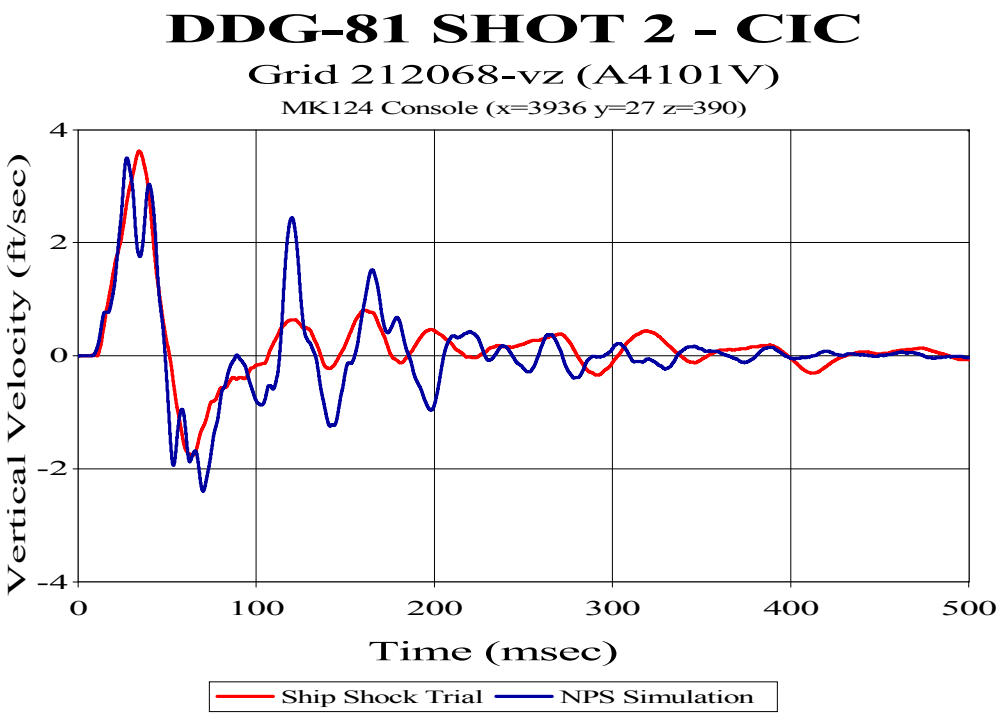

Figure 76. Deck Sensor A4101V: (RM = 0.0995, RP = 0.1985, RC = 0.1968)

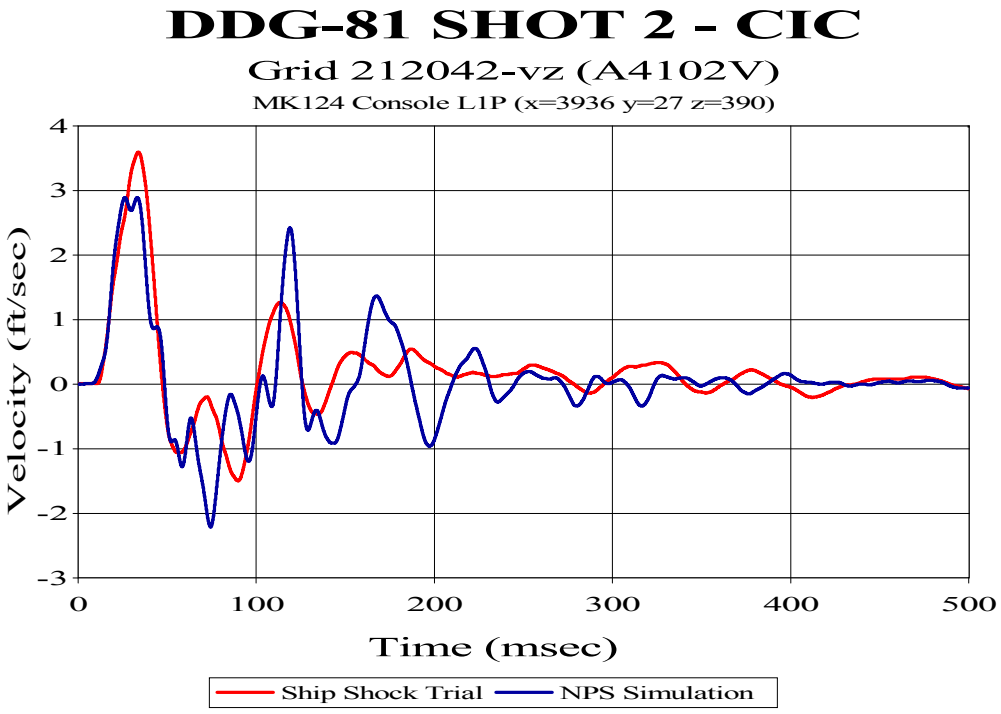

Figure 77. Deck Sensor A4102V: (RM = 0.0372, RP = 0.2234, RC = 0.2007)

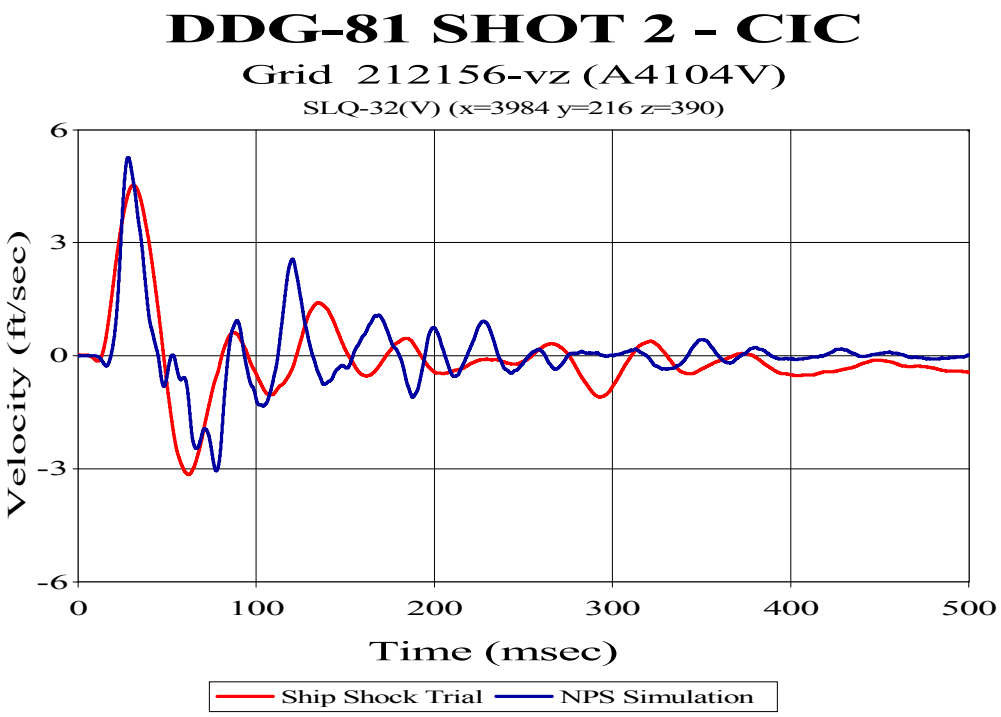

Figure 78. Deck Sensor A4104V: (RM = 0.0637, RP = 0.2739, RC = 0.2492)

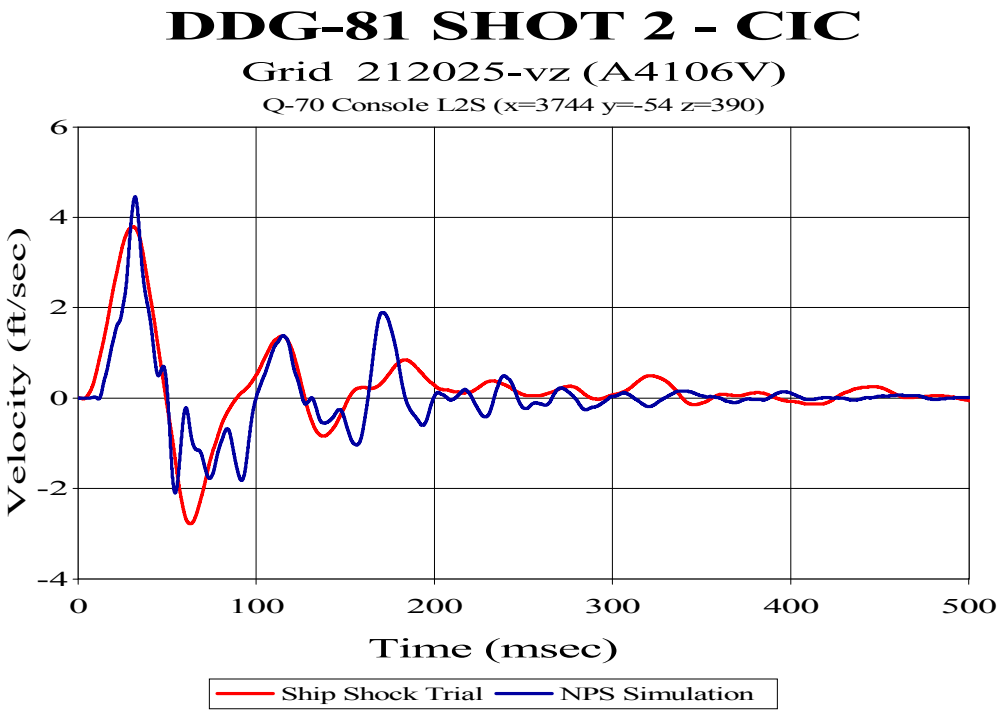

Figure 79. Deck Sensor A4106V: (RM = 0.0727, RP = 0.1815, RC = 0.1733)

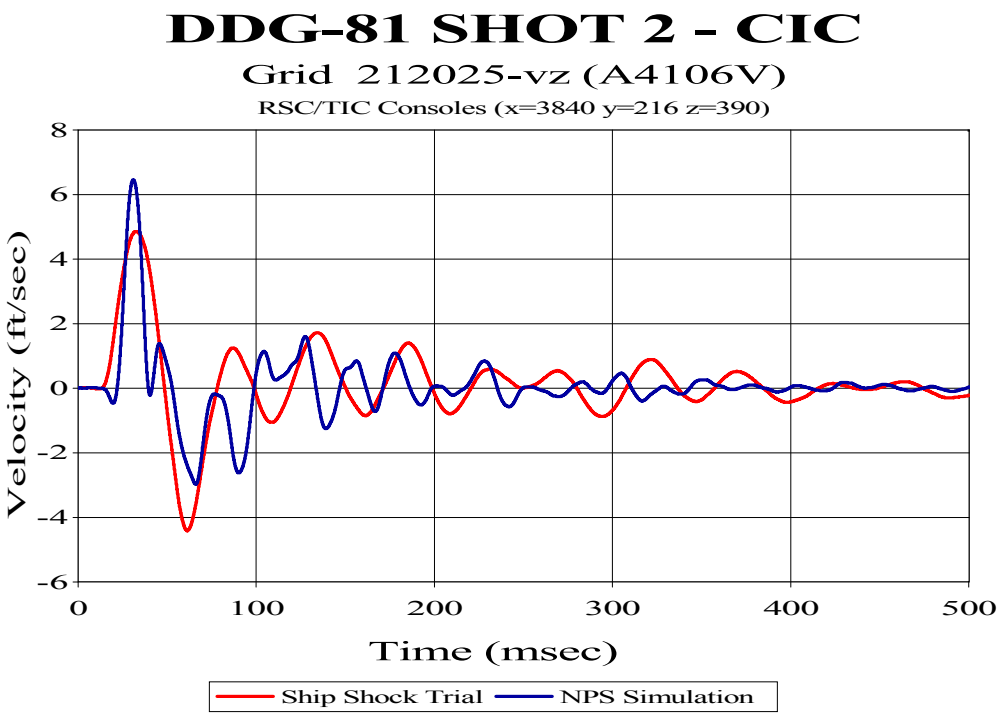

Figure 80. Deck Sensor A4108V: (RM = 0.1260, RP = 0.2862, RC = 0.2771)

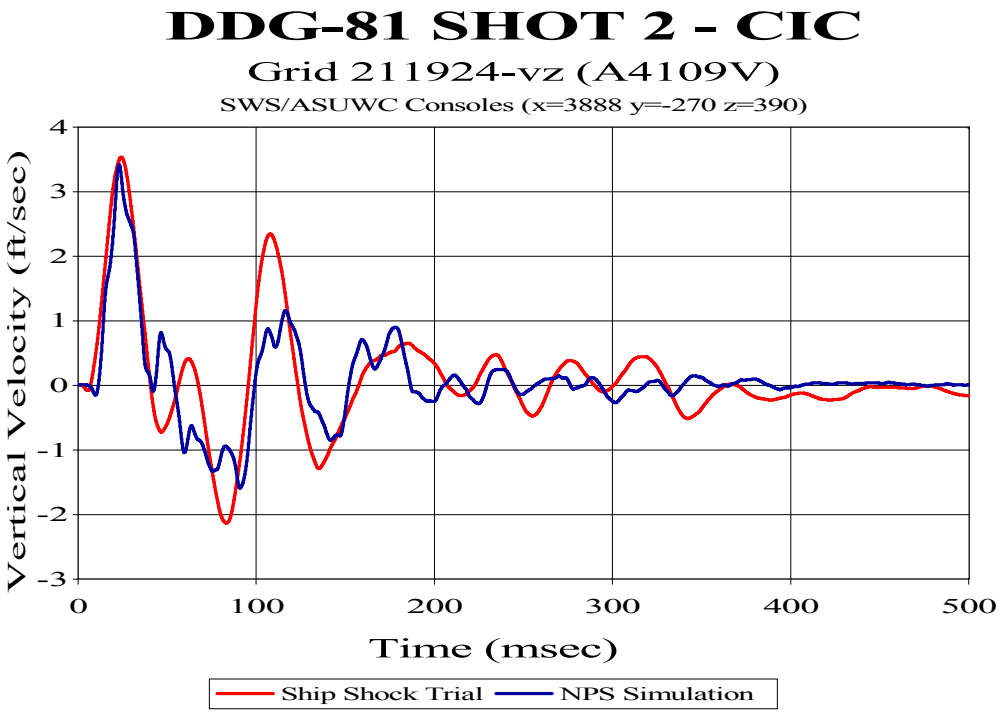

Figure 81. Deck Sensor A4109V: (RM = 0.1814, RP = 0.1995, RC = 0.2364)

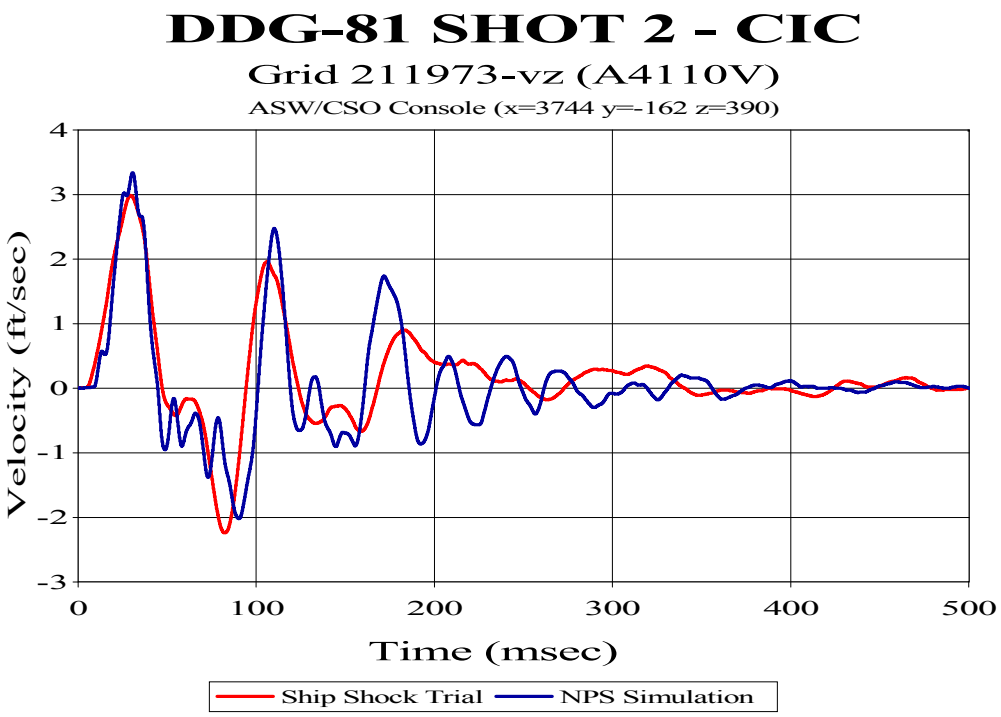

Figure 82. Deck Sensor A4110V: (RM = 0.0442, RP = 0.2132, RC = 0.1930)

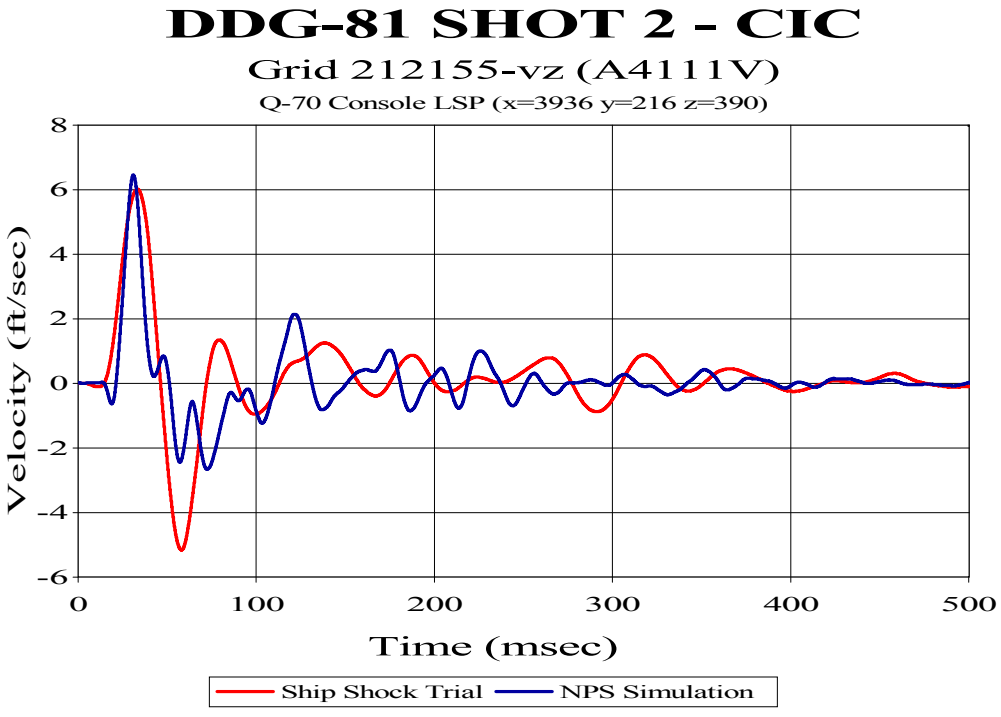

Figure 83. Deck Sensor A4111V: (RM = 0.1970, RP = 0.2737, RC = 0.2988)

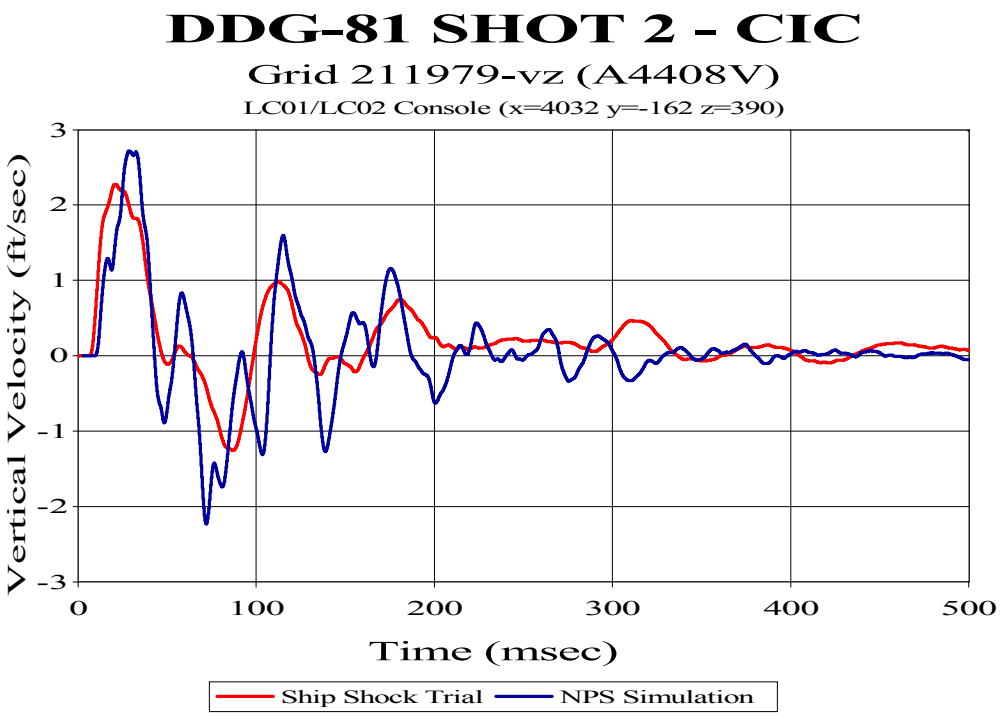

Figure 84. Deck Sensor A4408V: (RM = 0.1342, RP = 0.2397, RC = 0.2434)

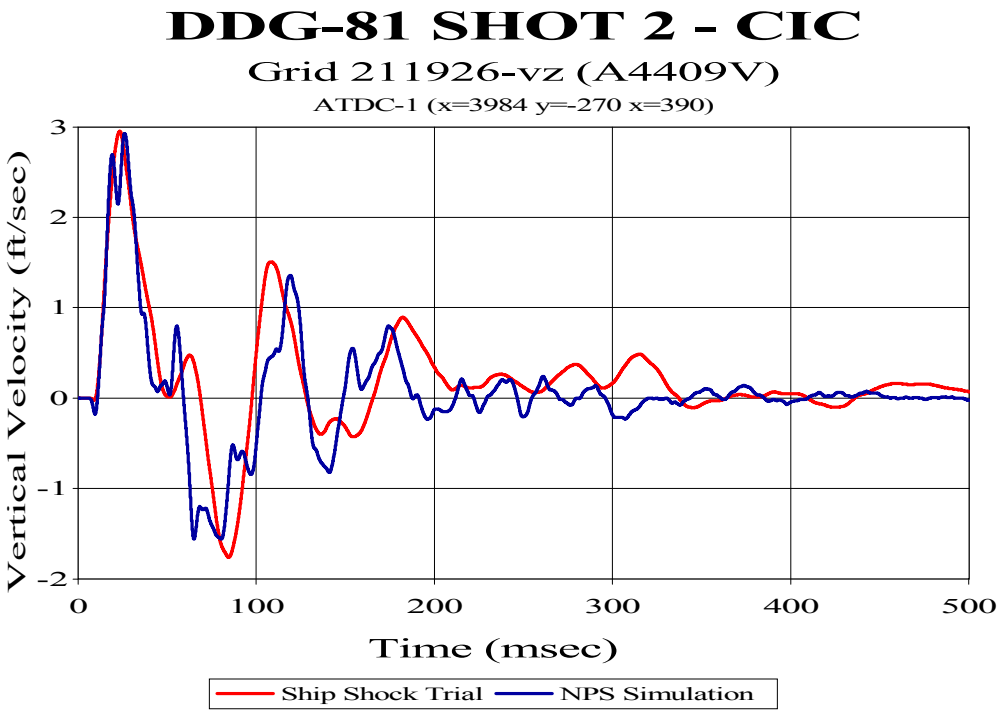

Figure 85. Deck Sensor A4409V: (RM = 0.0551, RP = 0.2097, RC = 0.1921)

C. SHOT 3

The following velocity plots are from the analysis of the Combat Information Center for Shot 3. The Russell's error factors for the corresponding data correlation follow each figure caption.

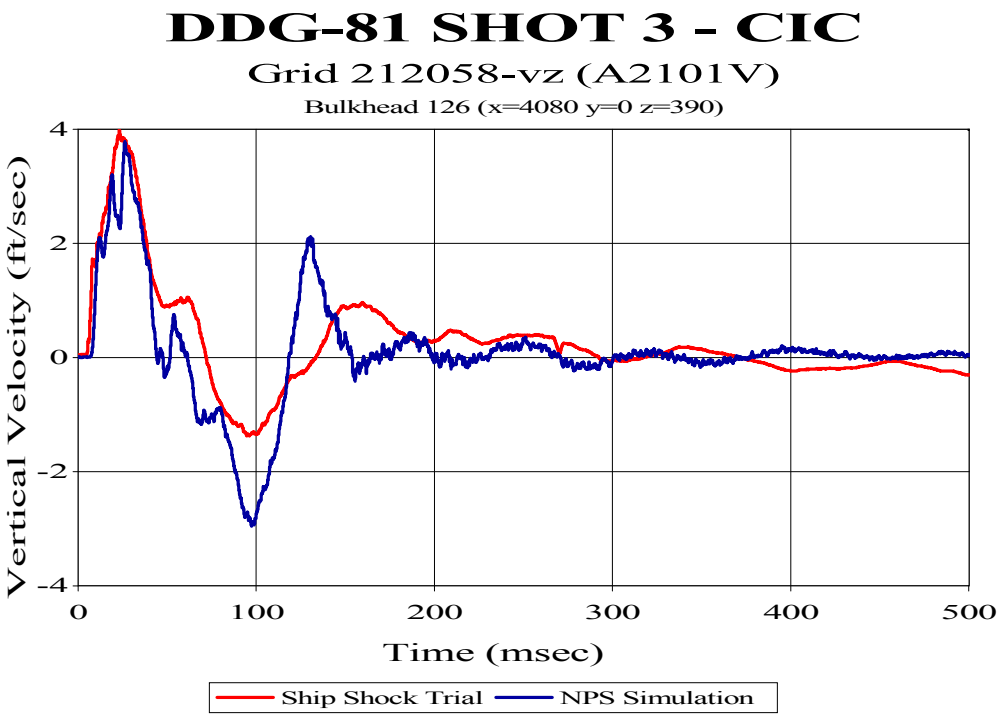

Figure 86. Bulkhead Sensor A2101V: (RM = 0.0295, RP = 0.2219, RC = 0.1896)

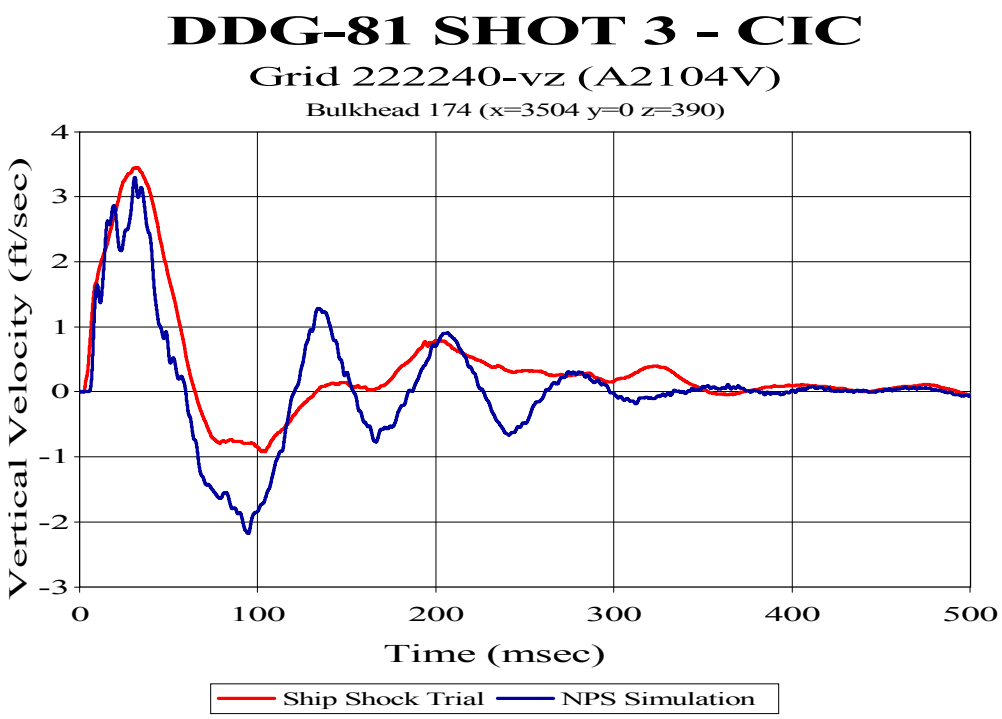

Figure 87. Deck Sensor A2104V: (RM = 0.0020, RP = 0.1895, RC = 0.1680)

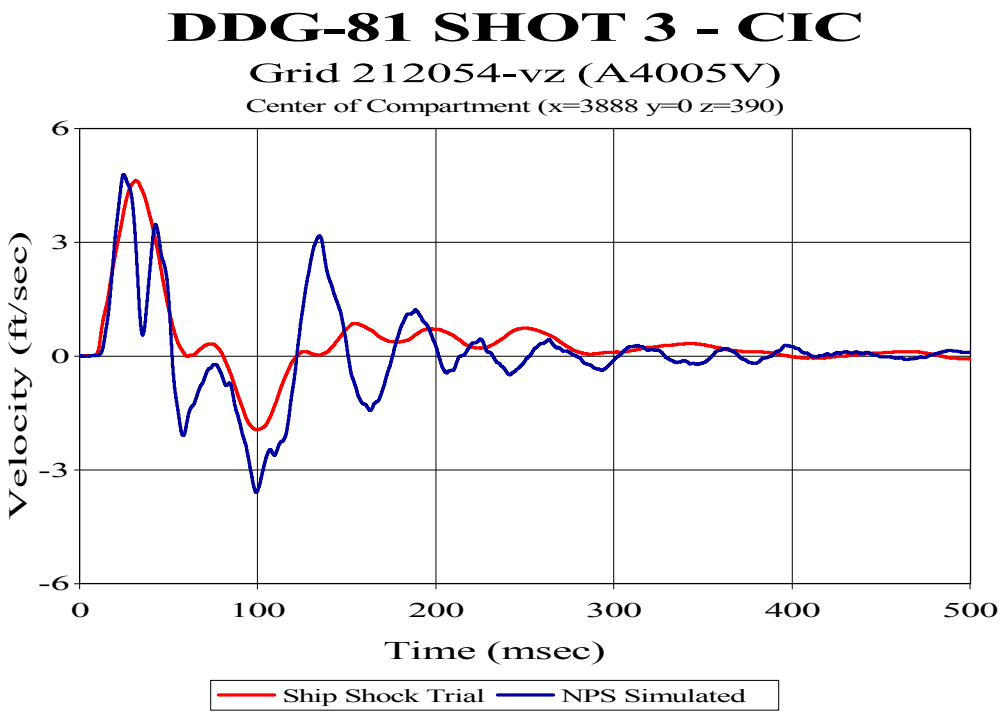

Figure 88. Deck Sensor A4005V: (RM = 0.1250, RP = 0.2521, RC = 0.2494)

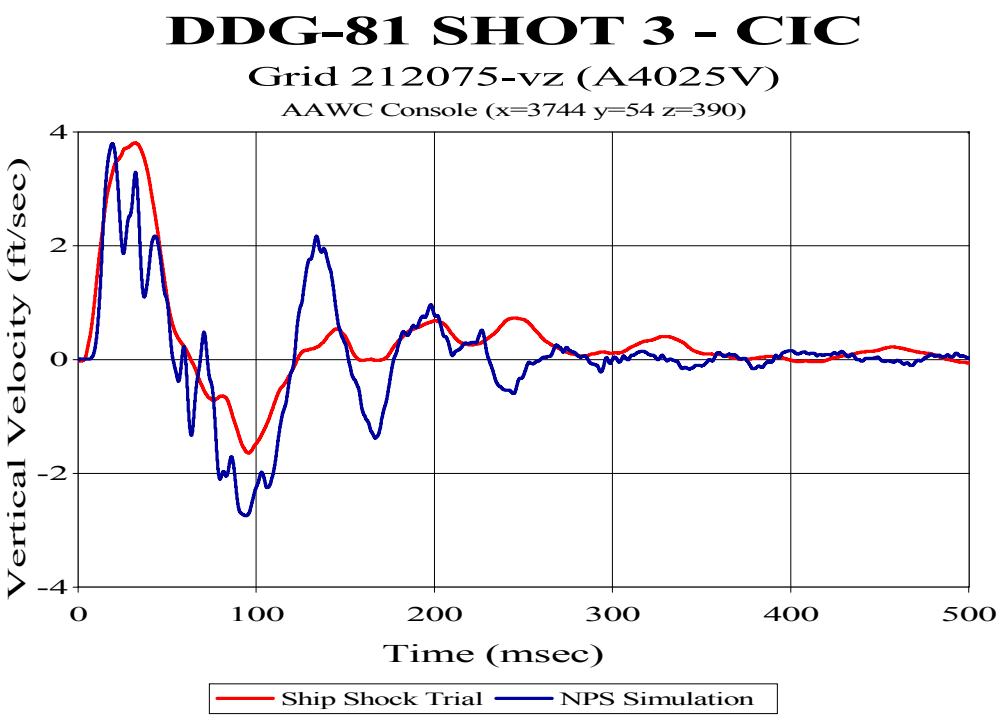

Figure 89. Deck Sensor A4025V: (RM = 0.0369, RP = 0.2048, RC = 0.1876)

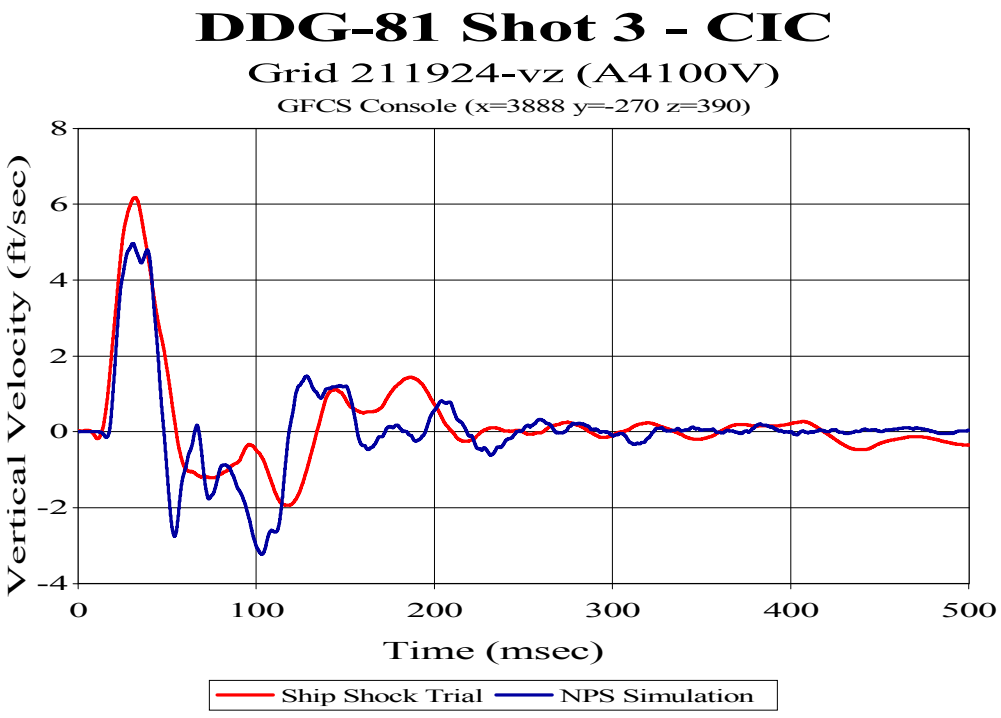

Figure 90. Deck Sensor A4100V: (RM = 0.0513, RP = 0.2190, RC = 0.1994)

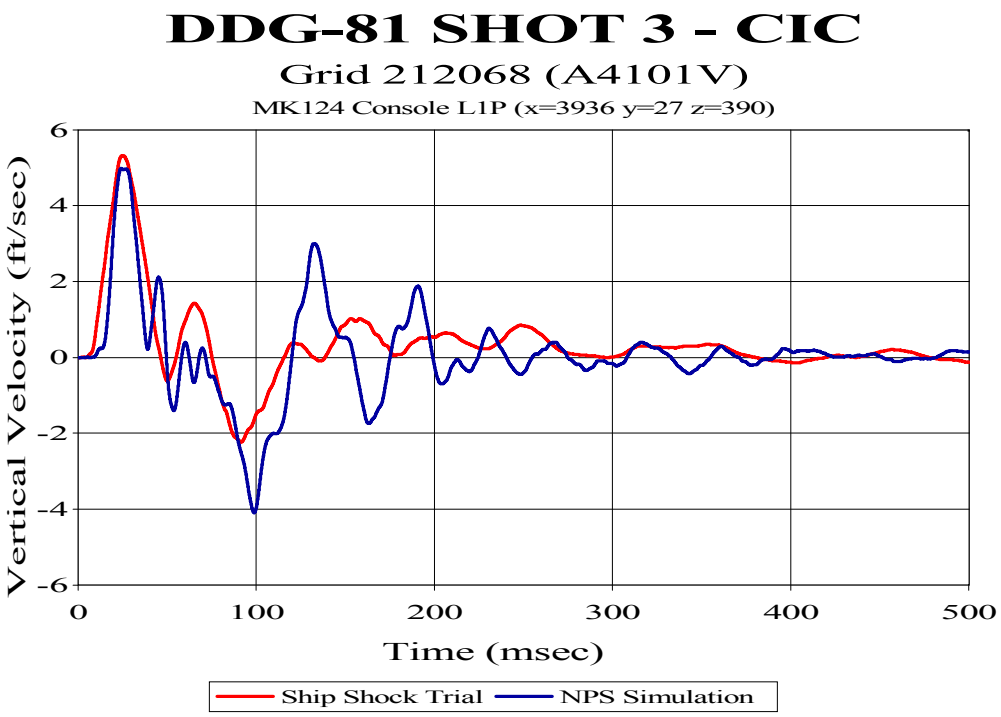

Figure 91. Deck Sensor A4101V: (RM = 0.0773, RP = 0.2520, RC = 0.2336)

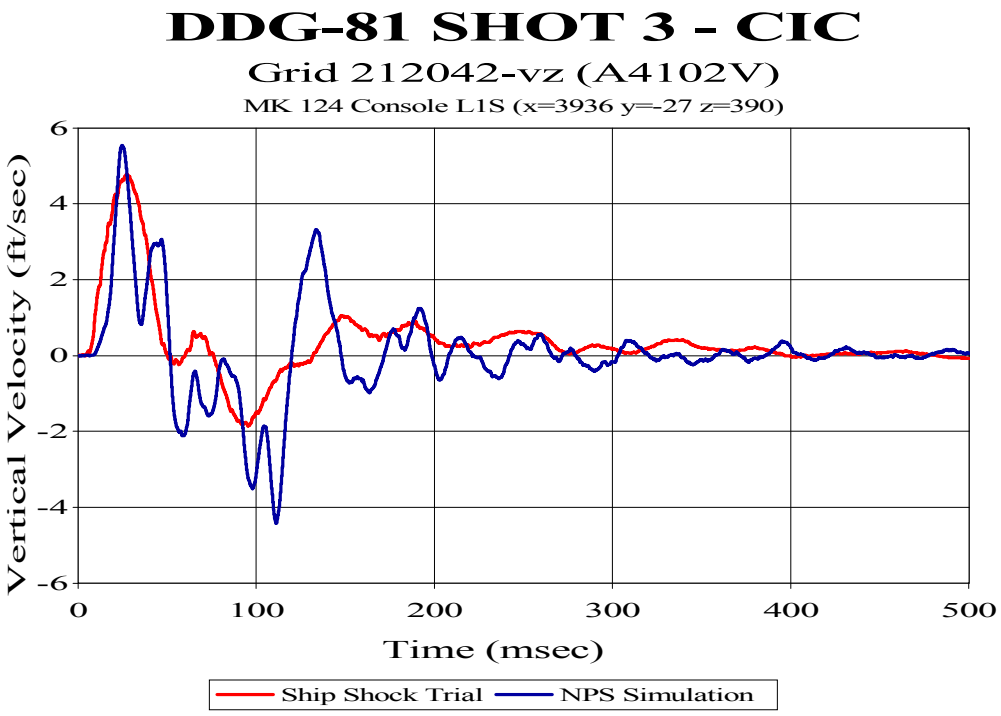

Figure 92. Deck Sensor A4102V: (RM = 0.1320, RP = 0.2779, RC = 0.2727)

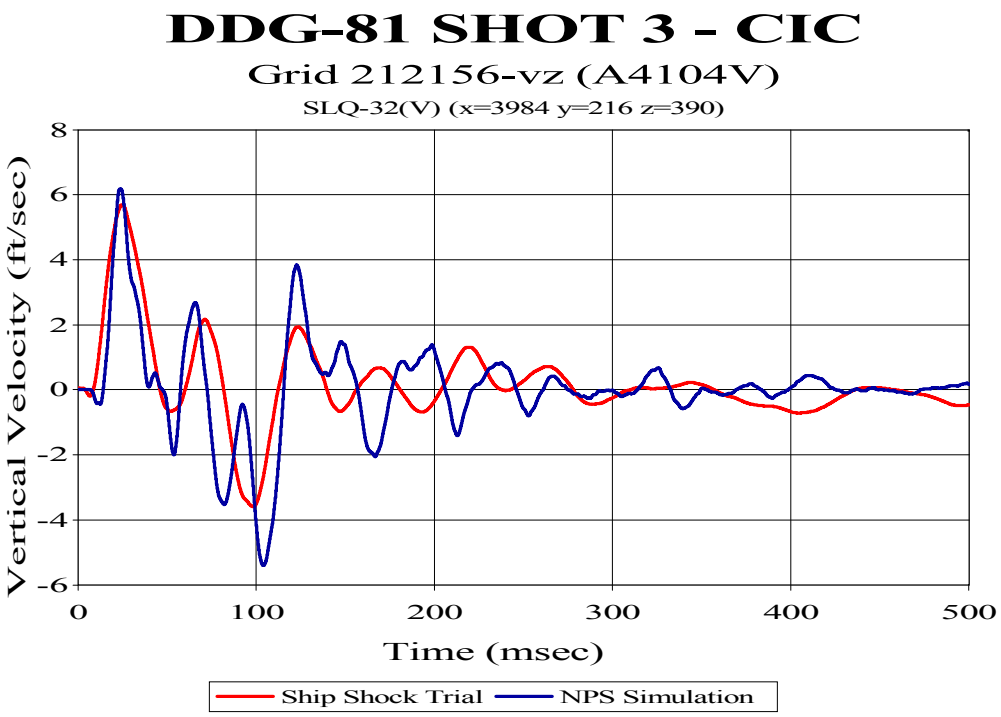

Figure 93. Deck Sensor A4104V: (RM = 0.0793, RP = 0.2736, RC = 0.2525)

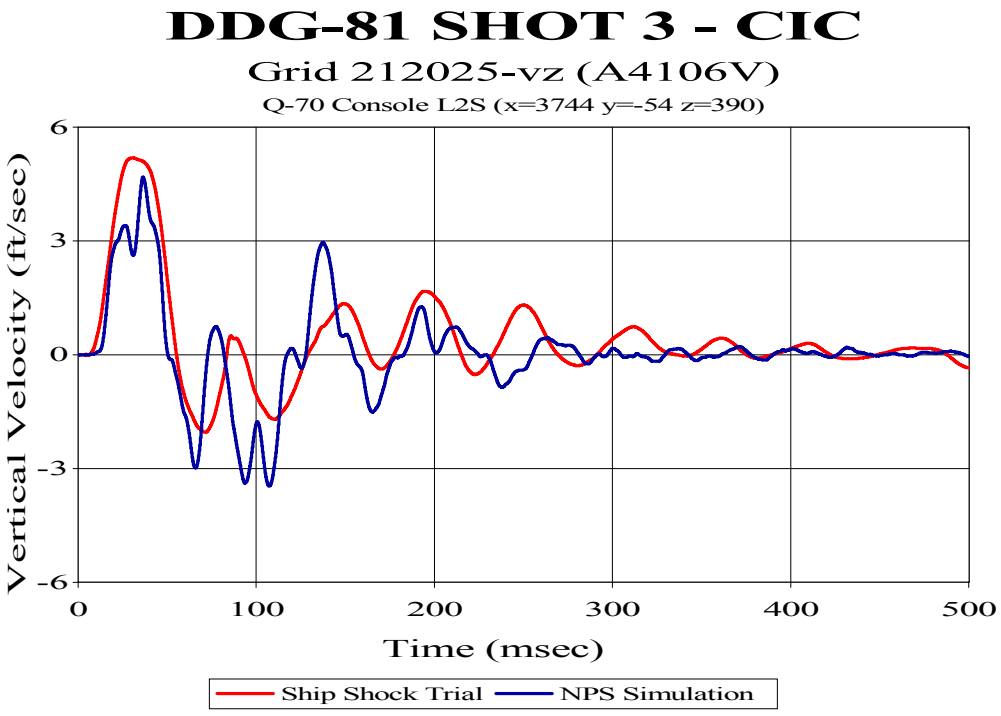

Figure 94. Deck Sensor A4106V: (RM = 0.0780, RP = 0.2334, RC = 0.2181)

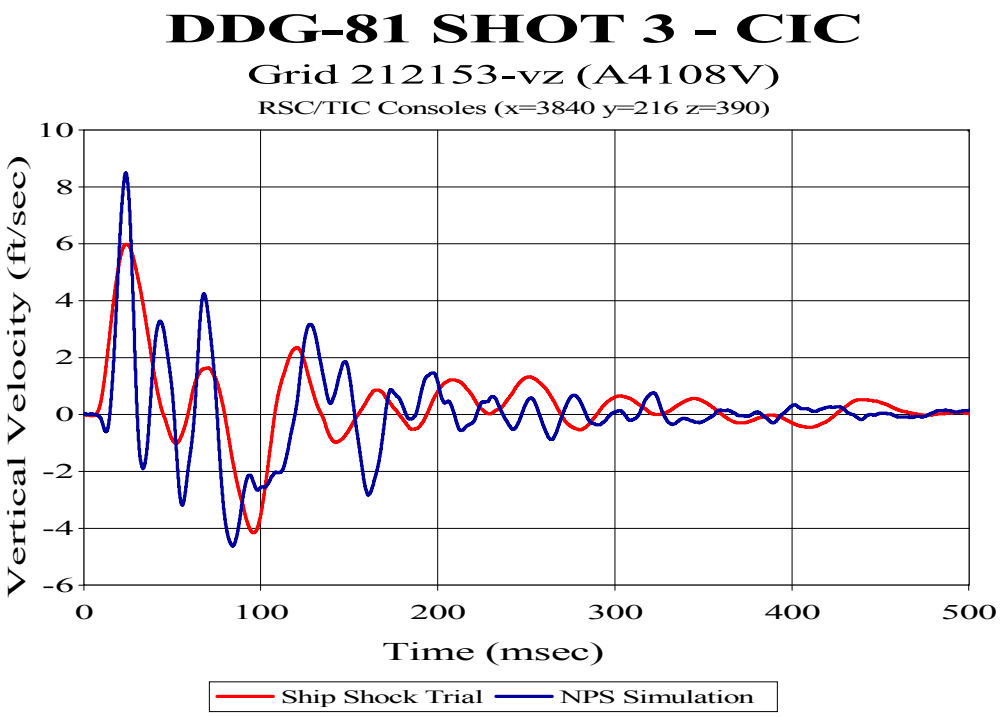

Figure 95. Deck Sensor A4108V: (RM = 0.1053, RP = 0.3095, RC = 0.2897)

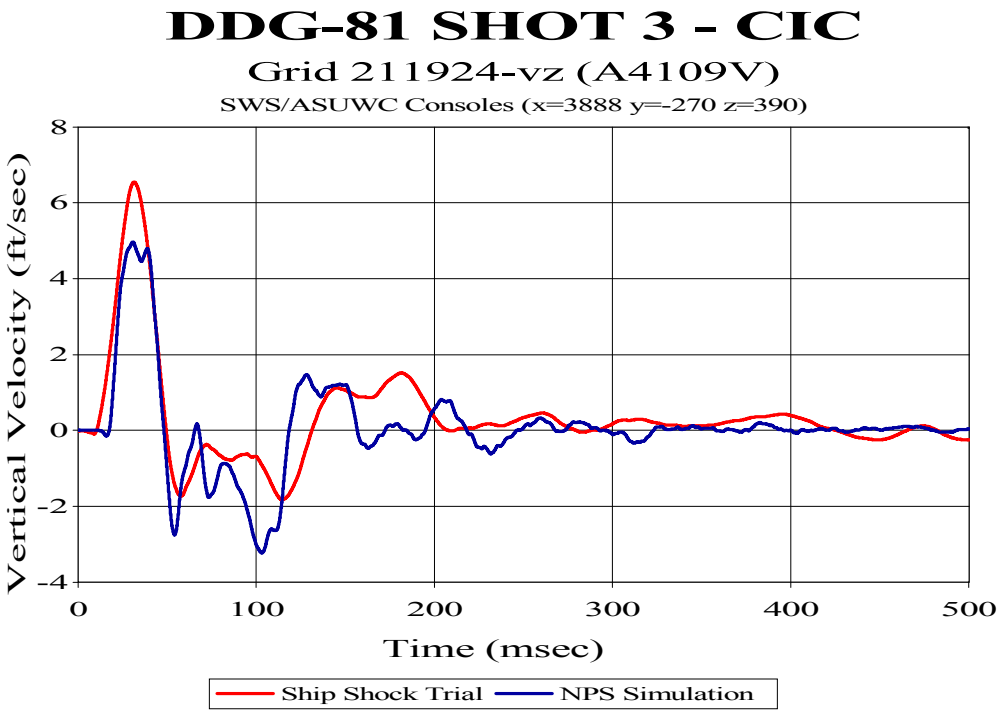

Figure 96. Deck Sensor A4109V: (RM = 0.0653, RP = 0.1927, RC = 0.1803)

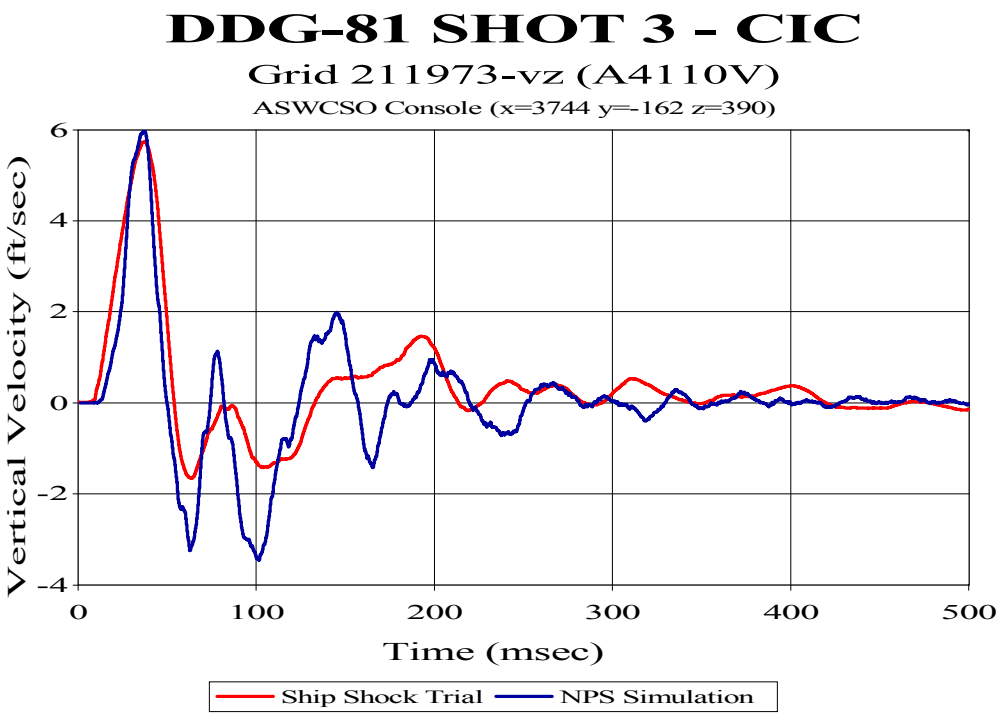

Figure 97. Deck Sensor A4110V: (RM = 0.0409, RP = 0.2075, RC = 0.1874)

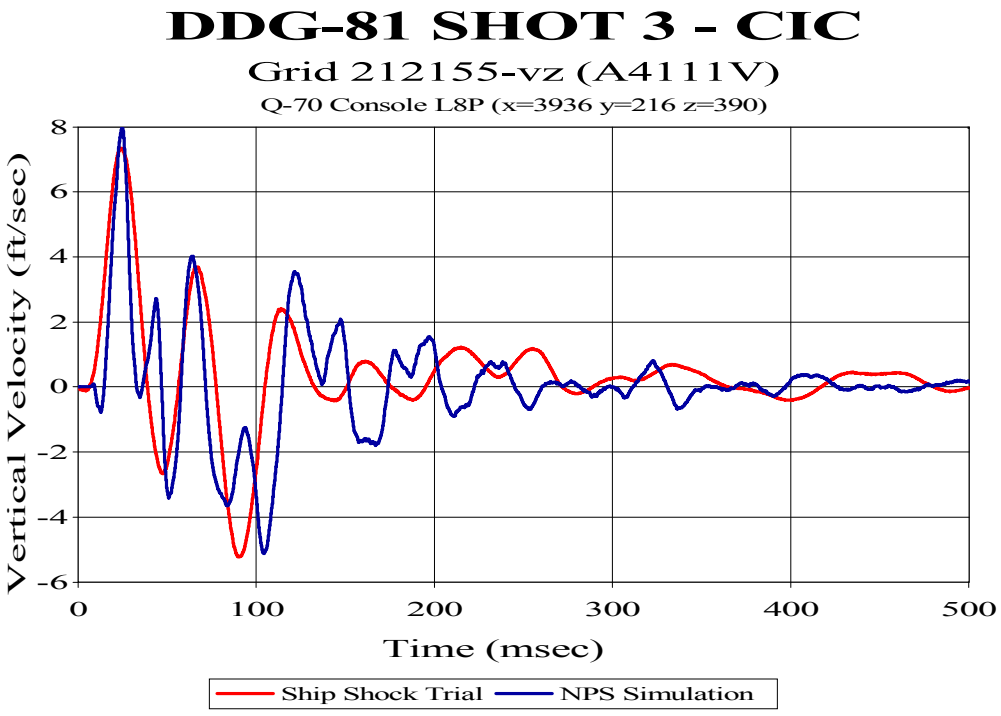

Figure 98. Deck Sensor A4111V: (RM = 0.0412, RP = 0.2951, RC = 0.2641)

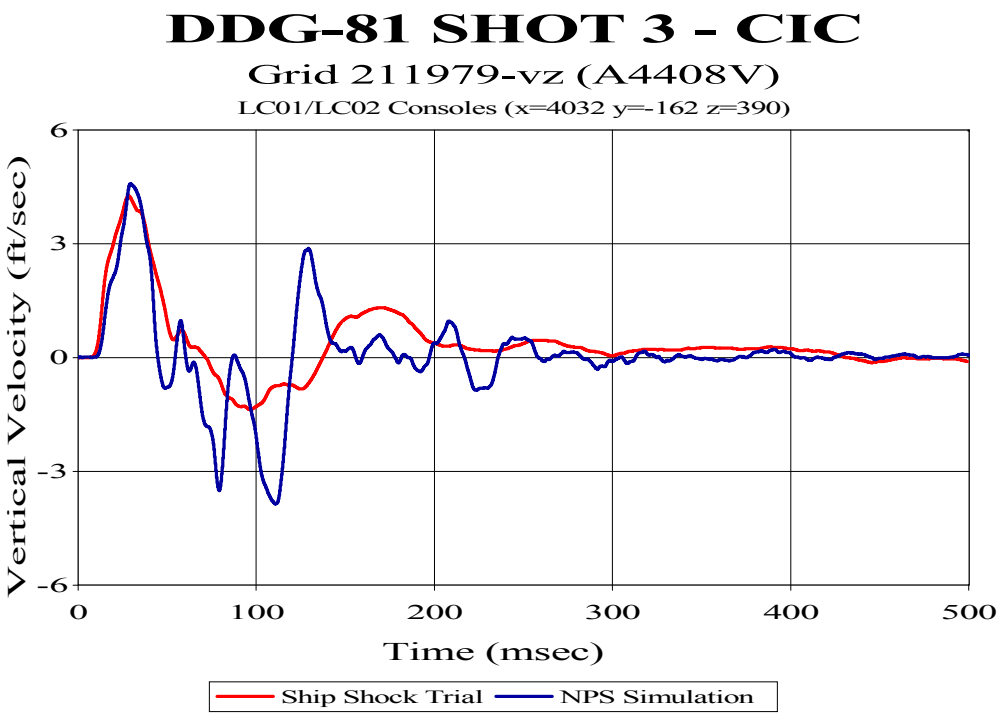

Figure 99. Deck Sensor A4408V: (RM = 0.1274, RP = 0.2727, RC = 0.2667)

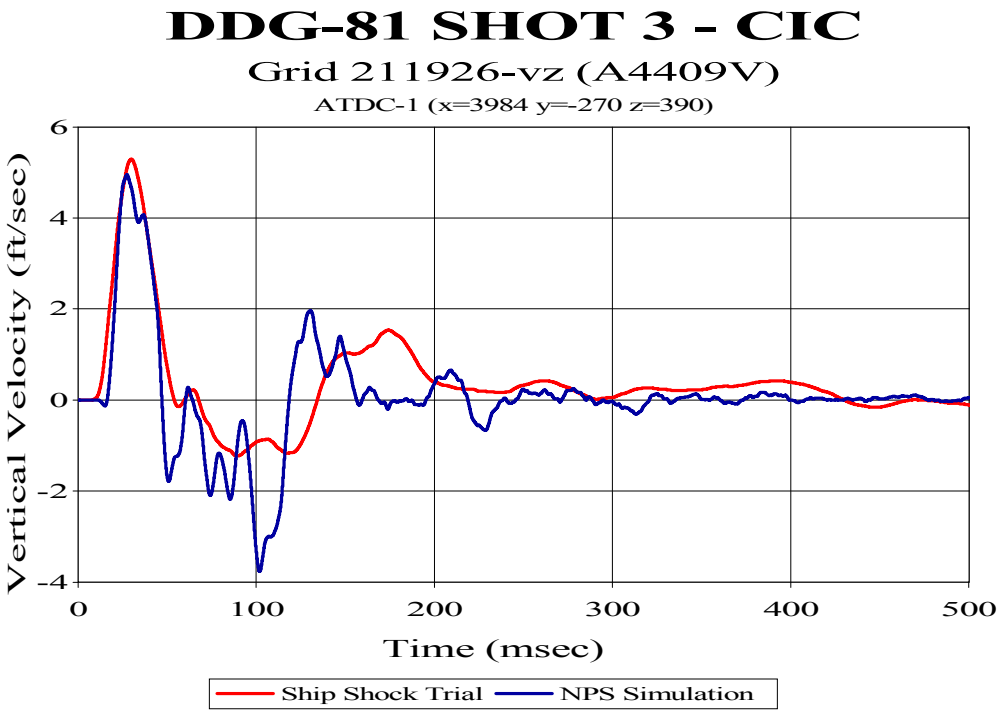

Figure 100. Deck Sensor A4409V: (RM = 0.0343, RP = 0.2223, RC = 0.1993)

APPENDIX C. ATHWARTSHIP VELOCITY PLOTS

A. SHOT 1

The following velocity plots are taken from the Athwartship analysis of Shot 1. The Russell's error factors for the corresponding data correlation follow each figure caption.

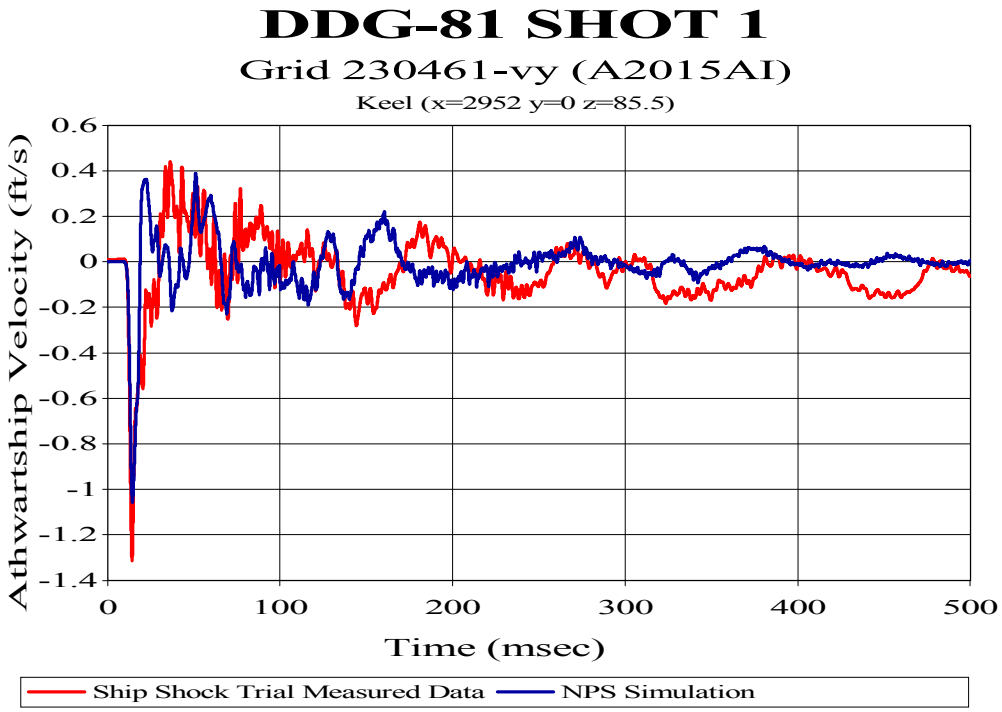

Figure 101. Keel Sensor A2015AI: (RM = 0.2403, RP = 0.3245, RC = 0.3578)

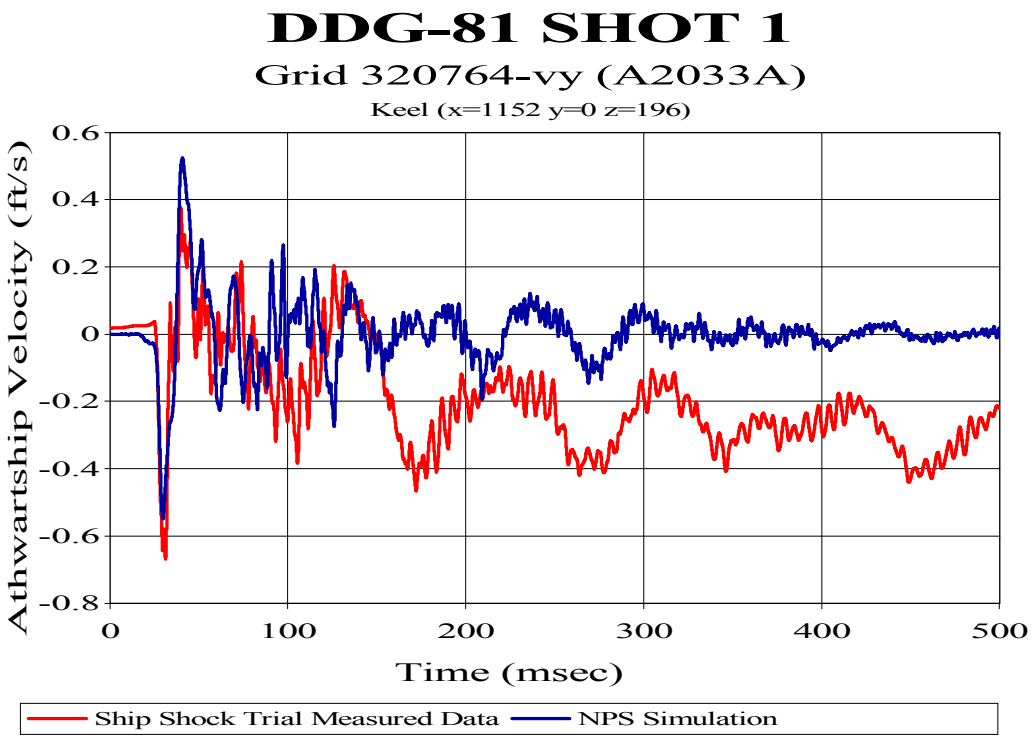

Figure 102. Keel Sensor A2033A: (RM = 0.0553, RP = 0.5207, RC = 0.4641)

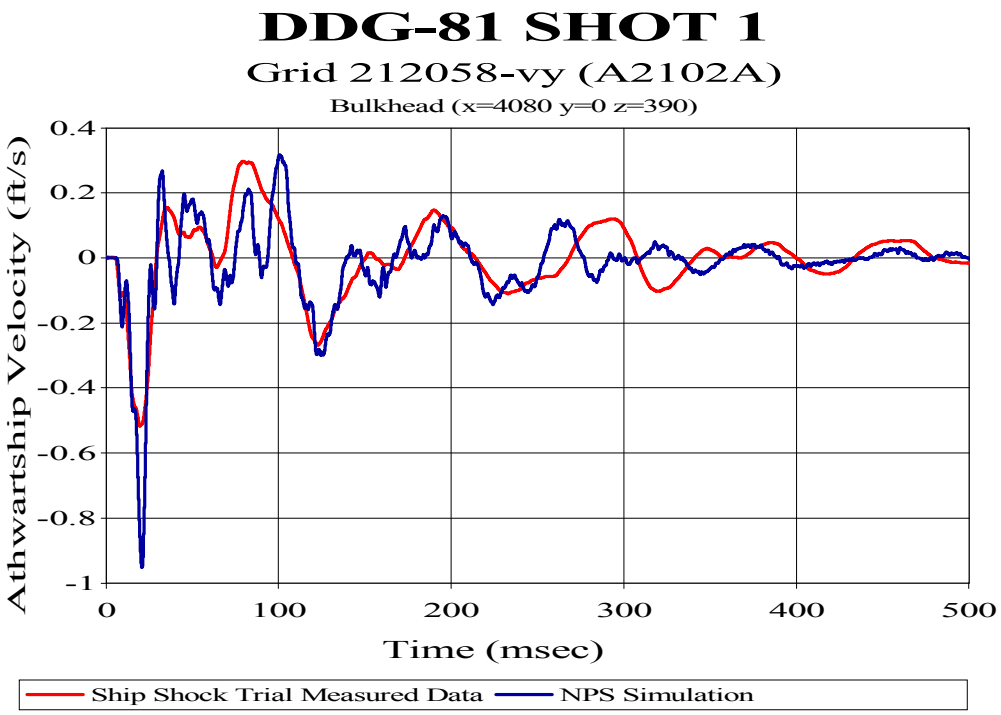

Figure 103. Bulkhead Sensor A2102AI: (RM = 0.0708, RP = 0.2367, RC = 0.2189)

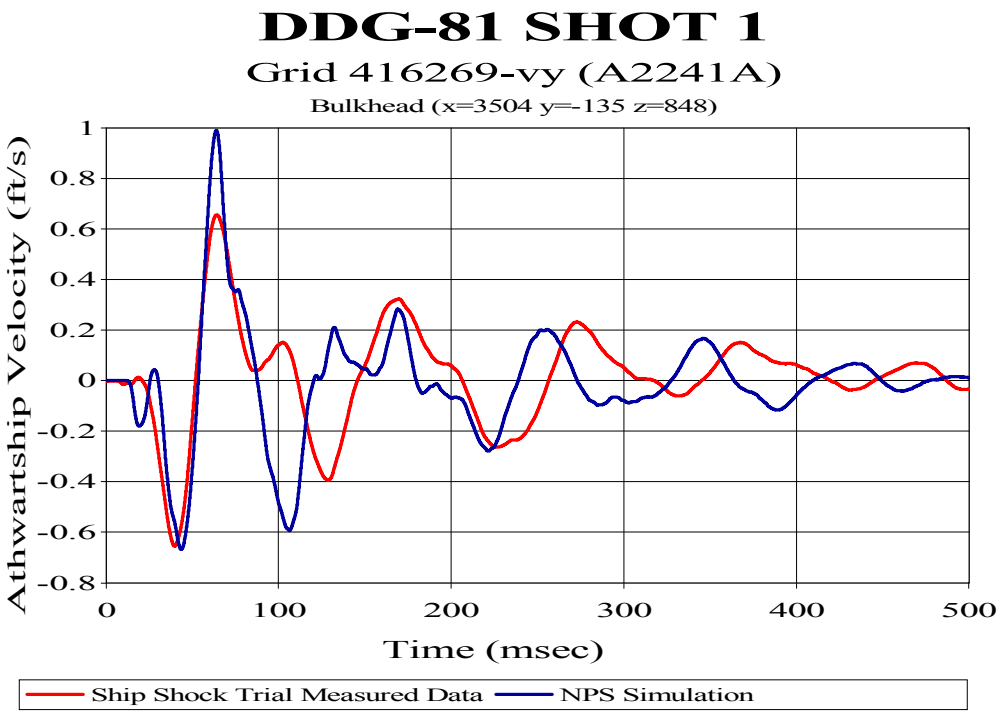

Figure 104. Bulkhead Sensor A2241A: (RM = 0.0847, RP = 0.3119, RC = 0.2864)

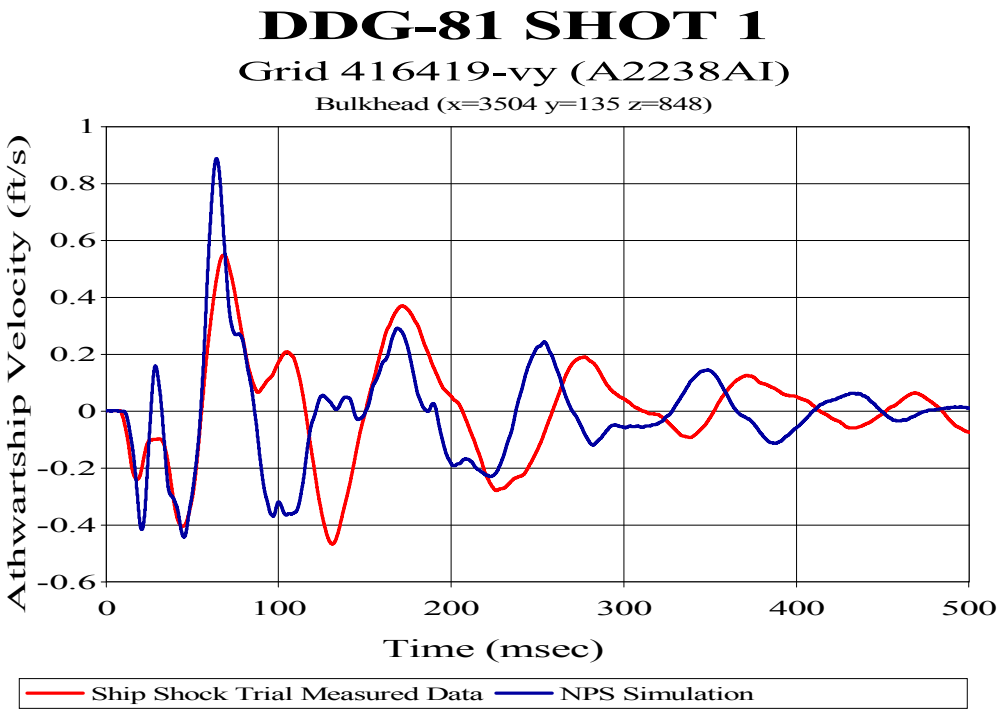

Figure 105. Bulkhead Sensor A2238AI: (RM = 0.0179, RP = 0.3542, RC = 0.3143)

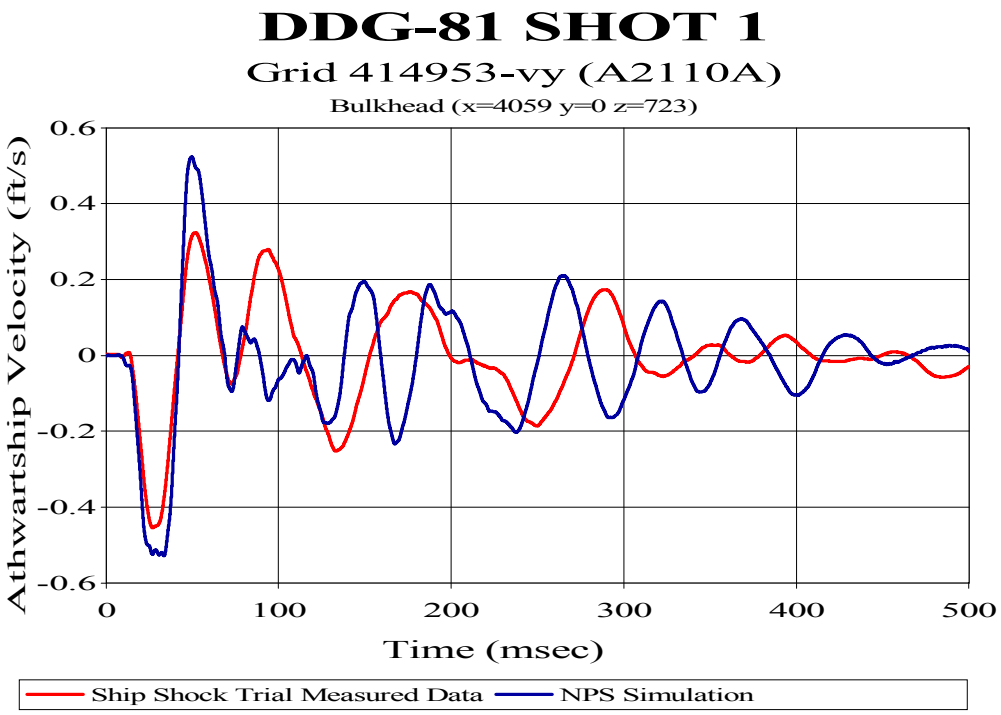

Figure 106. Bulkhead Sensor A2110A: (RM = 0.1393, RP = 0.3381, RC = 0.3241)

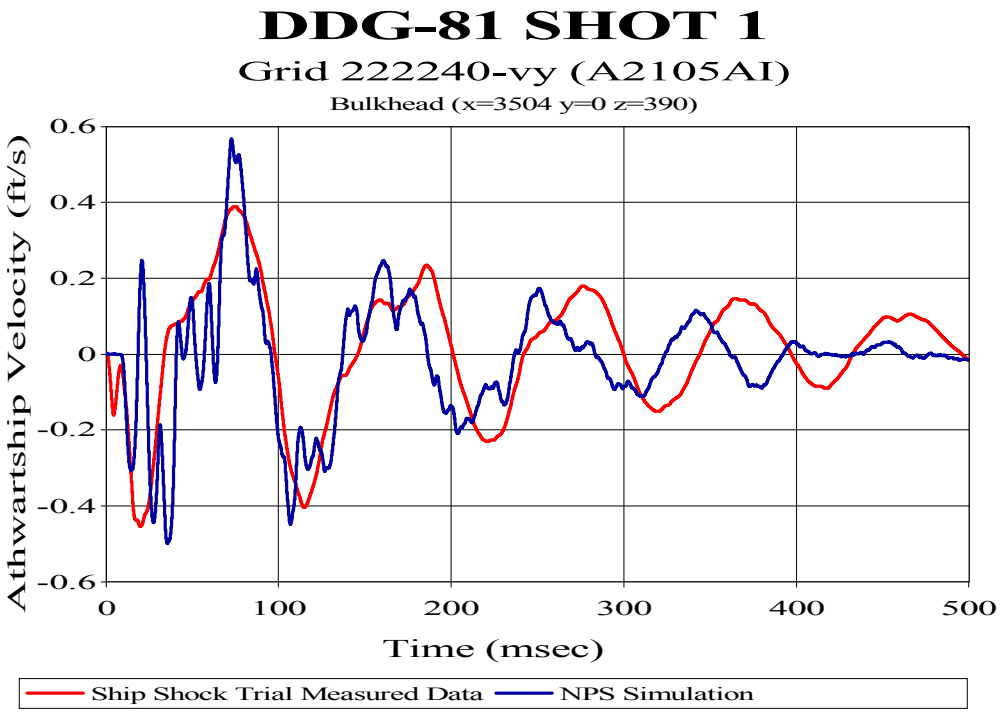

Figure 107. Bulkhead Sensor A2105AI: (RM = 0.0470, RP = 0.2873, RC = 0.2580)

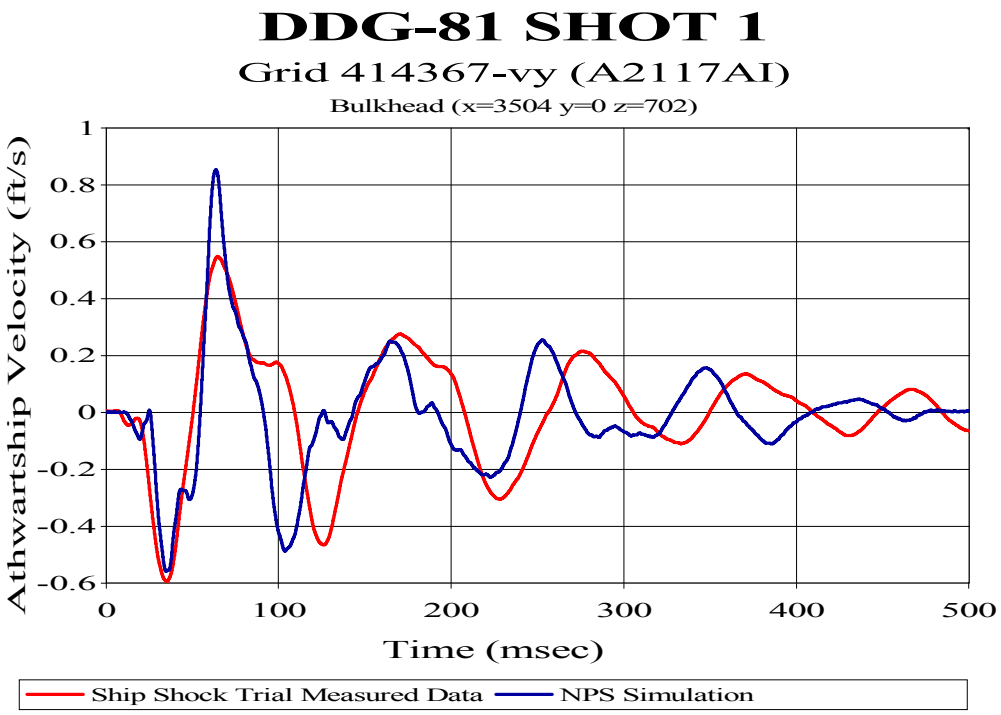

Figure 108. Bulkhead Sensor A2117AI: (RM = 0.0311, RP = 0.2997, RC = 0.2670)

B. SHOT 2

The following velocity plots are taken from the Athwartship analysis of Shot 2. The Russell's error factors for the corresponding data correlation follow each figure caption.

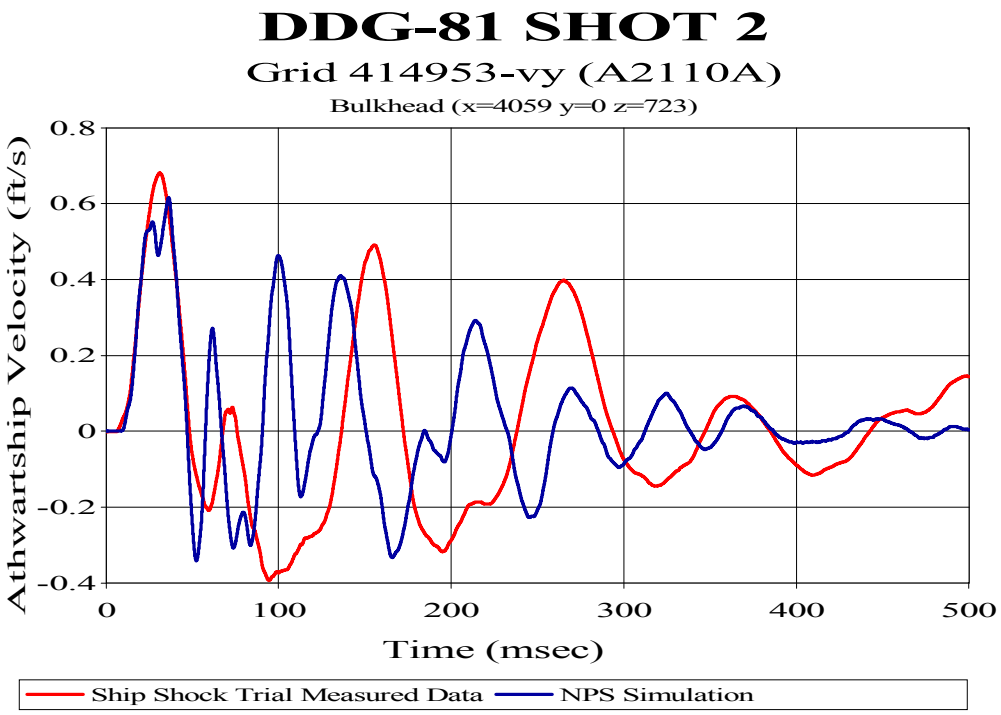

Figure 109. Bulkhead Senor A2110A: (RM = 0.1565, RP = 0.4387, RC = 0.4127)

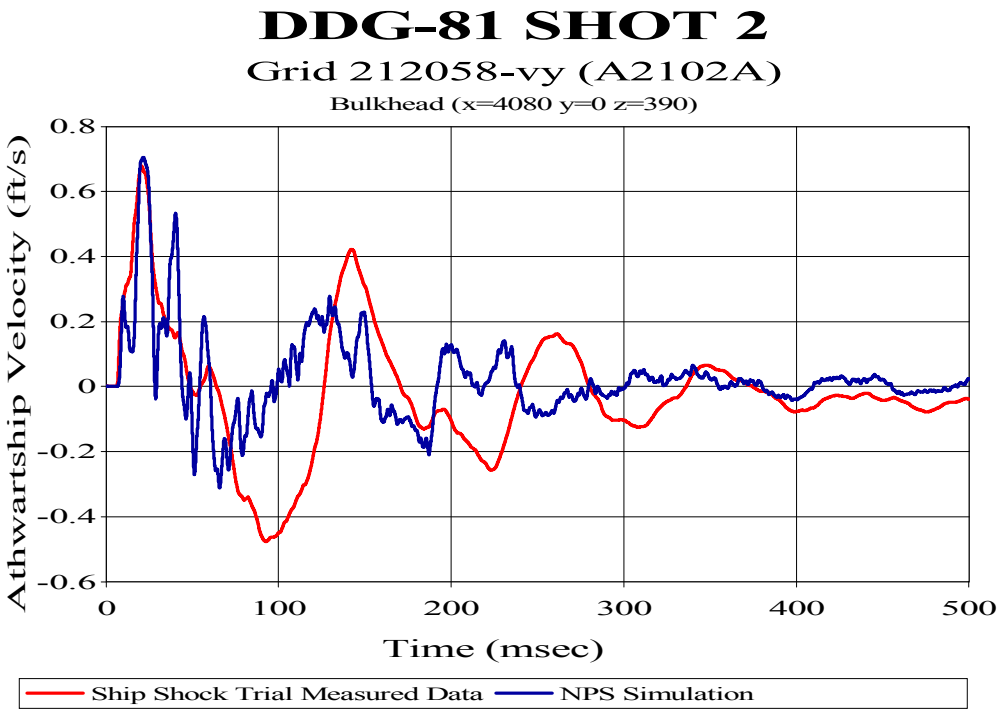

Figure 110. Bulkhead Sensor A2102A: (RM = 0.2431, RP = 0.3542, RC = 0.3807)

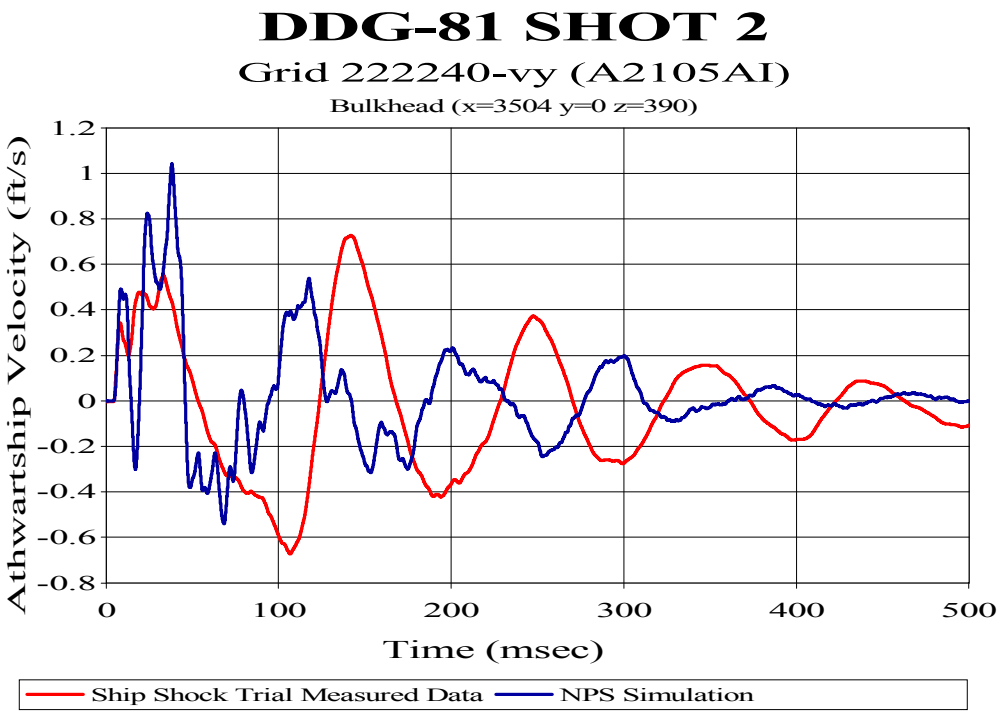

Figure 111. Bulkhead Sensor A2105AI: (RM = 0.1694, RP = 0.4986, RC = 0.4667)

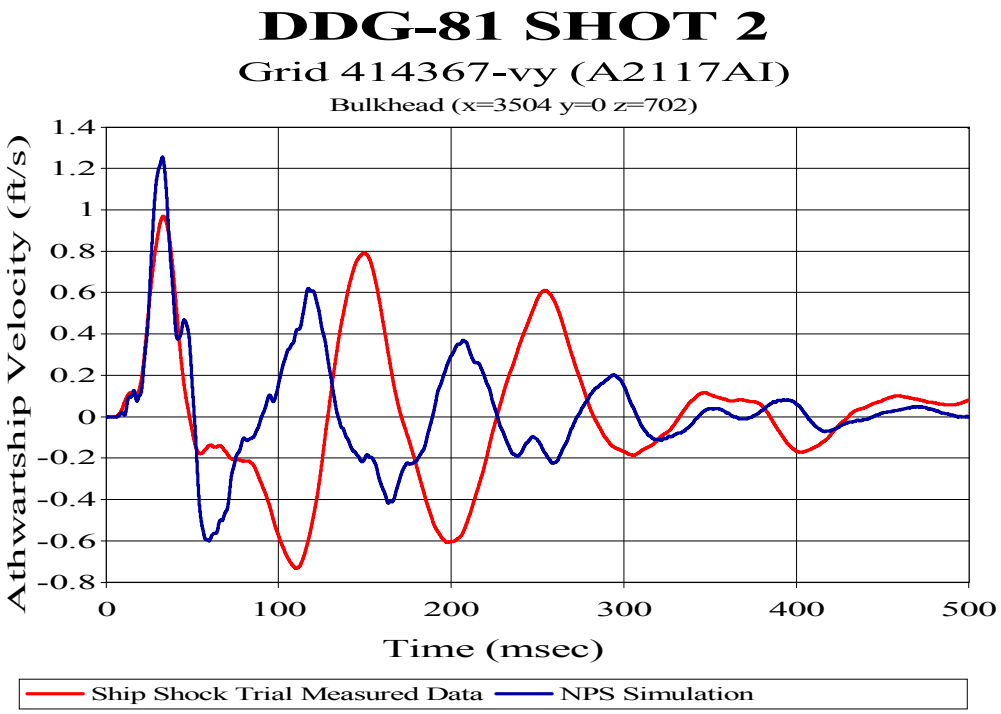

Figure 112. Bulkhead Sensor A2117AI: (RM = 0.1695, RP = 0.5077, RC = 0.4744)

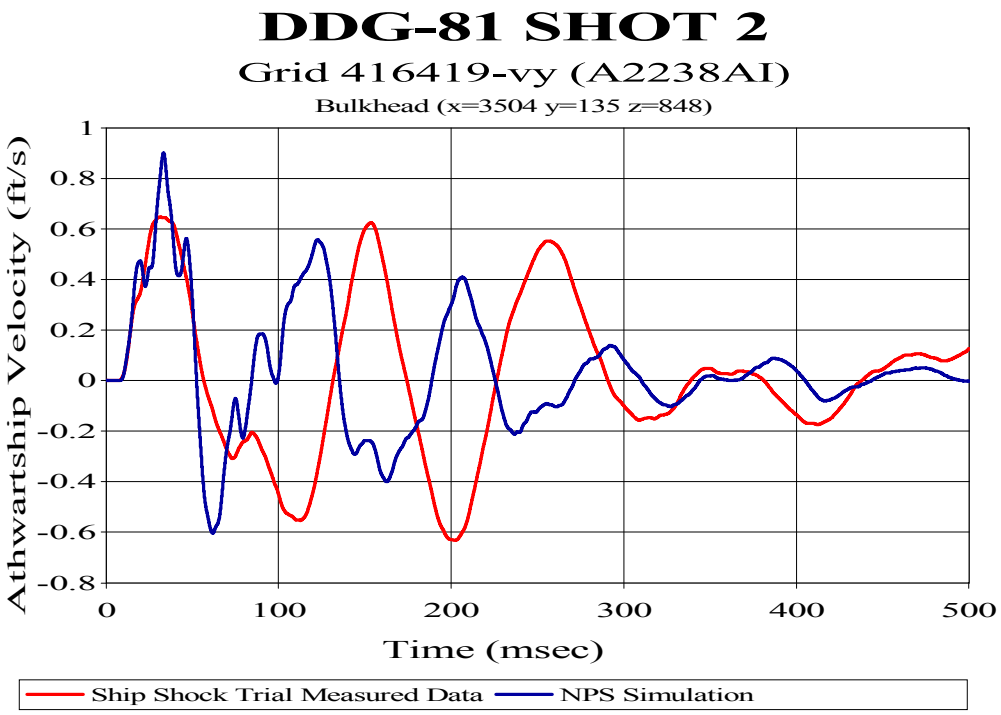

Figure 113. Bulkhead Sensor A2238AI: (RM = 0.1712, RP = 0.5305, RC = 0.4940)

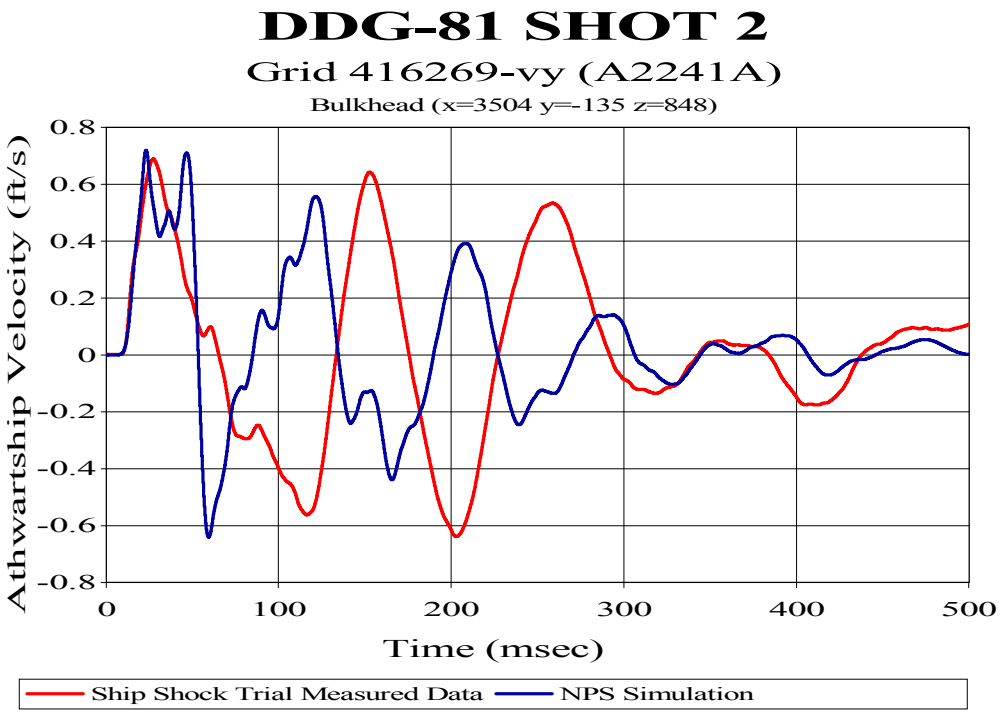

Figure 114. Bulkhead Sensor A2241A: (RM = 0.1735, RP = 0.5570, RC = 0.5170)

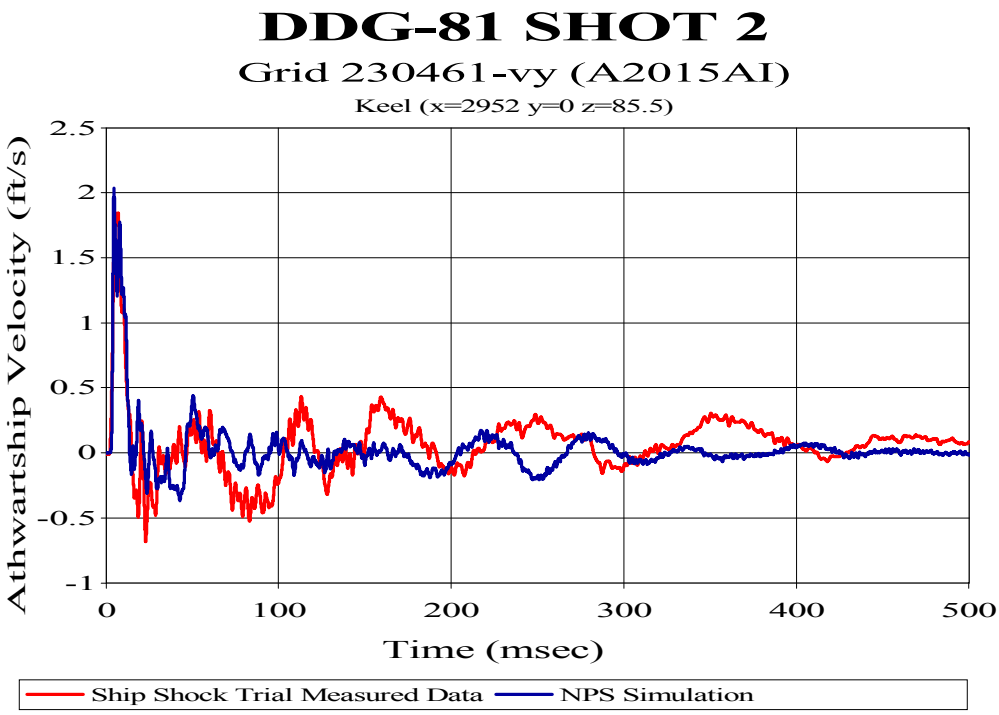

Figure 115. Keel Sensor A2015AI: (RM = 0.1488, RP = 0.2847, RC = 0.2847)

C. SHOT 3

The following velocity plots are taken from the Athwartship analysis of Shot 3. The Russell's error factors for the corresponding data correlation follow each figure caption.

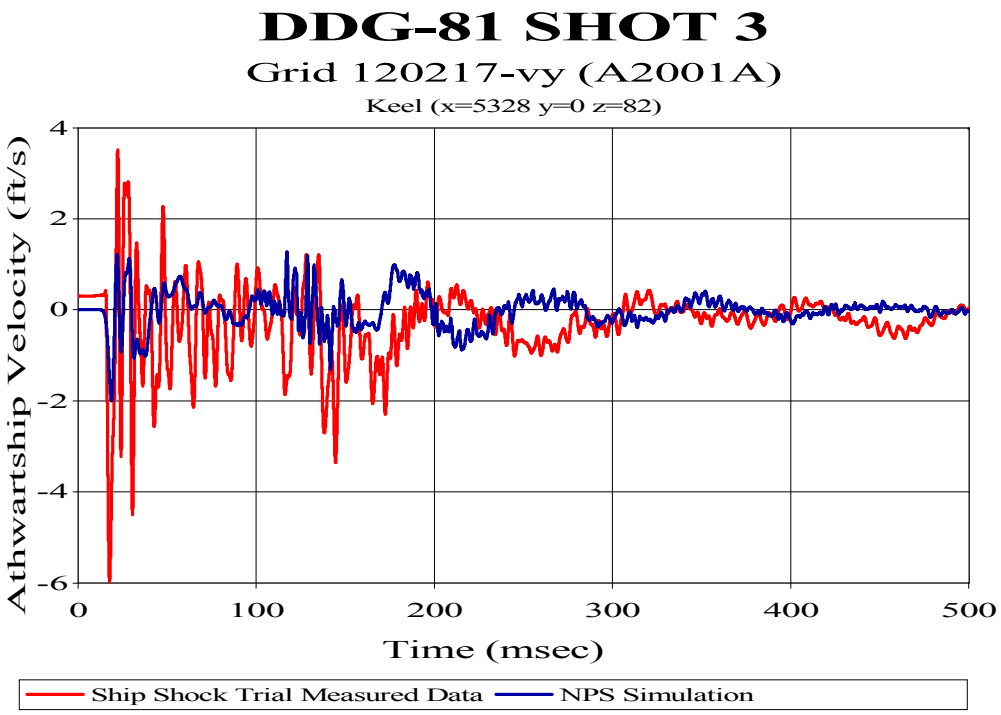

Figure 116. Keel Sensor A2001A: (RM = 0.4587, RP = 0.4203, RC = 0.5513)

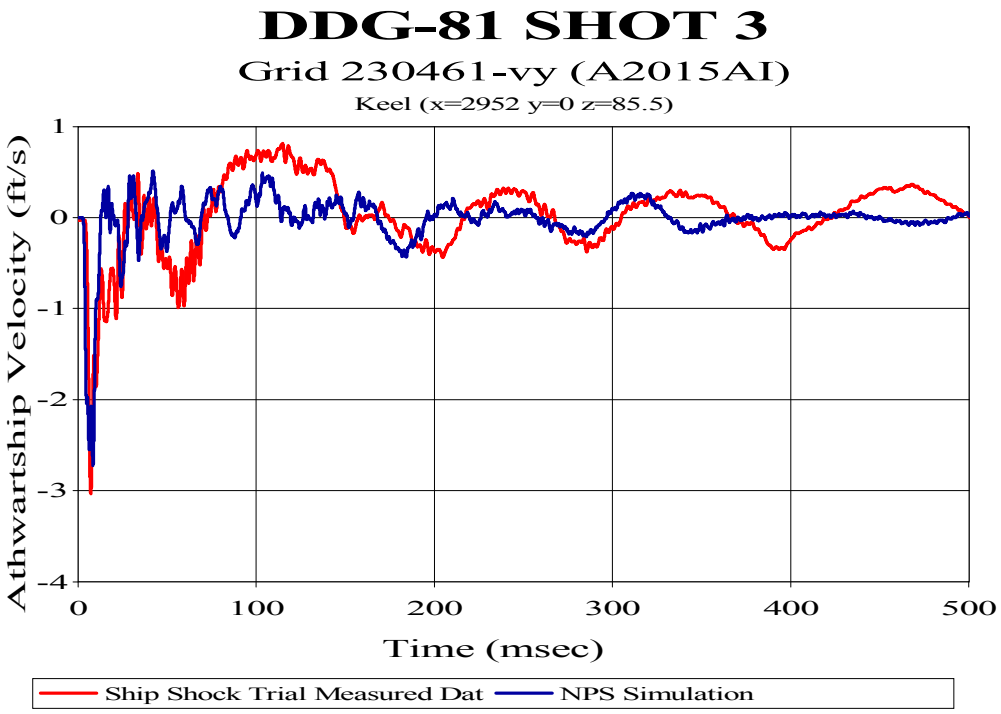

Figure 117. Keel Sensor A2015AI: (RM = 0.2428, RP = 0.3212, RC = 0.3568)

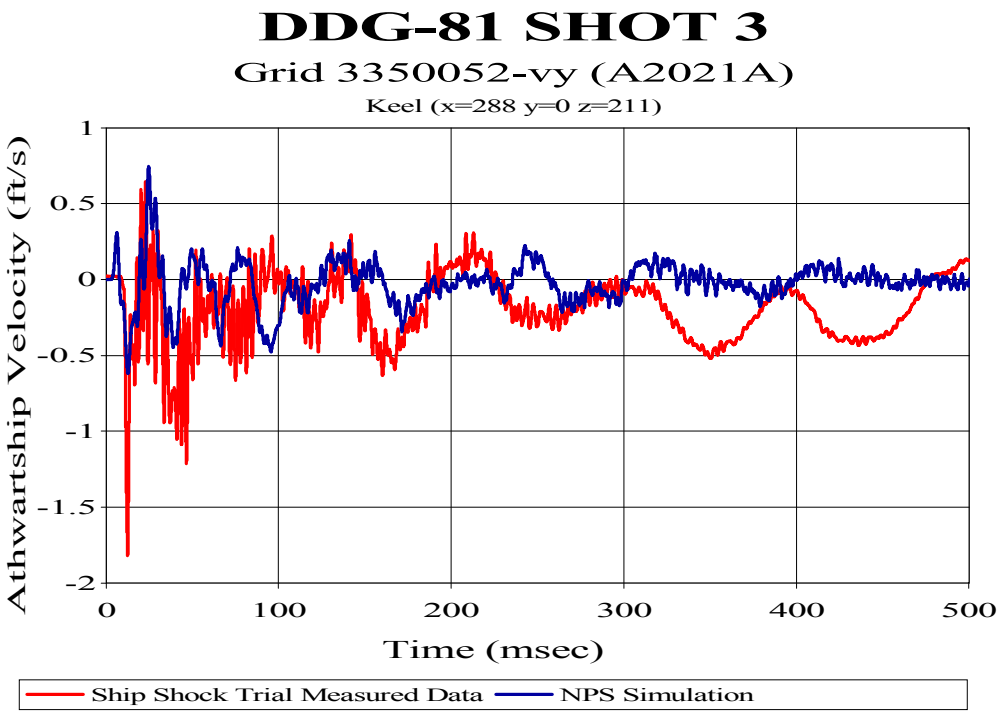

Figure 118. Keel Sensor A2021A: (RM = 0.4226, RP = 0.4295, RC = 0.5340)

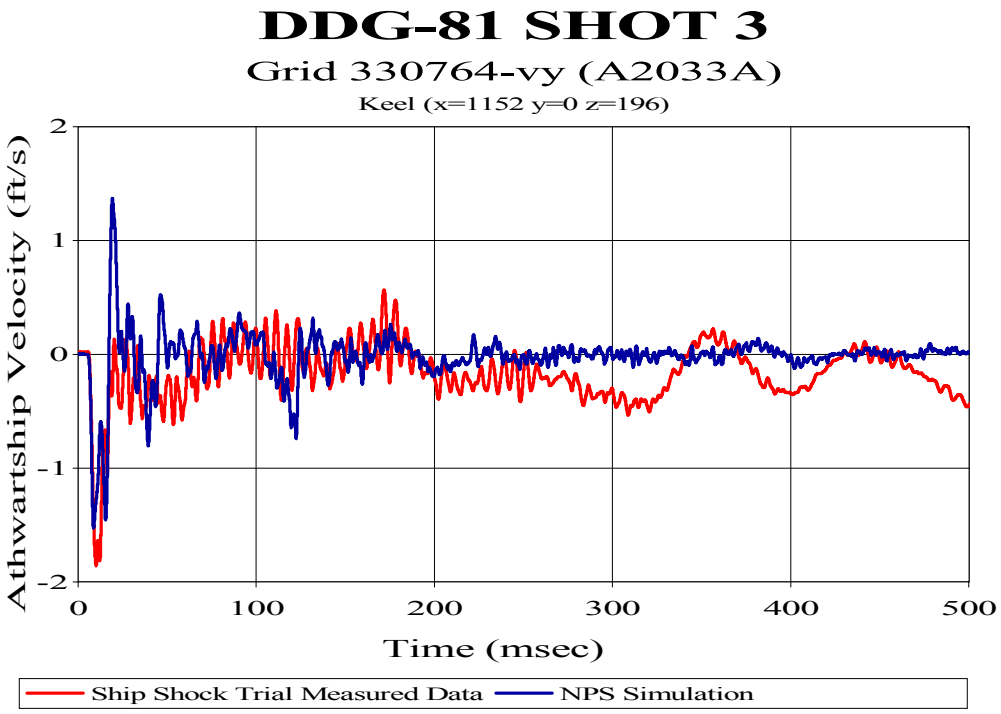

Figure 119. Keel Sensor A2033A: (RM = 0.2102, RP = 0.3771, RC = 0.3826)

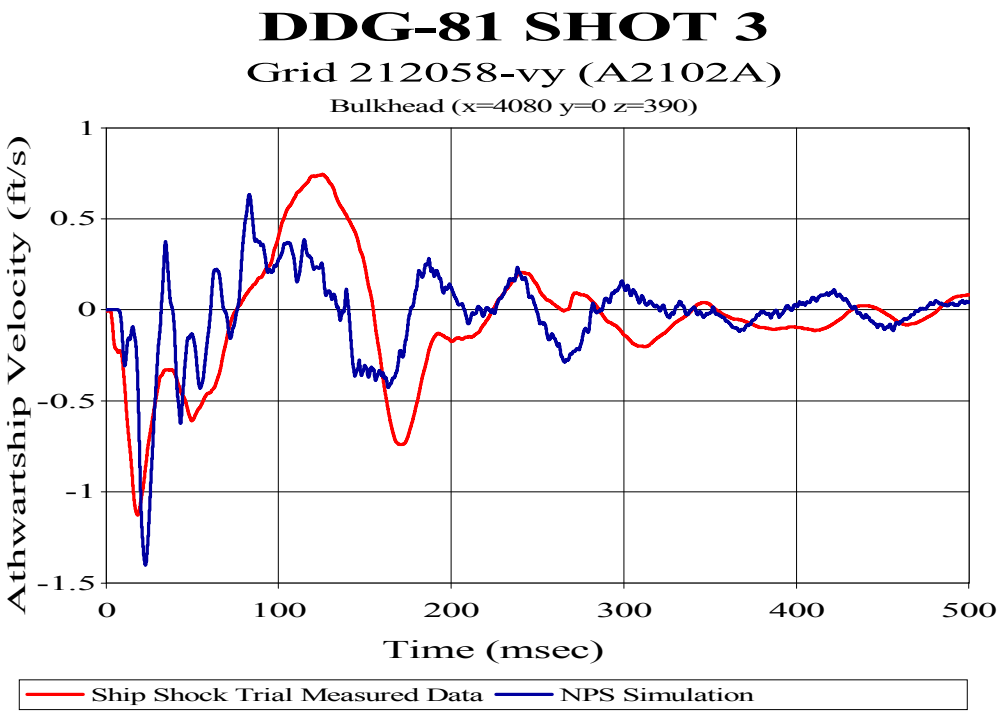

Figure 120. Bulkhead Sensor A2102A: (RM = 0.2265, RP = 0.3223, RC = 0.3491)

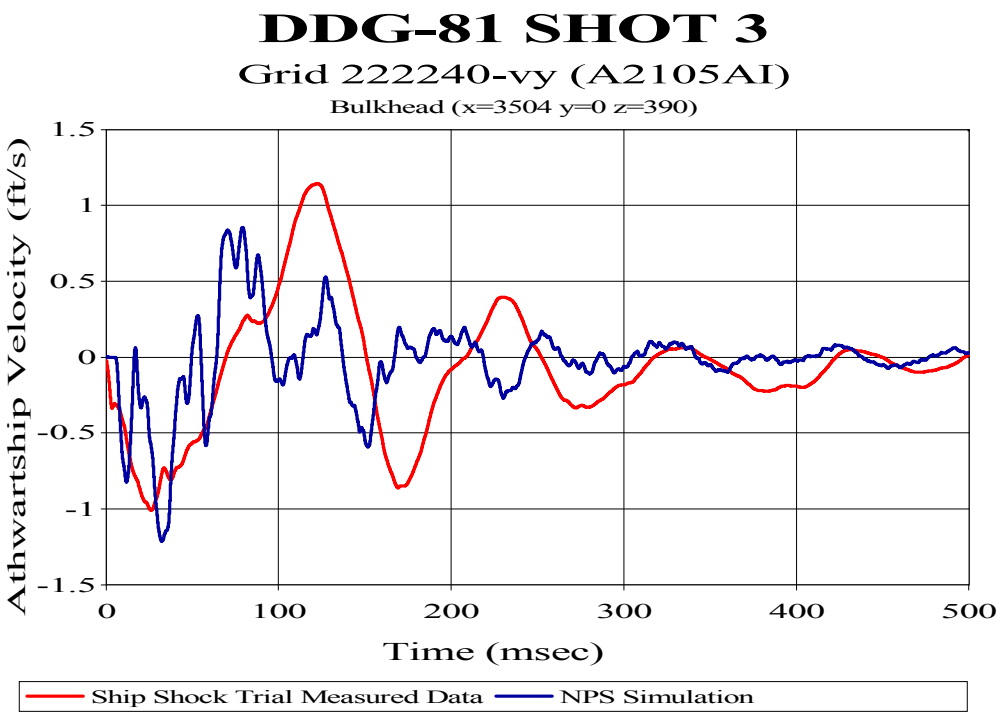

Figure 121. Bulkhead Sensor A2105AI: (RM = 0.2691, RP = 0.3725, RC = 0.4072)

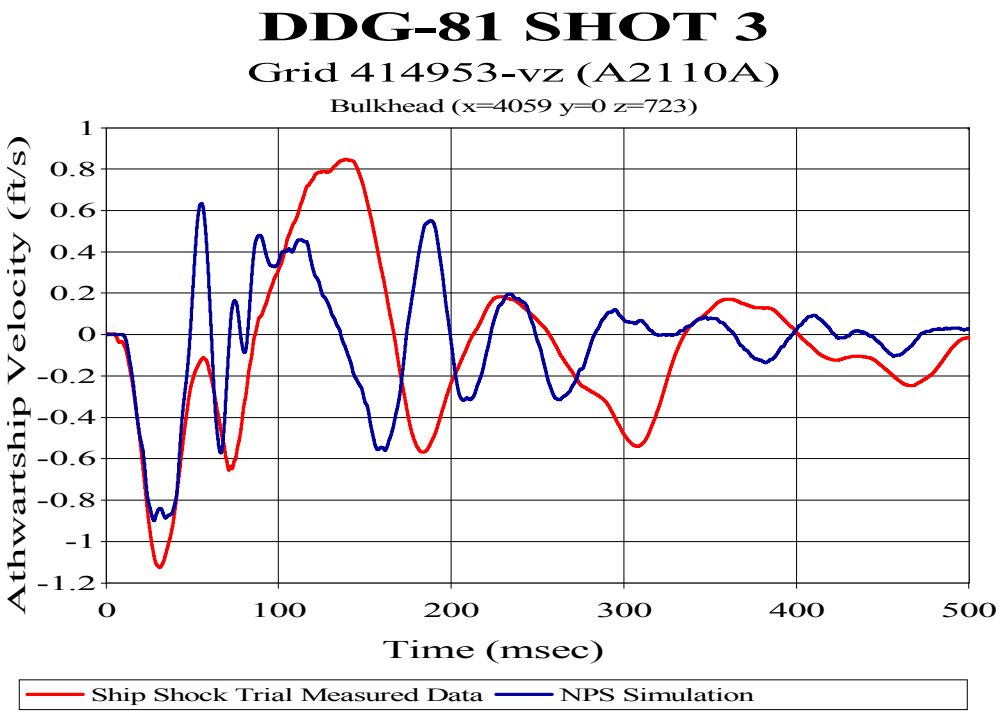

Figure 122. Bulkhead Sensor A2110A: (RM = 0.2156, RP = 0.3889, RC = 0.3941)

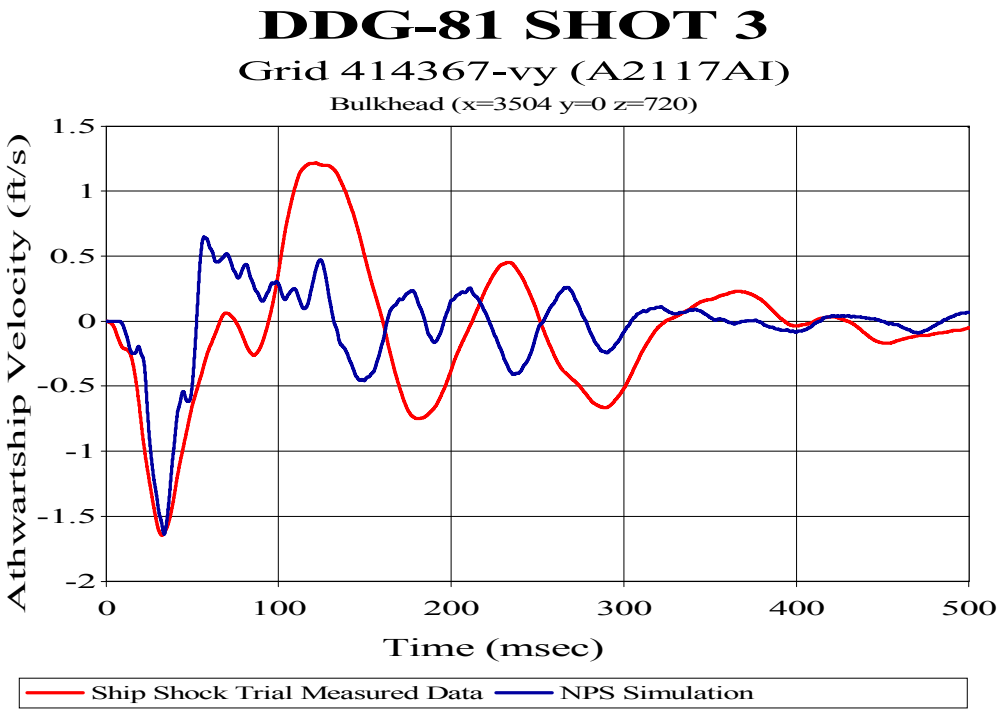

Figure 123. Bulkhead Sensor A2117AI: (RM = 0.3084, RP = 0.3551, RC = 0.4168)

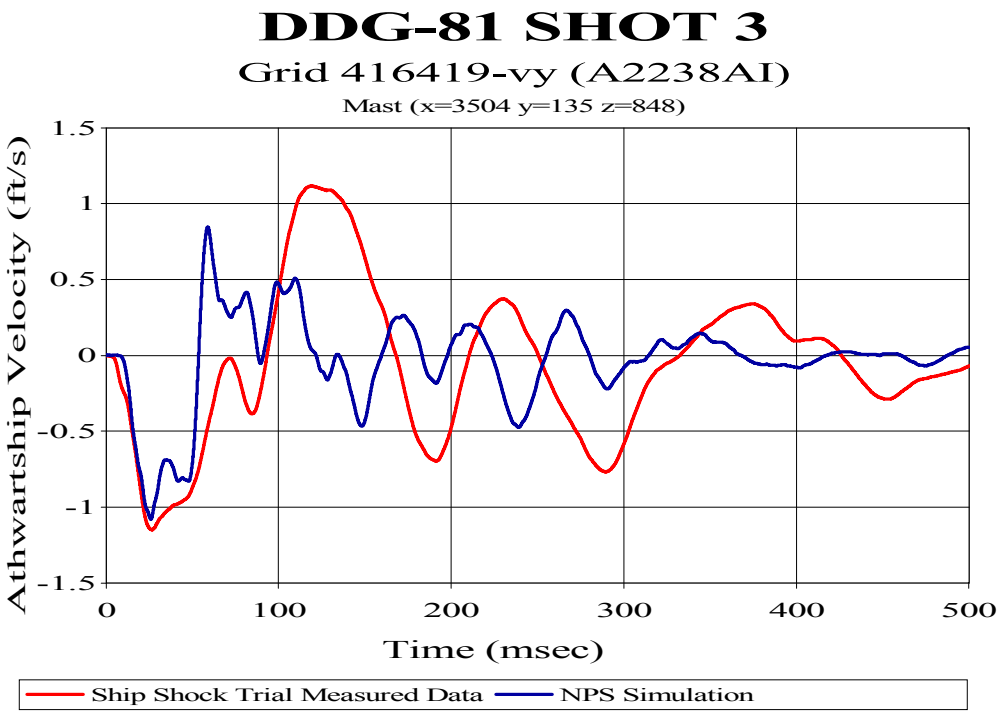

Figure 124. Mast Sensor A2117AI: (RM = 0.3248, RP = 0.3883, RC = 0.4487)

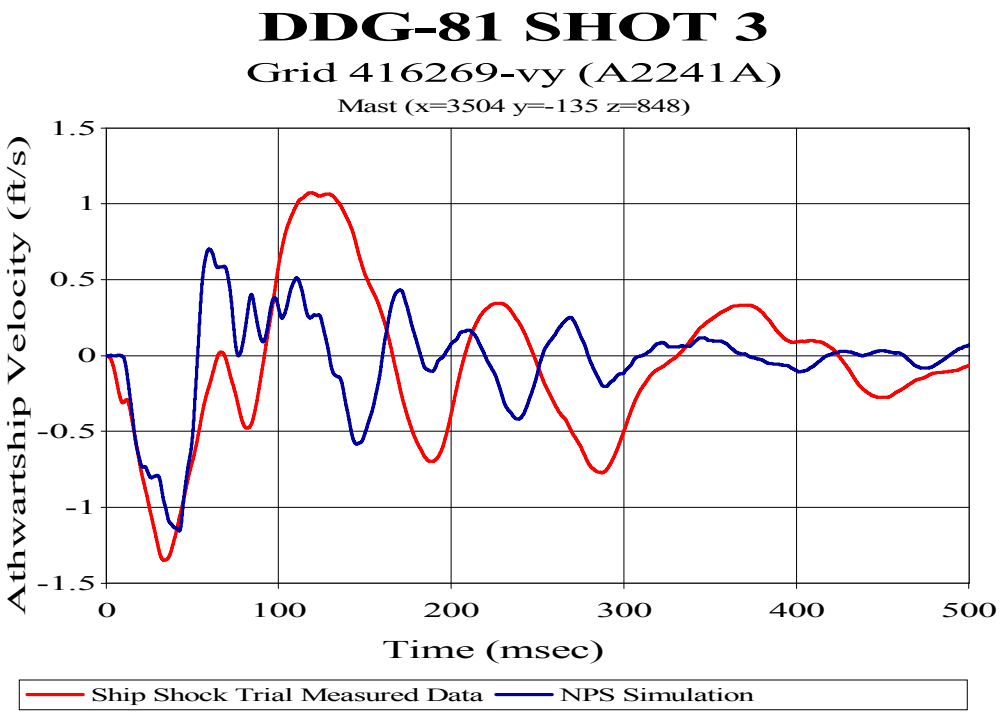

Figure 125. Mast Sensor A2241A: (RM = 0.2954, RP = 0.3741, RC = 0.4224)

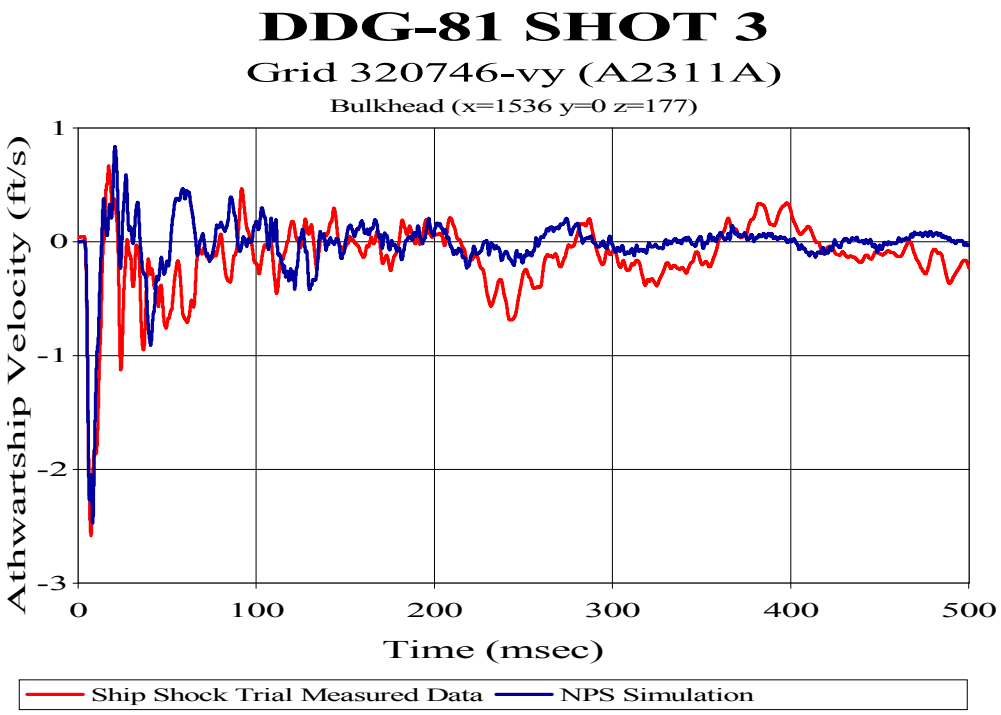

Figure 126. Bulkhead Sensor A2311A: (RM = 0.1937, RP = 0.3040, RC = 0.3194)

THIS PAGE INTENTIONALLY LEFT BLANK

APPENDIX D. RAYLEIGH DAMPING PROGRAM

The following program code was written using MATLAB® 6.1 release 12.1. The purpose of this program is to compute the Rayleigh damping coefficients for the damping comparison portion of this study.

```
% DDG-81 DAMPING COEFFICIENTS COMPARISON
% Ralyeigh Damping [C] = alpha [M] + beta [K]
% LT Jarema M. Didoszak, USN
% JUN 2003, Modified OCT 2003 from 3% to 4% Damping
% SVCL, Naval Postgraduate School, Monterey, CA

clc
format long

% NPS Damping
clear all
inputs=XLSREAD('nps');
zeta1= inputs(:,2);
omega1= inputs(:,1)*(2*pi);
A1= [1./(2*omega1), omega1/2];
alphabeta1=((conj(A1')*A1)^-1)*conj(A1')*zeta1
W=1:1885;
regen1=alphabeta1(1)./(2*W)+alphabeta1(2)*W/2;

% 4% and 4% damping
inputs=XLSREAD('44damping');
zeta44= inputs(:,2);
omega44= inputs(:,1)*(2*pi);
A44= [1./(2*omega44), omega44/2];
alphabeta44=((conj(A44')*A44)^-1)*conj(A44')*zeta44
W=1:1885;
regen44=alphabeta44(1)./(2*W)+alphabeta44(2)*W/2;

% 8% and 8% damping
inputs=XLSREAD('88damping');
zeta88= inputs(:,2);
omega88= inputs(:,1)*(2*pi);
A88= [1./(2*omega88), omega88/2];
alphabeta88=((conj(A88')*A88)^-1)*conj(A88')*zeta88
W=1:1885;
regen88=alphabeta88(1)./(2*W)+alphabeta88(2)*W/2;
```

```
figure(1)
plot(W/(2*pi),regen1,'b')
hold on
plot(W/(2*pi),regen44,'g')
plot(W/(2*pi),regen88,'r')
%legend('NPS DAMPING                    ', ...
 %     '4% DAMPING                     ', ...
  %    '8% DAMPING                      ')
plot(omega1/(2*pi),zeta1,'b')
plot(omega44/(2*pi),zeta44,'k.')
plot(omega88/(2*pi),zeta88,'k.')
axis([0 300 0.0001 0.35])
title('RAYLEIGH DAMPING')
xlabel('FREQUENCY (Hz)'), ylabel('DAMPING RATIO')
hold off

figure (2)
loglog(W/(2*pi),regen1,'b')
hold on
loglog(W/(2*pi),regen44,'g')
loglog(W/(2*pi),regen88,'r')
%legend('NPS DAMPING                    ', ...
 %     '4% DAMPING                     ', ...
 %     '8% DAMPING                     ')
loglog(omega1/(2*pi),zeta1,'b')
loglog(omega44/(2*pi),zeta44,'k.')
loglog(omega88/(2*pi),zeta88,'k.')
axis([2e-1 3e2 5e-3 1e1])
title('RAYLEIGH DAMPING')
xlabel('FREQUENCY (Hz)'), ylabel('DAMPING RATIO')
hold off
```

APPENDIX E. DAMPING VERTICAL VELOCITY RESPONSE PLOTS

1. SHOT 2 (500 MSEC)

The following vertical velocity plots are from the Shot 2 damping coefficient comparison. The Russell's error factor following each of the figure captions are only for the correlation between the simulations using the NPS damping values (α = 19.2, and β = 2.09E-06) and the measured data from the ship shock trial conducted at sea.

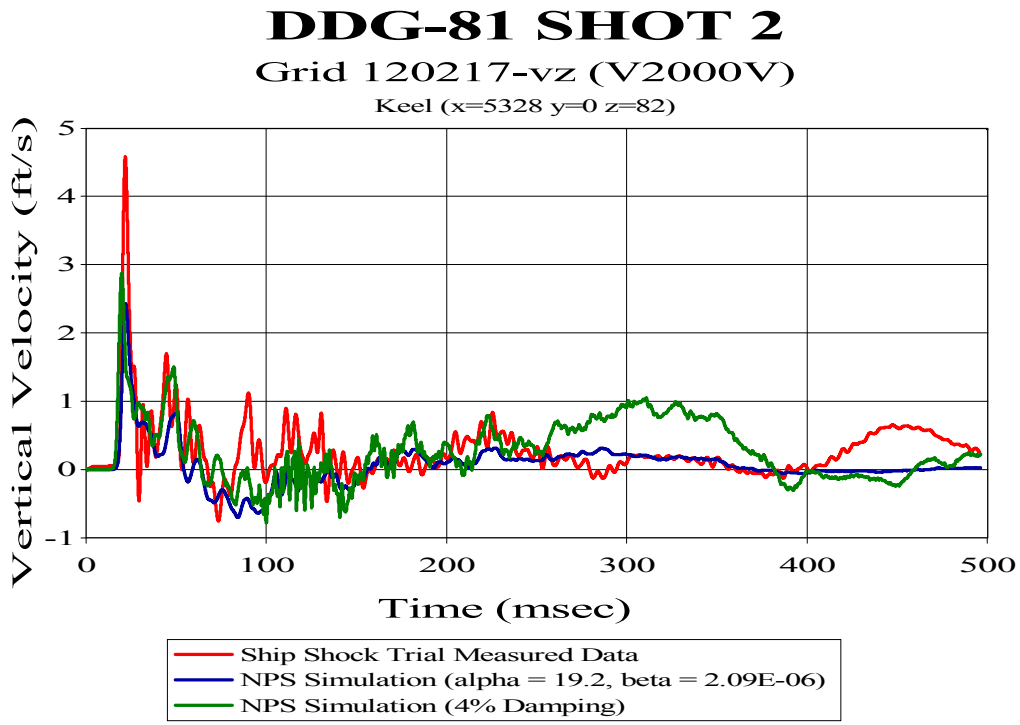

Figure 127. Keel Sensor V2000V: (RM = 0.3169, RP = 0.2887, RC = 0.3800)

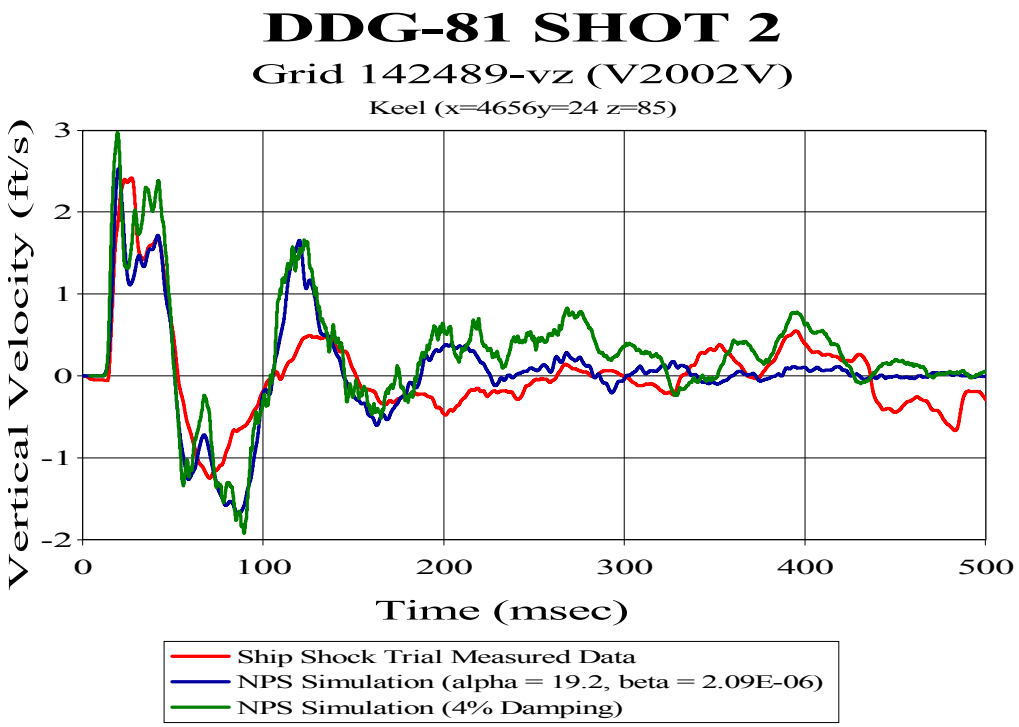

Figure 128. Keel Sensor V2002V: (RM = 0.0679, RP = 0.2175, RC = 0.2019)

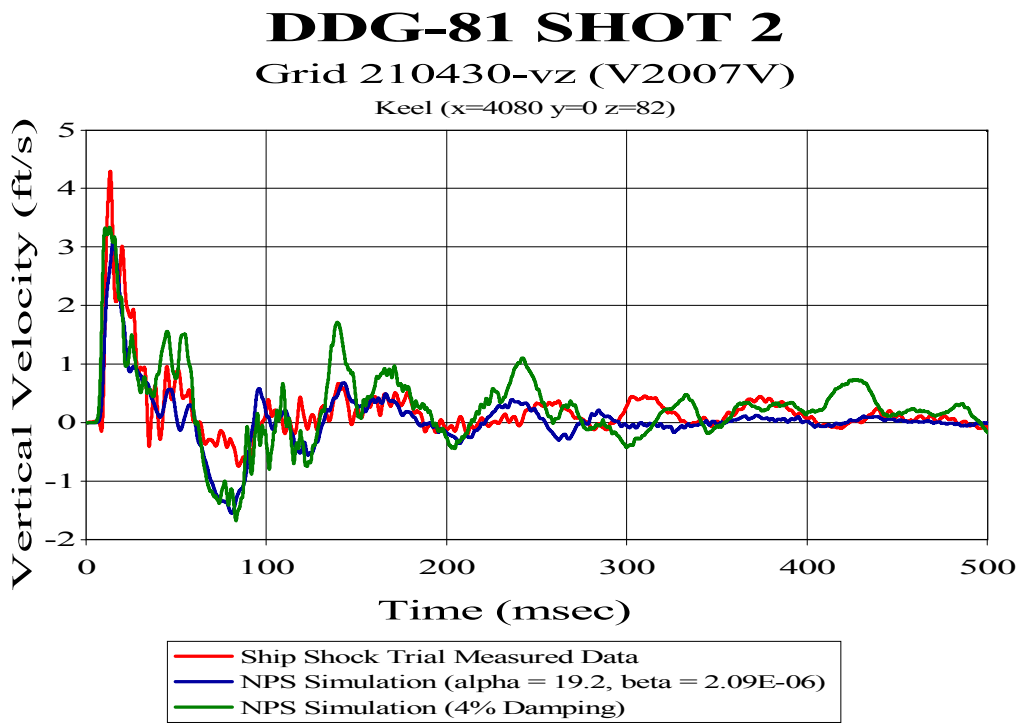

Figure 129. Keel Sensor V2007V: (RM = 0.0879, RP = 0.2164, RC = 0.2070)

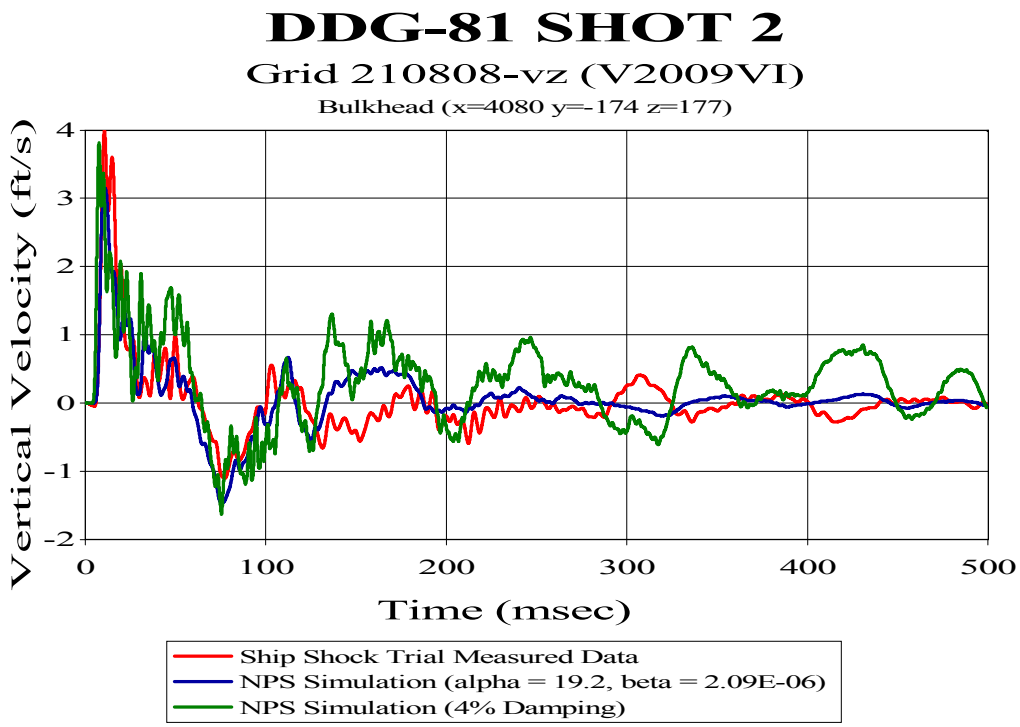

Figure 130. Bulkhead Sensor V2009VI: (RM = 0.0882, RP = 0.2272, RC = 0.2160)

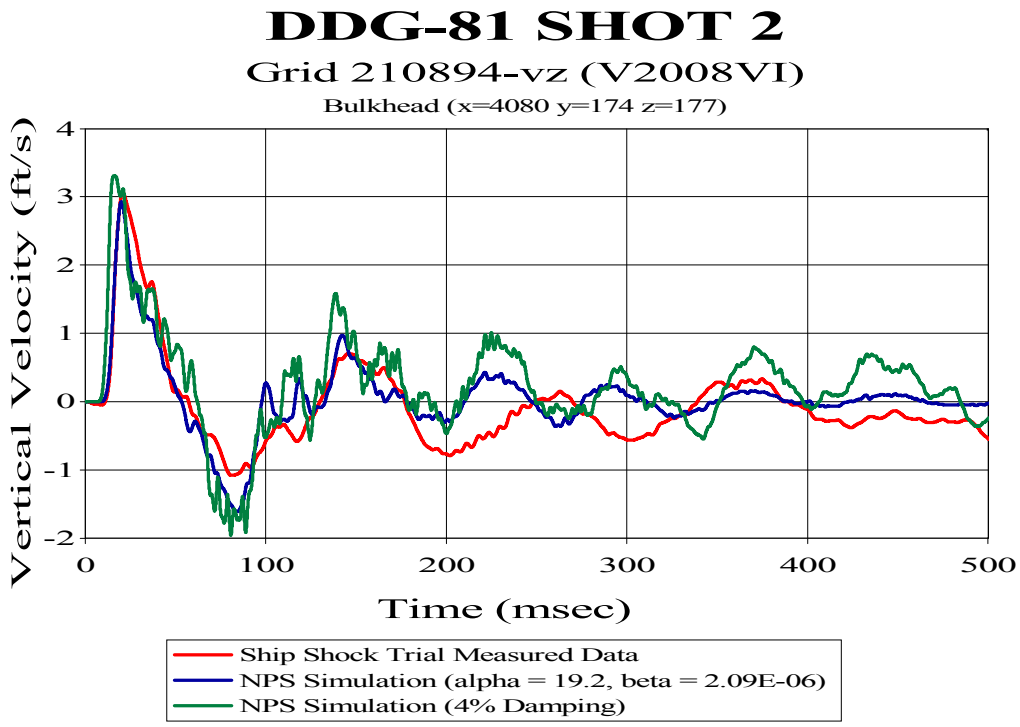

Figure 131. Bulkhead Sensor V2008VI: (RM = 0.1200, RP = 0.1932, RC = 0.2016)

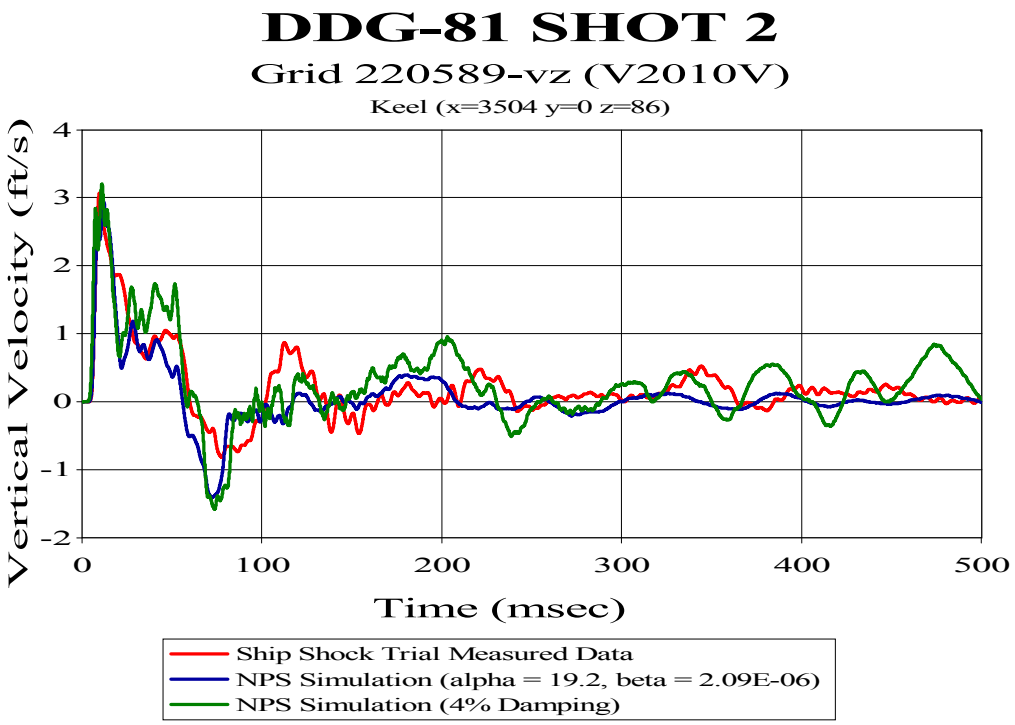

Figure 132. Keel Sensor V2010V: (RM = 0.0827, RP = 0.2070, RC = 0.1975)

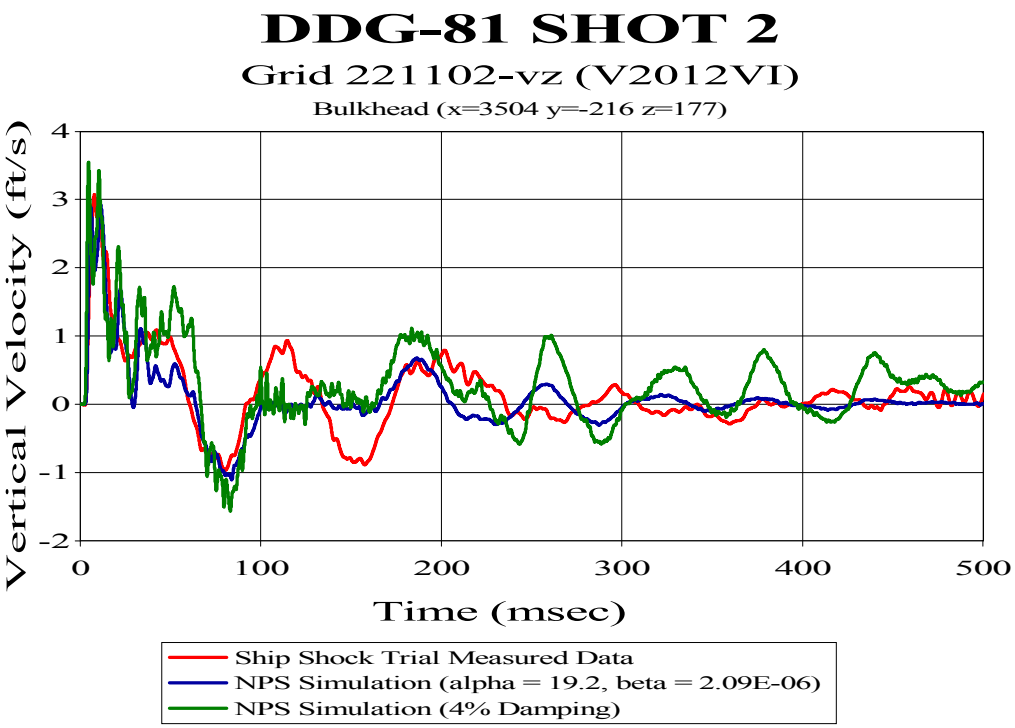

Figure 133. Bulkhead Sensor V2012VI: (RM = 0.1299, RP = 0.2211, RC = 0.2273)

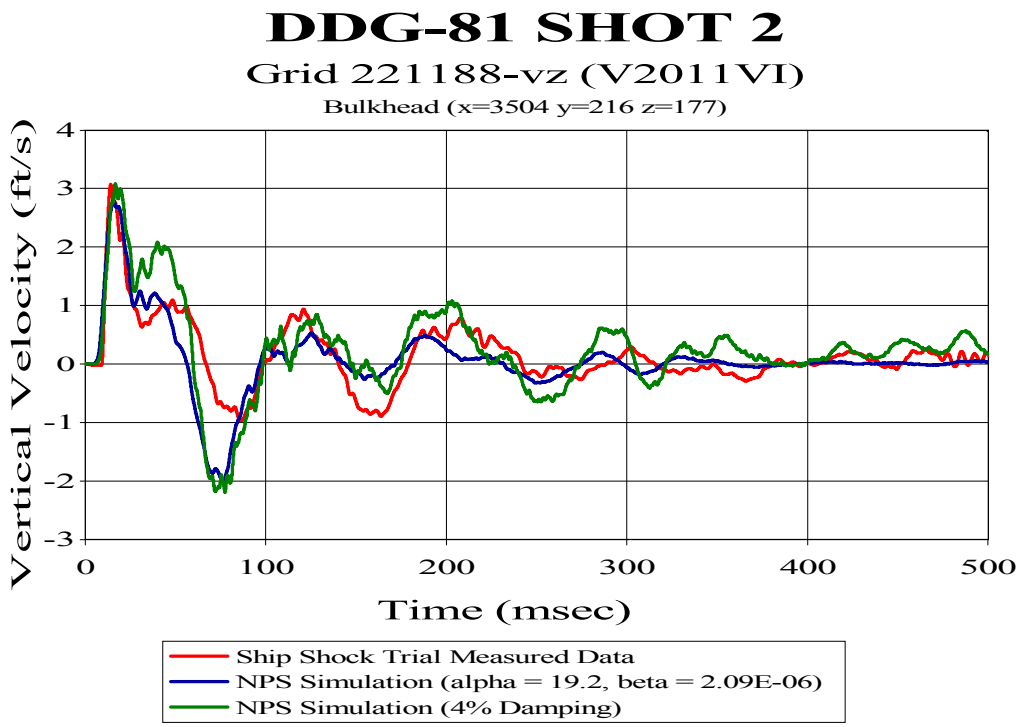

Figure 134. Bulkhead Sensor V2011VI: (RM = 0.0411, RP = 0.2240, RC = 0.2018)

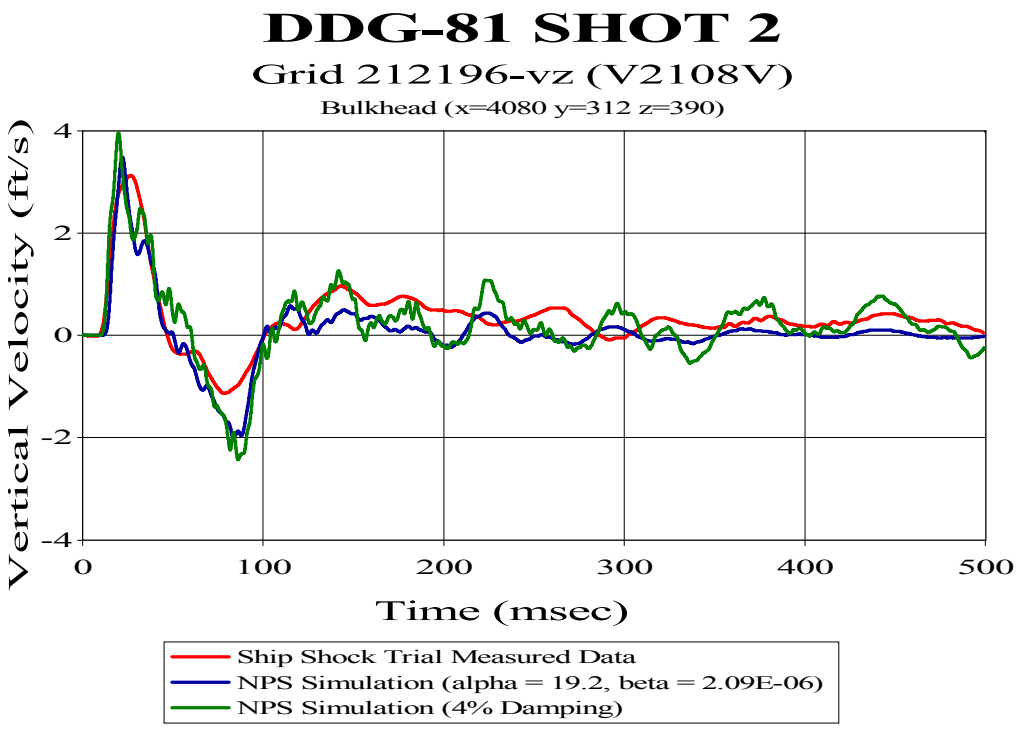

Figure 135. Bulkhead Sensor V2108V: (RM = 0.0809, RP = 0.1858, RC = 0.1796)

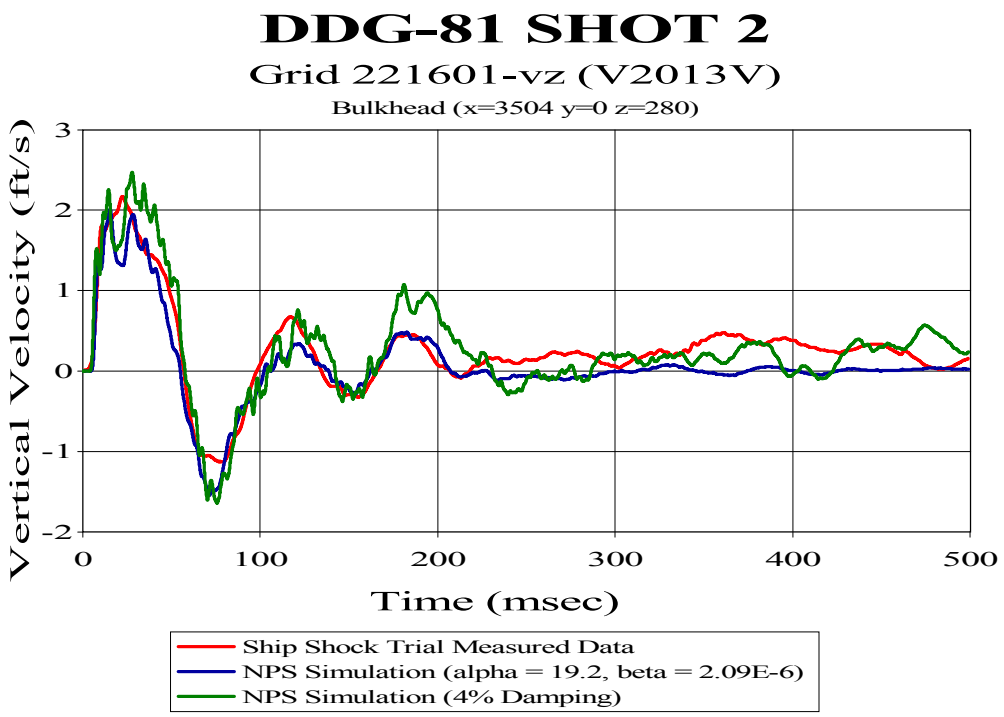

Figure 136. Bulkhead Sensor V2013V: (RM = 0.1049, RP = 0.1420, RC = 0.1565)

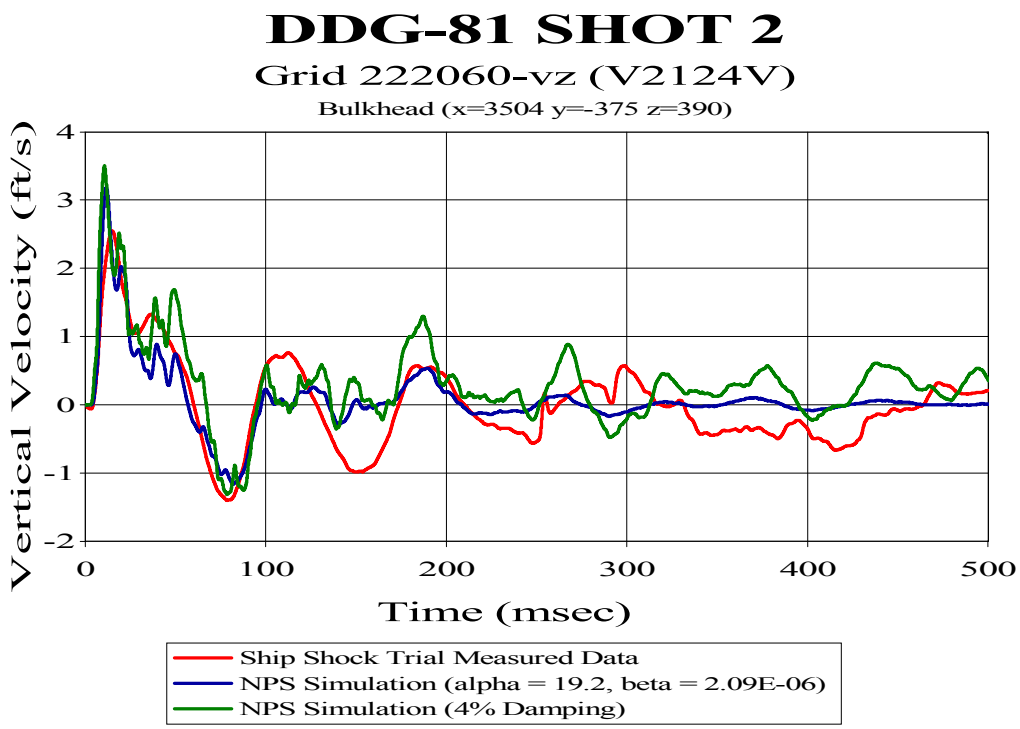

Figure 137. Bulkhead Sensor V2124V: (RM = 0.1793, RP = 0.2311, RC = 0.2456)

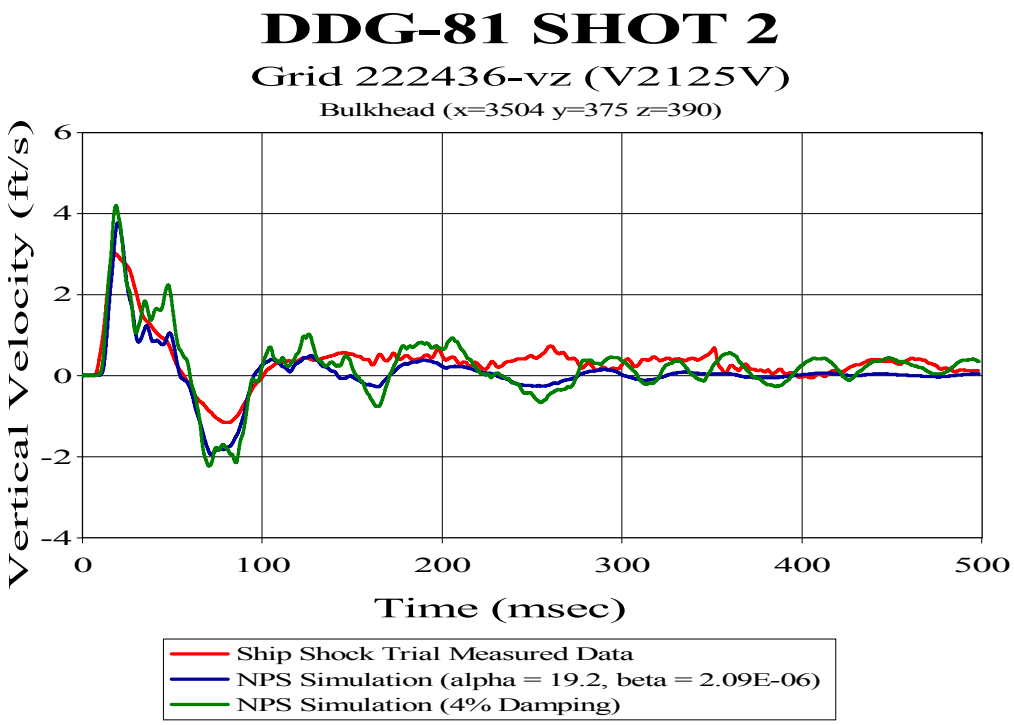

Figure 138. Bulkhead Sensor V2125V: (RM = 0.0214, RP = 0.1914, RC = 0.1707)

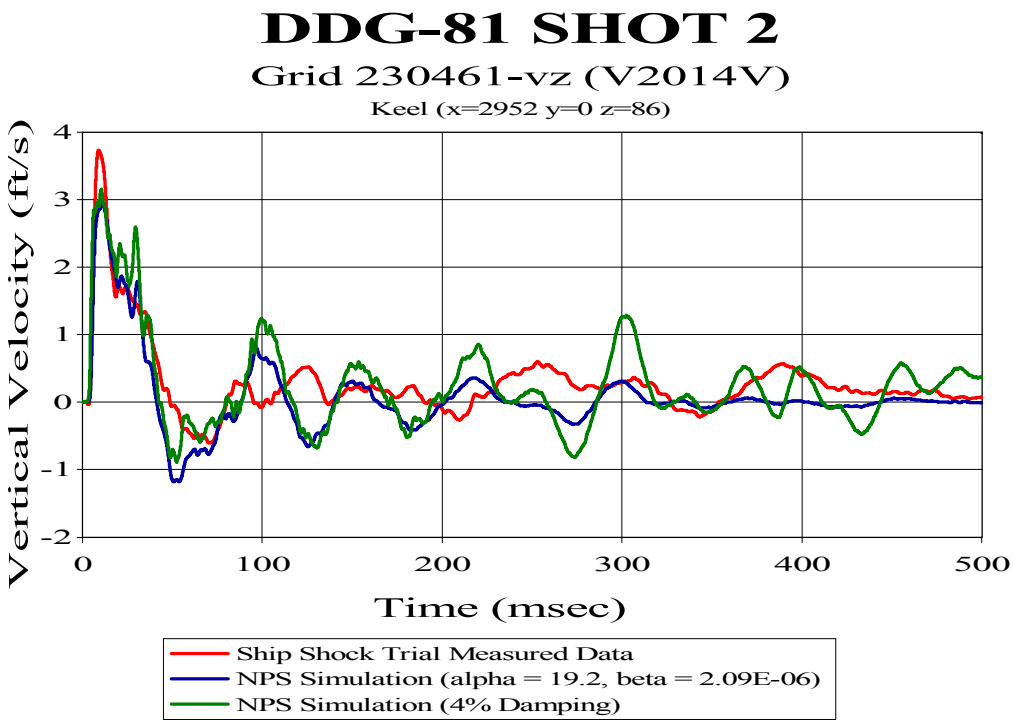

Figure 139. Keel Sensor V2014V: (RM = 0.0590, RP = 0.2126, RC = 0.1956)

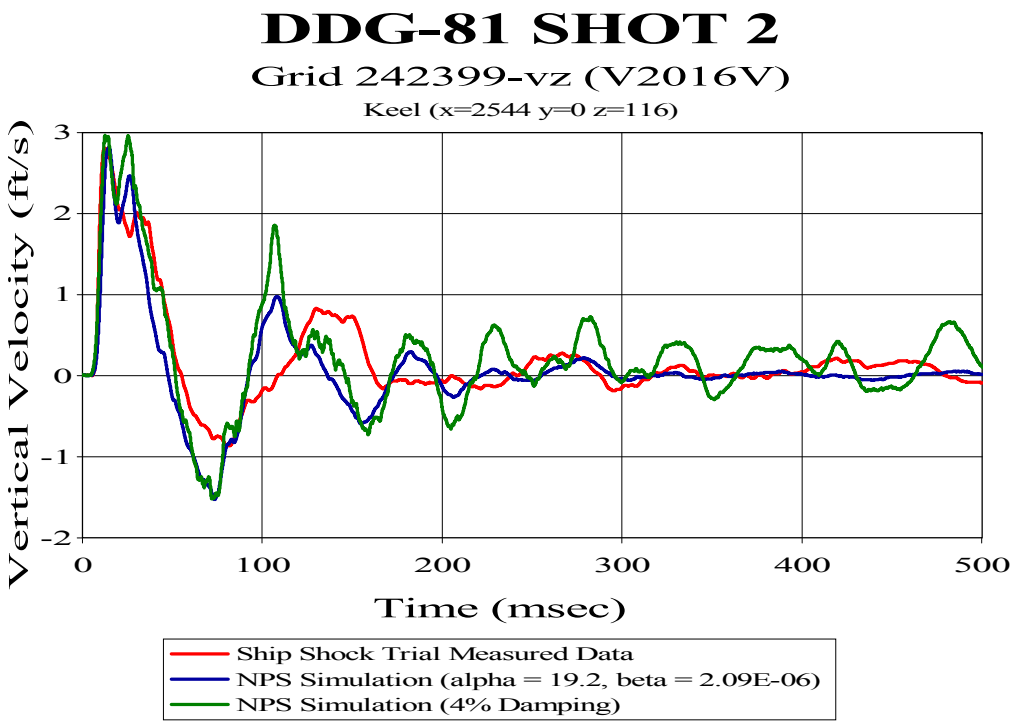

Figure 140. Keel Sensor V2016V: (RM = 0.0169, RP = 0.2038, RC = 0.1812)

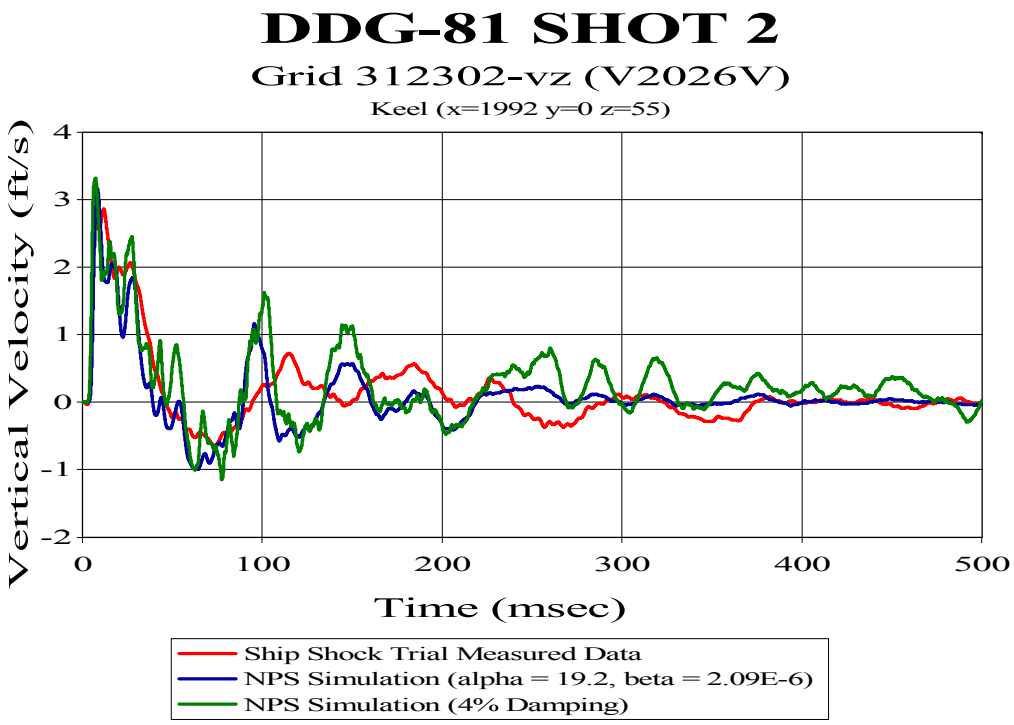

Figure 141. Keel Sensor V2026V: (RM = 0.0751, RP = 0.2185, RC = 0.2047)

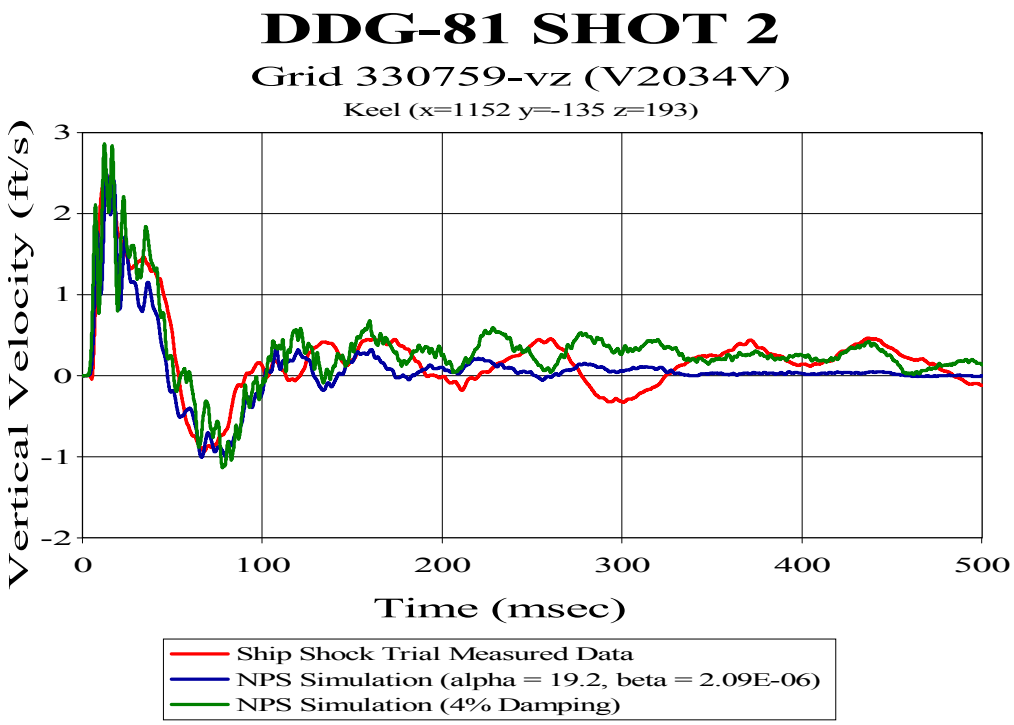

Figure 142. Keel Sensor V2034V: (RM = 0.1442, RP = 0.1874, RC = 0.2095)

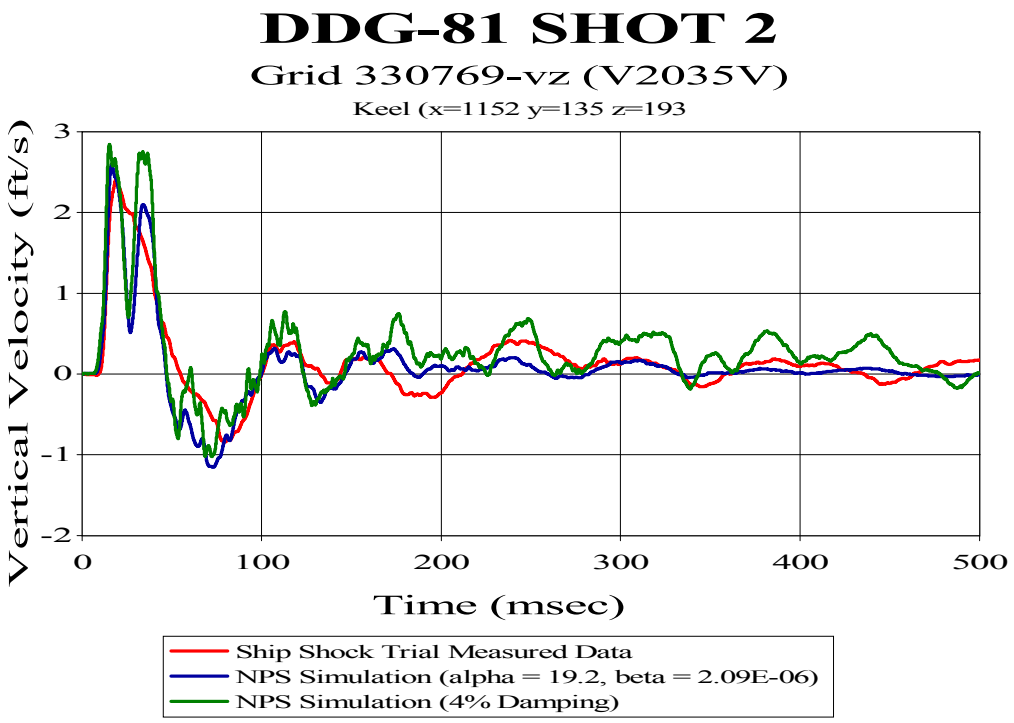

Figure 143. Keel Sensor V2035V: (RM = 0.0009, RP = 0.1692, RC = 0.1500)

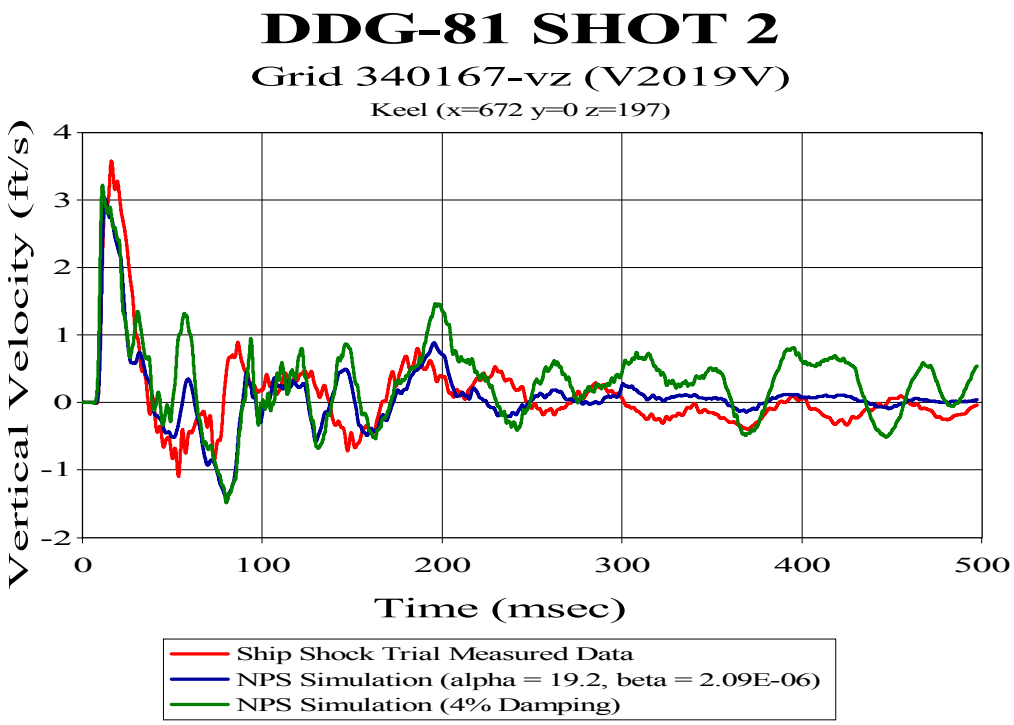

Figure 144. Keel Sensor V2019V: (RM = 0.1327, RP = 0.2391, RC = 0.2423)

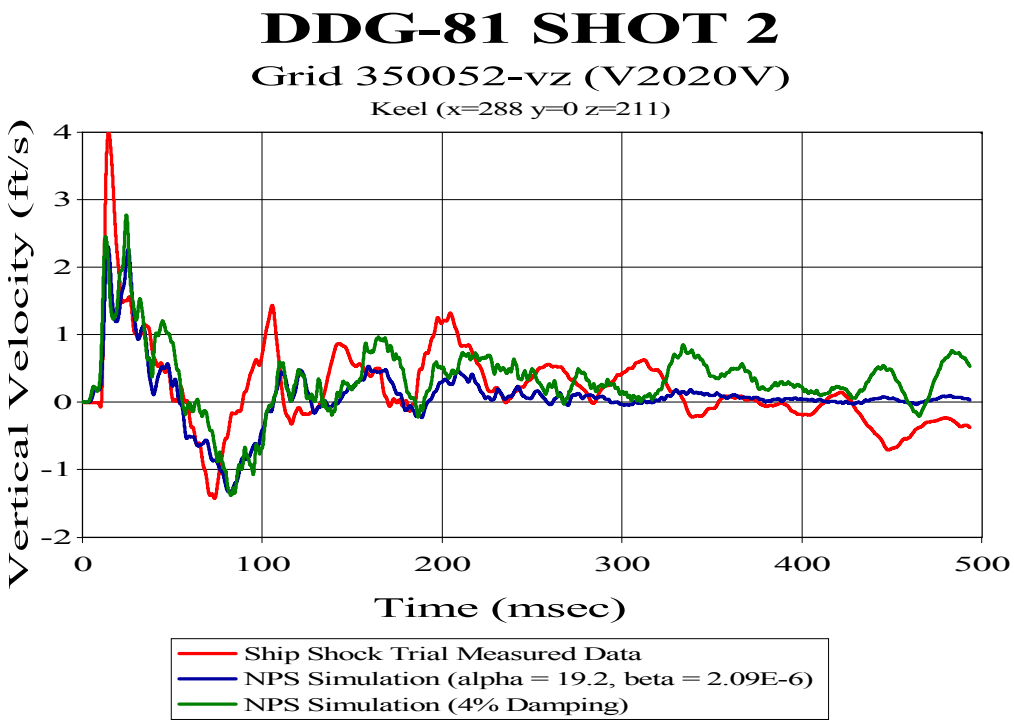

Figure 145. Keel Sensor V2020V: (RM = 0.2477, RP = 0.2657, RC = 0.3219)

2. SHOT 2 (250 MSEC)

The following vertical velocity plots are the supporting plots for the comparison of damping coefficients at selected sensor locations. These are a subset of the sensors listed in Section 1 of this appendix. These sensor locations were specifically chosen for further analysis since the simulations conducted using the NPS damping values provided poorer correlation with the measured ship shock trial data than did the simulations performed using the fixed 4% damping values.

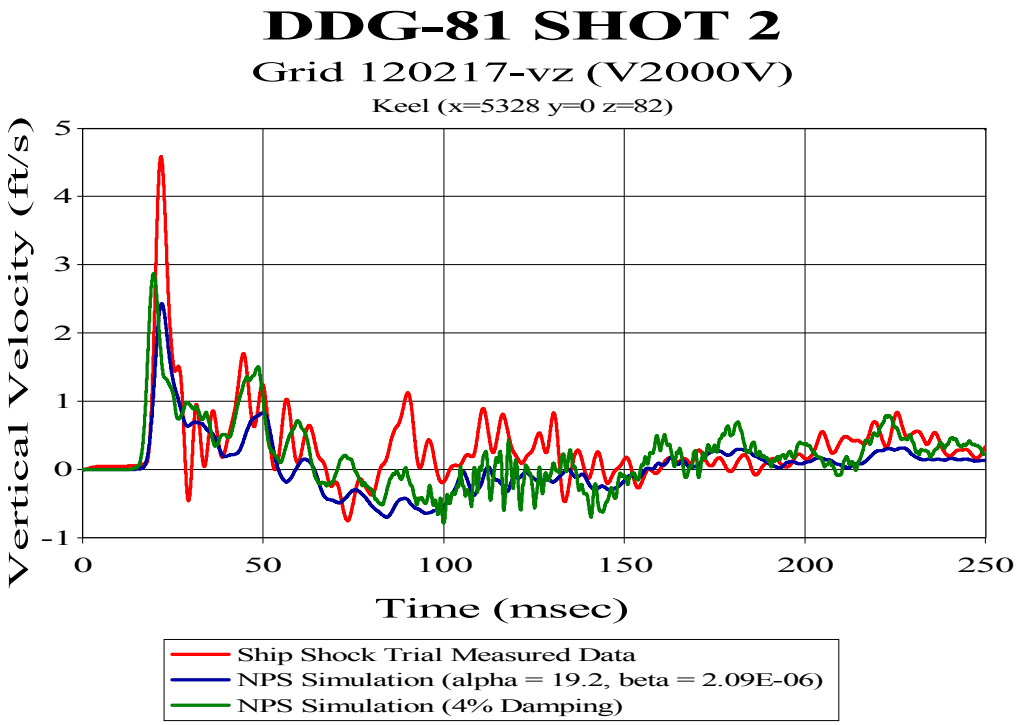

Figure 146. Keel Sensor V2000V: (RM = 0.2817, RP = 0.2599, RC = 0.3397)

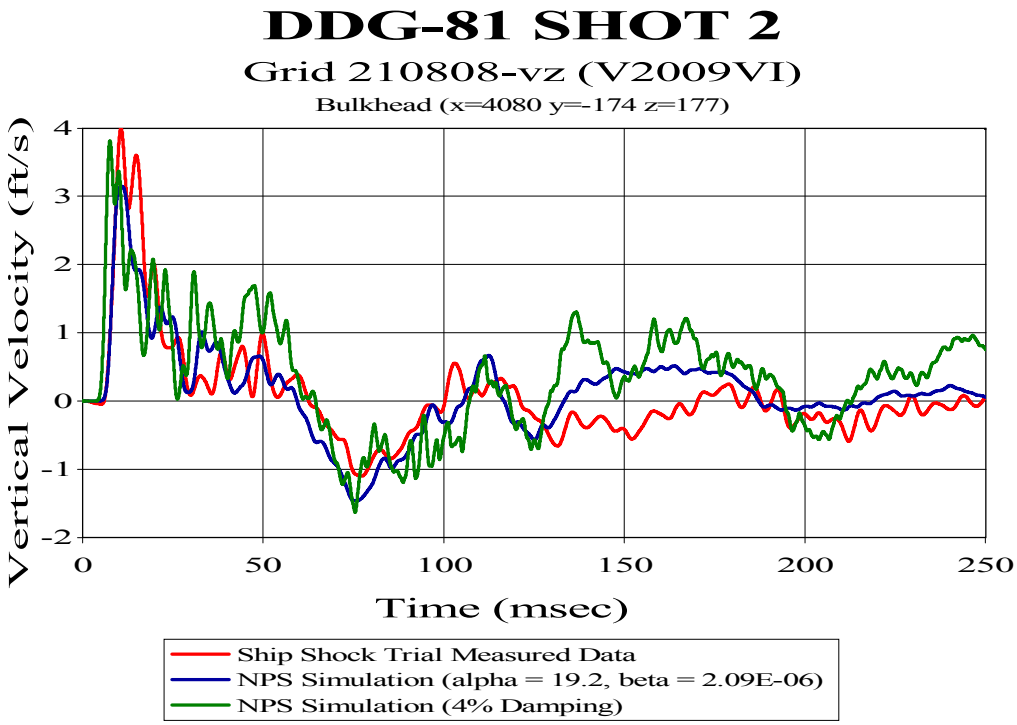

Figure 147. Bulkhead Sensor V2009VI: (RM = 0.0630, RP = 0.1868, RC = 0.1747)

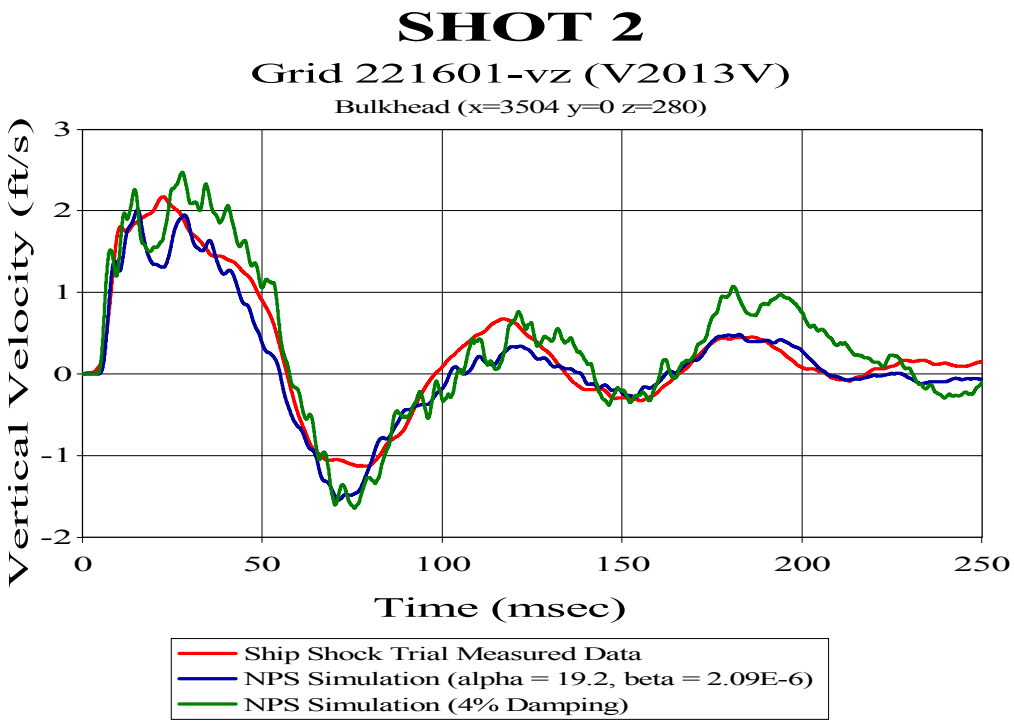

Figure 148. Bulkhead Sensor V2013V: (RM = 0.0700, RP = 0.0934, RC = 0.1034)

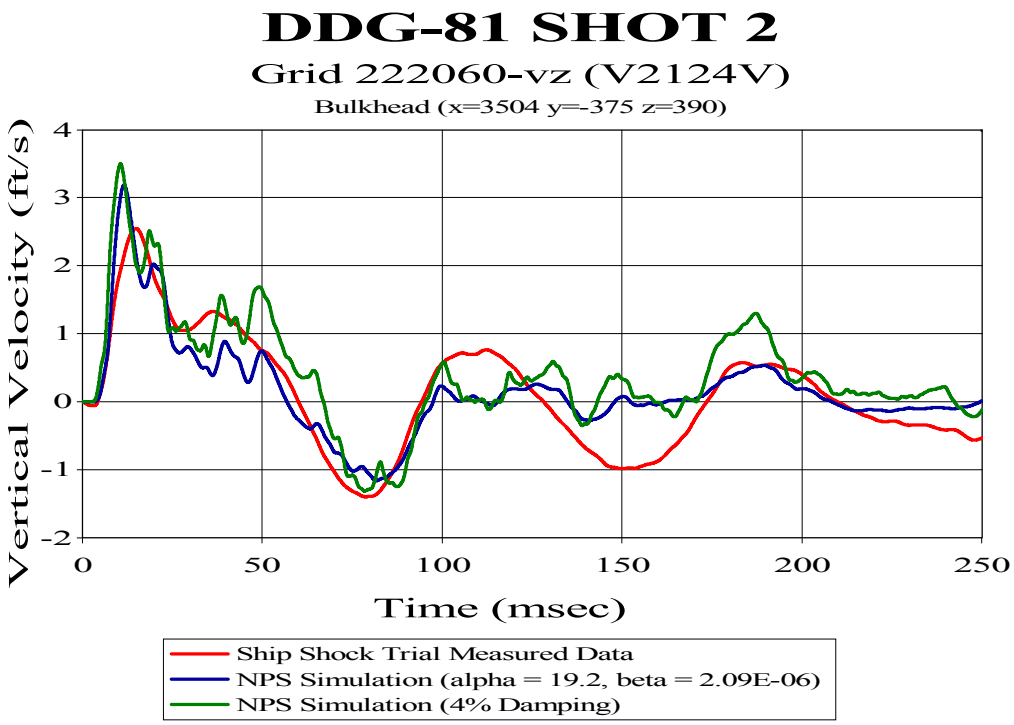

Figure 149. Bulkhead Sensor V2124V: (RM = 0.1418, RP = 0.1720, RC = 0.1976)

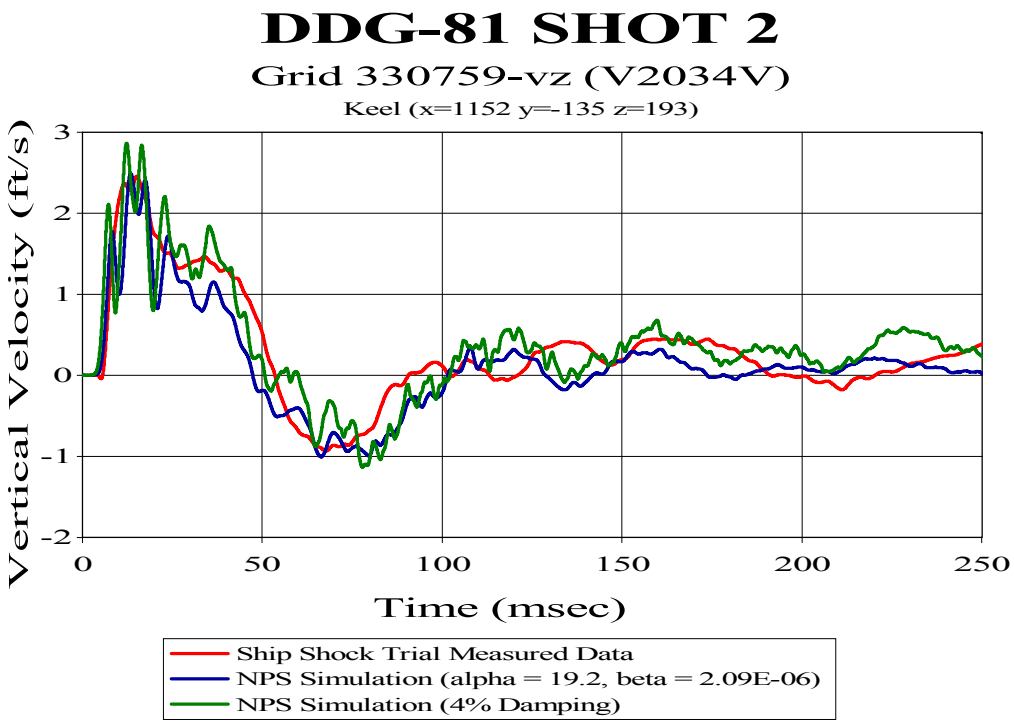

Figure 150. Keel Sensor V2034V: (RM = 0.1138, RP = 0.1456, RC = 0.1638)

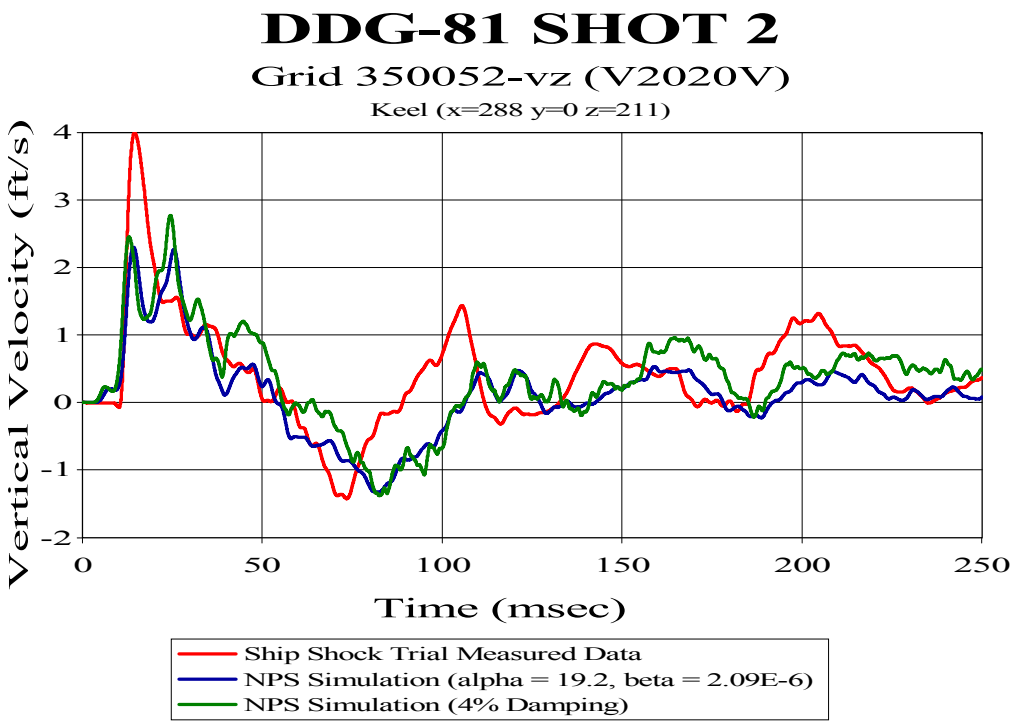

Figure 151. Keel Sensor V2020V: (RM = 0.2161, RP = 0.2423, RC = 0.2877)

LIST OF REFERENCES

1. NSWCCD/UERD, www.dt.navy.mil/sites/uerd/history.html, December 2003.

2. OPNAV Instruction 9072.2, "Shock Hardening of Surface Ships", 12 January 1987.

3. NAVSEA 0908-LP-000-3010A, Shock Design Criteria for Surface Ships, October 1994.

4. Military Specification, MIL-S-901D, Shock Tests, High Impact Shipboard Machinery, Equipment and Systems, Requirements for, March 1989.

5. DOT&E FY97 Annual Report, www.globalsecurity.org/military/library/budget/fy1997/dot-e/navy/97ddg51.html, November 2003.

6. Shin, Y. S. and Park, S. Y., "Ship Shock Trial Simulation of USS John Paul Jones (DDG 53) Using LS-DYNA/USA: Three Dimensional Analysis", 70th Shock and Vibration Symposium Proceedings, Vol. I, November 1999..

7. Mair, H. U., Reese, R.M., and Hartsough, K., "Simulated Ship Shock Tests/Trials?", www.ida.org/LFTEsimulation/documents/SSSTT.htm, October 2003.

8. Schneider, N. A., "Prediction of Surface Ship Response to Severe Underwater Explosions Using a Virtual Underwater Shock Environment", Master's Thesis, Naval Postgraduate School, Monterey, CA, 2003.

9. Shin, Y.S., "Naval Ship Shock and Design Analysis", Course Notes for Underwater Shock Analysis, Naval Postgraduate School, Monterey, CA 1996.

10. Cole, R.H., *Underwater Explosions*, pp. 1-15, Princeton University Press, 1948.

11. DeRuntz, Jr., J.A., *The Underwater Shock Analysis (USA) Manual*, Unique Software Applications, Colorado Springs, CO, May 1996.

12. Arons, A.B., et al, "Long Range Shock Propagation in Underwater Explosion Phenomena II", Underwater Explosion Compendium, Vol. 1, October 1949.

13. DeRuntz, Jr., J.A. "The Underwater Shock Analysis Code and Its Applications", 60th Shock and Vibration Symposium, Vol. I, pp. 89-107, November 1989.

14. Shin, Y.S., "Ship-Shock Modeling and Simulation with Applications Using LS-DYNA/USA Code, and Review of DDAM", Naval Postgraduate School, July 2002.

15. Geers, T. L., "Doubly Asymptotic Approximations for Transient Motions of Submerged Structures", Journal of the Acoustical Society of America, Vol. 64, pp 1500-1508, 1978.

16. DeRuntz, Jr. J. A. and Rankin, C. C., "Applications of the USA-STAGS-CFA Code to Nonlinear Fluid-Structure Interaction Problems in Underwater Shock of Submerged Structures," Proceedings of the 60th Shock and Vibration Symposium, 1989.

17. Shin, Y. S. and Santiago, L. D., "Surface Ship Modeling and Simulation", The ASME PVP, Vol. 351, pp. 29-34, 1997 ASME PVP Conference, July 1997.

18. Harrington, M. J., Gibbs & Cox, Inc., "DDG-51 Flight IIA Shock Simulation", Presentation at the Naval Postgraduate School, August 2002.

19. Riedel, J. S., DDG 51 Shipbuilding Program (PMS 400D), "USS WINSTON S. CHURCHILL (DDG 81) Shock Trial Overview", Presentation at Naval Postgraduate School, February 2002.

20. Hart, D. T., "Ship Shock Trial Simulation of USS Winston S. Churchill (DDG-81): Surrounding Fluid Effect", Master's Thesis, Naval Postgraduate School, Monterey, CA, 2003.

21. DeRuntz, Jr., J. A. and Shin, Y. S., "USA/LS-DYNA3D Software Training Course", Naval Postgraduate School, Monterey, CA, June 1996.

22. Shin, Y. S., "LS-DYNA Training Guide: Nonlinear Dynamic Analysis of Structures in 3-D Code Coupled with Underwater Shock Analysis Code for Ship Shock Modeling and Simulation", Naval Postgraduate School, July 2002.

23. Ceetron ASA, "GLview Pro Installation Guide & Tutorial: GLview Pro 6.3", Trondheim, Norway, 2001.

24. Russell, D. D., "Error Measures for Comparing Transient Data: Part I: Development of a Comprehensive Error Measure", 68th Shock and Vibration Symposium Proceedings, Vol. I, November 1997.

25. Russell, D. D., "Error Measures for Comparing Transient Data: Part II: Error Measure Case Study", 68th Shock and Vibration Symposium Proceedings, Vol. I, November 1997.

26. Russell, D. D., "DDG53 Shock Trial Simulation Acceptance Criteria", 69th Shock and Vibration Symposium, October 1998.

27. Rutgerson, S. E., NSWCCD/UERD Code 661, "Review of DDG 81 Modeling and Simulation Results", Presentation at Naval Postgraduate School, July 2003.

28. Shin, Y. S. and Ham, I., “Damping Modeling Strategy for Naval Ship System”, Tech. Report NPS-ME-03-003, Naval Postgraduate School, September 2003.

THIS PAGE INTENTIONALLY LEFT BLANK

INITIAL DISTRIBUTION LIST

1. Defense Technical Information Center
   Ft. Belvoir, Virginia

2. Dudley Knox Library
   Naval Postgraduate School
   Monterey, California

3. Mechanical Engineering Department Chairman, Code ME
   Naval Postgraduate School
   Monterey, California

4. Naval/Mechanical Engineering Curriculum Code 34
   Naval Postgraduate School
   Monterey, California

5. Professor Young S. Shin, Code ME/Sg
   Department of Mechanical Engineering
   Naval Postgraduate School
   Monterey, California

6. Michael J. Harrington
   Gibbs and Cox, Inc.
   Arlington, Virginia

7. Tim Zimmerman
   Gibbs and Cox, Inc.
   Arlington, Virginia

8. Michael C. Winnette
   Underwater Explosion Research Department (UERD)
   Naval Surface Warfare Center - Carderock Division
   West Bethesda, Maryland

9. Constintine Constant
   Naval Sea Systems Command
   Washington, District of Columbia

10. CAPT David H. Lewis, USN
    Program Manager, Aegis Shipbuilding
    Naval Sea Systems Command
    Washington, District of Columbia

11. CDR Jeff Riedel, USN
DDG-51 Class Post Delivery Manager (PMS 400PSA)
Naval Sea Systems Command
Washington , District of Columbia

12. Frederick A. Costanzo
Underwater Explosion Research Department (UERD)
Naval Surface Warfare Center - Carderock Division
West Bethesda, Maryland

13. Steven E. Rutgerson
Underwater Explosion Research Department (UERD)
Naval Surface Warfare Center - Carderock Division
West Bethesda, Maryland